Bolaamphiphiles as a novel drug delivery system in the treatment of diseases of the brain

Maclatchy, A.

BOLAAMPHIPHILES AS A NOVEL DRUG DELIVERY SYSTEM IN THE TREATMENT OF DISEASES OF THE BRAIN

AMY MACLATCHY

A thesis submitted in partial fulfilment of the requirements of the University of Westminster for the degree of Doctor of Philosophy

March 2020

Table of Contents

ABSTRACT

The incidence of central nervous system (CNS) diseases, such as glioblastoma, Alzheimer's disease and Parkinson's disease, will increase substantially in the next few decades. However, treatment for diseases of the brain is limited due to the restrictive physical and functional blood-brain barrier (BBB) dividing the brain and the vascular system. Bolaamphiphilic (BA) vesicles, produced from vernonia oil, encapsulate a wide range of therapeutic molecules, and offer an alternative drug delivery system to penetrate the brain to treat diseases of the CNS. We present novel anionic BA vesicles that cross biological barriers including the blood-brain barrier.

BA vesicles were characterised by dynamic light scattering, transmission electron microscopy, zeta potential analysis and size exclusion column chromatography. *In vitro* studies were performed on numerous CNS-representative and other cell lines - BV2 microglia, SH-SY5Y neurones, LN229 glioblastoma, HEK-293T epithelia, hCMEC/D3 endothelia and HASTR/ci35 astrocytes. *In vivo* studies were performed using C57BL/6 male mice. A novel methodology was developed to permit synthesis of the novel BAs first described here, directly from vernonia oil, the starting material.

This study has shown that a novel preparation of anionic BA form vesicles that encapsulate a range of different cargoes including tracer dyes and antibody fragments albeit with a low encapsulation efficiency. They do not influence cell viability or cause an acute immune response. They have been shown to penetrate the BBB *in vivo*. Analysis of the original BA material has shown to consist of two compounds, both of which have been synthesised and characterised.

The original material synthesised from vernonia oil and used to produce BA vesicles was thought to be cationic. However, after profiling the vesicles synthesised were found to have a negative zeta potential demonstrating that they are novel. They were further tested and found to cross biological barriers *in vitro*. Newly synthesised vesicles require further characterisation and optimisation to improve stability and encapsulation efficiency. The original anionic BA material has been shown to cross the BBB within 30 minutes of intravenous injection. These results demonstrate that whilst further studies are required this is a candidate drug delivery system to treat diseases of the brain.

Acknowledgements

This project and thesis would not be what it is without the dedication, support, motivation, encouragement, wisdom and supervision of my super supervisors, in particular Dr Mark Odell and Dr Simon McArthur, as well as Dr Saki Raheem and Professor Jimmy Bell. Thank you. Mark, thank you giving me this opportunity. Simon, thank you for all your patience, wisdom and selflessness. I cannot ever express the gratitude and appreciation of your support. Therefore, to you I dedicate this.

To my family, I want to say that you have been my backbone and best distraction anyone could have or want. You have provided stability and love constantly, most probably when I did not even deserve it. Thank you. To my girls, you can achieve anything you want, you are the most remarkable beings. And Jamie, thank you for all your support and encouragement. You are a remarkable man. Thank you. To you all I dedicate this to you.

A huge thank you to Erin MacLatchy for her patience and knowledge with formatting, and to Susan Simei-Cunningham for her time and guidance. You made this process much more manageable.

I wish to acknowledge Dr Sigrun Lange who has been a fantastic collaborator throughout my PhD, as well as introducing me to Dr Mariya Hristova. Thank you to Dr Mariya Hristova for coordination of the animal studies undertaken at UCL.

To my colleagues in the Research Centre for Optimal Health, Jimmy, Louise, Meliz, Jim, Rhys, and Ifi, thank you all for your guidance, support, feedback, conversations and doughnuts! Without it, this work would not be possible. Thank you.

Publications

1. Uysal-Onganer, P., MacLatchy, A., Mahmoud, R., Kraev, I., Thompson, P, R., Inal, J, M., and Lange, S. (2020). Peptidylarginine Deiminase Isozyme-Specific PAD2, PAD3 and PAD4 Inhibitors Differentially Modulate Extracellular Vesicle Signatures and Cell Invasion in Two Glioblastoma Multiforme Cell Lines. *International Journal of Molecular Sciences* 21(4):1495

   Abstract: Glioblastoma multiforme (GBM) is an aggressive adult brain tumour with poor prognosis. Roles for peptidylarginine deiminases (PADs) in GBM have recently been highlighted. Here, two GBM cell lines were treated with PAD2, PAD3 and PAD4 isozyme-specific inhibitors. Effects were assessed on extracellular vesicle (EV) signatures, including EV-microRNA cargo (miR21, miR126 and miR210), and on changes in cellular protein expression relevant for mitochondrial housekeeping (prohibitin (PHB)) and cancer progression (stromal interaction molecule 1 (STIM-1) and moesin), as well as assessing cell invasion. Overall, GBM cell-line specific differences for the three PAD isozyme-specific inhibitors were observed on modulation of EV-signatures, PHB, STIM-1 and moesin protein levels, as well as on cell invasion. The PAD3 inhibitor was most effective in modulating EVs to anti-oncogenic signatures (reduced miR21 and miR210, and elevated miR126), to reduce cell invasion and to modulate protein expression of pro-GBM proteins in LN229 cells, while the PAD2 and PAD4 inhibitors were more effective in LN18 cells. Furthermore, Kyoto Encyclopedia of Genes and Genomes (KEGG) pathways for deiminated proteins relating to cancer, metabolism and inflammation differed between the two GBM cell lines. Our findings highlight roles for the different PAD isozymes in the heterogeneity of GBM tumours and the potential for tailored PAD-isozyme specific treatment.

2. Kosgodage, U., Uysal-Onganer, P., MacLatchy, A., Mould, R., Nunn, A., Guy, G, W., Kraev, I., Chatterton, N, P., Thomas, L, E., Inal, J, M., Bell, J, D., and Lange, S. (2019). Cannabidiol Affects Extracellular Vesicle Release, miR21 andmiR126, and Reduces Prohibitin Protein in Glioblastoma Multiforme Cells. *Translational Oncology* 12(3):513-522

   Abstract: Glioblastoma multiforme (GBM) is the most common and aggressive form of primary malignant brain tumor inadults, with poor prognosis. Extracellular vesicles (EVs) are key mediators for cellular communication throughtransfer of proteins and genetic material. Cancers, such as GBM, use EV release for drug-efflux, pro-oncogenicsignaling, invasion and immunosuppression; thus, the

modulation of EV release and cargo is of considerableclinical relevance. As EV-inhibitors have been shown to increase sensitivity of cancer cells to chemotherapy, andwe recently showed that cannabidiol (CBD) is such an EV-modulator, we investigated whether CBD affects EVprofile in GBM cells in the presence and absence of temozolomide (TMZ). Compared to controls, CBD-treated cellsreleased EVs containing lower levels of pro-oncogenic miR21 and increased levels of anti-oncogenic miR126; these effects were greater than with TMZ alone. In addition, prohibitin (PHB), a multifunctional protein with mitochondrial protective properties and chemoresistant functions, was reduced in GBM cells following 1 h CBDtreatment. This data suggests that CBD may, via modulation of EVs and PHB, act as an adjunct to enhancetreatment efficacy in GBM, supporting evidence for efficacy of cannabinoids in GBM.

3. Kosgodage, U., Uysal-Onganer, P., MacLatchy, A., Kraev, I., Chatterton, N, P., Nicholas, A, P., Inal, J, M., and Lange, S. (2018). Peptidylarginine Deiminases Post-Translationally Deiminate Prohibitin and Modulate Extracellular Vesicle Release and MicroRNAs in Glioblastoma Multiforme. *International Journal of Molecular Sciences* 20(1):103

Abstract: Glioblastoma multiforme (GBM) is the most aggressive form of adult primary malignant brain tumour with poor prognosis. Extracellular vesicles (EVs) are a key-mediator through which GBM cells promote a pro-oncogenic microenvironment. Peptidylarginine deiminases (PADs), which catalyze the post-translational protein deimination of target proteins, are implicated in cancer, including via EV modulation. Pan-PAD inhibitor Cl-amidine affected EV release from GBM cells, and EV related microRNA cargo, with reduced pro-oncogenic microRNA21 and increased anti-oncogenic microRNA126, also in combinatory treatment with the chemotherapeutic agent temozolomide (TMZ). The GBM cell lines understudy, LN18 and LN229, differed in PAD2, PAD3 and PAD4 isozyme expression. Various cytoskeletal, nuclear and mitochondrial proteins were identified to be deiminated in GBM, including prohibitin (PHB), a key protein in mitochondrial integrity and also involved in chemo-resistance. Post-translational deimination of PHB, and PHB protein levels, were reduced after 1 h treatment with pan-PAD inhibitor Cl-amidine in GBM cells. Histone H3 deimination was also reduced following Cl-amidine treatment. Multifaceted roles for PADs on EV-mediated pathways, as well as deimination of mitochondrial, nuclear and invadopodia related

proteins, highlight PADs as novel targets for modulating GBM tumour communication.

Conferences

Westminster Doctoral Conference 2019- 15-minute presentation

BNA 2019 Festival of Neuroscience in Dublin 14th-17th April 2019- Poster presentation

Westminster Doctoral Conference 2018- Shot presentation

Westminster Doctoral Conference 2017- Poster presentation

Declaration of Contributors

The work undertaken in this thesis was performed and analysed by the author with the following exceptions:

Original bolaamphiphile production

The original bolaamphiphile material was produced by Professor Lawrence Williams and Dr Sumi Lee (Rutgers, USA).

Electron Microscopy

All electron microscopy work was undertaken at and provided by Research Complex at Harwell, as part of the national MRC platform initiative.

Animal Work

Animal work was undertaken at University College London (UCL) by Dr Mariya Hristova.

Bolaamphiphile vesicles

Protocol was designed by Dr Saki Raheem.

High resolution Mass Spectrometry

All HRMS data was performed at by Dr Emmanuel Samuel at School of Pharmacology, UCL.

List of Figures

List of Tables

List of Abbreviations

^{13}C - carbon

^{19}F - fluorine

^{1}H - Proton

ABC- ATP binding cassette

AChE- acetylcholine esterase

AD - Alzheimer's disease

ADME - adsorption, distribution, metabolism and excretion

AF546 – Alexa Fluor 546

AJs - adherens junction

ANOVA - Analysis of variance

AP2 - adaptor protein 2

ATCC- American Type Culture Collection

BA - bolaamphiphiles

BBB - blood-brain barrier

BBTB - blood-brain tumour barrier

BCRP - breast cancer resistance protein

BCSFB - blood cerebrospinal fluid barrier

BECs - brain endothelial cells

BM - basement membrane

BSA - bovine serum albumin

CD_3OD - deuterated methanol

$CDCl_3$ - deuterated chloroform

CED - convection enhanced diffusion

CMT - Carrier-mediated transporter

CNS - Central nervous system

CPPs - Cell penetrating peptides

CSF - cerebrospinal fluid

DAPI - 4',6-diamidino-2-phenylindole

DDS - drug delivery system

DLS- dynamic light scattering

DMAP- 4-(dimethylamino)pyridine

DMEM- Dulbecco's Minimum Essential Medium

DMF - dimethylformamide

DMF - dimethylformamide

DMSO- d_6 - deuterated dimethyl sulfoxide

DNA - deoxyribonucleic acid

DTT - dithiothreitol

EDTA- ethylenediaminetetraacetic acid

EGFR - epidermal growth factor receptor

ELISA - enzyme linked immunosorbent analysis

ESAMs - endothelial cell-selective adhesion molecules

Et_2O - diethyl ether

EtOAc - ethyl acetate

FACS - Fluorescence-activated cell sorting

FBS - foetal bovine serum

FITC- fluorescein isothiocyanate

FR- folate receptor

FS- forward scatter

FSC-A- forward scatter-area

FSC-H- forward scatter height

GFAP- glial fibrillary acidic protein

GLUT 1 - glucose transporter 1

HC -hydrocortisone

hEGF- human epidermal growth factor

hFGF- human fibroblast growth factor

HRMS - high resolution mass spectrometry

HRMS- High resolution mass spectrometry

Iba-1- ionised calcium binding adaptor molecule 1

ICV - intracerebroventricular

IDH - isocitrate dehydrogenase

IPTG- isopropyl β-D-1-thiogalactopyranoside

IR - Insulin receptor

ISF - interstitial fluid

IV- intravenous

JAMS - junctional adhesion molecules

K_2CO_3 – potassium carbonate

$KMnO_4$ - potassium permanganate

LAMs - leukocyte adhesion molecules

LAT1 - large amino acid transporter 1 receptor

LB- lysogeny broth

LDL - low-density lipoprotein

LDLR - low-density lipoprotein receptor

L-DOPA - levodopa

LPS- lipopolysaccharide

mAbs - Monoclonal antibodies

MeOH - methanol

MGMT - methylguanine methyltransferase

$MgSO_4$ - magnesium sulphate

MRPs - multidrug resistance-associated proteins

Na_2SO_4 – sodium sulphate

$NaHCO_3$ - sodium bicarbonate solution

NaOH - sodium hydroxide

NMR - Nuclear magnetic resonance

NTA - Nanoparticle Tracking Analysis

NVU - Neurovascular unit

OD - optical density

PBS- Phosphate-buffered saline

PD - Parkinson’s Disease

PDI - polydispersity index

PECAM-1/CD31- platelet endothelial cell adhesion molecule

PEG- Polyethylene glycol

Pet ether - petroleum ether

PFA- paraformaldehyde

P-gp - P-glycoprotein

PI- Propidium iodide

PLGA - poly(lactide-co-glycolide)

ppm - parts per million

R3-IGF-1- recombinant insulin-like growth factor

Rf - retention factor

RFP - red fluorescent protein

RMT - Receptor-mediated transporters

ROS - reactive oxygen species

scFv - single chain variable fragment

SDS-PAGE - Sodium dodecyl sulphate polyacrylamide gel electrophoresis

SLNs- solid lipid nanoparticles

SPSS- Statistical Package for the Social Sciences

SS- side scatter

SSC-A- side scatter- area

TAM- tumour associated microglia/macrophage

TBS - *tert*-butyldimethylsillane

TEER - Transendothelial cell electrical resistance

TFA -Trifluoroacetic acid

TfR - Transferrin receptor

TGN- Tris-Gylcerol-NaCl buffer

THF – tetrahydrofuran

TJs - Tight junctions

TLC - thin layer chromatography

TMS - trimethylsilane

TMZ - Temozolomide

TNF-α - Tumour necrosis factor-*α*

TPGS- d-α - tocopheryl polyetheylen gycol 1,000 succinate

TTfields - Tumour-treating fields

VE - vascular endothelial

VEGF - vascular endothelial growth factor

WHO - World Health Organisation

CHAPTER 1

1.1 Introduction

The incidence of diseases of the brain, such as Parkinson's disease (PD), Alzheimer's disease (AD) and glioblastoma, is forecast to increase as the global population as well as the aged population increases (Prince *et al*, 2016a; Feigin *et al*, 2017). AD is the most common form of dementia aetiologically characterised by the formation of protein aggregates called beta-amyloid plagues, as well as accumulation of mutated tau protein forming tau tangles within neurons (Alzheimer's Association, 2018). PD develops due to the loss of dopaminergic neurons located in the substantia nigra in the brain (Maiti, Manna and Dunbar, 2017; Surmeier, 2018). Gliomas are a brain cancer derived from glial cells, such as astrocytes, oligodendrocytes or ependymal cells (Louis *et al*, 2007; Hanif *et al*, 2017). They are the most common and aggressive of brain cancers in adults (Ohgaki and Kleihues, 2005; Verhaak *et al*, 2010) with poor mean survival of 14-15 months, and the more dismal recurrence survival of 5-7 months (De Witt Hamer *et al,* 2010; Sørensen *et al*, 2015; Hanif *et al*, 2017). It may be fair to assume that as the global population increases, so too will the global incidence. A recent study investigating epidemiology of conditions of the central nervous system (CNS), has found that in the 25 years from 1990-2015, both AD and PD saw the number of reported cases double (Feigin *et al*, 2017; Dorsey *et al*, 2018), with a prediction of 130 million suffering and diagnosed with AD by 2050 (Prince *et al*, 2016b). Duration is measured from diagnosis to death, there is no recovery from diseases such as AD and PD (Prince *et al*, 2016a). Unfortunately, there is no cure for these diseases, and treatment is palliative.

The impact of such statistics demonstrates the scope of this issue. However, there is a direct, as well as an indirect, burden. The indirect cost may be due to the loss of income by the patient or family member (Castro *et al*, 2010). Whereas the direct burden is associated with the cost of medical treatment and, depending on the status of the patient, social services (Castro *et al*, 2010). With the estimated worldwide cost of AD reaching (US) $1 trillion by 2018 (Prince *et al*, 2016b; Wimo *et al*, 2017) it can be appreciated that if the current statistics regarding increase of diagnosed patients, the cost, both financial and societal will also increase. These

brain diseases share the same challenge, despite their differing aetiologies, of an effective delivery of treatment.

The average time scale for drug discovery from concept to market is approximately 12 years at a cost that exceeds $1 billion (DiMasi *et al*, 2010; Van Norman, 2016; Mohs and Greig, 2017). Thus, demonstrating the challenges faced developing novel treatments. There have been no successful novel therapeutics for AD in the past 16 years despite the vast sums of money invested in numerous failed clinical trials (Sabbagh *et al*, 2019). High attrition rates of clinical trials is a further issue influencing and limiting discovery of novel treatments that can enter the brain (Morgan *et al*, 2012; Reichel, 2015; Vandenberghe *et al*, 2016; Chaturvedi *et al*, 2019). As a result, many pharmaceutical companies have reduced, downsized or closed their research centres, such as AstraZeneca, Johnson and Johnson, GlaxoSmithKline and Pfizer (Gautam and Pan, 2016; Hunter *et al*, 2018). With the lack of success, there is less investment at present in drug targeting (Pardridge, 2009; Chaturvedi *et al*, 2019).

This is not a recent development; Pardridge (2001) highlighted these shortcomings nearly two decades ago. However, there is a lack of investment in the targeting of novel compounds designed to treat diseases of the brain from within the pharmaceutical industry (Pardridge, 2009; Abbott, 2011). One of the deficiencies noted was that the majority of investment was focused towards drug discovery for CNS rather than drug delivery (Pardridge, 2009). The same rules used for pharmaceuticals for systemic treatment do not apply to the blood brain barrier (BBB). The challenges lie in the fact that the BBB prevents the effective delivery of compounds (Abbott, 2013). However, there appears to be a lack of understanding of the reasons for these failures including the target exposure, target engagement and the level of efficacy of the compound commensurate to the exposure and engagement (Morgan *et al*, 2012; Reichel, 2015).

1.2 Challenges for the delivery of therapeutics to treat diseases of the brain

There are a number of challenges for the delivery of therapeutics to treat diseases of the brain, requiring an understanding of the complexities surrounding the barriers that protect it (Chaturvedi *et al*, 2019). To treat a disease, a drug must be able to both elicit a suitable pharmacological effect (Reichel, 2015), and be able to reach

its site of action at a concentration sufficient/adequate in order to elicit this effect (Reichel, 2015). For therapeutics for the CNS, this second requirement is a major limitation, drugs must be able to cross the BBB and penetrate the brain parenchyma, against the natural role of the BBB as a barrier to xenobiotics, including most drugs (Alavijeh and Palmer, 2010; Chaturvedi *et al*, 2019). The design of therapeutics for the CNS must be based on the characteristics of the BBB (Pardridge, 1995). As a result, the neuropharmacokinetics and pharmacodynamics must account for this design of novel drug targeting (Reichel, 2015).

The BBB is a physical, functional, enzymatic and pharmacological barrier designed to protect and selectively restrict the entry of compounds into the brain (Bodor and Buchwald, 2002). The BBB is the interface of the vascular system and the central nervous system (CNS). It is a physical, functional and pharmacological barrier protecting and restricting entry of foreign substances and toxins (Abbott *et al*, 2010). The brain requires a strict homeostatic environment in order to perform its functions. As a result, the majority of therapeutics designed to treat diseases of the brain are unable to reach their intended target (Pardridge, 2009; Alavijeh and Palmer, 2010). The statics are quite sobering as approximately 98% of small drugs are prevented from crossing the BBB. Molecules, including therapeutics greater than 400 Da are also restricted. As a result of the selectively restrictive permeability of the BBB, hydrophilic or charged therapeutic agents are essentially prevented from crossing the BBB (Olanow *et al*, 1991; Garcia-Garcia *et al*, 2005) with many that do so being rapidly removed by the numerous efflux transporters found in the brain endothelial cells (BECs), for example p-glycoprotein (P-gp) or breast cancer resistance protein (BRCP) (Hartz and Bauer, 2011).

The only therapeutics that are able to penetrate to the brain parenchyma are small lipophilic drugs (Pardridge, 2002). The challenge in developing a therapeutic to cross the BBB is that there are a number of hurdles that the drug must overcome. The first of these hurdles is overcoming the BECs which differ from peripheral endothelial cells in that they lack fenestrations and have tight junction complexes, effectively restricting paracellular entry (Abbott, 2013; Miller, 2015; Arvanitis *et al*, 2019). Secondly, the BECs are limited in the expression of transmembrane transporters designed to selectively restrict entry to the brain to maintain

homeostasis (Pardridge, 2012; Abbott, 2013). Thirdly, the high expression of efflux transporters, the ATP Binding Cassette transporters protecting the brain from xenobiotics and foreign substances (McArthur *et al*, 2016). In order that we can understand the difficulties presented by the BBB we need to consider the case of need in respect of the delivery of a therapeutic agent to the brain.

1.3 The Structure and Function of the Blood Brain Barrier

The main functions of the BBB are to regulate homeostasis and protect the CNS by restricting the entry of toxins and foreign substances (Luissint *et al*, 2012; Obermeier, Daneman, and Ransohoff, 2013). Whilst doing this, it must selectively allow passage of nutrients and molecules and remove potentially toxic metabolic waste (Abbott, 2013; Daneman and Prat, 2015; McArthur *et al*, 2016). This is achieved by a combination of the physical and functional characteristics: the tight intercellular junctions, limited and selective transport systems and a highly effective and efficient family of ATP-binding cassette (ABC) efflux transporters such as P-glycoprotein (P-gp) and multi-drug resistance-associated proteins (MRP-1 and MRP-2) (Bart *et al*, 2000; Abbott, 2013; McArthur *et al*, 2016). This is further supported by the presence of a population of active phagocytes, in particular perivascular macrophages in vascular walls (Faraco *et al*, 2017).

The heavy demand for oxygen and glucose by the neurons is transported through the cerebral blood flow via the 600 kilometres of vascular network and across the BBB (Wong *et al*, 2013; Pulgar, 2019). The surface area of the BECs is estimated to be 15-25 m^2 (Wong *et al*, 2013; Pulgar, 2019). As a result of this vast network, it is thought that each neuron is within 20 µm of a capillary to ensure rapid solute equilibrium (Oldendorf et al, 1977; Wong *et al*, 2013; Sweeney et al, 2018).

The unique structure and hallmarks of the BBB are attributable to the neurovascular unit (NVU) comprised of pericytes, astrocytes, neurons, microglia, and specialised brain endothelial cells (BECs) as shown in figure 1.1A (Baeten and Akassoglou, 2011).

1.3.1 Brain endothelial cells

Brain endothelial cells (BECs) line the vast capillary network providing protection from pathogens and foreign substances, such as xenobiotics, and nourishment of

the CNS, whilst controlling and maintaining the homeostatic conditions of the extracellular neural environment (Blanchette and Daneman, 2015). The luminal membrane faces the circulation whilst the basolateral membrane faces the brain interstitial fluid (ISF) (Banks, 2019). A monolayer of BECs line the capillaries. However, in the narrowest regions of the capillaries the BECs form tight junctions with adjacent BECs (Banks, 2019). They are narrower than muscle endothelial cells at 200-500 nm in width (Coomber and Stewart, 1985; Abbott *et al*, 2010; Reichel, 2015).

BECs differ structurally and functionally from peripheral endothelial cells (ECs) in several ways (Abbott *et al*, 2006; Pinto *et al*, 2017). They lack fenestrations (Banks, 2019), display reduced pinocytosis (Gastfriend *et al*, 2018) and low expression of leukocyte adhesion molecules (LAMs) to limit the entry of immune cells (Langen, Ayloo and Gu, 2019). They have complex inter-endothelial junctions with contributions from both adherens and tight junction molecules (AJs and TJs, respectively) (Figure 1.1B) (Baeten and Akassoglou, 2011; Pinto *et al*, 2017) restricting paracellular transport to the brain. BECs have a high expression of the ABC transporters, such as P-gp transporter on both the luminal and abluminal membranes effectively removing potentially toxic and harmful substances and trafficking compounds into the brain parenchyma (Miller, 2015). In order to overcome the large energy requirements necessary for the demands of the ATP-binding cassette transporters and the sodium and potassium ATPase gates (Zlokovic, 2011), they express a larger number of mitochondria than peripheral ECs (Coomber and Stewart 1985). Routes of entry, such as intercellular pores and paracellular or transcellular channels and transporters, including caveolae, present on peripheral organs, are greatly limited at the BBB (Pardridge, 2012; Abbott, 2013; Obermeier *et al*, 2013). BECs are highly charged as a result of the TJs selectively restricting the entry of ions and small charged molecules resulting in the luminal surface being more polar than that of the abluminal (Blanchette and Daneman, 2015; Abbott *et al*, 2006; Sharif *et al*, 2018). The luminal membrane of BECs are lined with glycocalyx, a layer of negatively charged carbohydrates, providing a barrier between blood and endothelial cells (Abbott, 2013; Haeren *et al*, 2016; Kutuzov *et al*, 2018). They have recently been described as an endocrine tissue in

that they secrete and transport chemical signals across and out of the brain (Banks, 2019). Thus, further demonstrating their distinction to peripheral ECs.

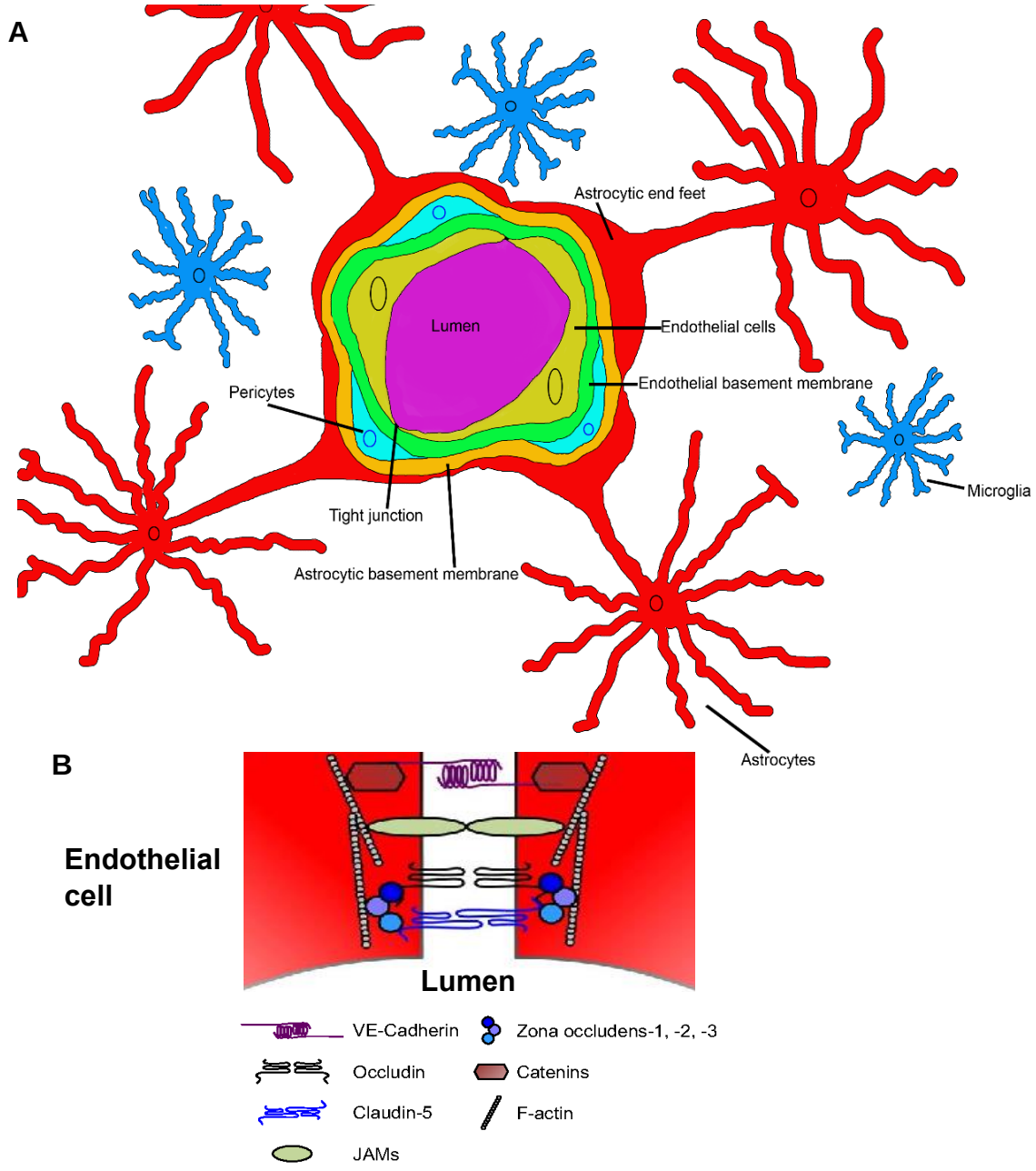

Figure 1.1 Structure of the neurovascular unit. A. Schematic representation of the neurovascular unit which comprises brain endothelial cells with the inter-endothelial tight junctions, endothelial and astrocytic basement membranes, pericytes, astrocyte end feet and microglia. **B.** Detail of inter-endothelial junctions and the molecular relationships between junctional complexes and the actin cytoskeleton. The tight junction complex consists of occludins, claudins and junctional adhesion molecules (JAMs). The C-terminus of the tight junction proteins bind to scaffolding proteins zona occludens-1, -2, and -3 which in turn link with the actin cytoskeleton. The adherens junctions comprise vascular endothelial (VE) cadherins which bind via catenins to the actin cytoskeleton. Adapted from McArthur *et al*, 2016, with permission.

1.3.1.1 Tight junctions and adherens junctions

Junctional complexes, such as tight junctions (TJs) and adherens junctions (AJs), located between adjacent endothelial cells, create a physical and functional barrier restricting the paracellular passage of molecules (Abbott *et al*, 2010). TJs are a complex of transmembrane proteins providing a physically limiting barrier between neighbouring endothelial cells (Luissant *et al*, 2012; Savaiva *et al,* 2016). Due to their polarity they form a highly selective diffusion barrier restricting delivery of pharmaceuticals (Ballabh *et al*, 2004; Bicker *et al*, 2014; Blanchette and Daneman, 2015; Tietz and Englehardt, 2015).

Inter-endothelial junctions between BECs are complex, multi-part structures, including TJs, AJs, junctional adhesion molecules (JAMS) and endothelial cell-selective adhesion molecules (ESAMs) (Tietz and Englehardt, 2015; Freskgård and Urich, 2017; Stamatovic *et al*, 2016). Occludin, claudin-5 and JAMs, membrane linker proteins, all form homodimer bridges linking adjacent endothelial cells (Cummins, 2012; McArthur *et al*, 2016; Stamatovic *et al*, 2016). Intracellular accessory proteins, such as zonula occludens-1, -2, and 3, act as scaffolding proteins connecting the cytoplasmic tails of transmembrane proteins occludin and claudin-5 to F-actin, providing the rigidity to the TJs (Almutairi *et al*, 2016; Cummins, 2012; Stamatovic *et al*, 2016). ESAMs interact, as the other proteins, with zonula occludens in the plasma membrane of the adjacent cells, to mediate the linkage formed with the actin cytoskeleton, creating an additional physical barrier, further restricting permeability (Stamatovic *et al*, 2016). AJs form junctional complexes between neighbouring ECs and are composed of the transmembrane protein vascular endothelial (VE)-cadherin binding to intracellular catenins, (Harris and Nelson, 2010; Luissint *et al*, 2012; Tietz and Englehardt, 2015). The transmembrane protein-protein links provide greater protection and limited entry of foreign substances across the BBB. Each of these elements is important in forming the BBB. As a result of such interactions, a difference in polarity between the apical and basolateral sides of BECs is created. The measurement of this structural and functional characteristic is referred to as the transendothelial electrical resistance (TEER).

TEER is a measurement of the tightness of the BBB, controlling transportation of molecules into and out of the cell (Abbott *et al*, 2006; Blanchette and Daneman, 2012; Srinivasan *et al*; 2015). It has been measured at 1500 Ω cm^2 (Crone and Christensen, 1981), but has been estimated to be as high as 5000 Ω cm^2 in humans (Lauschke, Frederiksen, and Hall, 2017; Srinivasan and Kolli; 2019). The tighter the TJs the higher the TEER, thus influencing the level of transcellular and paracellular entry of molecules and compounds (Redzic, 2011). The TEER of other barriers of the body is considerably less than that of the BECs, such as the brain cerebrospinal fluid barrier 150 Ω cm^2 (Saito and Wright, 1984; Redzic, 2011) or other tissues of 3-33 Ω cm^2 (Crone and Christensen, 1981; Redzic, 2011). This highlights the distinct, restrictive, protective and unique characteristics of the BBB.

1.3.2 Basement membranes

The basement membrane (BM) is located between the endothelial cells and astrocytic end feet and is composed of extracellular matrix proteins secreted from the pericytes, BECs and astrocytes (Baeten and Akassoglou, 2011). The BM is comprised of two closely apposed membranes - the endothelial and the astrocytic BM, also referred to as the glia limitans (Baeten and Akassolou, 2011; Blanchette and Daneman, 2015; Daneman and Prat, 2015; Pinto *et al*, 2017). The membranes are lined with extracellular receptors, involved in cell-cell and cell-matrix communication (Baeten and Akassoglou, 2011). The BMs are also involved in the prevention of leukocyte permeation due to the presence of laminins secreted from the BECs and astrocytes (Baeten and Akassoglou, 2011; Pinto *et al*, 2017; Wang *et al*, 2006). These basal laminae play an important role in the structure of the BBB acting as a support for the endothelial cells, as well as communicating with and providing nutrients for the parenchyma (Baeten and Akassoglou, 2011; McArthur *et al*, 2016). Embedded within the basement membranes are pericytes.

1.3.3 Pericytes

Pericytes, through their interactions with the endothelial cells, are involved in the development, differentiation, maturation and regulation of the BBB (Obermeier *et al*, 2013; Jackson *et al*, 2017). The number of pericytes is directly proportional to that of endothelial cells and is referred to as the endothelium/pericyte ratio (Jackson *et al*, 2017). Pericytes, along with perivascular macrophages, are the first line of

immunologic defence involved in phagocytosis (Thomas, 1999; Guillemin and Brew, 2004; Faraco *et al*, 2017). They are involved in the regulation of cerebral blood flow and capillary diameter (Bell *et al*, 2010; Winkler *et al*, 2014; Jackson *et al*, 2017). Pericytes and astrocytic end feet, the distal end of astrocyte processes, regulate permeability of the BBB through their interaction with the basement membranes and induction of TJ formation (Bell *et al*, 2010; Obemeier *et al*, 2013; Winkler *et al*, 2014).

1.3.4 Astrocytes

Astrocytes, the most abundant type of glial cell, provide structural support to the cerebral blood vessels, maintaining homeostasis of fluid, electrolytes, amino acids and neurotransmitters, the control of cerebral blood flow and removal of metabolic waste from the parenchyma (Takano *et al*, 2006; Wolburg-Buchholz *et al*, 2009; Baeten and Akassoglou, 2011; Bicker *et al*, 2014; McArthur *et al*, 2016;). Astrocytes, through their endfeet, ensheath microvessels in the CNS (Wolburg-Buchholz *et al*, 2009; Daneman, 2012; Bicker *et al*, 2014). *In vitro* astrocytes have been shown to influence and induce the expression of BEC characteristics such as P-glycoprotein and TJs in non-CNS endothelial cells (Abbott *et al*, 2006; Alvarez *et al*, 2013), demonstrating their influence over the integrity of the BBB. They are involved in numerous functions including neuronal development and synapse formation (Liddelow and Barres *et al*, 2017). They have been suggested to be responsible for brain ageing (Clarke *et al*, 2018), neurodegenerative disease (Liddelow and Barres *et al*, 2017), and are potentially neuroprotective after traumatic brain injury (Shinozaki *et al*, 2017). These factors have been observed in numerous studies investigating models of reactive astrocytes demonstrating the heterogeneity within the population cells (Molofsky *et al*, 2012; Zamanian *et al*, 2012; Liddelow and Barres *et al*, 2017). This highlights the complexity of the populations of astrocytes and their roles in health and disease.

1.3.5 Microglia

Microglia are known as the macrophages of the brain, providing immunity through regulation of both innate and adaptive immune responses (Gomez-Nicola and Perry, 2015). Through constant surveillance of the brain parenchyma, they respond acting as phagocytes ingesting and degrading debris, such as dead cells, and

harmful agents including pathogens (Davalos *et al*, 2005; Nimmerjahn, Kirchhoff and Helmchen, 2005; Yin *et al*, 2017). They are involved in the integrity of the brain, from normal development and function to repair (Tremblay *et al*, 2011; Bicker *et al*, 2014; Gomez-Nicola and Perry, 2015; McArthur *et al*, 2016). Microglia are involved in the normal development of the brain through interactions with neurons to promote differentiation and survival by production and release of specific neurotrophic factors including insulin growth factor (Michell-Robinson *et al*, 2015; Yin *et al*, 2017). They are involved in tissue repair and maintaining homeostasis (Derecki *et al*, 2013). However, microglia convert to a pro-inflammatory phenotype during disease and brain injury (Derecki *et al*, 2013; Eggen *et al*, 2013). This has a negative impact as is observed with diseases such as Alzheimer's disease and glioma that they are implicated in progression and proliferation (Hambardzumyan, Gutmann and Kettenmann, 2016; Wolf, Boddeke, and Kettermann, 2017). Such a response demonstrates the adaptive characteristics of the microglial cells in maintaining plasticity of the brain (Nimmerjahn, Kirchhoff and Helmchen, 2005; Tremblay *et al*, 2011; McArthur *et al*, 2016).

1.4 Routes of Entry

Both the BBB and the brain require the entry of molecules, such as glucose, in order to provide the high levels of energy needed to maintain healthy functioning (Benarroch, 2014). The metabolic waste produced must also be removed. As the brain is so heavily protected and entry into the brain and across the BBB is restricted and, in some instances, prevented, molecules enter and exit via endogenous transport pathways and a number of mechanisms, such as transcytosis or diffusion (Freskgård and Urich, 2017). There is a lower expression of endogenous transport systems on the BBB (Stewart, 2000; Pardridge, 2005), further restricting and limiting the entry of molecules and compounds required for the brain. However, the systems located on both the apical and basolateral sides of the BECs are specific to the requirements of the brain (Patching, 2017). The pathways and mechanisms involved include:

- Paracellular entry (Bicker *et al*, 2014; Saraiva *et al*, 2016; Pinto *et al*, 2017)

- Macropinocytosis, absorptive mediated transport and receptor mediated transport, which includes both clathrin-mediated and caveolae-mediated transport; are the main vesicular pathways of the BBB (Goulatis and Shusta, 2017).
- Carrier-mediated transporters (Pardridge, 2005; Ohtsuki and Terasaki, 2007; Abbott, 2013; Lajoie and Shusta, 2015)
- ATP binding cassette (ABC) efflux pumps (Abbott, 2013; Qosa *et al*, 2015; Strazielle and Ghersi-Egea, 2015; van Tellingen *et al*, 2015; Freskgård and Urich, 2017) (Figure 1.2)

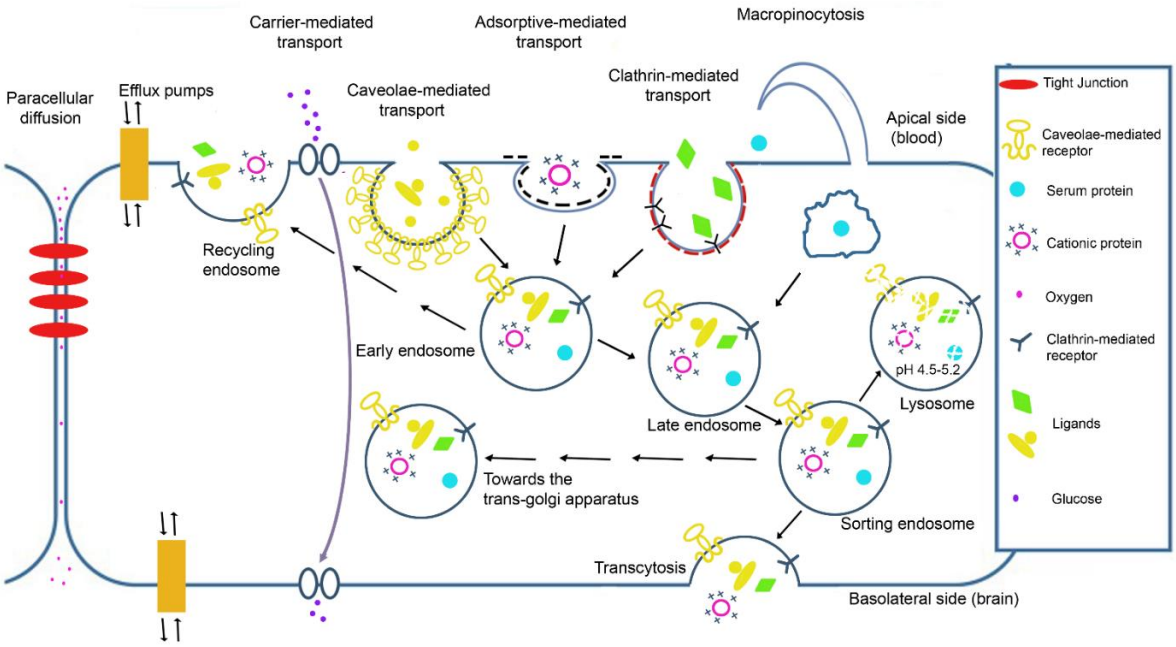

Figure 1.2. The different modes of transport into and across the BBB. The routes of entry of the BBB include paracellular diffusion, efflux pumps, carrier-mediated transport, adsoptive-mediated transport, macropinocytosis and receptor-mediated transport, including both caveolae- and clathrin-mediated transport. The material packaged within each delivery system may be transcytosed to the basolateral side via the endosome, delivered for further distribution within the cell, recycled thus exiting the cell, or be digested in the lysosome.

1.4.1 Paracellular diffusion

Paracellular diffusion is the route by which molecules diffuse at the site of the TJs, in the instance of ions and gaseous molecules, or across the plasma membrane of the BECs for lipophilic substances (Bicker *et al*, 2014; Saraiva *et al*, 2016; Pinto *et al*, 2017). However, due to the formation of the TJs between adjacent cells that regulate diffusion, paracellular transport is severely restricted (Wong *et al*, 2013).

This is due to the limited intercellular pore size, approximately 1 nm (Sarin, 2010; Furtado *et al*, 2020). As a result, small molecules and ions are effectively prevented from crossing (Abbott *et al*, 2010; Wong *et al*, 2013). Diffusion across the membranes is specific to lipophilic compounds that are able to cross dependent upon criteria such as size and the number of hydrogen bonds (Pardridge, 2005; Furtado *et al*, 2020).

1.4.2 Transcytosis and endocytosis

Transcytosis involves the transportation of vesicles through the cell, from one side of the plasma membrane to the contralateral, for example, from the luminal to the abluminal of the brain endothelial cells (Okamoto, 1998; Stewart, 2000) (Figure 1.3A). Whereas endocytosis is the process in which extracellular compounds, such as proteins and lipids, are internalised to the cell by the fusion of the plasma membrane to form vesicles (Doherty and McMahon, 2009) (Figure 1.3B). There are a number of pathways involved in endocytosis once the vesicle is internalised (Okamoto, 1998; Henry *et al*, 2012; Goulatis and Shusta, 2017) (Figure 1.2). The vesicle fuses with endosomes to form the early endosome (Huotari and Helenius, 2011; Scott, Vacca and Gruenberg, 2014). The function of the early endosome is to act as the initial sorting station to determine the destination of the cargo to regulate the pathways of the vesicle (Huotari and Helenius, 2011; Scott, Vacca and Gruenberg, 2014). During this process the internalised cargo will be either recycled, redirected towards the trans-golgi network, degraded or transcytosed (Okamoto, 1998; Huotari and Helenius, 2011; Scott, Vacca and Gruenburg, 2014). The initial binding of the ligand to the receptor determines the fate of the endosome and its cargo (Freskgärd and Urich, 2017).

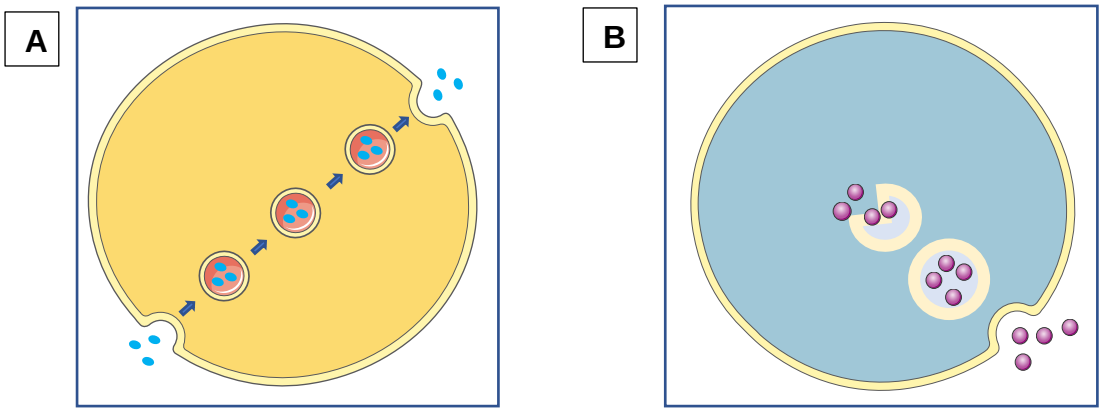

Figure 1.3. The different pathways of vesicle transportation after entry into the cell. A) Transcytosis. The transport of vesicles through the cell from the side they are formed to the other where they are released. **B) Endocytosis**. The process by which compounds from the extracellular matrix are internalised by the cell membrane. The cell membrane fuses together to form a vesicle which transports the molecules encapsulated within the vesicle inside the cell.

1.4.3 Macropinocytosis

Although macropinocytosis is one of the pathways in which molecules transcytose, there are few macropinocytic vesicles present on the BBB (Brightman and Reese, 1969). Macropinocytosis is the non-selective uptake of extracellular fluid (Lim and Gleeson, 2011; Goulatis and Shusta, 2017). It is a signal dependent process involving the rearrangement of the cytoskeleton and ruffling of the plasma membrane to form vesicles (Lim and Gleeson, 2011; Goulatis and Shusta, 2017). These vesicles differ from other vesicles in that they do not have a coating and appear much larger (0.2 µm- 5 µm) than clathrin (100 nm) and caveolae- mediated transport (Lim and Gleeson, 2011).

1.4.4 Adsorptive-mediated transport systems

Adsorptive-mediated transport is involved in the transport of cationic molecules (Goulatis and Shusta, 2017). Due to the electrostatic interactions between anionic moieties, such as sialic acid, present on the luminal cell membrane, positively charged molecules, such as glycoproteins, are non-specifically invaginated and transcytosed through the cell to be exocytosed from the abluminal membrane by heparan sulphates (Bickel et al, 2001; Hervé et al, 2008; Lu, 2012; Abbott, 2013).

1.4.5 Receptor-mediated transport

Receptor mediated transport (RMT) is the vesicular transport of materials from the apical membrane of BECs to the basolateral side (Jones and Shusta, 2007). It involves the interaction of a ligand to a specific receptor located on the surface of the BEC (Jones and Shusta, 2007; Goulatis and Shusta, 2017). This complex results in the invagination of the membrane to form an intracellular transport vesicle (Brown and Greene, 1991). This initiates transport of the vesicle through the BEC cytosol to the basolateral membrane to be transcytosed and released (Jones and Shusta, 2007; Huotari and Helenius, 2011; Scott, Vacca and Gruenburg, 2014). RMT includes both clathrin-mediated and caveolae-mediated transport vesicular pathways of the BBB (Goulatis and Shusta, 2017).

Receptor-mediated transporters are involved in the selective transportation of larger molecules, such as transferrin, insulin, and low-density lipoprotein, across the BBB to the brain (Pardridge, 2002). This process involves the formation of vesicles through the binding of a ligand, such as insulin or transferrin, to its specific receptor, for example insulin receptor (IR) or transferrin receptor (TfR), respectively, located on the luminal plasma membrane (Guo *et al*, 2012; Bicker *et al*, 2014; Lajoie and Shusta, 2015). These receptors, as well as the low-density lipoprotein receptor (LDL-R), are highly expressed on the BBB (Goulatis and Shusta, 2017). The vesicles are either transcytosed through the 200 nm of cytoplasm to the abluminal membrane to the brain parenchyma or mediated towards the endosomal pathway for degradation (Pardridge, 2002; Lajoie and Shusta, 2015; Goulatis and Shusta, 2017). As previously mentioned, both clathrin-mediated and caveolae-mediated transport are examples of RMT.

1.4.5.1 Clathrin-mediated transport

Clathrin-mediated transport involves the interaction of the adaptor protein complexes, adaptor protein 2 (AP2), and clathrin in the formation of endocytic vesicles (Goulatis and Shusta, 2017; Lim and Gleeson, 2011). Assembly of the lattice-like clathrin coat is initiated through the binding and recruitment of the specific ligand and the transmembrane receptors to adaptor protein complexes and clathrin (Lim and Gleeson, 2011; Schmid, 1997). Thus, the assembly of proteins, as well as the intrinsic curvature of the clathrin coating, encourage the bending and

invagination of the membrane to form the vesicle (Ungewickell and Hinrichsen, 2007). Budding and packaging of the clathrin coated endosomal vesicle is completed on fission from the plasma membrane (Schmid, 1997). The transferrin receptor is an example of the clathrin mediated transport system (Goulatis and Shusta, 2017; Jefferies et al, 1984). On disassembly of the network of clathrin and adaptor proteins, the endosomal vesicle fuses with the early endosome where the cargo and receptors are sorted and are either transcytosed, degraded or recycled, the latter is exclusive to the receptors (Mayor and Pagano, 2007; Huotari and Helenius, 2011; Goulatis and Shusta, 2017).

1.4.5.2 Caveolae-mediated transport

Caveolae are specialised lipid rafts which converge in regions of the plasma membrane, involved in endocytosis, exocytosis, regulation of cholesterol and signal transduction (Hommelgaard et al, 2005; Thomas and Smart, 2008; Bastini and Parton, 2010; Parton and del Pozo, 2013). The regions in which caveolae structures are located are rich in saturated phospholipids, sphingolipids, cholesterol and lipid-linked proteins (Xu *et al*, 2015; Andreone *et al*, 2017). They are composed of proteins called caveolin (Kovtun *et al*, 2015). Caveolae appear in different conformations (Thomas and Smart, 2008), such as flask like shaped invaginations (Parton, Joggerst and Simons, 1994; Gumbleton *et al*, 2000; Bastini and Parton, 2010) or tubular structures (Benlimame *et al*, 1998). Cholesterol dependent caveolae appear flat (Rothberg *et al*, 1992). The low-density lipoprotein (LDL) receptor is located in these lipid rich regions on the plasma membranes of BECs, demonstrating that caveolae-mediated transport involves the transcytosis of LDL to the brain parenchyma (Méresse *et al*, 1991; Candela *et al*, 2008). The formation of the caveolae vesicles involves the interaction of the caveolin coating proteins and cavin protein complex, and budding involves GTPase dynamin (Bastini and Parton, 2010; Preston, Abbott and Begley, 2014; Andreone *et al*, 2017).

1.4.6 Carrier-mediated transport

Carrier-mediated transporters (CMT) are located on the endothelial membranes and shuttle small hydrophilic molecules and essential nutrients to the brain such as glucose (GLUT 1) and amino acids (Large neutral amino acid- LAT-1) (Pardridge, 2005; Ohtsuki and Terasaki, 2007; Abbott, 2013; Lajoie and Shusta, 2015). These

transporters are important in the regulation, support and functioning of the CNS (Ohtsuki and Terasaki, 2007; Abbott, 2013). Due to the presence of numerous mitochondria of the BECs and the high energy requirements of the brain fed almost exclusively by glucose (Oldendorf, Cornford and Brown, 1977; Benarroch, 2014), the GLUT1 transporter is one of the most abundant transporters of the BBB (Patching, 2017).

1.4.7 ATP binding cassette (ABC) transporters

ATP binding cassette (ABC) efflux pumps are responsible for the active transport of exogenous and endogenous molecules across membranes (Abbott *et al*, 2010; Abbott, 2013; Qosa *et al*, 2015; Strazielle and Ghersi-Egea, 2015; van Tellingen *et al*, 2015). Whilst these transporters are located on tissues and organs involved in adsorption, distribution, metabolism and excretion, they are highly expressed on the BBB (Robey *et al*, 2018). ABC efflux transporters play an important role in the protection of the brain through the removal of potentially harmful xenobiotics, as well as metabolic waste (Ashraf, Kao and Bendayan, 2014). However, they do this indiscriminately such that therapeutics designed for treatment of diseases such as glioblastoma, epilepsy and HIV, are also excluded and excreted (Miller, 2015). The level of expression relates directly to the accumulation and concentration of drug in the brain (Chan *et al*, 2013; Miller and Cannon, 2014).

Of the seven ABC transporter family, A-G, the three most studied families include ABCB (specifically ABCB1), ABCC and ABCG (specifically ABCG2) due to their multidrug resistance (Xiong *et al*, 2015; Leandro *et al*, 2019). One of the most important of this family though, is the protein P-glycoprotein (P-gp or MDR1), encoded for by the gene *ABCB1*. This protein, located on the luminal surface of the BECs (Berarroch, 2012; Robey *et al*, 2018), acts to remove many pharmaceutical and non- pharmaceutical compounds, including many chemotherapeutics (Redzic, 2011; Xiong *et al*, 2015; Thomsen *et al*, 2017).

The ABCC family consists of the multidrug resistance-associated proteins 1-6 (MRP1-6) located on both the luminal and abluminal membranes of BECs (Hartz and Bauer, 2011; Berarroch, 2012; Miller, 2015; Dréan *et al*, 2018). Substrates of MRP transporters are primarily, though not restricted to, chemotherapeutics as for P-gp transporter (Xiong *et al*, 2015). *ABCG2* encodes for the breast cancer

resistance protein (BCRP) transporter located on the luminal surface of BECs (Berarroch, 2012). Substrates include tyrosine kinase inhibitors, such as gefitinib, antineoplastic agents, including mitoxantrone, and antibiotics (Robey *et al*, 2007).

Many ABC transporters are also expressed on astrocytes, pericytes, microglial cells and neurons (Löscher and Potschka, 2005; Ashraf et al, 2012; Sanchez-Covarrubias et al, 2014; Qosa et al, 2015). Whilst this mechanism is highly effective at protecting the brain from foreign substances and maintaining the homeostatic environment, for treating diseases of the brain, such as glioblastoma, this can prove extremely challenging. ABC transporters have also been reported to be overexpressed on glioblastoma cells conferring chemoresistance (Khamisipour et al, 2016; Dréan et al, 2018).

1.5 Challenges faced developing a drug delivery system to the brain

There are a number of factors influencing the delivery of drugs to the brain such as the restrictive, functional and pharmacological characteristics of the BBB, as previously mentioned (Section 1.1). However, the drug itself also presents itself with numerous challenges including the pharmacokinetics of the drug (adsorption, distribution, metabolism and excretion - ADME), size, charge, lipophilicity, solubility, binding to plasma proteins and permeability (Alavijeh *et al*, 2005; Bergström, 2005; Mannhold, 2005; Manallack, 2007).

1.5.1 Pharmacokinetics

The two most important characteristics of the ability of a drug to cross cell membranes include lipophilicity and solubility (Bergström, 2005; Mannhold, 2005). The acid-base dissociation constant, pKa, influences the ability of a drug to cross biological barriers (Manallack, 2007). This is based on the Henderson-Hasselbalch equation:

$$pH = pKa + \log 10 \frac{[A-]}{[HA]}$$

where pH is the acidity of a buffer solution, pKa is the pH at which half of the drug is deprotonated/ionised, [A^-] is the concentration of the conjugate base (accepting protons) and [HA] is the concentration of the acid (donating protons) (Manallack, 2007). The equation describes the interaction of the drug in its ionised and non-

ionised state which in turn relates to the lipophilicity and solubility of a drug and the pH of the environment in which it is interacting (Po and Senozan, 2001; Manallack, 2007). A soluble or ionised drug is unable to cross a biological barrier. The rare exception is where a carrier mediated transporter exists, for example levodopa (L-DOPA) transported by the large amino acid transporter 1 receptor (LAT1) (Tsuji, 2005). However, the more lipophilic or non-ionised a drug the more permeable it is, leading to non-specific absorption throughout the body and influencing the concentration of the drug. Nonetheless, there are factors that influence and may prevent rapid uptake.

The molecular weight and the number of hydrogen bonds a therapeutic can make influence its ability to penetrate the BBB (Habgood *et al*, 2000; Pardridge, 2003). Small drugs, which do not exceed 400-500 daltons (Da) appear to cross the BBB (Habgood *et al*, 2000). However, the more hydrogen bonds a molecule can form reduces the delivery of the drug across the BBB (Habgood *et al*, 2000). One such example is histamine, which is only 111 Da. It contains three nitrogen atoms that can form hydrogen bonds with water, and these prevent penetration across the BBB (Pardridge, 2003). When developing and designing a drug delivery system, such factors need to be considered.

Penetration of compounds/drugs to the CNS is dependent upon a number of factors such as the rate (speed of delivery) and the extent (the concentration of the drug that crosses) (Reichel, 2015). Each of these factors have their own rate limiting steps. It is considered that the rate limiting factor influencing the rate at which a compound crosses the BBB is dependent upon the cerebral blood flow (CBF) and the permeability at the site of entry (Reichel, 2015). Other factors include the mechanism by which the compound requires to enter the brain, the transporters present at the BBB and the binding of the compound to plasma proteins (Reichel, 2015).

1.5.2 Drug extrusion from the BBB

As previously mentioned, the ABC transporters are involved in adsorption, distribution, metabolism and excretion (ADME) through the influx of molecules and the removal of waste and xenobiotics (Section 1.4.7) (de Lange, 2004; Neuwelt *et al*, 2011). Paradoxically, the ABC transporters not only protect the brain from

xenobiotics, they also extrude certain drugs required to treat diseases of the brain through multidrug resistance (de Lange, 2004; Mahringer and Fricker, 2016; Robey *et al*, 2018). Acquired multidrug resistance is the ability of cells to develop resistance, after having been directly exposed, to drugs and their analogues (de Lange, 2004). The challenges faced are compounded by vast categories of substrates for the ABC transporters, most specifically P-gp transporters (Sanchez-Covarrubias *et al*, 2014), including chemotherapeutics, antibiotics, antiepileptics, antidepressants and HIV-1 protease inhibitors (Mahringer and Fricker, 2016).

The expression signatures of these transporters are also dependent upon CNS pathogenesis, for example overexpression of transporters P-gp, Bcrp, Mrp1 and Mrp 2 is observed with epilepsy, in AD and PD P-gp expression is downregulated (Mahinger *et al*, 2011) whilst overexpression of P-gp has been implicated in multidrug resistance of cancers such as glioblastomas (Haar *et al*, 2012; Miller, 2015; Qosa *et al*, 2015). Down regulation of P-gp and Brcp transporters, exporters of beta-amyloid plagues, is thought to facilitate the accumulation these neurotoxic proteins observed in AD (Mahinger *et al*, 2011). Whilst overexpression of ABC transporters on tumour cells is believed to reduce the accumulation and hence efficacy of therapeutics through extrusion (Wijaya, Fukuda and Schuetz, 2017). Both *in vivo* and *in vitro* studies have demonstrated an overexpression in ABC transporters correlating to higher resistance of chemotherapeutics including, but not limited to, etoposide (Nakai *et al*, 2009), a topoisomerase inhibitor, and alkylating agents carmustin and temozolomide (Goldwirt *et al*, 2014).

1.6 Circumventing the BBB

Due to the protective mechanisms of the BBB, drug delivery is intrinsically challenging. There are only a small number of drugs that are able to cross the BBB that treat diseases such as epilepsy, affective disorders and chronic pain (Ajay *et al*, 1999). Therefore, techniques have been developed in order to circumvent the BBB altogether.

In order to overcome the physiochemical characteristics and challenges of the BBB a drug delivery system must fulfil certain criteria, as mentioned previously (section 1.1 and 1.3), to deliver therapeutics to the target site. The key requirements for a successful drug delivery system have been suggested by Popov *et al* (2012) are

stability in blood, the ability to penetrate biological barriers and to demonstrate site specificity for target organs. Further requirements include the reduction of side effects, biocompatibility, retention of biological functionality and biodistribution (De Jong and Borm, 2008; Nagpal *et al*, 2013).

A number of techniques have been used in order to circumvent the BBB or improve the delivery of drug across the BBB. One such example of the latter, is to increase the lipophilicity of the drug (Pardridge, 2003; Lu *et al*, 2014). Whilst this can lead to increased membrane permeation, this permeation will be non-specific potentially leading to unwanted toxic effects (Pardridge, 2003; Manallack, 2007; Nagpal *et al*, 2013). This further results in non-target specificity and uptake which in turn influences both the pKa and pharmacokinetics, ultimately altering the concentration of drug available for delivery to the brain (Pardridge, 2003; Manallack, 2007). Increasing the lipophilicity of the therapeutic may also increase the molecular weight which can in turn restrict the drug from traversing the BBB (Pardridge, 2003). Therefore, rather than altering the drug, further techniques have focused on circumventing the BBB for drug delivery.

1.6.1 Trans-cranial drug delivery

Trans-cranial drug delivery involves the use of invasive techniques designed to bypass the BBB (Gabathuler, 2010; Vogelbaum and Aghi, 2015). They include: intracerebroventricular (ICV) delivery, intracerebral implantation and convection enhanced diffusion (CED) (Pardridge, 2005; Vykhodtseva *et al*, 2008; Cohen-Pfeffer et al, 2017). ICV consists of a reservoir of drugs implanted under the scalp connected to a catheter delivering therapeutics to the cerebrospinal fluid of the ventricles (Temsamani *et al*, 2000; Pathan *et al*, 2009). Intracerebral implantation involves the delivery of therapeutics using controlled-release polymer implants (Brem *et al*, 1991; Fung *et al*, 1996). As these methods rely on diffusion across the brain, the concentration of the therapeutic from the site of administration to the brain parenchyma is seriously limited (Pardridge, 2005; Vykhodtseva *et al*, 2008). A further limiting factor may be a result of the initial steep drug concentration locally, potentially leading to toxicity to the surface of the brain (Pardridge, 2016).

Convection enhanced diffusion is an alternative transcranial technique. Fluid containing a therapeutic is delivered, using a continuous pressure gradient, via a

catheter to the brain parenchyma (Bobo *et al*, 1994; Kunwar *et al*, 2010; Vogelbaum and Aghi, 2015). In studies in mice, the forced infusate demonstrated a preferential flow along white matter tracks, which appears to be linked to astrogliosis (Ai *et al*, 2003; Voges *et al*, 2003; Pardridge, 2005). This demonstrates the limitations and potential concerns with such methods for humans.

1.6.2 Trans-nasal delivery

There are a number of therapies using the nasal route as a technique to circumvent the BBB using devices such as nebulisers and atomisers (Suman *et al*, 1999; Moller *et al*, 2011; Djupesland, 2013a), nanocarriers, examples include nanoparticles and nanogels (Khan *et al*, 2017) and further strategies including vasoconstriction and mucoadhesion (Perez *et al*, 2012). The rationale of trans-nasal delivery involves the delivery of the drug from the submucosal space to the arachnoid membrane, to enter the olfactory cerebral spinal fluid (CSF) and thus the BBB (Pardridge, 2005). However, it appears there are several factors preventing these events occurring (Pardridge, 2005). Due to the rapid clearance of CSF, drugs delivered to this locale, regardless of route of entry, will swiftly be removed and enter the peripheral bloodstream, and this is observed with ICV (section 1.6.1) (Pardridge, 2005). However, it has been suggested that delivery may occur via the trigeminal nerves, potentially bypassing the CSF (Liu *et al*, 2011; Djupesland *et al*, 2013b; Sisa *et al*, 2019). Nonetheless, the arachnoid membranes, one of the three layers of the meninges involved in protecting the brain, consist of TJ's similarly restrictive and preventative as the BECs (Kristensson and Olsson, 1971). Further limitations include restricted volume of administration of drugs, low permeability of hydrophilic drugs and short retention time influencing drug absorption (Wu *et al*, 2008; Lochhead and Thorne, 2012; Erdő *et al*, 2018). Anatomically, the olfactory region for rodents (50% of the nasal mucosa) and human (3-5% of the nasal mucosa) differs such that detection is difficult to track in CSF of humans (Graff and Pollack, 2004; Westin *et al*, 2005; Pardridge, 2012).

1.6.3 Cerebrospinal fluid vs blood-brain barrier delivery

Drug delivery to the brain is a complex process due to the barrier produced by the BBB. CSF has been used an alternative to overcome this barrier (Rediz, 2011; Pardridge, 2012 and 2016). Drugs can be injected directly into the CSF; however,

penetration of the brain parenchyma is limited by diffusion (Pardridge, 2016). Therefore, it is a perceived misconception to measure drug concentration from the lumbar puncture (CSF) as an indicator of drug concentration of the brain interstitial fluid (ISF) (Pardridge, 2012 and 2016; Rizk *et al*, 2017). The BBB and blood cerebrospinal fluid barrier (BCSFB) are functionally and physiologically diverse (Pardridge, 2012; Rizk *et al*, 2017). The BBB is the interface of the vascular system and the CNS, and the BCSFB is the interface of the vascular system and CSF (Pardridge, 2012). The BCSFB comprises epithelial cells lining the choroid plexus (Pardridge, 2012). Anatomically, the BCSFB has a higher expression of pinocytotic vesicles, which includes clathrin-mediated, caveolae-mediated and macropinocytotic vesicles (Coomber and Stewart, 1986; Strazielle and Ghersi-Egea, 2013). However, this difference also appears to influence the functionality of the barrier indicating a site of high endocytic activity (Strazielle and Ghersi-Egea, 2013).

The CSF compartment is separated from the blood by the choroid plexus (Pardridge, 2017). The primary role of the BCSFB is to secrete cerebrospinal fluid from the cerebral epithelial cells of the choroid plexus (Redzic, 2011). Delivery and exchange of molecules between the cerebrospinal fluid and interstitial fluid, the fluid that surrounds the brain parenchyma, are dependent upon similar factors governing the BBB such as size and lipophilicity, presence of receptors and concentration gradients (Abbott *et al*, 2018). Therapeutics injected to the CSF in fact preferentially distribute to the blood rather than the brain (Pardridge, 2016). The surface area of the BBB and the number of capillary supplying and distributing blood within the brain parenchyma is considerably greater, 130-fold and 10-fold respectively, than that of the choroid plexus, thus influencing the potential uptake and concentration of drugs the brain is exposed to (Pardridge, 2016). This work demonstrates that this method is an unsuitable alternative.

1.6.4 BBB Disruption

BBB disruption has been used to circumvent the BBB. It is the physical disruption of the BBB to allow for paracellular entry. Methods include chemical disruption and ultrasound (Khan *et al*, 2017). One of the earliest chemical disruption techniques, osmotic shock, employed the injection of a hypertonic solution, mannitol, to

instigate cell shrinkage leading to opening of the tight junctions (Neuwelt *et al*, 1979; Brasnjevic *et al* 2009). However, disruption to the BBB does not discriminate which molecules can access the brain, and allows entry to potentially toxic plasma proteins, such as albumin (Guo *et al*, 2012).

The use of focused ultrasound to transiently disrupt the BBB to improve drug delivery is another technique employed in order to circumvent the BBB (Hynynen et al, 2003; Kobus et al, 2016; Aryal et al, 2017). Janowicz et al (2019) used focused ultrasound to deliver AD antibody therapeutics in mice. There was no difference in uptake from the site of sonication or the whole brain. As a result of the appearance of skull distortions, this technique has been modified to improve the specificity with the introduction of intravenously injected microbubbles to allow for the use of a lower frequency, due to the oscillation of the microbubbles (Hynynen et al, 2006; Liu et al, 2016). Goutal et al (2018) demonstrated that disruption of the brain did not influence the delivery of erlotinib (an ATP inhibitor). Therefore, suggesting that further research is required to ensure the efficacy of delivery of specific therapeutics using this technique, and that there are no long-term health risks through the disruption of the BBB (Mäger et al, 2016).

1.6.5 'Trojan Horses' for endogenous transport systems

Although the expression of specific receptors is lower for the BBB than other tissues, there are a number of receptors found that are overexpressed, such as the transferrin receptor, insulin receptor and low-density lipoprotein receptor (Guo *et al*, 2012; Gao, 2016). As a result, endogenous transporters have been targeted as a potential drug delivery system, more specifically the transferrin receptor (TfR) has been the most widely targeted (Gao, 2016; Pardridge, 2006 and 2017). Trojan horse technology has been modified to investigate delivery of therapeutics across the BBB by 'piggy backing' the endogenous receptor. The Trojan horse is a receptor specific monoclonal antibody (mAb) designed to bind to the endogenous receptor, then penetrate the BBB with a fused therapeutic peptide (Pardridge, 2006 and 2017). Despite the specificity of ligands to the receptor, it has been reported that the antibody binds to a region separate to the endogenous ligand rather than competing (Skarlatos, Yoshikawa and Pardridge, 1995). A further limitation is that

such receptors are located systemically indicating the possibility of non-brain specific uptake.

1.6.6 Prodrugs

A prodrug is a therapeutic that in its native state is biologically inactive. However, on arrival at the target site is activated. An example of a prodrug is levodopa (L-DOPA), the precursor to dopamine, and the therapeutic used for the treatment of Parkinson's disease (PD). Due to its structure, L-DOPA has a high affinity for a carrier mediated transporter (CMT) the large amino acid transporter 1 receptor (LAT1). Once L-DOPA is delivered to the brain, it is decarboxylated by the enzyme dopamine decarboxylase converting it from L-DOPA to dopamine (Pardridge, 2006). Another example is Temozolomide (TMZ) an alkylating chemotherapeutic in the treatment of glioblastomas (Zhang *et al*, 2012). Once taken up, it is rapidly metabolised to the active form involved in methylation of purine bases of DNA (5-aminoimidazole-4-carboxamide or AIC) (Zhang *et al*, 2012). Whilst these treatments can cross the BBB, there are specific drawbacks. L-DOPA is non-specifically metabolised throughout the body leading to a number of side effects. Whereas the specific obstacle surrounding TMZ is chemoresistance, observed in some glioblastomas overexpressing protein methylguanine methyltransferase (MGMT).

1.6.7 Liposomes

Liposomes are colloidal drug carriers. They are bilayered vesicles carrying their payload within the lumen of the vesicle (Lian and Ho, 2001). The composition of the liposome membrane contains biocompatible materials, such as cholesterol, designed to improve its stability and capacity to cross biological barriers including the BBB (Brasnjevic *et al*, 2009; Kabanov and Batrakova, 2017). The formulation and composition of the bilayer will determine the size of the liposome from nanometres to micrometres (Sharma and Sharma, 1997; Lian and Ho, 2001; Kabanov and Batrakova, 2017). There are numerous benefits to encapsulating a therapeutic within a colloidal drug carrier as they can reduce the potential for adverse side effects and protect against enzymatic interactions with the drug, potentially improving bioavailability (Brasnjevic *et al*, 2009; Kabanov and Batrakova, 2017). However, liposomes are rapidly removed from cells by efflux

pumps (Tamai and Tsuji, 2000; Kabanov and Batrakova, 2017) and have a relatively low encapsulation capacity (Grinberg *et al*, 2010). Liposomes have also demonstrated aggregation in plasma hampering their delivery (Ishida *et al*, 2002; Zhang *et al*, 2016). Cationic liposomes have a rapid clearance in tissues such as lung, spleen and liver (Thurston *et al*, 1998).

1.6.8 Exosomes

Exosomes are extracellular vesicles that originate from endosomes (Alvarez-Erviti *et al*, 2011). They are produced from intraluminal vesicles formed in multivesicular bodies of late sorting endosomes that are transported to the plasma membrane for exocytosis (Kallumi and LeBleu, 2020). They are endogenous vesicles of approximately 40-160 nm in size encapsulating a range of constituents from RNA to proteins (Alvarez-Erviti *et al*, 2011; Kallumi and LeBleu, 2020). They can be engineered to deliver a range of therapeutics including siRNAs (Alvarez-Erviti *et al*, 2011), and can also be synthesised to mimic the characteristics of endogenous exosomes (Jang *et al*, 2013; Oh *et al*, 2015). For example, exosomes have been engineered to express the rabies virus glycoprotein (RVG), to target neurons and glial cells, in order to deliver siRNAs specific to BACE1, a protease that cleaves the amyloid precursor protein (APP) involved in the aggregation of β-amyloid protein, resulting in knockdown of this gene (Alvarez-Erviti *et al*, 2011). However, there are a number of limitations to the therapeutic use of exosomes, including difficulties in endosomal isolation and purification as well as their heterogenous sizes (Furi *et al*, 2017; Li *et al*, 2019). Moreover, the use of endogenous exosomes is limited by differential shape, cargo and production efficiency by differing cell types (Mentkowski *et al*, 2018; Li *et al*, 2018).

1.6.9 Bolaaamphiphiles

Bolaamphiphilic (BA) compounds are molecules with either one or two long alkyl carbon chains, or, in some instances, macrocyclins such as porphyrins or steroids connected by hydrophilic head groups (Escamilla and Newkome, 1994; Fuhrhop and Fritsch, 1986; Fuhrhop and Wang, 2004). However, for this thesis the focus is on BAs comprised of a carbon chain with polar head groups. The word ‘bola’ originates from South America relating to a missile weapon consisting of two ball shaped heads connected by a cord (Fuhrhop and Fritsch, 1986). In 1951, the term

‘bolaform electrolyte’ was used to describe a hydrophobic chain connected to ionic headgroups at either end (Fuoss and Edelson, 1951; Fuhrhop and Fritsch, 1986).

1.6.9.1 Structure of bolaamphiphiles

Synthetic BAs are based on monolayered lipid membranes produced by archaea (Fuhrhop and Fritsch, 1986). BAs produced from archaea are difficult to isolate, as a result their architecture has been reproduced (Grinberg *et al*, 2010). However, rather than the characteristic ether bonds designed to enable archaea to inhabit highly acid environments, synthetic BAs are formed by ester bonds (Fuhrhop and Fritsch, 1986; Fariya *et al*, 2014). Synthetic BAs are composed of one or two hydrophobic chains connected by two hydrophilic head groups (Han *et al*, 2004). There are a number of potential combinations of head groups or moieties for BAs as they do not need to be identical nor polar (Fuhrhop and Fritsch, 1986; Han *et al*, 2004). The head groups can compose of different moieties to form asymmetric or symmetric compounds (Fuhrhop and Fritsch, 1986; Han *et al*, 2004; Nuraje *et al*, 2013). They can form numerous different structures based on the length of the hydrophobic portion and presence of a moiety, such as nanotubules (Fuhrhop *et al*, 1993; Shimizu *et al*, 2005), nanorods (Fuhrhop *et al*, 1993; Shimizu *et al*, 2005), ribbons (Shimizu and Masuda, 1997), spherical vesicles (Grinberg *et al*, 2010), cylindrical vesicles (Fuhrhop and Wang, 2004; Shimizu *et al*, 2005; Singh *et al*, 2018), helices (Shimizu and Masuda, 1997) and fibrous structures (Franceschi *et al*, 2000, Grinberg *et al*, 2010). Fariya *et al* (2014) reported that condensation and substitution reactions are utilised in the production of BAs composed of α,ω-diols, -diamines, -dihalides and dicarboxylates.

Theoretically, BAs encapsulate a higher volume by default as the lumen volume should be greater than that of a bilayered vesicle of the same size (Puri *et al*, 2009). They are deemed more stable due to the transmembrane configuration of the membrane protecting from delamination (Puri *et al*, 2009; Singh *et al*, 2018). By virtue of the monolayer lipid membrane, BAs are less likely to fuse with lipid membranes, referred to as lipid exchange, as well as themselves than bilayered vesicles (Puri *et al*, 2009). As a result, they exhibit the potential to cross the biological barrier intact (Puri *et al*, 2009).

Vernonia oil, obtained from *Vernonia galamensis* has been utilised as a suitable oil to synthesise BA molecules with a range of different head groups (Grinberg *et al*, 2008; Grinberg *et al*, 2010). BAs can form a mono-layered membrane in the form of a raft when in aqueous/polar solutions. When disrupted by ultrasound the raft forms vesicles encapsulating molecules present in the aqueous solution. They are similar to liposomes, mentioned previously (section 1.6.7), as they form vesicles encapsulating cargo in the lumen (Popov *et al*, 2010). They are biocompatible and certain BA derivatives with choline head groups have been suggested to cross the BBB (Dakwar *et al*, 2012; Popov *et al*, 2012 and 2013). However, unlike liposomes, BA form monolayered vesicles, increasing their potential encapsulation capacity (Puri *et al*, 2009; Popov *et al*, 2010). This is also advantageous as there is less lipid-lipid exchange between biological membranes and the vesicles in comparison to liposomes with their bilayer membrane, with the potential to retain both their structure and cargo (Puri *et al*, 2009; Popov *et al*, 2010). They are reportedly more stable than liposomes (Grinberg *et al*, 2010). As BA vesicles encapsulate their cargo, they can increase the bioavailability, and reduce adverse side effects if they can be made to target particular sites (Zhang *et al*, 2015).

1.6.9.2 Applications of bolaamphiphiles

BAs have been used for a number of applications such as gene delivery (Gupta *et al*, 2015), electronics and drug delivery (Nuraje *et al*, 2013). BAs, synthesised from jojoba oil, have been investigated for the delivery of siRNAs due to the electrostatic interactions between the cationic headgroups and anionic properties of the siRNA (Gupta *et al*, 2015).

BAs have the potential to be used as a brain drug delivery system. Popov *et al*, (2012) suggested that using an acetylcholine ester group would be hydrolysed by the presence of CNS derived acetylcholine esterase (AChE) preventing their egress. Dakwar *et al* (2012) showed in mice that vesicles made from such BAs when loaded with fluorescein isothiocyanate (FITC)-labelled BSA, delivered intravenously, penetrate all major organs. In the presence of the peripherally- acting AChE inhibitor, pyridostigimine, vesicle stability increased and significant levels of labelled BSA were found in the brain. As pyridostigimine is licensed for the treatment of myasthenia gravis (Maggi and Mantegazza, 2011) it is proposed that

it will be safe for adjunct therapy. These vesicles were subsequently reported to have been used to successfully treat brain HIV infections with encapsulated drugs normally excluded by the BBB, however, a full report of this study has not yet been published (Heldman *et al.,* 2014). A further property of positively charged BAs is their ability to bind siRNA on their surface. Studies have been reported showing their successful delivery of siRNA, bound on the vesicle exterior, to neuroblastomas (Kim *et al*, 2013 and 2020).

The precise mechanism whereby this group of BA vesicles can cross the BBB has not been demonstrated. It has been hypothesised on the basis of limited data to occur through transcytosis (Fenhart *et al*, 1999, Dakwar *et al*, 2012). It is not clear if the acetylcholine head group is required for uptake or if some character of the backbone fatty acid chain derived from vernonia oil imparts this capability. It is clear that their stability in whole serum is limited (approximately two hours) and that pyridostigimine more than doubles this (to five hours). The question arises as to whether BA vesicles could be an effective delivery system for glioblastomas. Chemotherapeutics, such as etoposide, have difficulty crossing the BBB (Bart *et al*, 2000). A study demonstrating the use of folic acid and lactoferrin tagged poly(lactide-co-glycolide) (PLGA) nanoparticles encapsulating etoposide for treatment of glioblastomas appeared to target tumours though compromised the viability of the BBB (Kuo and Chen, 2015). Using brain penetrating BA vesicles encapsulating cytotoxic drugs such as etoposide could be an effective method to deliver to glioblastomas.

1.7 Hypothesis and aims

BAs produced from vernonia oil can be used as a suitable drug delivery system to treat diseases of the brain.

The overall aim of the project is to develop a robust methodology in order to produce stable BA vesicles to ultimately cross the BBB and delivery therapeutics to the brain to be used as an effective drug delivery system to treat diseases of the brain.

In order to test the hypothesis and reach the overall aim there are several criteria and objectives to ensure the drug delivery system is suitable. Therefore, the main

objectives will be to test the physicochemical properties of the vesicles. The system will need to be profiled for size, charge/stability, and encapsulation efficiency, as well as to test the ability of the vesicles to encapsulate various tracer dyes, molecules and drugs (Chapter 2). Secondly, it is important to investigate the potential toxic effects of BA vesicles and to determine whether they are taken up by both brain cell types and cells representative of putative clearance pathways, studies that will be further supported by analysis of vesicle uptake *in vivo* (Chapter 3). The final objective of this thesis is to produce a protocol to improve the overall yield of the BA material (Chapter 4).

CHAPTER 2

2.1 Challenges surrounding penetrating the blood-brain barrier

The lack of pharmaceuticals that can successfully penetrate the brain is one of the challenges faced in treating CNS disorders. The BBB protects the brain and maintains the homeostatic environment of the CNS, which is essential for healthy neuronal function (Daneman, 2015). It is a highly effective pharmacological, metabolic and physical barrier, and is the primary impediment for delivery of treatment for diseases of the brain. Therapeutic agents are restricted from crossing the BBB based on their lipid solubility, molecular size, the number of hydrogen bonds that can be formed and charge (Olanow *et al*., 1991; Garcia-Garcia *et al*, 2005; Banks and Greig, 2019). Large molecules are unable to penetrate the BBB due to the limited expression of receptors located on the brain endothelial cells (BECs). The tight junctions of the BECs also prevent paracellular entry of >98% of small molecules across the BBB to the brain (Pardridge, 2005; Pardridge, 2012, He *et al*, 2018). Chemotherapeutics, such as etoposide, are effectively ejected from BECs by the ABC transporters (Bart *et al*, 2000, Wang *et al*, 2019). Thus, developing a delivery system that is capable of delivering drugs to the brain whilst ensuring the integrity of the brain and the functions of the barrier are not compromised is a significant challenge.

The measurement of drug efficacy is the ability of the drug to reach the target site in its unbound state to elicit its response (Warren, 2018). Encapsulation of drugs in vesicles and nanoparticles may thus allow for greater delivery of a therapeutic to the target site, restricting non-specific interactions and allowing for more of the therapeutic to be delivered. This would reduce the potential for unwanted side effects, whilst increasing bioavailability. An example is the non-pegylated liposomal doxorubicin (NPLD), Myocet™, used to treat ovarian and breast cancer (Leonard *et al.*, 2009). Doxorubicin is an anthracycline, a cytotoxic drug which is also cardiotoxic (Von Hoff *et al*, 1979). Encapsulation of doxorubicin within the lumen of the liposome has been shown to reduce cardiotoxicity and improve delivery to highly vascularised sites, such as tumours (Leonard *et al.*, 2009). Bolaamphiphiles (BAs) may be used for similar applications, specifically to cross the BBB and deliver drugs to the brain.

2.1.1 Bolaamphiphiles as a vehicle for drug delivery

BA vesicles can encapsulate molecules, including therapeutic agents, present in the original solution in which they form rafts prior to ultrasound disruption (Popov *et al*, 2010). GLH-20 (figure 2.1), a cationic BA molecule with an acetylcholine head group, forms vesicles that apparently cross the BBB via transcytosis (Dakwar *et al*, 2012; Popov *et al*, 2012). GLH-20 vesicles are hydrolysed by acetylcholinesterase (AChE) (Popov *et al*, 2012) which is found in appreciable amounts in the brain, as well as throughout the periphery and (as pseudocholinesterase) in the blood, where it is responsible for terminating nerve transmission by cleaving the neurotransmitter acetylcholine into acetic acid and choline (Gjerløff *et al*, 2014; Watabe *et al*, 2014). In these studies on GLH-20, pyridostigmine was used to inhibit circulating cholinesterase lysing the vesicles (Popov *et al*, 2012; Dakwar *et al*, 2012).

BAs present several advantages over the liposome vesicles that have been used previously. Most notably, they are capable of forming monolayered vesicles (Popov *et al*, 2010), and are thus less likely to interact with the cell membrane and are therefore more likely to remain intact (Grinberg *et al*, 2008; Popov *et al*, 2010). Moreover, bolaamphiphile vesicles have the potential to encapsulate a higher payload than liposomes, with evidence suggesting that they may be able to encapsulate small proteins (Dakwar *et al*, 2012). Thus, they are likely to prove a significantly more efficient therapeutic delivery system.

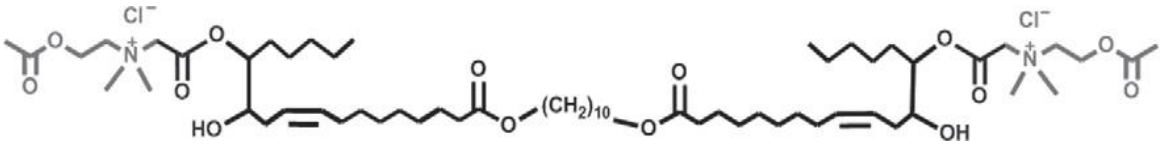

Figure 2.1. The molecular structure of bolaamphilphilic compound GLH-20. GLH-20 is synthesised from vernolic acid. The acetylcholine head groups of the bolaamphiphile enable the vesicles to be lysed by acetylcholinesterase.

2.1.1.1 Antibody fragments

New generation anti-cancer therapeutics have been designed linked to small chain variable fragments (scFv) that target them to specific antigen expressing cells (Flynn *et al*, 2016; Zammarchi *et al*., 2016). ADCT-502 is one such antibody drug conjugate (ADC) that targets HER-2 expressing tumours (Zammarchi *et al*, 2016). However, to effectively treat glioblastomas with such therapeutics, they must

access the brain. Whilst whole antibodies are large molecules and thus may be difficult to encapsulate, antibody fragments comprised of the variable heavy and variable light regions of the antibody, and containing the important antigen binding site, are smaller and may offer an alternative approach. The fragment scFv 4D5-8RFP (figure 2.2) is smaller than an antibody (52 kDa as opposed to 150 kDa, respectively), but retains the antigen binding characteristics (Markiv et al., 2011). scFv 4D5-8RFP is specific to human breast and ovarian cancer, binding to the HER2 protein, and is engineered to contain the red fluorescent protein to identify cells expressing HER2 (Eigenbrot *et al*, 1992; Markiv *et al*, 2011). To model the ability of BAs, to carry therapeutic proteins, including antibody fragments, across the BBB, scFv 4D5-8RFP has been selected.

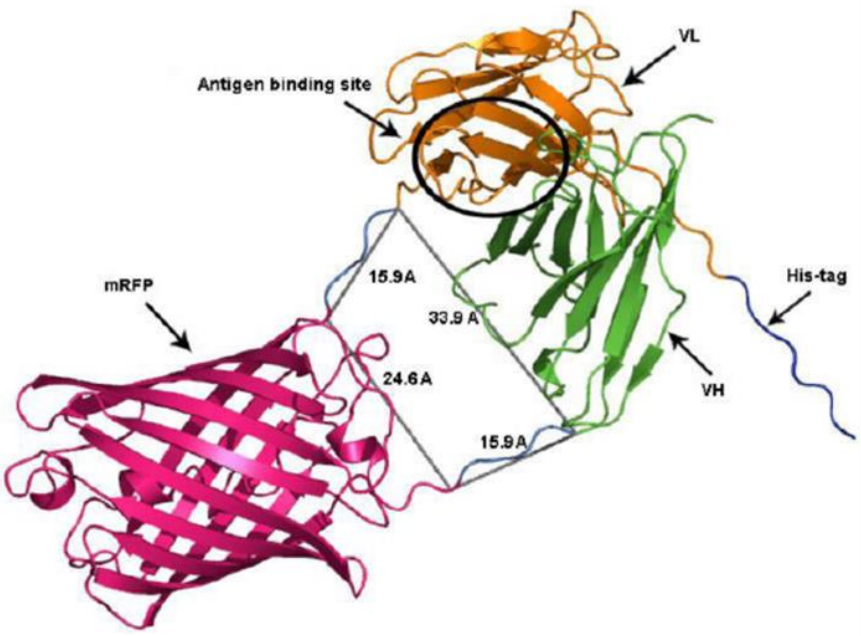

Figure 2.2. A 3D model of REDantibody molecule. The scFv 4D5-8RFP is comprised of variable heavy and light chains (green and yellow domains, respectively) attached through linkers to the red fluorescent protein domain (mRFP) [Reproduced with permission from Markiv *et al*, 2011].

2.2 Aims:

The overall objective is to investigate the capabilities of the BA vesicles as a drug delivery system *in vitro.*

1. To investigate the encapsulation of small molecules such as the dyes propidium iodide (PI), Alexa Flour 546 and larger molecules such as scFv 4D5-8RFP

2. To investigate the size and stability of these vesicles

3. To investigate the physical characteristics of the vesicles and their different cargoes

2.3 Methods

2.3.1 Materials- source of reagents

Table 2.1. The list of materials and their suppliers used throughout chapter 2.

MATERIALS	SUPPLIER	ADDRESS
Candida Antarctica lipase B (CALB) (Novozym 435) (catalog # 06-3123)	Strem Chemicals	Newtown, Cambridge, UK
uranyl acetate (catalog # AGR1260A)	Agar Scientific	Stanstead, Essex, UK
DMEM (catalog # BE12-614F), PBS (catalog # BE17-516F), Trypsin/EDTA (catalog # CC-5012), penicillin/streptomycin (catalog # 09-757F),	Lonza	Slough, UK
EtOH (catalog # 20821.330DP)	VWR Chemicals	Leicestershire, UK
Cholesterol (catalog # C8667), cholesteryl hemisuccinate (catalog # C6512), glycerol (catalog # G5516), Brilliant Blue R (catalog # S5130)	Sigma Aldrich	Irvine, UK
Fetal bovine serum heat inactivated (catalog # FB-1001H)	Biosera	East Sussex, UK
TEMED (catalog # 17919), acetic acid (catalog # 10384970), 1,10 decanediol (catalog # 10403515), petroleum ether (catalog # 42085.K7), ethyl acetate (catalog # 22912.K2), Pierce™ unstained protein MW marker (catalog # 26610), CellMask Plasma Membrane stain (catalog # C10046), DAPI (4',6-diamidino-2-phenylindole) (catalog # D1306), propidium iodide (catalog # BMS500PI),	Thermo Fisher Scientific	Loughborough, Leicestershire, UK

MATERIALS	SUPPLIER	ADDRESS
chloroform (catalog # C2432), methanol (catalog # 10675112		
Formaldehyde (catalog # 104003), sodium dodecyl sulphate (catalog # 817034), bromophenol blue (catalog # 108122), toluene (catalog # 108331), diethyl ether (catalog # 309966), chloroacetic acid (catalog # 800412), ampicillin (catalog # 171254), tetracycline (catalog # 58346), chloramphenicol (catalog # 220551), IPTG (catalog # 420322), imidazole (catalog # 104761), Triton X-100 (catalog # X100), mowiol (catalog # 475904) , Ni-NTA agarose resin (catalog # GE17-5268-01), sepharose CL-4B beads (catalog # CL4B200)	MERCK- Sigma Aldrich	Darmstadt, Germany
Alexa Fluor 546 (catalog # A10237)	Invitrogen	Renfrewshire Scotland
Acti-stain-488 phalliodin (catalog # PHDG1)	Cytoskeleton, Inc	Denver, USA
Tris (catalog # 60040), glycine (catalog # G36050), yeast extract (catalog # Y20025), NaCl (catalog # S23020), kanamycin (catalog # K22000), acrylamide (catalog # A11275), ammonium persulphate (catalog # A20500), tryptone (catalog # T60060), lysozyme (catalog # L38100), dithiothreitol (DTT) (catalog # D11000)	Melford	CheImsworth, Ipswich, UK
Anhydrous $MgSO_4$ (catalog # 33337.36)	Alfa Aesar-Fischer Scientific	Heysham, Lancashire, UK

2.3.2 Synthesis of bolaamphiphile GLH-20

A crude vernonia oil preparation was obtained from Arno Hugo (University of the Free State, Bloemfontein, South Africa). The general scheme for the synthesis is shown in figure 2.3. Synthesis of BAs was performed in collaboration with Dr Sumi Lee and Professor Lawrence Williams (Rutgers, USA) Grinberg *et al* (2008). The

addition of 1,10-decanediol and an immobilised *Candida antarctica* lipase B (CALB) (Novozym 435), as the catalyst, with toluene for 8 hours generated product 3. Toluene was dissolved in the mixture of product 3 with the addition of chloroacetic acid at 100 ^{o}C for 21 hours monitored by thin layered chromatography (TLC). Diethyl ether was added to the cooled mixture and washed, twice with 5% (w/v) sodium bicarbonate solution and four times with water. The final step was the addition of acetylcholine at 60 ^{o}C for 3 hours to produce the GLH-20 BA compound.

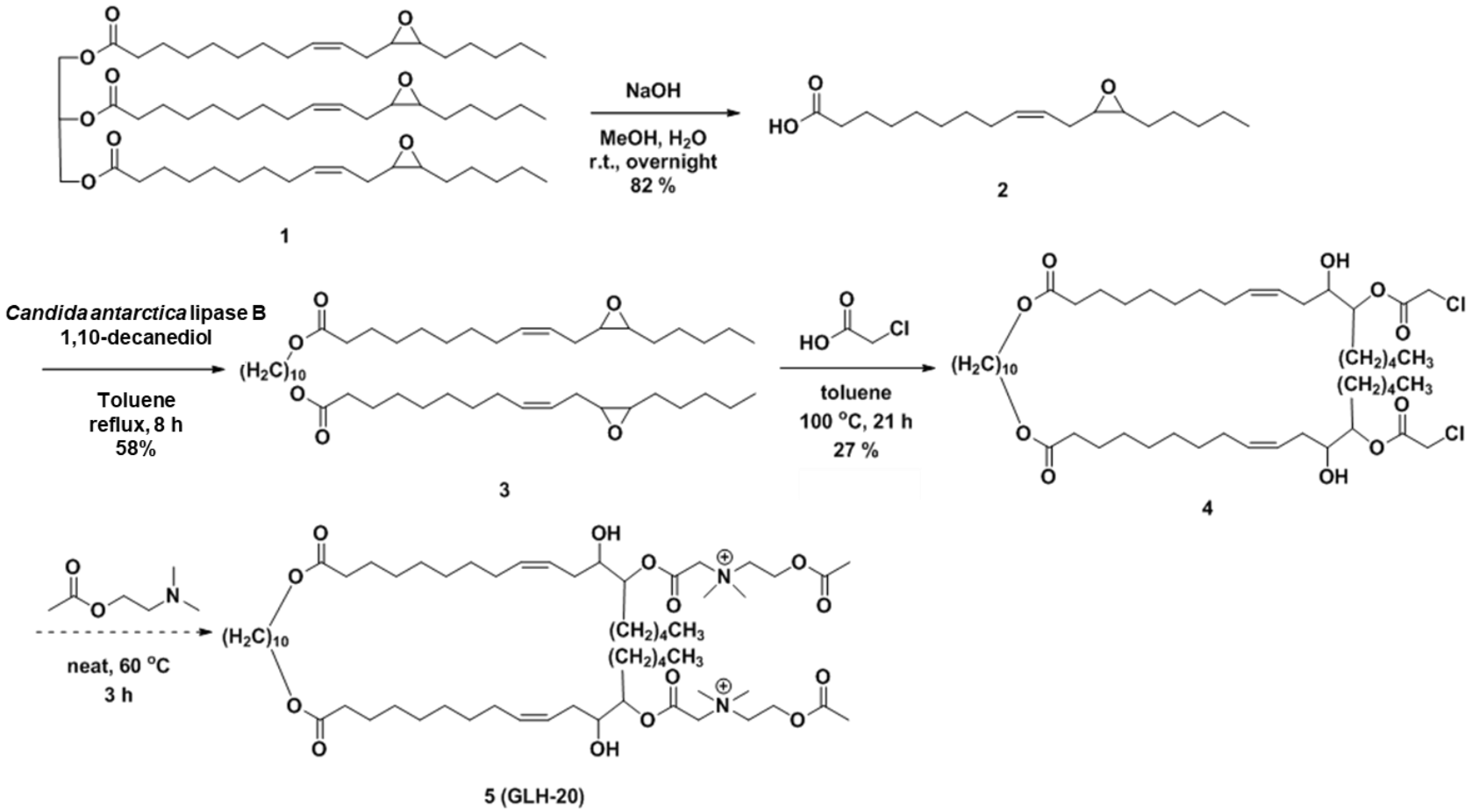

Figure 2.3 Schematic representation of the production of GLH-20 bolaamphiphile. There are four steps involved in the production of GLH-20 BAs. The first step is the hydrolysis of esters, followed by the coupling reaction in the presence of the catalyst *Candida antarctica* lipase B (Novozym 435). Step 3 involves the addition of chloroacetic acid. The final step is the addition of acetylcholine. The methods have been improved for stability and yield.

2.3.3 Protein expression and purification

Rosetta gami BL21-DE3 (kindly given by Dr Anatoliy Markiv), containing a plasmid expressing the red fluorescent protein 4D5-8RFP, were inoculated into lysogeny broth (LB - 10 g/l tryptone, 10 g/l yeast extract and 5 g/l sodium chloride) (Sezonov, Joseleau-Petit and D'Ari, 2007) containing 100 µg/ml ampicillin, 12.5 µg/ml tetracycline, 15 µg/ml kanamycin and 34 µg/ml chloramphenicol, then grown overnight at 37ºC with shaking. The overnight culture was diluted 1/100 into pre-warmed LB broth with antibiotics as above and incubated at 37ºC under agitation at 250 rpm until an optical density (595nm) of 0.5-0.8 was reached. Flasks were placed on ice for 30 minutes, after which 0.3 mM isopropyl β-D-1-thiogalactopyranoside (IPTG) was added and the culture was incubated for a further 20 hours at 20ºC under agitation at 250 rpm. Bacterial cells were then pelleted at 4800 x g for 20 minutes using a Heraeus Megafuge 40 centrifuge, then resuspended in Tris-Glycerol-NaCl (TGN) buffer (50 mM Tris, pH 7.5, 250 mM NaCl, 10% v/v glycerol) with 10 mM imidazole, approximately 25 ml per litre of original culture. These cells were stored at -80ºC.

To purify overexpressed protein frozen cells were defrosted in an ice/water bath. Lysozyme was added to 1 mg/ml final and incubated on ice for 30 minutes, followed by addition of Triton X-100 to 0.1% v/v final concentration with a further incubation on ice for 30 minutes. Lysed cells were then sonicated using a MS73 probe (Bandelin Sonopuls, Germany) for a minimum of 3 x 30 second bursts at 40% maximum amplitude in an ice-water bath. Cell debris and sheared DNA was removed by centrifugation at 25,000 x rpm using a Sorvall T-865 ultracentrifuge. Soluble protein was then incubated with Ni-NTA agarose resin (GE Healthcare, Sweden). Ni-NTA agarose beads were prepared by centrifuging for 1 minute at 1500 x rpm using a Universal 320R centrifuge before resuspending in TGN 10 mM imidazole buffer. Beads were washed twice more with this buffer before adding to the protein supernatant. The mixture was then agitated gently at 4ºC before beads were collected by centrifugation for 1 minute at 1000 x rpm using a Universal 320R centrifuge. Beads were resuspended in TGN with 10 mM imidazole, poured into a 25 ml chromatography column (Bio-Rad, Hertfordshire, UK) then washed with a minimum of 50 column volumes of TGN with 10 mM imidazole. Protein was eluted

with 5 column volumes of Tris 50 mM pH 7.5, glycerol 10% v/v, NaCl 100 mM and imidazole 250 mM.

2.3.4 Sodium dodecyl sulphate polyacrylamide gel electrophoresis (SDS-PAGE)

Equivalent volumes of protein samples and Laemmli buffer (4% w/v SDS, 20% v/v glycerol, 200 mM dithiothreitol (DTT), 0.01% w/v bromophenol blue and 0.1 M Tris HCl), were mixed and denatured by heating at 95°C for 10 minutes, to linearise the protein, and centrifuged at 13000 x g for 5 minutes using a Universal 320R Hettrich centrifuge prior to loading onto a 12% polyacrylamide gel (resolving gel - 0.375 M Tris, pH 8.8, 40% w/v polyacrylamide, polymerised by the addition of TEMED and 10% w/v ammonium persulphate in a 1:5 ratio: stacking gel -125 mM Tris, pH 6.8, 4-5% w/v polyacrylamide, again polymerised by the addition of a 1:5 ratio of TEMED and 10% w/v ammonium persulphate). Samples and molecular weight ladder (MW 116 - 14.4 kDa) (Thermo Fisher Scientific, UK) were then separated by electrophoresis at 180 V for 45 minutes in running buffer (250 mM Tris, pH 7.5, 1.92 M glycine, 1% w/v SDS).

Gels were stained with Coomassie Brilliant Blue (methanol 40% v/v, acetic acid 10% v/v, dH_2O and 0.25% w/v Brilliant Blue R) for 30 minutes on a shaker at 60 rpm and destained (in the same buffer omitting 0.25% Brilliant Blue R) for visualisation of protein separation.

2.3.5 Synthesis of vesicles

The compounds encapsulated were AF546 in PBS (final concentration 125 mM), propidium iodide in PBS (final concentration 125 µg/ml propidium iodide) and scFv 4D5-8RFP in PBS (final concentration 4.6 µM).

BA (10 mg/ml) was mixed with cholesterol (1.6 mg/ml), and cholesteryl hemisuccinate (CHEM) (2.1 mg/ml) and dissolved in chloroform. A rotary evaporator (Stuart®) under vacuum at 35^{o}C was used to remove the solvent. The BA mixture was rehydrated with 0.01 M PBS alone or the desired molecule (125 mM for AF546, 125 µg/ml propidium iodide, and 4.6 µM scFv 4D5-8RFP) in PBS or 10 mM NaCl and transferred to ice. The mixture was sonicated using an MS73 probe sonicator (Bandelin) for 12 mins at 40% amplitude, performing 15s pulses

and pausing for 10s (390 pulses in total). Vesicle size was measured using dynamic light scattering (DLS) (Section X). A Nanopartica Analyser SZ-100, (Horiba UK Ltd, UK) was used for profiling empty, propidium iodide, AF546 and scFv 4D5-8RFP encapsulated vesicles (see section 2.2.6). Vesicles were stored in 0.01 M PBS or 10 mM NaCl at 4^{o}C.

2.3.6 Vesicle purification

A 200 ml column of Sepharose CL-2B beads was prewashed with two volumes of vesicle buffer (0.01 M PBS or 10 mM NaCl) before addition of 500 µl of vesicle preparation; PBS was used for empty vesicles. Fractions were collected as 1 ml volumes with vesicle containing fractions located using DLS and confocal microscopy (see sections 2.3.7 and 2.3.13, respectively).

3.3.6 Dynamic Light Scattering

Dynamic light scattering (DLS) is a technique used to establish the physiochemical properties of a particle, such as the hydrodynamic diameter, also referred to as the z-average, and the polydispersity index (PDI) (ISO22412, 2017). DLS measures the random interactions of particles in suspension, also referred to as Brownian motion, when a laser is directed on the sample. This causes light to scatter as the particles randomly diffuse through a liquid. The size of the particles reflects the speed at which they interact. DLS measures the intensity of these random and temporal fluctuations of the light that is scattered from the particles in the sample.

Samples of either neat or purified vesicles were loaded into semi-micro disposable cuvettes diluted 1:10 in deionised water and particle sizes were measured using a Nanopartica Analyser SZ-100 (Horiba) with a range of 0.3 nm - 0.8 µm. A minimum of three measurements were taken of each sample. The dispersion medium viscosity is 0.895 mPa·s for the deionised water and PBS that the samples were measured in.

2.3.8 Electron microscopy

Diluted vesicle samples in 0.01 M PBS (1:100) were applied onto freshly glow-discharged (negatively) carbon-coated copper grids (300 mesh). The grids were negatively stained with 2% w/v uranyl acetate using the touching drop method (Rubinstein, 2007). Images were obtained using transmission electron microscope

(JEM-2100, JEOL) as part of the service provided by the Research Complex at Harwell, as part of the national MRC platform initiative.

2.3.9 Vesicle Stability

The zeta potential of the vesicles was measured monthly over a four-month period. Samples of either empty or AF546 encapsulated vesicles, that had yet to be purified by size exclusion chromatography, were injected into a capillary cell, alongside vesicle preparations diluted 1:10 in deionised water. Zeta potentials were measured using a Nanopartica Analyser SZ-100 (Horiba). Three readings were taken for each sample.

2.3.10 Autofluorescence spectra analysis

Preparations of 100 µl empty vesicles and PBS were examined in triplicate in a 96 well microplate (Nunc) using a CLARIOstar fluorescence plate reader (BMG Labtech) for a full spectrum scan.

2.3.11 Cell lines

Cell lines, neuroblastoma SH-SY5Y and LN229 glioblastoma (ATCC), used for vesicle uptake studies were chosen as representative of the cells of the brain during disease. SH-SY5Y is a model cell for Parkinson's disease. LN229 is a glioblastoma derived cell line. Cells were grown in Dulbecco's Minimum Essential Medium (DMEM) with 5% v/v foetal bovine serum (FBS, previously heat decomplemented by 30-minute incubation at 56˚C; Biosera Ltd., UK), 1% v/v penicillin and streptomycin. Cells were incubated at 37ºC for 3-4 days under 5% v/v CO_2 until 70% confluent.

2.3.12 Routine cell culture

All cell line work was performed in a laminar flow hood with aseptic technique. Cells were maintained in sterile 75 cm^2 flasks. Cells were passaged when they appeared 70% confluent. Spent media was removed and cells were washed with sterile 0.01 M PBS without Ca^{2+} for 5 minutes at 37ºC. PBS was removed and 0.25% w/v trypsin, 1 mM EDTA was added and cells were incubated for 5 minutes at 37ºC. Following dilution of trypsin with fresh medium containing 5% v/v FBS, cells were counted using a haemocytometer, centrifuged at 800 x g using an IEC CL30

centrifuge for 5 minutes, resuspended and re-plated for further growth or experimentation at 15,000 cells/cm^2 in appropriate medium.

Chamber slides were seeded with 1x10^5 SH-SY5Y or LN229 cells/cm^2 and cultured for 2-3 days. Cells were then incubated for 30 minutes, LN229, with final concentration of 3.5 µg/ml AF546 encapsulated vesicle in media prior to removal of spent medium, washing with PBS, fixing by immersion in 4% v/v formaldehyde in PBS for 10 minutes. SH-SY5Y cells were washed and counterstained for 1-hour incubation with 1:1000 dilution of CellMask™ Plasma Membrane stain (Thermo Fisher Scientific), to stain the plasma membrane. LN229 cells were washed and counterstained with phalloidin-acti-stain-488 (Cytoskeleton Inc) (1:140 dilution), for visualisation of the cytoskeleton, for 20 minutes. DAPI (final concentration 50 ng/ml), to define the nuclei, was used for 10 minutes. Chamber slides were then washed and mounted with Mowiol 4-88 (24% w/v glycerol, 9.6% w/v Mowiol, dH_2O, 0.2 M Tris, pH 8.5).

2.3.13 Confocal microscope

Confocal microscopy was used to determine the peak fractions of vesicles in unknown samples and in uptake studies. Following adjustment of gain and offset, cells and vesicles were imaged at 1024 x1024 resolution, using an oil immersion x63 objective on a Leica LSM880 laser scanning confocal microscope running Zen software. A minimum of 3 images were collected per well. Lasers used were 405 nm diode laser (for DAPI stain), 488 nm Argon-Krypton (for Phalliodin cytoplasmic staining), 561 nm diode (for AF546), and 633 nm HeNe (for the plasma membrane stain).

2.3.14 Encapsulation efficiency of bolaamphiphile vesicles

The encapsulation concentration is a quantitative indication of the efficiency of encapsulation of the delivery system. It is a measure of the amount of molecule incorporated in the delivery system which is defined as the percentage of molecule in the system (final concentration) relative to the initial concentration of molecule (Papadimitrious and Bikiaris, 2009). The encapsulation efficiency of the vesicles was calculated using following formula from equation 1:

$$encapsulation\ efficency\ (\%) = \frac{final\ concentration}{initial\ concentration} \times 100$$

The concentration of encapsulated AF546 was determined by comparison with a standard curve consisting of serial dilutions of AF546, range 0.1- 100 µM assayed by fluorescence spectrophotometry. Preparations of 100 µl vesicles or standards were examined in triplicate in a 96 well microplate (Nunc) using a CLARIOstar fluorescence plate reader (excitation filter 540-20 nm, emission filter 590-30 nm) (BMG Labtech). Linear regression analysis was performed using MARS Data Analysis Software (BMG Labtech). Fluorescence values for encapsulated vesicles were compared with linear regression results to determine the final concentration. A typical standard curve is presented in figure 2.4.

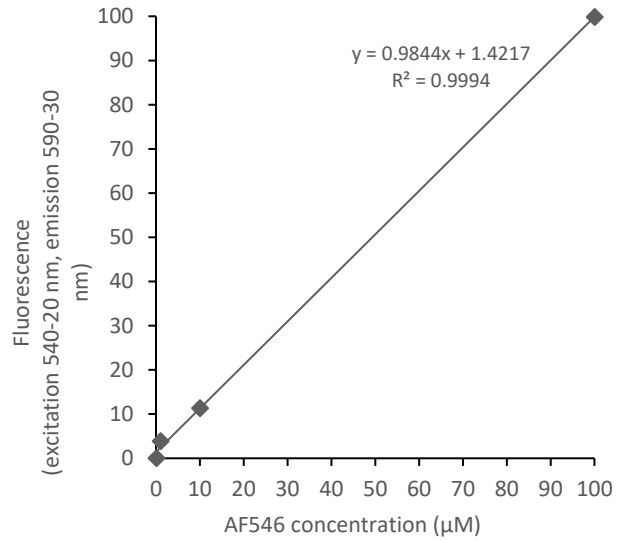

Figure 2.4 Standard curve of Alexa Fluor 546 concentrations. 0.1-100 µM of AF546 were assayed by fluorescent spectrophotometry (excitation 540-20 nm, emission 590-30 nm) to determine the concentration of AF546 encapsulated within vesicles. R^2=0.9994

2.3.15 Statistical Analysis

Results are expressed as mean ± standard error of mean (SEM). All statistical analysis was performed using SPSS (version 25). Data was analysed using one-way ANOVA test with post *hoc* analysis using Tukey's honest significant difference test. Values of $p \leq 0.05$ were considered significant.

2.4 Results

To investigate the capabilities of our BA vesicles as a drug delivery system *in vitro,* they were encapsulated with tracer dyes, including PI and AF546. To explore the ability to carry therapeutic proteins the BA vesicles were encapsulated with antibody fragment scFv 4D-8RFP, recombinantly expressed and purified from *E. coli*. *In vitro* work for PI and scFv 4D5-8RFP encapsulated vesicles is carried out in chapter 3.

2.4.1 Expression of scFv 4D5-8RFP

The antibody recognising the HER2 protein incorporating the red fluorescent protein, scFv 4D5-8RFP (figure 2.2) was produced in Rosetta gami (DE3) *E.coli*, purified using nickel affinity chromatography and analysed by SDS-PAGE (figure 2.5). The product obtained was consistent with that seen previously. The full length polypeptide species has a molecular weight of 52 kDa which was seen. In addition two major cleavage products were seen which is consistent with previous observations. Markiv *et al* (2011) reported frequent cleavage of either one side or other of the flexible, variable region as observed (figure 2.5). The purity of the full-length protein, 77%, was determined using Image J (Baker *et al*, 2019), by comparison with the molecular weight of the full length polypeptide. The cells expressing the protein were bright red. It was decided that the protein was sufficiently pure to be concentrated and for its encapsulation to be studied.

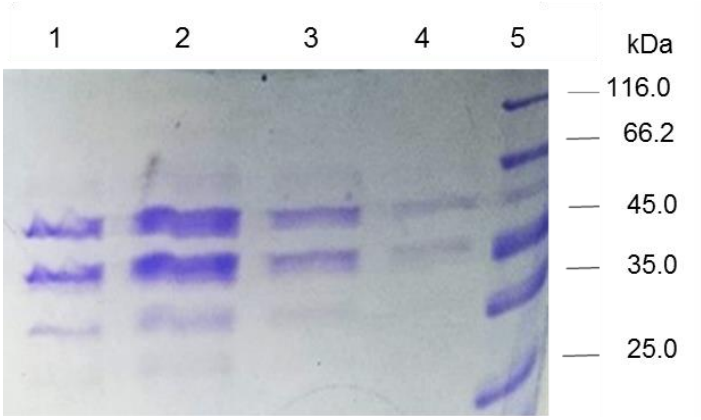

Figure 2.5. Purification of fluorescent scFv 4D5-8RFP. Recombinant 4D5-8RFP expressed in *E.coli*, was purified by Ni-NTA affinity chromatography resolved by 12% w/v SDS-PAGE and stained with Coomassie Brilliant Blue R250. Lanes 1-4: Ni-NTA column elutions lane 5: molecular weight markers, 116, 66.2, 45.0, 35.0, 25.0, 18.4 and 14.4 kDa.

2.4.2 Dynamic light scattering characterisation of empty, AlexaFluor 546, Propidium Iodide and scFv 4D5-8RFP encapsulated vesicles

The vesicles were synthesised with PBS (empty vesicles), AF546, PI or scFv 4D5-8RFP. The starting BA material obtained from Professor William's group (Rutgers) was combined with cholesterol and cholesteryl hemmisuccinate as described in section 2.4 (Grinberg *et al*, 2005). Their physical properties were characterised by DLS (table 2.2).

Table 2.2. Dynamic light scattering and polydispersity analysis measurements of empty vesicles, and vesicles encapsulating either Alexa Fluor 546, propidium iodide or antibody fragment scFv 4D5-8RFP (n=3).

Vesicles	Empty	Alexa Fluor 546	Propidium iodide	scFv 4D5-8RFP
Z-Average (nm) (mean ± SEM)	183.7 ± 1.3	183.5 ± 3.0	182 ± 2.1	307.3 ± 4.7
PDI (mean ± SEM)	0.3 ± 0.0	0.3 ± 0.0	0.3 ± 0.0	0.3 ± 0.0

Vesicles encapsulating scFv 4D5-8RFP are nearly 70% larger than empty or those encapsulating the tracer dyes, which were of remarkably uniform size. However, scFv 4D5-8RFP is a larger molecule at 52 kDa than AF546 (1080 Da) and PI (668 Da). PI and scFv 4D5-8RFP encapsulated vesicles have been physically characterised in this chapter, and further *in vitro* work has been undertaken in Chapter 3.

2.4.3 Electron microscopy

In order to verify and further characterise the size and the morphology of our BA vesicles, transmission electron microscopy (TEM) was used. Prior to purification by size exclusion chromatography, empty vesicles diluted 1:10 demonstrate particle sizes ranging from 100-190 nm consistent with DLS analysis (figure 2.6).

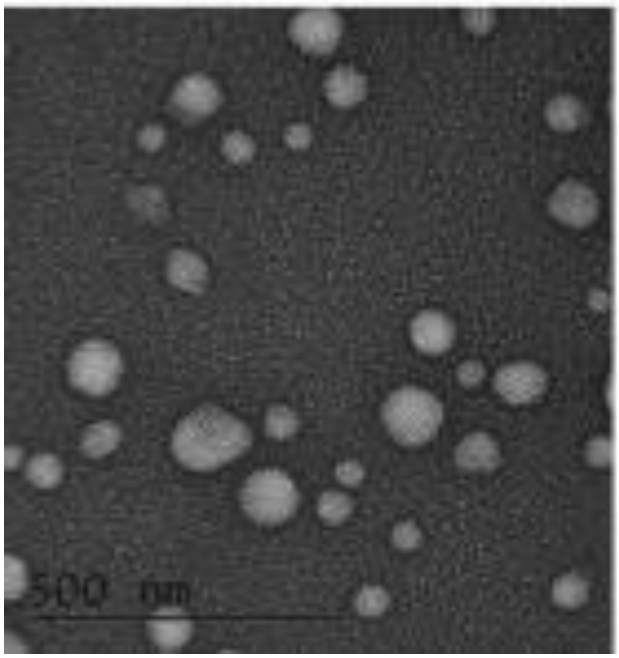

Figure 2.6. Electron microscope imaging of empty bolaamphiphilic vesicles. Vesicle size indicated by scale bar, mean size verified by dynamic light scattering (DLS) as 180 nm. Image taken on a JEM-2100 microscope at the Research Complex at Harwell.

2.4.4 Size exclusion chromatography for the purification of vesicles

Following encapsulation, vesicles were separated from non-encapsulated dye by size exclusion chromatography on a 200 ml Sepharose CL-2B column. Eluting fractions were profiled by DLS to identify the population of vesicles purified away from free dye. Free PI was observed visually between fractions 47 to 55. For the AF546 encapsulated vesicles, non-encapsulated/unbound dye was observed eluting in fractions 24-29. No colouration was observed for the antibody fragment vesicles by eye as was visible for the PI and AF546 encapsulated vesicles. Purified samples were verified by DLS measurements.

DLS was used to profile the purified vesicle fractions to determine the location of purified vesicles. From the DLS profile, AF546 encapsulated vesicles were found in fractions 8-14 (table 2.3). The profiles of F10 and F11 demonstrate low PDI, indicating a more monodispersed population, with size distributions similar to that of the neat vesicles, prior to purification. Therefore, both F10 and F11 were used in further experimental work. This distribution was also observed with the DLS profiles of the antibody fragment and PI fractions.

Table 2.3. Analysis of Alexa Fluor 546 vesicle fractions purified by CL-2B chromatography. The Z-average and polydispersity index (PDI) readings of purified fractions of AF546 encapsulated GLH-20 vesicles (n=3).

Fraction number	F8	F9	F10	F11	F12	F13	F14
Z-average (nm) (mean ± SEM)	771.5 ± 124.5	339.3 ± 288.5	184.0 ± 1.9	189.4 ± 1.8	249.9 ± 62.9	195.6 ± 3.6	203.7 ± 330.3
PDI (mean ± SEM)	0.6 ± 0.01	0.2 ± 0.1	0.2 ± 0.1	0.2 ± 0.2	0.3 ± 0.1	0.4 ± 0.1	0.4 ± 0.2

2.4.5 Zeta potential of vesicles

Zeta potential is a measure of the surface potential and can be used to assess stability and propensity for aggregation. If the effective charge is low, then the repulsion between the individual vesicles will similarly be low. A charge on vesicles between +10 mV and -10 mV is considered to be effectively neutral (Clogston and Patri, 2011). A surface potential in this range indicates that the vesicles have the potential to aggregate with time. The zeta potential of the various vesicles made was therefore analysed to give an indication of their stability (table 2.4).

Table 2.4. Zeta potential measurements of bolaamphiphilic vesicles. Empty vesicles or vesicles encapsulating AF546, PI or antibody fragment were shown to have negative zeta potentials and are therefore, anionic (n=3).

Vesicles	Empty	Alexa Fluor 546	Propidium iodide	scFv 4D5-8RFP
Zeta potential (mV) (± SEM)	-65.7 ± 1.4	-42.2 ± 0.6	-23.0 ± 1.6	-5.0 ± 1.2

All samples indicated that the electric repulsion was great enough that they are considered to be stable with the exception of the antibody fragment, scFV 4D5-8RFP, as the potential falls below the -10 mV to +10 mV range (Clogston and Patri, 2011). However, the charge was unexpectedly negative, which is inconsistent with the structure of GLH-20 which would possess a positive zeta potential. It is hypothesised that the original material was not GLH-20 and that an unexpected product had resulted during the production. This indicating a novel material. It was decided therefore to test the uptake of these vesicles to determine if the material still had properties capable of facilitating cellular delivery.

2.4.6 Preliminary in vitro work uptake of Alexa Fluor 546 encapsulated vesicles

To investigate the delivery capabilities of the BA vesicles, and whether they are able to penetrate biological barriers *in vitro,* studies were undertaken using a neuronal cell line representative of the brain. Newly synthesised AF546 vesicles, approximately 1 week since synthesis, were selected for AF546's photostability and strength of signal. Plasma membrane stain, CellMask, was used for staining the cell membrane. Uptake of AF546 encapsulated vesicles was assessed by confocal microscopy following a two-hour exposure. AF546 vesicle uptake can be seen as fluorescent yellow spots within the cells, suggesting that the vesicles are potentially still intact (figure 2.7). What is clear is that these negatively charged vesicles penetrate biological membranes.

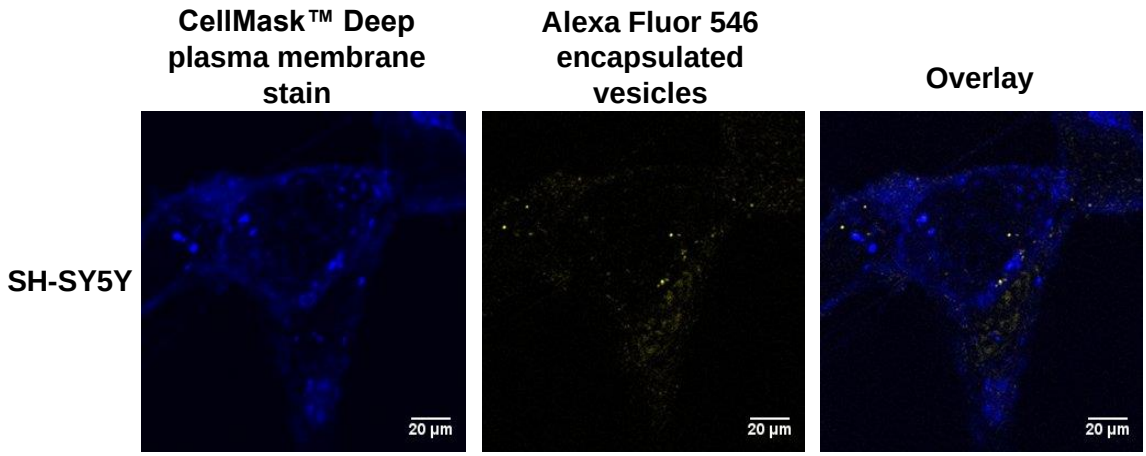

Figure 2.7. Uptake of Alexa Fluor 546 encapsulated vesicles in SH-SY5Y neuroblastoma cell line. Confocal microscopic image of SH-SY5Y cells incubated for 2 h with final concentration of 3.5 µg/ml of AF546 encapsulated vesicles at 37 ^{o}C in 5% CO_2 in air. Vesicles encapsulating AF546 (yellow) were counterstained with 1:1000 dilution of CellMask Deep plasma membrane marker (blue). Scale bar = 20 µm.

2.4.7 Long term stability of vesicles

The zeta potential of the vesicles is negative–demonstrating that the vesicles are negatively charged (table 2.4). To evaluate the stability of the purified AF546 vesicles, zeta potential measurements were taken over a four-month time course (table 2.5). Vesicles were stable for 3 months at 4^{o}C. Their potential drops by approximately 10% between months 2 and 3 and by 25% between months 2 and 4.

Table 2.5. Zeta potential measurements of Alexa Fluor 546 encapsulated vesicles over a four-month time frame (n=3).

Month	0	1	2	3*
Zeta potential (mV) (mean ± SEM)	-44.2 ± 0.6	-42.2 ±1.1	-37.3 ± 0.8	-33.4 ± 5.3

This zeta potential indicated the AF546 encapsulated vesicles were stable for 3 months at 4^{o}C. The decrease is zeta potential is significant (p=0.023) for the final reading against the initial reading using a one-way ANOVA whilst still remaining significantly above the stability limit defined by Clogston and Patri (2011).

2.4.8 In vitro work uptake of Alexa Fluor 546 encapsulated vesicles.

In order to investigate the uptake of purified AF546 vesicles by potential targets within the brain we used glioblastoma cell line, LN229, it is an ideal target to assess whether vesicles can enter relevant brain cells. Uptake of AF546 encapsulated vesicles assessed by confocal microscopy following a thirty-minute exposure, revealed vesicle uptake. There was possible vesicle lysis as AF546 can been seen in diffuse staining of the cytosol of the cells (figure 2.8) as opposed to the punctate staining in SH-SY5Y cells (figure 2.7). A greater fluorescence signal of AF546 is observed in the encapsulated vesicles compared to the control of free AF546.

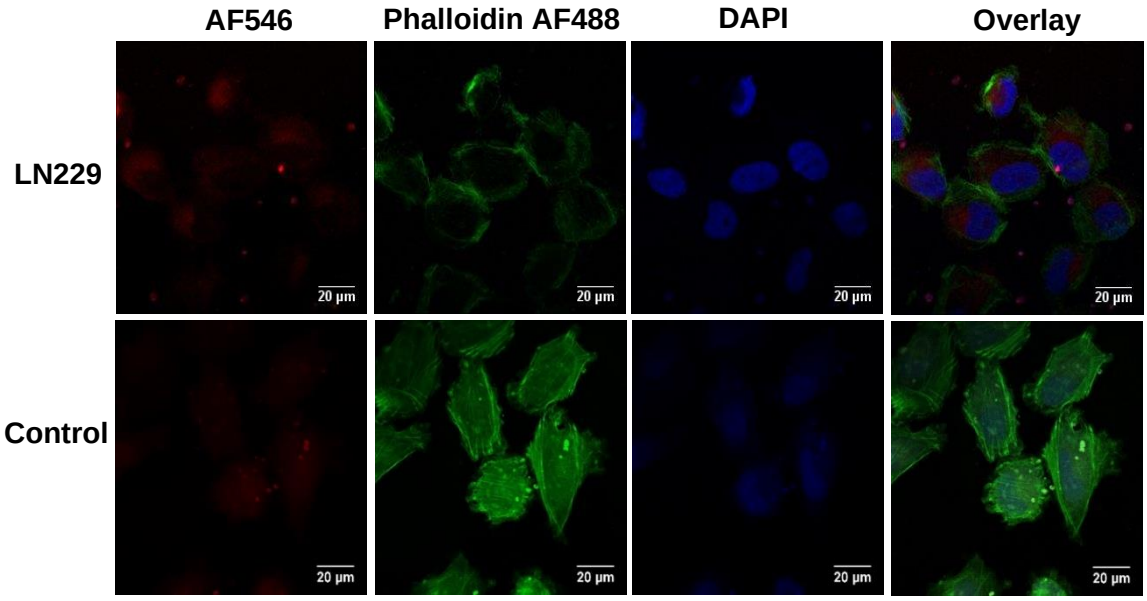

Figure 2.8. Confocal images of Alexa Fluor 546 encapsulated vesicle uptake, and non-encapsulated Alexa Fluor 546 (control), in the human glioblastoma cell line LN229. Cells were treated for 30 minutes with a final concentration of 3.5 µg/ml of purified AF546 (red) encapsulated vesicles, at 37°C in 5% v/v CO_2 in air, prior to counterstaining with 0.1 µM AF488-conjugated phalloidin (green), and 50 ng/ml DAPI (blue), fixation with 4% w/v formaldehyde and confocal microscopy. Staining of AF546 is apparent in the cytoplasm of the LN229 cells only. Scale bar = 20 µm.

As part of the *in vitro* work undertaken, and as AF546 is diluted in PBS prior to vesicle synthesis, the autofluorescence of the PBS was studied to ensure PBS does not autofluoresce, giving false readings. The fluorescence spectrum demonstrates that empty vesicles follow the same spectrum as PBS with lower fluorescence intensity (figure 2.9).

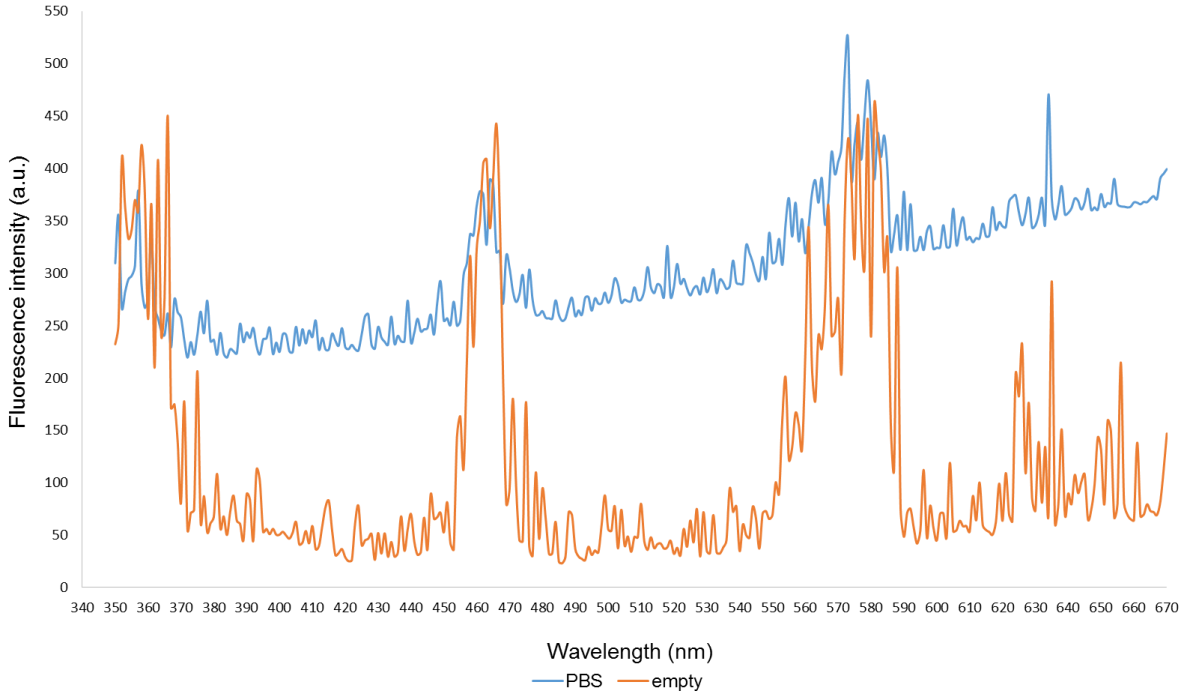

Figure 2.9. Autofluorescence spectra of PBS and empty vesicles using CLARIOstar fluorescent plate reader.

2.4.9 Linear regression analysis to determine the encapsulation efficiency and concentration of Alexa Fluor 546 and propidium iodide encapsulated vesicles.

To determine the concentration of AF546 from the purified fractions (figure 2.10) and hence, the encapsulation efficiency of the vesicles, fluorescence readings (AF546 excitation and emission spectrum is 556 and 573 nm, respectively and the filters used include excitation 540-20 nm, emission 590-30 nm) of the encapsulated AF546 vesicles was measured and compared against a standard curve derived from a dilution of the AF546 employed in these assays (figure 2.4). From the initial concentration of AF546 (125 mM) the highest concentration of Alexa Fluor after purification was measured at 18.72 ± 1.55 µM by a fluorescence plate reader (figure 2.10), allowing an encapsulation efficiency to be measured of 0.02% for the peak fraction (F11), using the equation presented in section 2.3.14.

Of the 7 purified fractions of AF546 encapsulated vesicles measured using a CLARIOstar fluorescence plate reader (figure 2.10) the total encapsulation efficiency of the preparation was calculated at 0.04%, using the same calculation as mentioned above. Although more fractions were measured, the plate reader could only detect a signal in the fractions recorded. This makes the assumption that there

is no quenching of the Alexa Fluor signal by the BA material. An absorption spectrum of empty BA vesicles across the range 340-670 nm revealed no apparent light absorption, consistent with this.

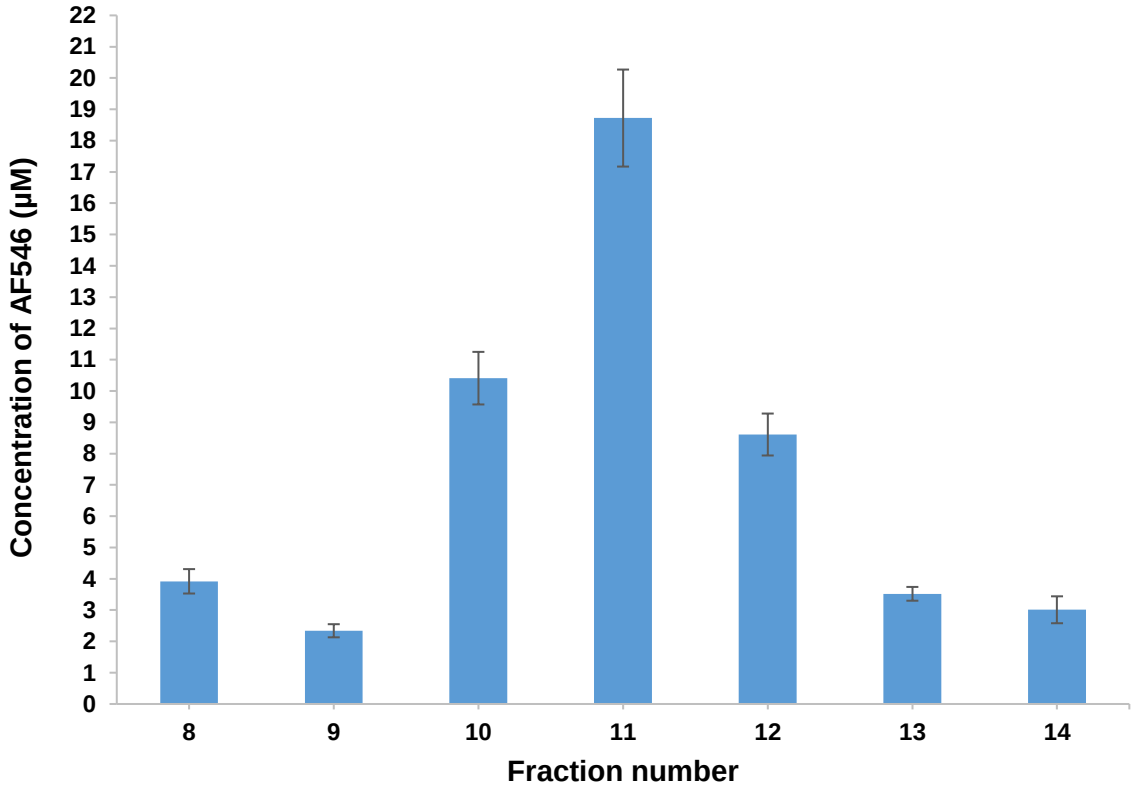

Figure 2.10. The encapsulation concentration of Alexa Fluor 546 encapsulated vesicles as calculated from the linear regression (Figure 2.4). Preparations of vesicles were examined using a CLARIOstar fluorescence plate reader (excitation filter 540-20 nm, emission filter 590-30 nm). From the measurements, fraction 11 of the purified vesicle population had the greatest concentration of AF546 (n=3).

2.5 Discussion

This study set out to manufacture vesicles from GLH-20 material applied by our collaborators. The material should have been the BA GLH-20 which has an acetylcholine head group giving the resulting BA and its derived vesicles a positive charge. The material produced vesicles of a size consistent with previous reports when combined with cholesterol and cholesterol hemi-succinate, however, the vesicles produced had a negative zeta potential. This investigation has revealed that this novel bola material was capable of forming vesicles encapsulating a number of dyes and an scFv fragment. Furthermore, the vesicles were capable of

penetrating neuronal cells *in vitro*. These vesicles retained a stable negative zeta potential over a period of four months at 4°C, attesting to good stability.

The original formulation of the GLH-20 vesicles, prepared Dr Sumi Lee and Professor Lawrence Williams (Rutgers), was deemed to have a low yield as compared to other studies synthesising vernonia oil vesicles (Popov *et al*, 2010). However, this was not problematic as this was a proof of concept study. The material was then being tested to establish if we could encapsulate a variety of payloads for delivery to neuronal cells and specific types of such cells, for example glioblastomas. Vesicles were produced to see whether it was possible to encapsulate a large molecule such as the scFV 4D5-8RFP antibody fragment. Vesicles were first encapsulated with tracer dye molecules such as AF546 and PI to study their consistency with previous work and their uptake by cells.

Dyes to encapsulate in vesicles were selected due to their specific properties and size. AF546 has a relatively low molecular weight (1080 Da), however it would not be expected to cross the BBB. It has a fluorescent intensity several fold brighter than that of Cy dyes, rhodamine or fluorescein with an increased photostability (Panchuk-Voloshina *et al*, 1999; Berlier *et al*, 2003) and is non-toxic. PI (0.668 kDa) is a nuclear stain excluded from living cells. scFv 4D5-8RFP was selected as a test molecule that would show if it was possible to deliver next generation drugs that can target specific cells whilst carrying chemotherapeutic payloads. The antibody (52 kDa) recognises human epidermal growth factor receptor 2 (HER2). Whilst HER2 is overexpressed primarily in breast and ovarian cancers, it has also been observed to be amplified in other cancers including glioblastomas (Yan *et al*, 2015). It was also included as a proof of principle in relation to the possible transport of scFv conjugated drug molecules across the BBB. Furthermore, scFv 4D5-8RFP expresses the red fluorescent protein, enabling imaging using either confocal or epifluorescent microscopy.

2.5.1 Characterisation of BA vesicles

There are a number of parameters to characterise for a drug delivery system, the two main parameters being size and shape/structure (Mourdikoudis, Pallares, and Thanh, 2018). It is necessary to standardise such techniques in order to maintain reproducibility and alignment for testing and characterising such systems

(Björnmalm, Faria, and Caruso, 2016; Mulverny *et al*, 2016; Gao and Lowry, 2018; Mourdikoudis, Pallares, and Thanh, 2018). Therefore, we have followed the techniques for characterisation that other studies have followed in the development of BA vesicles (Popov *et al*, 2010; Dakwar *et al*, 2012). We have used DLS, TEM and size exclusion chromatography in order to characterise our BA vesicles.

GLH-20 vesicles produced by Dakwar *et al* (2012), encapsulating bovine serum albumin conjugated to fluorescein isothiocyanate (BSA-FITC) were 203.8 ± 4.8 nm in comparison to their empty vesicles of 104.7 ± 2.5 nm. BSA is a larger molecule (66 kDa) than the scFv we employed (52 kDa). Similarly to the Dakwar study, the size of our scFv encapsulated vesicles was considerably larger than our empty vesicles. It might appear the larger the molecule the larger the size of the vesicle (Gdowski *et al*, 2015). This is true when comparing the neat, AF546 and PI encapsulated vesicles to the antibody fragment. Other factors that may influence the size of the vesicles in addition to the molecular weight of the encapsulated material include the concentration of the polymer material and surface tension (Abyadeh *et al*, 2017). Further considerations may be due to the interactions between the vesicle material and the antibody fragment (Zeng *et al*, 2011; Press *et al*, 2017). The pH of the solution of cargo to be encapsulated can influence the interaction between the carrier formulation and molecule to be encapsulated (Press *et al*, 2017).

TEM highlights the range of variability in our sample, which is further supported and indicated by the PDI value. This is perhaps inevitable as this is a sample of the unpurified vesicles. According to Danaei *et al* (2018) a PDI of 0.3 and below, which are the values we recorded, indicates a homogenous population. Perhaps this should be revised as there is heterogeneity in our neat sample. Once they have been purified by size exclusion chromatography, the vesicles should be eluted according to their sizes, as is performed for proteins, the larger molecules eluting first and the smallest molecules eluting later (Stetefeld *et al*, 2016). They will also be separated from the media (including unincorporated payload material) in which they were synthesised. The fractions of purified vesicles profiled in this study using DLS, did not appear to separate based on size. The DLS readings appear to show that the vesicle sizes of the peripheral fractions have anomalous readings either side of the peak fractions. One hypothesis may be that these results are due to the

low concentration of vesicles at that size. If the concentration of the sample is too low, the number of scattered light events may be too low to measure accurately (Lim *et al*, 2013). The DLS is sensitive to large particles, as they scatter more light, potentially skewing the data (Bhattacharjee, 2016; Stetefeld *et al*, 2016). It may be that the smaller vesicles are unstable and therefore aggregate causing the instability, or it may be a result of the low concentration (Lim *et al*, 2013, Maguire *et al*, 2018). As we are searching for the peak population it may be expected that vesicles would appear in each of the fractions in a heterogenous sample. If this is the case, the lack of sensitivity is a limitation when using low concentrations of sample with the DLS. As the concentration of vesicles that we are working with appears small this may skew the results. Nonetheless, on locating the peak fractions, the DLS detected measurements similar to the initial readings of the unpurified sample. The fluorescent plate reader also verified this, as the peak fluorescence signal was detected in the same fraction, supporting the use of DLS in this instance. A technique which could overcome this limitation is Nanoparticle Tracking Analysis (NTA) (Mehn *et al*, 2017). NTA is a method based on Brownian motion that identifies and track individual particles in solution, allowing the measurement of particle size distribution and particle concentration (Filipe *et al*, 2010; Mehn *et al*, 2017).

2.5.2 Zeta potential and stability

The zeta potential is a measure of electrostatic repulsion/attraction between nanoparticles in solution and therefore, a measure of stability - the greater the electrostatic repulsion the less likely the vesicles will aggregate. A nanoparticle with a zeta potential value > ± 30 mV is considered highly stable (Patel and Agrawal, 2011). The zeta potential of the empty vesicles had the greatest negative potential. This result was not anticipated as the vesicles were expected to be cationic and therefore should have a positive zeta potential. The zeta potential of all the vesicles was negative, indicating that the BA material from which the vesicle has been synthesised are not only anionic, but novel. No formulation of anionic BA vesicles derived from vernonia oil has been reported. The formulation of the vesicles is therefore not the formulation we set out to have synthesised and must also be further explored (see chapter 4). Our novel BA vesicles were taken up *in vitro* indicating that regardless of the charge they possess, they were still able to cross

the cell membrane in SH-SY5Y and LN229 cells. Anionic vesicles have been investigated as potential drug delivery systems to treat CNS diseases (Lockman *et al*, 2004). After 1 minute of exposure, anionic nanoparticles, of a similar size to our BA vesicles and highly negative zeta potential, were shown to cross the BBB in rats at a higher concentration than cationic nanoparticles. Contrary to these author's initial hypothesis the particles were not repelled or excluded by the negative charge of the BBB. It would be of interest to investigate if an increase in exposure time, increases the uptake of the anionic particles. This would be undertaken in human endothelial cells, such as hCMEC/D3, as they are first cells on the BBB that the vesicles would have to overcome *in vivo*.

Chattopadhyay *et al* (2008) investigated the uptake and release of anionic solid lipid nanoparticles (SLNs) in immortalised human endothelial cells hCMEC/D3. These particles, of a similar size to our BA vesicles, encapsulated the tracer dye rhodamine 123 (R123), a fluorescent tracer specific for mitochondria. They found that uptake of the tracer dye was higher for the encapsulated dye than for the non-encapsulated dye. They suggested the irregular uptake within the cell population observed in their microscopy images was a result of Brownian motion and electrostatic interactions (Chattopadhyay *et al*, 2008). Due to the anionic properties of biological barriers it is important to investigate mechanisms by which the anionic BA vesicles can penetrate. Different cell lines will help to characterise different uptake kinetics (Korang-Yeboah *et al*, 2015). This should be explored for future work, using different cell lines to investigate the level of uptake. Different biological barriers have differing apicobasal membrane polarity, which is important to consider particularly when comparing to the transendothelial electrical resistance (TEER) values for the BBB and peripheral organs (Crone and Christensen, 1981; Redzic, 2011). Our BA vesicles present an interesting and potentially novel drug delivery system which requires further investigation.

An important parameter in drug delivery for BA vesicles is vesicle stability (Puri *et al*, 2009). The zeta potential can provide an insight, *in vitro,* of the stability of the vesicles *in vivo (*Bhattacharjee, 2016). Popov *et al* (2010), investigated the storage of GLH-20 encapsulating carboxyfluorescein at room temperature and 4°C. GLH-20 vesicles were observed to be no longer stable after 13 days. Our empty and

AF546 BA vesicles demonstrated high stability, as a result of the ability to repel other particles based on their zeta potential. This zeta potential is dependent upon the properties of the material used for the vesicle formulation and the solvent the analytes are suspended in (Joseph and Singhvi, 2019). Low zeta potential values, as observed with scFv 4D5-8RFP encapsulated vesicles, may be influenced by van der Waals interactions/attractions which may lead to aggregation (Clogston and Patri, 2011; Joseph and Singhvi, 2019; Savage, Hilt and Dziubla, 2019). On measuring the zeta potential, if the isoelectric point is reached the electrostatic repulsion between particles/vesicles diminishes and the attraction of forces such as van der Waals are more dominant (Pfeiffer *et al*, 2014). The antibody fragment has an isoelectric point of 6.5 and is therefore soluble at physiological pH (7.4) (Markiv *et al*, 2011). It is therefore, suggested that perhaps the interactions between the antibody fragment and the vesicles may be influencing the overall isoelectric point of the vesicles, which in turn is influencing the low zeta potential, indicating carrier-cargo interactions influencing vesicle behaviour. It cannot be discounted that the low zeta potential may be a result of the solvent the BA vesicles were suspended in, which was deionised water. As deionised water produces carbonic acid in the presence of carbon dioxide, this can lower the pH of deionised water, thus influencing the zeta potential of the vesicles. However, Jesus *et al* (2016) observed that the zeta potential of their particles, encapsulating different concentrations of recombinant hepatitis B surface antigen, was influenced by the addition of chitosan rather than the concentration of protein or the solvent the analyte was suspended in.

2.5.3 Encapsulation efficiency

Encapsulation efficiency is paramount in the development of a drug delivery system and is an indication of the potential efficacy (Furtado *et al*, 2018; Çalış *et al*, 2019). The concentration of encapsulated AF546 is limited in comparison to the initial concentration of AF546 added to the original synthesis. One hypothesis may be that as AF546 is a negatively charged molecule, the repulsion between the vesicles and AF546 may be influencing the encapsulation efficiency. Press *et al* (2017) believe that interactions between the carrier (BA vesicles) and the cargo (molecule encapsulated) can influence encapsulation. Although the charge may have an influence, this may not be the overarching factor regarding the low incorporation

value. It may be worth investigating encapsulating cargoes that have a higher concentration (Halayqa and Domańska, 2014; Derman, 2015). The same studies should be reprised with an increase in AF546 concentration to investigate if the charge of cargo has influenced the encapsulation efficiency as will be seen in no change in encapsulation efficiency. Conversely, if the charge is not influencing the efficiency then there will be an increase in encapsulation and therefore, fluorescent signal as measured using a fluorescent plate reader as used previously.

As the concentration of the polymer may be a factor influencing encapsulation efficiency (Yeo and Parks, 2004; Bozzuto and Molinari, 2015), perhaps increasing the concentration of BA material with cholesterol and cholesteryl hemisuccinate may increase the overall encapsulation efficiency (Harayqa and Domańska, 2014; Derman, 2015, Kim *et al*, 2020). The relevant dose will be dependent upon a number of parameters including the encapsulation efficiency, the therapeutic to be encapsulated and the therapeutic dose (Bozzuto and Molinari, 2015). Bozzuto and Molinari (2015) indicate that in many cases the toxic effects of the drug are not dissimilar to the therapeutic dose. We need to ensure that the vesicles are not only able to encapsulate an effective dose in order to elicit the response it is designed to induce, but that the vesicles are able to deliver that dose to the target site (Kita and Dittrich, 2011).

Factors that influence the encapsulation efficiency include solubility of the polymer in organic solvent, concentration of polymer, solubility of solvent, the rate of removal of solvent, the ratio of dispersed phase (the vesicles/delivery system) and continuous phase (the liquid in which they are dispersed) (Yeo and Parks, 2004; Sun and Chiu, 2005; Bozzuto and Molinari, 2015). Other factors include morphology of the vesicles/nanoparticles, such as size and shape (Sun and Chiu, 2005). The effect of the solvent solubilising the lipid material may not be a factor for our vesicles as according to Ong *et al* (2016) chloroform is the most suitable solvent. Liposomes prepared with chloroform were shown to have the highest negative zeta potential as well as highest encapsulation efficiency (Ong *et al*,2016). It appears there may be other factors influencing this efficiency, such as the material and formulation. The rate of solidification may be a factor that can be investigated in the future. One observation was the effect of over sonication on the size of the vesicles (Taurozzi *et al*, 2010). This is referred to as coagulation. The sonicated

material is influenced by numerous factors, such as increased collision frequency, increased localised pressure and temperature gradients, from the acoustic energy that conversely forms aggregates of the primary particles (Aoki *et al*, 1987; Taurozzi *et al*, 2010). Although only observed once, it was seen to be adversely influencing the size of vesicles and it might be of interest to investigate different techniques such as such as ethanol injection, a method in which our BA material is dissolved in ethanol then injected in an aqueous buffer to form vesicles (Huang *et al*, 2010; Shaker *et al*, 2017; Kim *et al*, 2020). Perhaps an alternative method may be to use a water bath sonicator as perhaps factors such as the temperature and the intensity of the sound waves may be inversely influencing the encapsulation efficiency. Hadian *et al* (2014) investigated the effect of water bath sonication against probe sonication and a combination of the two and how that influenced efficiency for liposomes encapsulating omega-3 fatty acids. They found that the water bath did not improve encapsulation efficiency for liposomes.

Popov *et al* (2013) investigated the effect of encapsulation of analgesic peptides in different pH conditions to optimise encapsulation. The different peptides, including leu-enkephalin and kyotorphin, were encapsulated in 3 different pH conditions (pH 3.5, 7.4 and 9.5) to investigate how this influences encapsulation efficiency due to the isoelectric point of each of the analgesic peptides. Their findings appear to support the higher the pH the greater the encapsulation concentration of two analgesics- leu-enkephalin and kyotorphin. In the instance of leu-enkephalin the increase was nearly 5-fold as the pH increased from 3.5 (2.9%) to 9.5 (16.7%). As leu-enkephalin is a neutral molecule pH 7.4 by increasing the pH the molecule becomes negatively charged and their vesicles were cationic. This may explain the increase in encapsulation efficiency seen as a result of a favourable cargo-carrier interaction (Harayqa and Domańska, 2014). Thus, indicating that unfavourable steric interactions between AF546 and our vesicles may explain the low encapsulation efficiency that we have observed. It will be important to investigate this further in the future.

2.6 Future studies

The preliminary uptake studies undertaken only demonstrate qualitatively that the AF546 vesicles were able to cross the cellular membrane of SH-SY5Y and LN229

cells. Further work is required to quantify the uptake kinetics *in vitro* and ultimately *in vivo* and content release. Although the vesicles may appear punctate in the SH-SY5Y cells it needs further work to investigate whether the vesicles are intact. This would be performed using tracer dyes that bind to compartments or molecules within the cell, such as propidium iodide which binds to nucleic acids. The kinetics of cargo uptake and release will need to be investigated in different cell lines.

Harayqa and Domańska (2014) increased the polymer concentration of their poly(DL-lactide-co-glycolide) nanoparticles encapsulating psychotic therapeutics which resulted in an increased encapsulation. However, the resulting nanoparticles were in the 300 nm range. The addition of poly(vinyl alcohol) (PVA), a biodegradable polymer. decreased this size however this lowered the encapsulation efficiency. Derman (2015) found that increasing the concentration of cargo, caffeic acid phenethyl ester loaded, in PLGA nanoparticles increased the encapsulation efficiency. As we are interested in increasing the encapsulation efficiency, increasing the polymer concentration should be investigated for future studies as well as increasing the concentration of the cargo.

To measure the encapsulation efficiency and quantify the concentration of scFv 4D5-8RFP antibody fragments encapsulated within the lumen of our BA vesicles. The vesicles will need to be dissolved in suitable solvent or media such as Triton-X 100 (Popov *et al*, 2012). The released antibody fragments will need to be separated from the vesicle material via centrifugation (Popov *et al*, 2012). The protein will be in the supernatant which can be quantified by either measuring the fluorescence using a fluorescent plate reader creating a standard curve as done previously (section 2.3.15) to calculate the concentration of antibody fragment released from the vesicles (Popov *et al*, 2010 and 2012), or by creating a protein assay from the antibody fragment, producing a standard curve from the stock concentration of antibody fragment, from which the concentration can be calculated (Gdowski *et al*, 2015).

Although the zeta potential for AF546 encapsulated vesicles over a period of 3 months demonstrates the stability of the vesicles being stored at 4 °C, the decrease over the 3-month time frame does show a small but statistically significant decrease. However, the zeta potential does not drop below -30 mV which

demonstrates, despite the significant drop, the vesicles are still very much stable (Clogston and Patri, 2011; Patel and Agrawal, 2011). The vesicles were stored in dH_2O, which may influence the charge and, by extension, the zeta potential. The vesicles, therefore, should also be resuspended and stored in a physiologically relevant buffer system, such as PBS during the analysis.

Further work would include the encapsulation of dye such as pHrodo dye to investigate the effect of pH and the encapsulation efficiency. The fluorescence of pHrodo increases with lower pH (Ogawa *et al*, 2010). Popov *et al* (2013) observed an increase in encapsulation efficiency as pH increased. Therefore, to replicate this effect we would use a pH sensitive dye such as pHrodo to measure the increase in fluorescence on encapsulation efficiency. These vesicles could also be used to investigate the porosity of the vesicles, by investigating the effect the external environment has on the internal environment of the vesicles. This would be important for future interactions to determine the effect of the external environment on the encapsulated therapeutic.

Incorporation of additional lipids such as polyethylene glycol (PEG) with liposomes has been used with conflicting results on encapsulation efficiency. Folate PEGylated liposomes increased encapsulation efficiency compared to PEGylated liposomes (Cho *et al*, 2014), whereas Garinot *et al* (2007) observed no change and Muralidharan *et al* (2014) a reduction. Therefore, it would be of interest for future studies to incorporate the folate PEGylation with our vesicles in order to increase encapsulation efficiency. PEGylation has been linked to increase efficiency of drug delivery through prolonged systemic circulation due to reduced opsonisation (Zeng *et al*, 2011; Press *et al*, 2017). It appeared to increase the uptake of liposomes encapsulating chemotherapeutics (Gabizon *et al*, 2003). However, an increase in the condition palmer-plantar erythrodysesthesia has been linked to the PEGylation of PEGylated liposomal doxorubicin (Lorusso *et al*, 2007). The non-PEGylated version of the same liposome, encapsulating the same drug (doxorubicin) demonstrated limited to no effects (Leonard *et al*, 2019). Therefore, we will investigate the effect of incorporation of PEGylation of our vesicles by performing toxicity and immunogenicity studies to monitor any potential change.

2.7 Conclusions

The original synthesis undertaken was designed to produce GLH-20 cationic vesicles. Dakwar *et al* (2012) had used these vesicles to demonstrate that encapsulated FITC conjugated BSA could cross the BBB *in vivo*. Initially we had wanted to investigate the use of GLH-20 encapsulating an antibody fragment. During the profiling and characterisation of the BA vesicles the zeta potential was negative indicating that the vesicles were anionic and indeed novel and unexpected. The material synthesised was not the original GLH-20 material, indicating that a novel product has been synthesised. The only step which differs from the experimental procedure is the initial step of hydrolysis of the esters. This may have influenced the synthesis downstream. From our own investigations the method used appeared to be non-selective at hydrolysing the esters as well as non-selectively opening of the epoxide groups. As a result of the material producing novel vesicles, further investigation was undertaken to explore what this material was and is reported in Chapter 4. Further work was undertaken to determine the potential of these vesicles. The BA vesicles are not only novel, they have a negative zeta potential, they were shown to cross biological barriers as shown in preliminary *in vitro* uptake studies and have been shown to encapsulate different cargoes. Therefore, it is important to further investigate their potential as a drug delivery system. It is recommended that future *in vitro* work include toxicity, viability and immunogenicity to investigate their safety and utility. It is also proposed that future work includes uptake in other cell lines representative of the body and brain, and that the release kinetics is further investigated. Finally, it is recommended in order to investigate the potential of these BA vesicles as a drug delivery system *in vivo* using an animal model.

CHAPTER 3

3.1 Introduction

As shown in the previous chapter, BA vesicles are suitable carriers to be used for drug delivery and are capable of penetrating biological barriers *in vitro*. Directly delivering drugs across the cerebromicrovascular wall is the most effective means of treating diseases of the brain, but due to the physical, functional and pharmacological restrictions of the BBB, this route of drug administration to the brain is greatly limited (Abbott, 2013; Daneman and Prat, 2015; McArthur *et al*, 2016; Pardridge, 2007). Developing a drug delivery system capable of penetrating the BBB and carrying a variety of cargoes into the brain parenchyma is thus a very appealing goal for treatment of the numerous neurological and psychological diseases of the brain, for which glioblastoma serves as a typical example.

3.1.1 Safety and utility of vesicles

Prior to clinical testing further, challenges surrounding the drug delivery system must be addressed. The main purpose of *in vitro* testing is to assess the potential of the vesicle/formulation causing an adverse effect *in vivo* (Dobrovolskaia and McNeil, 2013). *In vitro* testing is used as a surrogate indicator to rapidly evaluate of the effects *in vivo*. Performing these studies enables an understanding of potential acute responses. These include release, localisation and toxicity/inflammation. Therefore, it is important to investigate the safety and utility of the system.

Prior to undertaking such studies there are several factors that should be considered, including selection of a relevant model, selection of an end-point, choosing appropriate controls, appropriate range of *in vitro* assays to test vesicles and understand how the results of the assay translates *in vivo*, to ensure there is relevant and translatable *in vitro/in vivo* correlation (Dobrovolskaia and McNeil, 2013). The advantages of *in vitro* studies extend to cost, speed and ethical considerations (Kumar *et al*, 2017). There are several assays that can be used to assess safety, including proliferation assays, apoptosis and necrosis assays, oxidative stress assays and DNA damage assays (Kumar *et al*, 2017). Whilst it is fundamental to test toxicity, it is of equal importance to address any immunogenic responses as inflammation in the CNS can be an indicator of pathology (Dobrovolskaia and McNeil, 2013). As there is a paucity of toxicity and viability

studies performed for BAs, we will be undertaking numerous assays to profile the BA vesicles from the previous chapter (Fariya *et al*, 2014).

Moreover, the rate at which the vesicles are taken up and cross biological barriers and release their contents *in vitro* provide evidence regarding their bioavailability *in vivo* (Korang-Yeboah *et al*, 2015; Jain and Thareja, 2019). There are a number of factors which ultimately influence this from the cell line used, the formulation of the vesicles, the pH of the environment and the temperature (Siepmann and Göpferich, 2001; Fu and Kao, 2010; Korang-Yeboah *et al*, 2015). The release profile is an important parameter to include for the utility of a drug delivery system (Korang-Yeboah *et al*, 2015).

As outlined in chapter 1, we believe that BA vesicles represent an efficient drug delivery system and have undertaken studies to examine their effectiveness. Following the production and physical characterisation of the BA material detailed in chapter 2, the safety and utility of these vesicles will be tested in cellular and whole animal models.

3.2 Specific Aims:

1. To evaluate potential adverse effects caused by the vesicles using brain relevant immortalised cell lines

2. To investigate the ability of different cells of the brain to take up and lyse vesicles carrying different cargoes

3. To test the ability of BA vesicles carrying different cargoes to enter the brain *in vivo*

4. To monitor BA vesicle distribution *in vivo*

3.3 Methods

3.3.1 Materials- source of reagents

Table 3.1 The list of all materials and their suppliers used throughout chapter 3.

MATERIALS	SUPPLIER	ADDRESS
rat collagen (catalog # 08-115)	EMD millipore	Darmstadt, Germany
DMEM (catalog # BE12-614F), PBS (catalog # BE17-516F), Trypsin/EDTA (catalog # CC-5012), penicillin/streptomycin (catalog # 09-757F), EGM2 MV (catalog # CC-3202), and catalog # CC-4147 for the following reagents: hydrocortisone (HC), human epidermal growth factor (hEGF), human fibroblast growth factor (hFGF), recombinant insulin-like growth factor (R3-IGF-1), vascular endothelial growth factor (VEGF), ascorbic acid, and gentamicin	Lonza	Slough, UK
Fetal bovine serum heat inactivated (catalog # FB-1001H)	Biosera	East Sussex, UK
Annexin A5-FITC detection kit (catalog # 640914)	BioLegend	California, USA
calf collagen (catalog # 9007-34-5), glycerol (catalog # G5516), sucrose (catalog # S0389)	Sigma Aldrich	Irvine, UK
Propidium Iodide (catalog # BMS500PI), N2 nutrient supplement (catalog # 17502048), Blasticidin S (catalog # A1113902), CellMask Plasma Membrane stain (catalog # C10046), actinomycin D (catalog # 11805017), DAPI	Thermo Fisher Scientific	Loughborough, Leicestershire, UK

(4',6-diamidino-2-phenylindole) (catalog # D1306), PrestoBlue (catalog # A13261), Lipopolysaccharide (LPS) (catalog # 00-4976-03), TNF-α ELISA kit (catalog # BMS607-3), bovine serum albumin (catalog # B14)		
$CaCl_2$ (catalog # C1016), formaldehyde (catalog # 104003), Mowiol (catalog # 475904)	MERCK- Sigma Aldrich	Darmstadt, Germany
Tris (catalog # 60040)	Melford	CheImsworth, Ipswich, UK

3.3.2 Cell lines

Cell lines used for vesicle uptake studies were chosen as representative of the cells found in the brain. Human SH-SY5Y neuroblastoma (American Type Culture Collection- ATCC), human LN229 glioblastoma (ATCC), human hCMEC/D3 cerebromicrovascular endothelial cells (VH Bio Ltd.), human HASTR/ci35 astrocytes (Prof T. Furihata, Kyoto University, Japan) and murine BV2 microglia (Prof E. Blasi, University of Modena and Reggio Emilia, Italy). For comparison with other body tissue types the human kidney cell line HEK-293T (ATCC) was used. SH-SY5Y, LN229, BV2 and HEK-293T cells were grown in Dulbecco's Minimum Essential Medium (DMEM) (Lonza, Basel, Swizterland) with 5% v/v fetal bovine serum (FBS, previously heat decomplemented by 30 minute incubation at 56˚C; Biosera Ltd., UK), 1% v/v penicillin and streptomycin. The human endothelial cell line, hCMEC/D3 (VHBio Ltd) was grown in complete EGM-2 medium supplemented with gentamicin (50 µg/ml), 2.5% v/v FBS, ascorbic acid solution (1 µg/ml), hydrocortisone (0.2 µg/ml) , human epidermal growth factor (hEGF) (5 ng/ml), human fibroblast growth factor (hFGF) (10 ng/ml), insulin-like growth factor-1 (R3-IGF-1) (20 ng/ml) and human vascular endothelial growth factor (hVEGF) (0.5 ng/ml) (Lonza, Basel, Switzerland). Endothelial differentiation medium was replaced by EGM-2 omitting VEGF prior to experimentation. The HASTR/ci35 immortalised astrocyte line was grown in DMEM supplemented with N2 nutrient mix (Thermo Fisher Scientific UK Ltd.), blasticidin S (4 µg/ml), 10% v/v FBS and 1% v/v

penicillin and streptomycin (Lonza). Differentiation media for the astrocytes was as above, but omitted blasticidin S.

All cells were incubated for 3-4 days until 70% confluent at 37˚C, or 33˚C for HASTR/ci35, under 5% v/v CO_2. HASTR/ci35 cells, once differentiation medium was added, were then grown at 37˚C under 5% v/v CO_2 until confluent.

3.3.3 Routine cell culture

All cell line work was performed in a laminar flow hood with aseptic technique. Cells were grown in sterile 75 cm^2 flasks; in the case of hCMEC/D3 and HASTR/ci35 cells these were previously coated with 15 µg/cm^2 type I collagen. Cells were passaged when they appeared 70% confluent. Spent media was removed and cells were washed with sterile 0.01 M PBS without Ca^{2+} for 5 minutes at 37°C. PBS was removed and 0.25% w/v trypsin, 1 mM EDTA was added and cells were incubated for 5 minutes at 37°C. Following dilution of trypsin with fresh medium containing 5% v/v FBS, cells were counted using a haemocytometer, centrifuged at 800 x g using an IEC CL30 centrifuge, resuspended and re-plated for further growth or experimentation at 15,000 cells/cm^2 in appropriate medium.

Chamber slides were seeded with 1x10^5 SH-SY5Y, HEK-293T, BV2 or LN229 cells/cm^2 and cultured for 2-3 days. Cells were then incubated for 2-24 hours with a sample of the vesicle fraction in media prior to removal, washing, fixing by immersion in 4% v/v formaldehyde in PBS for 10 minutes. Cells were washed and counterstained with phalloidin-acti-stain-488 (Cytoskeleton Inc; 1:140 dilution), for visualisation of the cytoskeleton, for 20 minutes. Cells were stained with 50ng/ml 4',6-diamidino-2-phenylindole, dihydrochloride (DAPI; Thermo Fisher Scientific) for 10 minutes to define nuclei. Cells stained with CellMask™ Plasma Membrane stain (1:1000 dilution, Thermo Fisher Scientific) were incubated for 1 hour. Cells were then washed in PBS and mounted with Mowiol 4-88 (40% w/v glycerol, 9.6% w/v Mowiol, 0.2 M Tris, pH8.5).

3.3.4 Annexin A5-Propidium Iodide Viability Assay

12 well plates (Nunc) were seeded with 0.5 x 10^6 cells- human astrocytic (HASTR/ci35) or endothelial (hCMEC/D3) cells and cultured for 3-4 days at 37ºC under 5% v/v CO_2 in standard growth medium. Cells were either untreated, treated

with 0.1 µg/ml actinomycin D (ThermoFischer Scientific), PBS, or various concentrations of empty vesicles (50 µg/ml, 25 µg/ml, 10 µg/ml and 5 µg/ml in PBS) and incubated overnight. Cells were washed with PBS-/- and centrifuged at 1000 g for 5 min at room temperature. Cells were then resuspended in binding buffer (0.01 M PBS with 0.1% w/v BSA and 1 mM $CaCl_2$) containing annexin A5-FITC (0.45 µg, Biolegend Inc., USA) and propidium iodide (0.9 µg) before being incubated at room temperature in the dark for 15 min. After incubation, 400 µl of additional binding buffer was added to the cell suspension, and gently mixed. Samples were kept on ice in the dark, until analysed by flow cytometry, using the 488 nm blue laser and the FITC and PerCP-Cy™5.5 filters. Single stains were used for compensation of these fluorochromes. Flow cytometric analysis was performed using a BD FACSCanto II (BD Biosciences) and FACS Diva Software. Cells were gated using forward scatter (FS) and side scatter (SS) to distinguish from and exclude cellular debris. Data were analysed using FlowJo software (Treestar Inc, OR, USA). A typical annexin A5-FITC profile for HASTR/ci35 cells is shown in figure 3.1

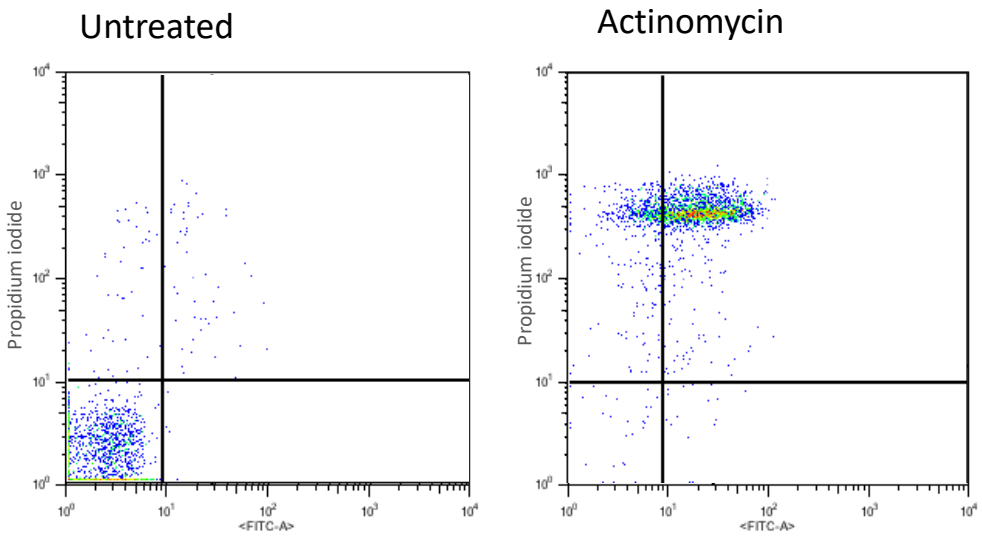

Figure 3.1. A typical annexin A5-FITC profile for healthy and apoptotic HASTR/ci35 cells. Immortalised astrocytes were either untreated or treated with 0.1 µg/ml cytotoxic drug, actinomycin D**.** Untreated cells show a high concentration of healthy cells, whilst the treated cells indicate a higher population of early and late apoptotic cells. Each of the four quadrants represents the stages of cell health- healthy (bottom left), early apoptotic (bottom right), late apoptotic (top right) and necrosis (top left).

3.3.5 PrestoBlue viability assay

Endothelial cells, hCMEC/D3, were seeded at a density of $1x10^4$ cells/cm^2 on to a collagen coated 96 well plate (Sterillin) and cultured for 2-3 days. Cells were treated with either medium only (negative control), PBS (negative control), 10 µg/ml Actinomycin D (positive control) or 50 µg/ml empty vesicles for 24 hours at 37°C, 5% CO_2. PrestoBlue was added at 1:10 dilution to each well and incubated for 10 minutes at 37°C. Fluorescence was measured using CLARIOstar plate reader using filters 545-20/600-40 nm.

3.3.6 TNF-α ELISA

Cells of the murine microglial line, BV2, were seeded at a density of $1.5x10^5$ cells/cm^2 onto 48 well plates (Sterillin) and cultured for 2-3 days. Cells were then treated with either medium only, 10 µg/ml lipopolysaccharide (LPS) (Jin *et al*, 2018; Barabutis *et al*, 2019) or 50 µg/ml empty vesicles for 24 hours at 37°C, 5% CO_2 in triplicate. Sample medium was collected and TNFα content was measured with a murine TNF-α solid-phase enzyme linked immunosorbent analysis (ELISA), (ThermoFisher). Recombinant mouse TNFα was used to establish a standard curve at 1000, 500, 250, 125, 62.5, 31.25, 15.625 and 7.8125 pg/ml (figure 3.2) according to the manufacturer's instructions. End-product absorbance at 450nm was measured using a CLARIOstar plate reader (BMG Labtech, Germany).

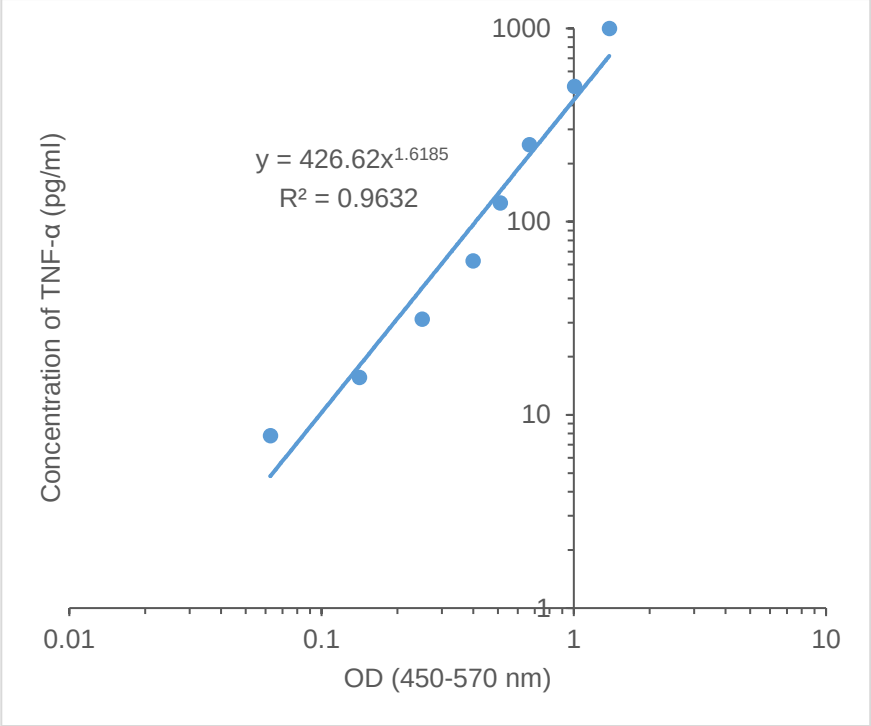

Figure 3.2. Standard curve of TNF-α concentrations (1000 – 7.8125 pg/ml) assayed by spectrophotometry (OD 450 – 570 nm) to determine the inflammatory response caused by 50 µg/ml vesicles to murine microglial cell line, BV2, after 24 hour exposure.

3.3.7 Release kinetics of propidium iodide encapsulated vesicles

LN229 glioma cells were seeded at a density of $1x10^5$ cells/cm^2 on 24 well plates and treated with purified PI encapsulated vesicles for different times (4, 3, 2, 1 hour and 30 minutes). Spent medium was removed, and cells were washed in 0.01 M PBS. Once PBS was aspirated cells were trypsinised for 5 minutes. Detached cells were collected and centrifuged for 5 minutes at 800 x g using an IEC CL30 centrifuge. The supernatant was aspirated, and the pellet was resuspended in final concentration of 50 ng/ml DAPI for 5 minutes. Cells were once again centrifuged as described above. The supernatant was aspirated, and cells were resuspended in cold PBS. Samples were kept on ice in the dark, until analysed by flow cytometry using the violet (405 nm) and blue (488 nm) lasers and the DAPI and PerCP-Cy™5.5 filters. Analysis was performed as described in section 3.3.4. Figure 3.3 shows the gating strategy in order to determine single cell from the populations of events using the flow cytometer.

3.3.8 Confocal microscope

Confocal microscopy was used to determine the peak fractions of vesicles in unknown samples and in uptake studies. Following adjustment of gain and offset, cells and vesicles were imaged at 1024x1024 resolution, using an oil immersion x63 objective on a Leica LSM880 laser scanning confocal microscope running Zen software. A minimum of 3 images were collected per well. Lasers used were 405 nm diode laser (for DAPI stain), 488 nm Argon-Krypton (for PI), 561 nm diode (for RFP of the antibody fragment), and 633 nm HeNe (for the plasma membrane stain).

PI encapsulated vesicles have a maximum excitation wavelength of 493 nm and the emission wavelength of 636 nm. For vesicles encapsulating AF546 and scFv 4D5-8RFP the excitation wavelengths are 556 nm and 584 nm respectively, and emission values are 573 nm and 607 nm respectively. Excitation and emission wavelengths for DAPI were 358 nm and 461 nm, respectively. CellMask™ plasma membrane stain has an excitation wavelength maximum of 649 nm and emission wavelength maximum of 699 nm. Cytokeletal stain, phalloidin-acti-stain-488, excites at 495 nm and 518 nm is the maximum emission wavelength

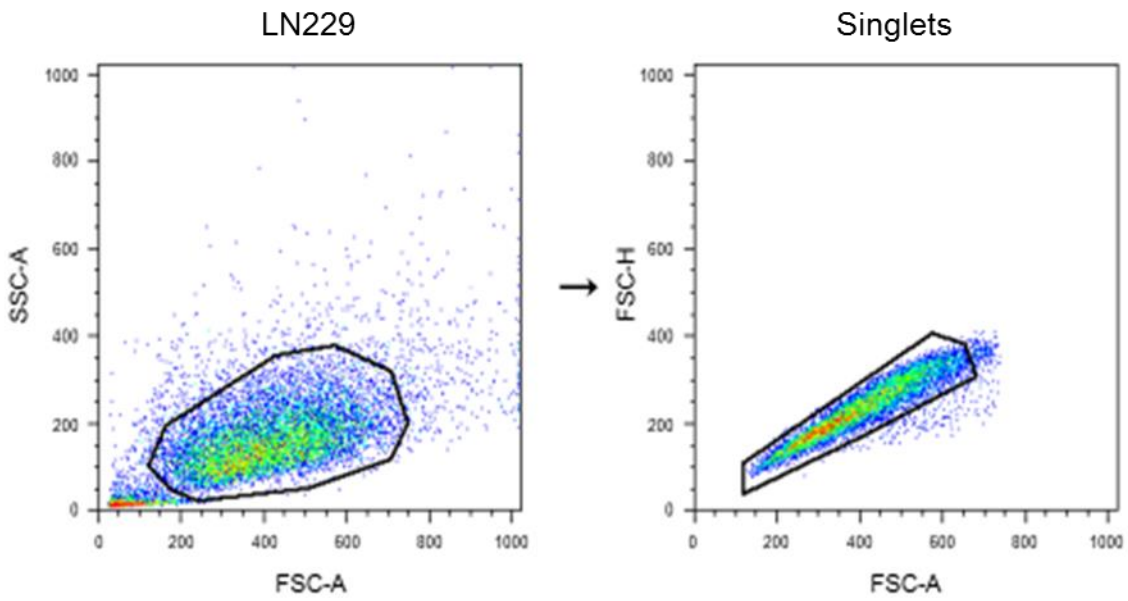

Figure 3.3. Gating strategy for flow cytometry analysis. The cell populations with low forward and side scatters and high forward and side scatters were established in order to locate single cell events. This is then gated to include the population of LN229 cells of interest. Flow cytometry dot plot on the left shows side scatter- area (SSC-A) versus forward scatter-area (FSC-A), referring to the population of events that represents the LN229 cells of interest. This population is 'gated' and then further analysed using the forward scatter height (FSC-H) against forward scatter area (FSC-A) is used to determine the singlets or single cell events to improve accuracy.

3.3.9 Animal Studies

All animal experiments were performed in accordance with the UK Animals (Scientific Procedures) Act of 1986 and relevant EU legislation. Animal studies were undertaken at University College London (UCL) under procedure project licence number 70/8784.

In order to investigate the ability of the GLH-20 encapsulated vesicles to traverse the BBB *in vivo* studies were performed using 7-week old male C57BL/6 mice (4 mice per test, of which there were 5 tests, n=20). Mice were purchased from Charles River. Mice were kept in individual ventilated cages under controlled lighting (12h on, and 12h off) with free access to standard mouse chow and drinking water.

125 µl of sample containing 12.5 µg/ml of the BA starting material (non-encapsulated AF546, encapsulated AF546, encapsulated scFv 4D5-8RFP, non-

encapsulated scFv 4D5-8RFP and empty vesicle control) were administered intravenously, through the tail vein, by Dr Mariya Hristova and colleagues at UCL. Mice were sacrificed (Pentoject, 0.6-0.8ml/kg) 30 minutes after injection and perfused with ice-cold, filtered PBS, by Dr Mariya Hristova. Tissues were collected (brain, kidneys, heart, liver, lungs, and subcutaneous adipose tissue- inguinal pad) by Dr Simon McArthur, and snap frozen. Half of each brain was snap frozen, whilst the other half was collected in 4% v/v formaldehyde in 0.01 M PBS for fixation for 24h at 4˚C, prior to cryoprotection in 30% w/v sucrose and freezing on dry ice. Frozen brain, lung, heart and kidney tissue was sectioned (20 µm coronal sections for brain) using an OTF5000 cryostat (Bright Instruments Ltd., Cambridge, UK). All slices, except fixed brains, were counterstained with 0.1 µg/ml DAPI and mounted under Mowiol 4-88 on glass microscope slides for epifluorescence microscopic imaging.

3.3.10 Epifluorescence microscope

Epifluorescence microscopy was used to analyse mouse tissue samples. Fluorescence was detected using the Leica CTR5000 fluorescent microscope with MetaMorph software. Tissue samples were imaged at 1024x1024 resolution, using either dry (x40 objective) or oil immersion (x63 objective). A minimum of 3 images were collected per well.

Filters used were DAPI and RFP to visualise fluorescent dyes DAPI or AF546 and scFv 4D5-8RFP, respectively.

3.3.11 Homogenisation of tissue samples

Frozen organ samples (brain, liver, heart, lungs, kidney, subcutaneous adipose tissue - inguinal fat pad, and tibialis anterior skeletal muscle) with encapsulated AF546, free AF546 and empty vesicles were placed individually in Eppendorf tubes to thaw and weighed. 0.25% v/w Triton X-100 final was added to each tube and homogenised by maceration (SHMI homogeniser, Stuart) at 35000 rpm for 15 secs. Samples were centrifuged (SIGMA 1-16K, Sigma) at 16000 x g for 15 minutes at 4°C and the supernatant was carefully collected. 100 µl of supernatant samples and standards (serial dilutions of AF546, range 0.1- 100 µM) were prepared in triplicate in a 96 well microplate (Nunc) and analysed using a CLARIOstar fluorescence plate reader (excitation filter 540-20 nm, emission filter 590-30 nm)

(BMG Labtech). The concentration of encapsulated vesicles against free AF546 in the mouse organs was determined by comparison with an AF546 standard curve (serial dilutions of AF546, range 0.1- 100 µM). Alexa Fluor concentrations were normalised by tissue weight and against background fluorescence from animals treated with empty vesicles.

3.3.12 Statistical Analysis

All statistical analysis was performed using SPSS (version 25). Quantitative data were assessed for normality of distribution using the Kolmogorov-Smirnov test, prior to analysis by one-way ANOVA test with Tukey's HSD *post hoc* test. A value of $p < 0.05$ was considered significant.

3.4 Results

Prior to *in vitro* investigations, the vesicles must be shown to be non-toxic. Therefore, the annexin A5 apoptosis and PrestoBlue viability assays were used on cell lines representative of the cells of the BBB and other major organs of the body.

3.4.1 BA vesicles are non-toxic

In order to investigate the toxicity of the vesicle material, an annexin V apoptosis assay was performed on representative cells of the brain (HASTR/c35i immortalised human astrocytes and hCMEC/D3 immortalised human cerebromicrovascular endothelial cells). Empty vesicles were added at dilutions of 50 µg/ml, 25µg/ml, 10 µg/ml and 5µg/ml from the purified peak fractions.

Treatment of HASTR/ci35 immortalised human astrocytes with empty vesicles (concentrations ranging from 5 µg/ml to 50 µg/ml) had no effect on cell viability after either 24 hours or 7 days exposure (Figures 3.4 and 3.5). In contrast, vesicles at the highest concentrations (50 µg/ml and 25 µg/ml) caused a significant increase in the proportion of hCMEC/D3 human cerebromicrovascular endothelial cells in the early phase of apoptosis after 24 hours exposure (Figure 3.6).

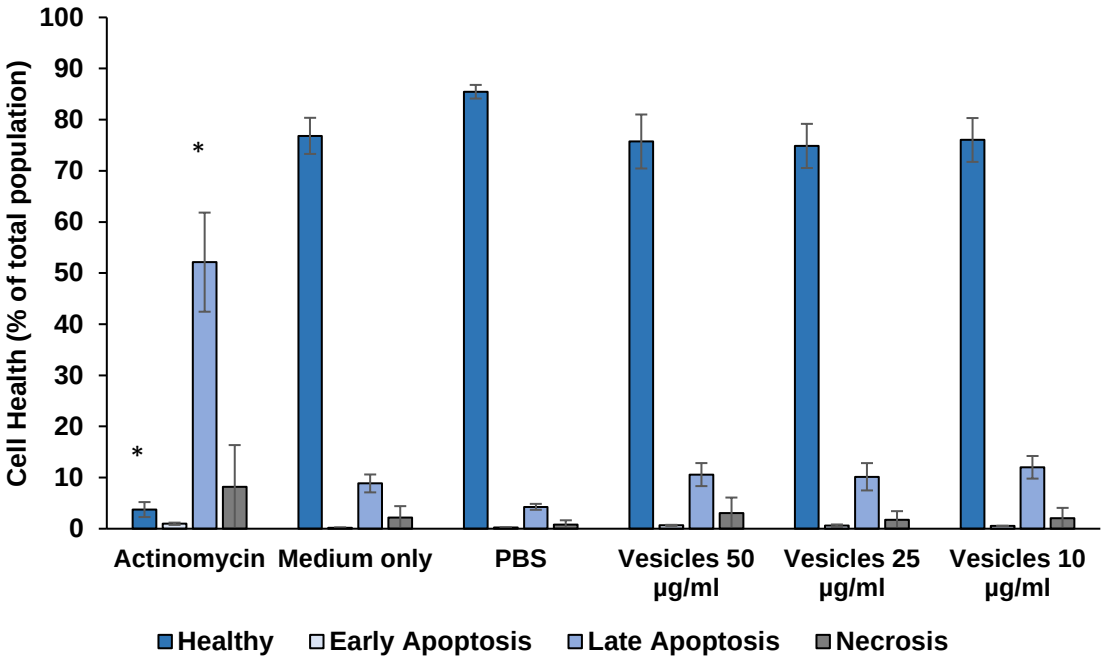

Figure 3.4. Incubation of HASTR/ci35 immortalised human astrocytes with bolaamphiphile vesicles for 24 hours does not increase apoptosis. Cells were incubated with 10 µg/ml actinomycin D (positive control), medium only (negative control), 0.01 M PBS (vehicle control) or empty vesicles diluted 50 µg/ml, 25 µg/ml or 10 µg/ml in 0.01 M PBS vehicle for 24 hours. Apoptosis was evaluated using the annexin V apoptosis assay (see section 3.3.4). Data are mean +/- sd; n=3; * $p<0.05$ vs. medium only.

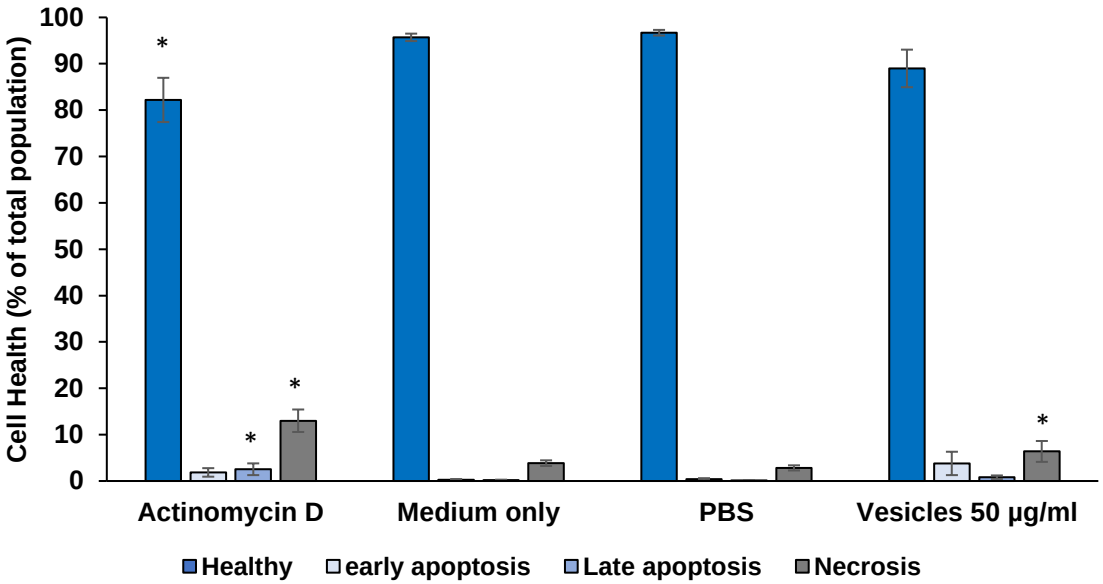

Figure 3.5. Incubation of HASTR/ci35 immortalised human astrocytes with bolaamphiphile vesicles for 7 days does not cause appreciable levels of apoptosis. Cells were incubated with empty vesicles diluted 50 µg/ml in 0.01 M PBS vehicle, medium only (negative control), 0.01 M PBS (vehicle control) or 10 µg/ml actinomycin D (positive control) for seven days. Apoptosis was evaluated using the annexin V apoptosis assay (see section 3.3.4). Data are mean +/- sd; n=3; * $p<0.05$ vs. medium only.

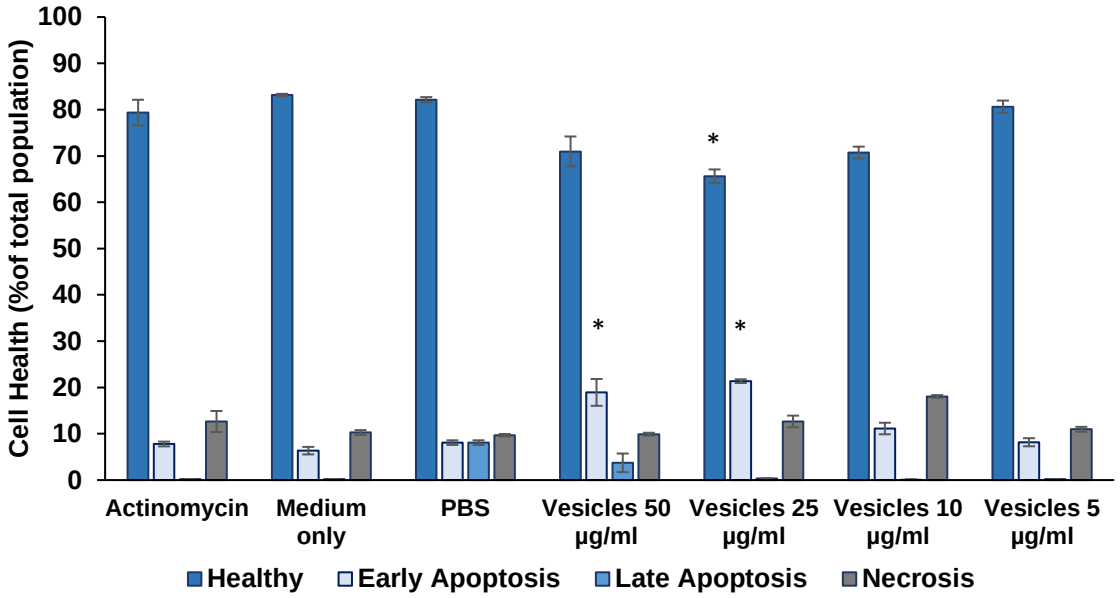

Figure 3.6. Incubation of hCMEC/D3 immortalised human endothelia with bolaamphiphile vesicles for 24 hours appears to cause low levels of cytotoxicity. Cells were incubated with 10 µg/ml actinomycin D (positive control), medium only (negative control), 0.01 M PBS (vehicle control) or empty vesicles diluted 50 µg/ml, 25 µg/ml, 10 µg/ml or 5 µg/ml in 0.01 M PBS vehicle for 24 hours. Apoptosis was evaluated using the annexin V apoptosis assay (see section 3.3.4). Data are mean +/- sd; n=3; * $p<0.05$ vs. medium only.

3.4.2 Proliferation studies of vesicles

In order to investigate effects of the BA vesicles on cellular proliferation *in vitro* the PrestoBlue assay was performed (Helm *et al*, 2017). Treatment of hCMEC/D3 human cerebromicrovascular endothelial cells with 50 µg/ml empty vesicles had no adverse effect on cell viability after 24 hours exposure using the PrestoBlue assay (figure 3.7).

Viability of hCMEC/D3 endothelial cells was not compromised after 24-hour incubation with bolaamphiphilic vesicles. However, actinomycin D significantly reduced cell viability.

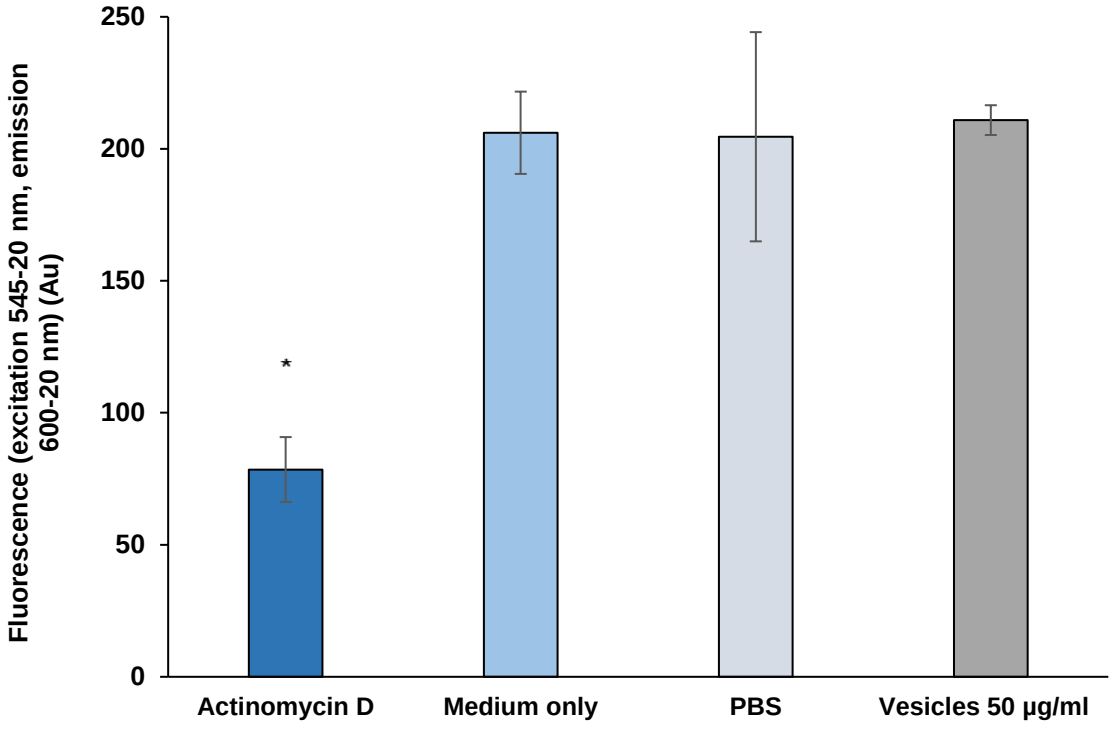

Figure 3.7. Incubation of hCMEC/D3 immortalised human endothelia with bolaamphiphile vesicles for 24 hours does not affect cell viability. Cells were incubated with 10 µg/ml actinomycin D (positive control), medium only (negative control), 0.01 M PBS (vehicle control) or empty vesicles diluted 50 µg/ml in 0.01 M PBS vehicle for 24 hours. Apoptosis was evaluated using the PrestoBlue assay (section 3.3.5). Data are mean +/- sd; n=6; * $p<0.05$ vs. medium only.

3.4.3 BA Vesicles do not cause TNF-α release in BV2

An ELISA (enzyme-linked immunosorbent assay) for TNF-α was performed after 24 incubation of murine microglial cells with either 50 µg/ml empty vesicles, medium only or 10 µg/ml LPS (figure 3.8). No production of TNF-α was observed in response to vesicles, suggesting the BA vesicles are unlikely to cause an inflammatory response.

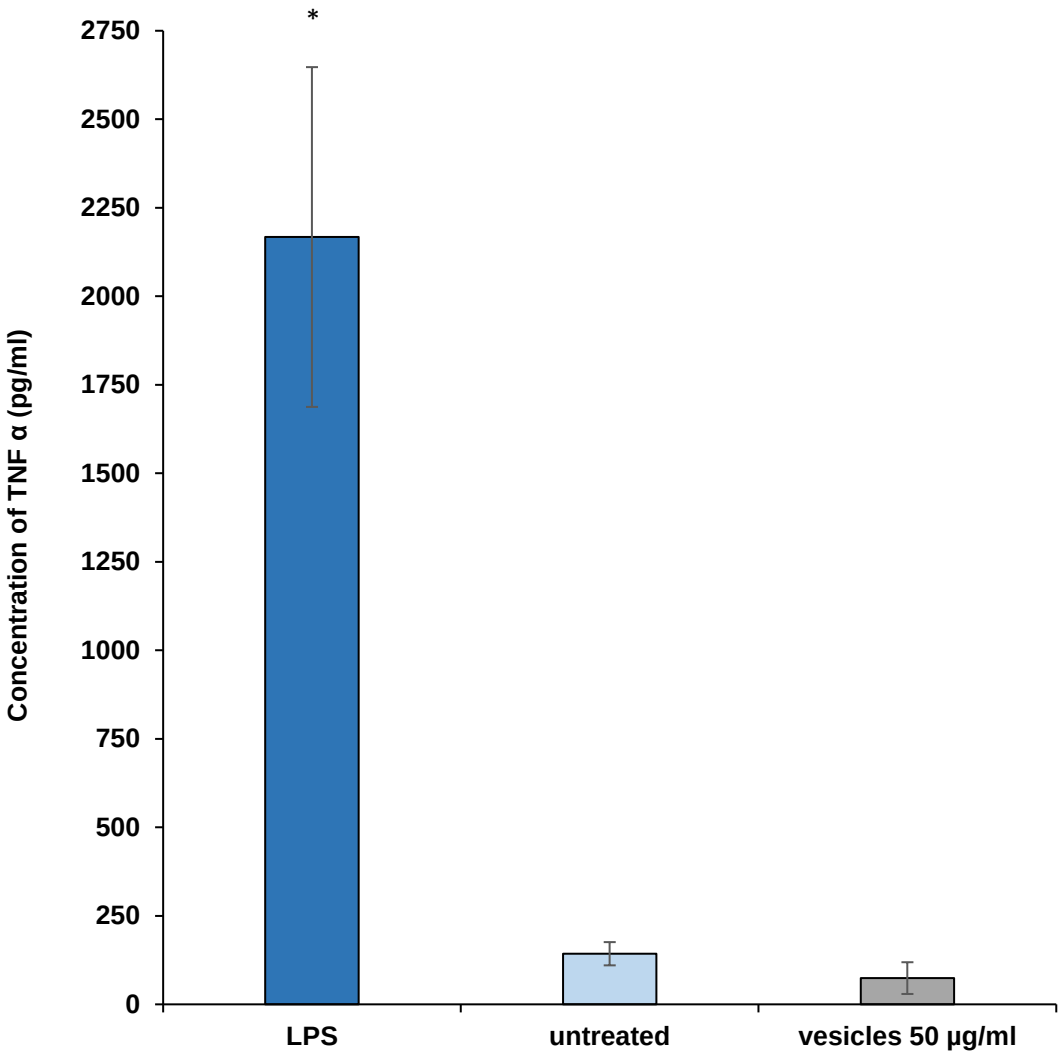

Figure 3.8. Incubation of murine microglial cells, BV2, for 24 hours with empty vesicles do not produce an inflammatory response. Cells were incubated with 10 µg/ml LPS (positive control), medium only (negative control), or empty vesicles diluted 50 µg/ml in 0.01 M PBS vehicle for 24 hours. Inflammation was evaluated using the TNF α ELISA (see section 3.3.6). Data are mean +/- sd; n=3. $p<0.05$ vs. untreated only.

3.4.4 Profiling and uptake of propidium iodide encapsulated vesicles

Propidium iodide (PI) is a nucleic acid stain unable to penetrate viable cells with an intact plasma membrane. Therefore, only cells which had taken up and subsequently lysed these vesicles should show any nuclear fluorescent signal. Moreover, as PI will not cross viable cell membranes, living cells that exhibit fluorescence must have accumulated vesicle encapsulated PI.

The human neuroblastoma cell line, SH-SY5Y, the mouse microglial cell line, BV2, and the human kidney cell HEK-293 were used. Whilst SH-SY5Y and BV2 cell parents are found in the brain parenchyma and thus represent typical neural populations, the HEK-293 cells, derived from human kidney epithelial cells, served as a useful control to represent the principle clearance organ, the kidney. Uptake and indication of vesicle opening was apparent in both the microglia and kidney epithelial cell lines after 24 hours treatment with vesicles, but little fluorescence was observed in neuroblastoma cells (figure 3.9). Nuclear binding was not observed for HEK-293 or SHSY5Y cells in the control study. However, the BV2 cells nuclear binding of PI is apparent indicating PI has penetrated the cell membrane.

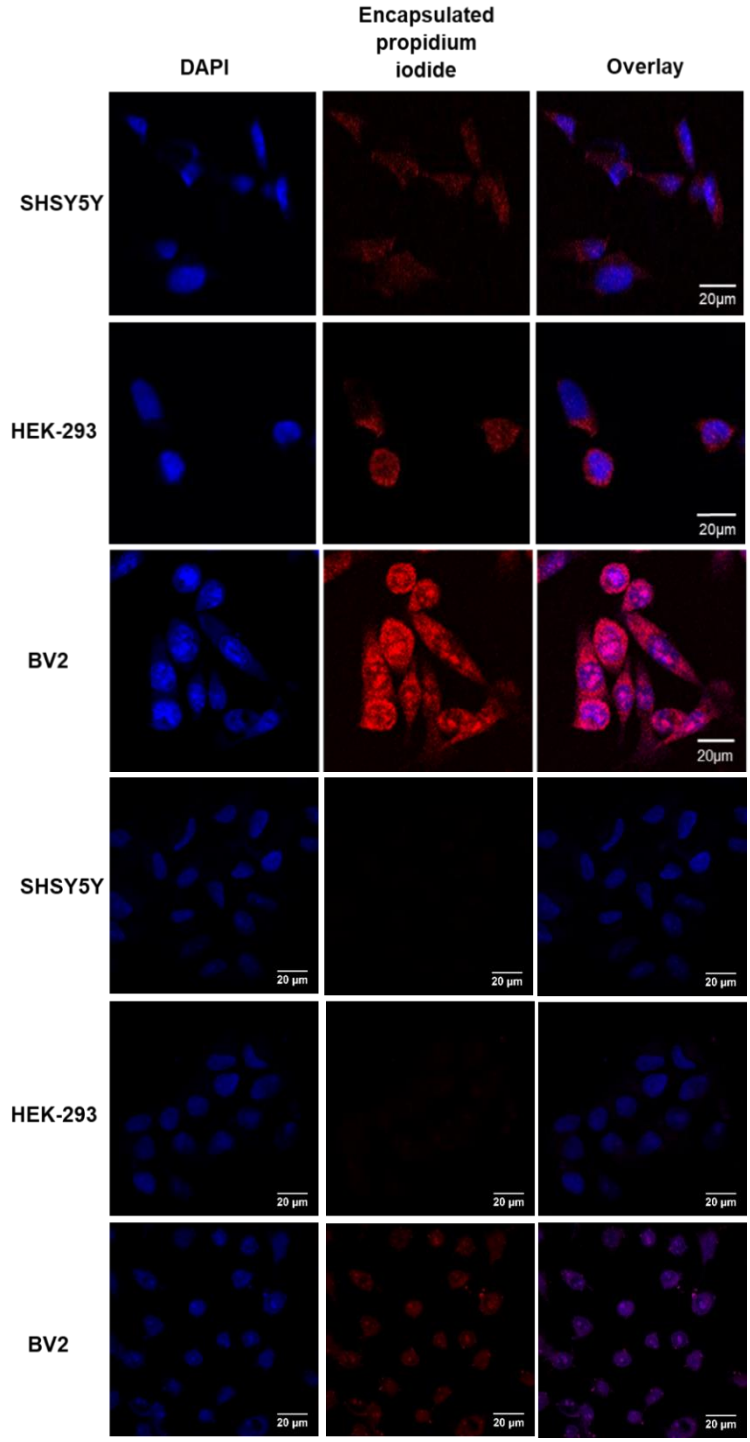

Figure 3.9. Signs of vesicle opening in microglia and kidney epithelium-derived cell lines, but not in neuroblastoma cells after 24h exposure. Confocal images of SH-SY5Y neuroblastoma, HEK293 kidney epithelial and BV2 microglial cells were treated for 24 hours with purified propidium iodide-containing vesicles and non-encapsulated propidium iodide at 37°C in 5% CO_2 in air, prior to fixation with 4% formaldehyde and counterstaining with 50 ng/ml DAPI. Confocal microscope images (x 63 oil objective) were taken of the samples at excitation 358 nm, emission 461 nm for DAPI, excitation 493nm and emission 636nm for propidium iodide. Scale bar = 20 μm

3.4.5 Time-dependency of vesicle uptake in LN229 glioblastoma cell lines

Complementing the uptake studies in which PI was encapsulated in the vesicles and was shown to bind to DNA in 24 hours (figure 3.9), we investigated the time-dependency of vesicle uptake and opening using the LN229 glioblastoma cell line. Whilst the previous study demonstrates that the vesicles were lysed it does not give a specific time point. It is important to investigate the time frame at which the vesicles are lysed, and PI is released to understand the kinetics of the vesicles. Therefore, flow cytometry was used in order to quantify the release kinetics of PI vesicles from LN229 cells over a four-hour period, revealing a time-dependent increase in PI staining (figure 3.10) that was statistically significant by 2h post-exposure. Typical density plots are presented in figure 3.11

Epifluorescent images indicate that nuclear labelling was clearly evident after 30 minutes incubation with propidium iodide containing vesicles, and the staining increased in intensity concomitant with exposure times (figure 3.12). This increase is significant from hour 2 to hour 4. The spread of PI and DAPI staining increases over the course of the study. Non-encapsulated PI is also observed binding to nucleic acids within 30 minutes. Thus, demonstrating that PI can penetrate the cell membrane of LN229 cells.

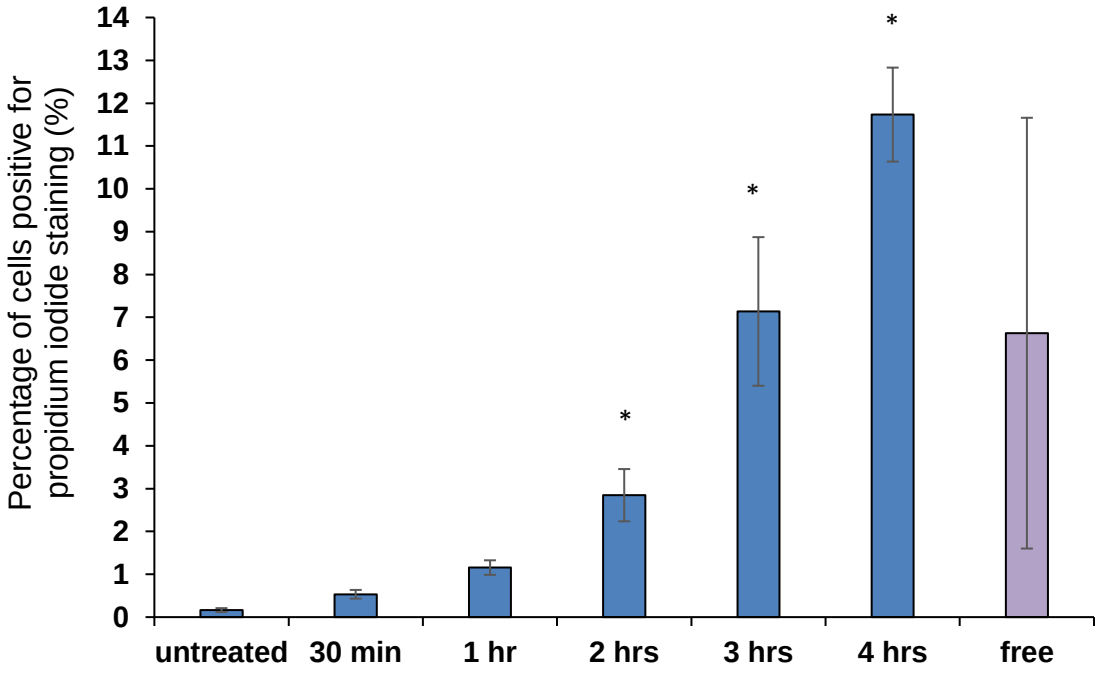

Figure 3.10. Flow cytometry analysis of glioblastoma cell line, LN229, incubated with propidium iodide encapsulated vesicles over 4-hour time frame. Flow cytometry analysis of LN229 cells incubated at 30 minutes, 1, 2, 3 and 4 hours at 37^{o}C with bolaamphiphile vesicles encapsulating PI. Uptake and release increases over time as observed by an increase in propidium iodide signal. Data are mean +/- sd; n=3. $p<0.05$ vs. untreated only.

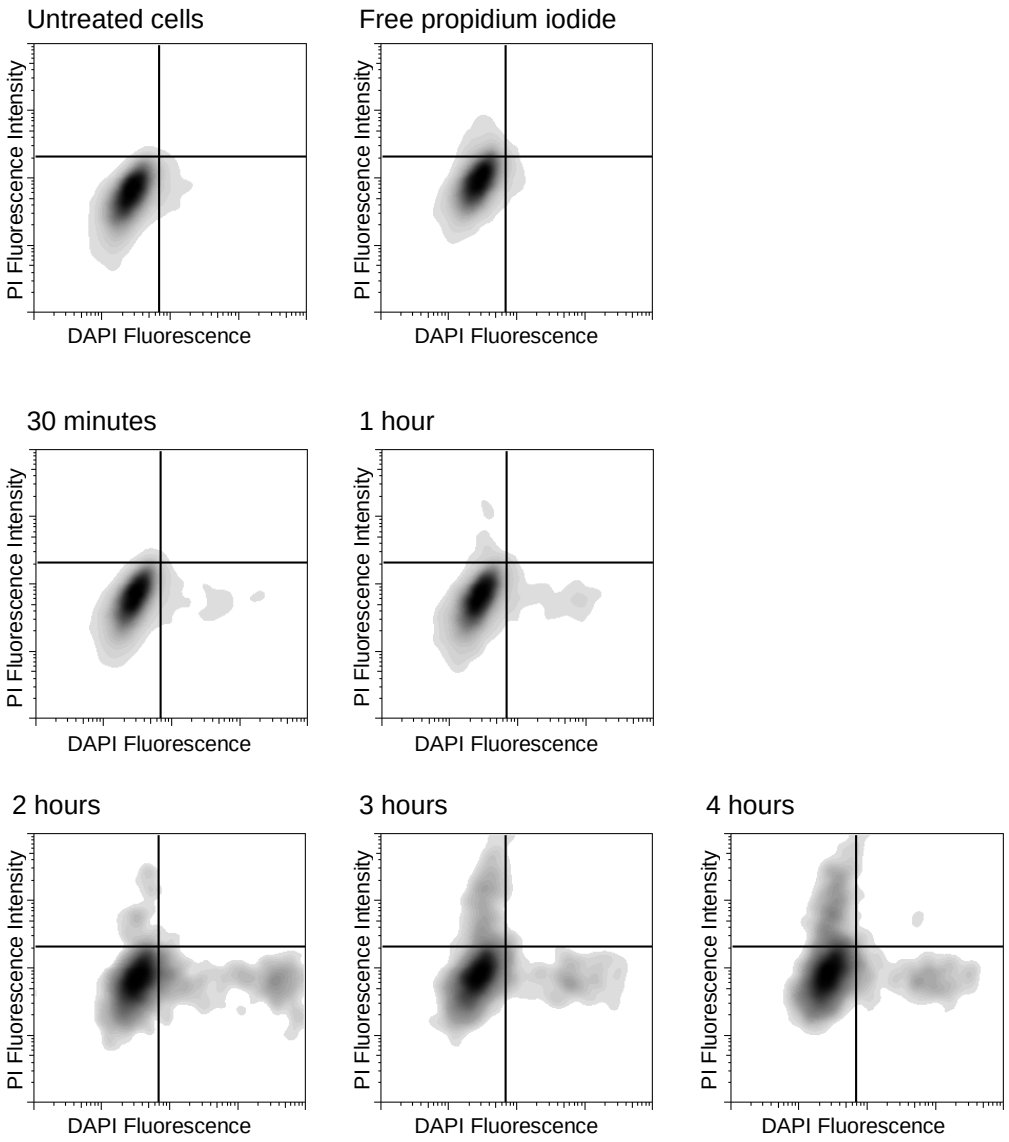

Figure 3.11. Images of flow cytometry analysis of glioblastoma cell line, LN229, incubated with propidium iodide encapsulated vesicles over 4-hour time frame. Flow cytometry analysis of LN229 cells incubated at 30 minutes, 1, 2, 3 and 4 hours at 37ºC with bolaamphiphile vesicles encapsulating PI and counterstained with nuclear stain DAPI. The PI and DAPI signal intensify over time. As more PI is taken up and released from the vesicles, binding increases as well as the nuclear staining signal. The plots were generated in FlowJo.

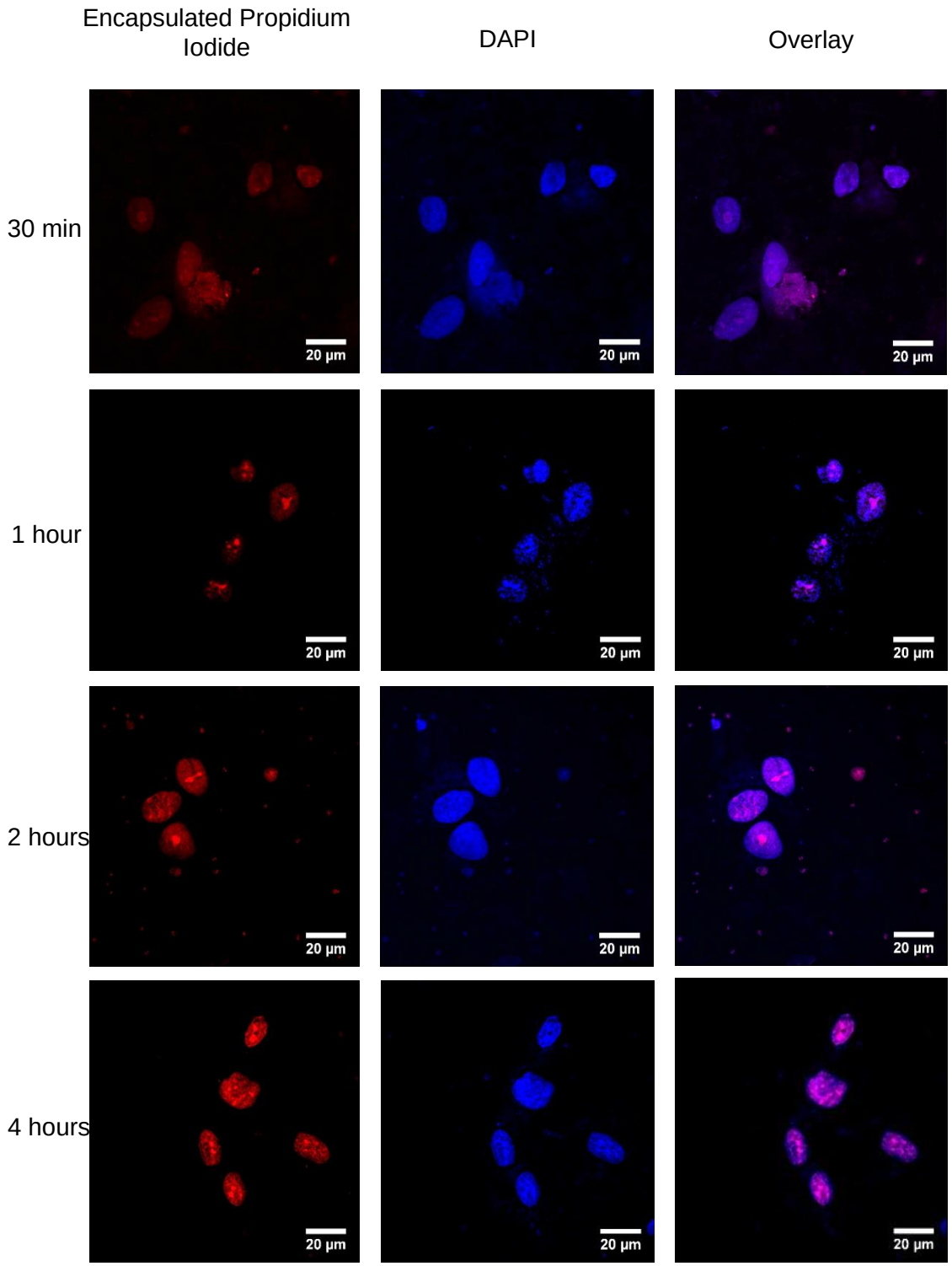

Figure 3.12. Time course of uptake and release of propidium iodide encapsulated vesicles in glioblastoma cell line, LN229. Confocal microscopic image of LN229 cells incubated at 30 minutes, 1, 2 and 4 hours at 37ºC with bolaamphiphile vesicles encapsulating PI (red), counterstained with DAPI (blue). Nuclear labelling, indicative of propidium iodide release, is clearly evident and increases as the time course continues. Scale bar = 20 µm.

3.4.6 Profiling and uptake of antibody fragment encapsulated vesicles

Antibody fragment scFV 4D5-8RFP is specific to the HER-2 receptor which is overexpressed in cancerous tissue including breast and ovarian (Markiv *et al*, 2011). In order to investigate the uptake of antibody fragment encapsulate vesicles SH-SY5Y cells were incubated for 2 hours with scFV 4D5-8RFP encapsulated vesicles and unencapsulated scFV 4D5-8RFP antibody fragment as our control. Cells were counterstained with deep red plasma membrane stain and imaged using confocal microscopy. Vesicles are taken up by SH-SY5Y cells and are punctate and intact (figure 3.13).

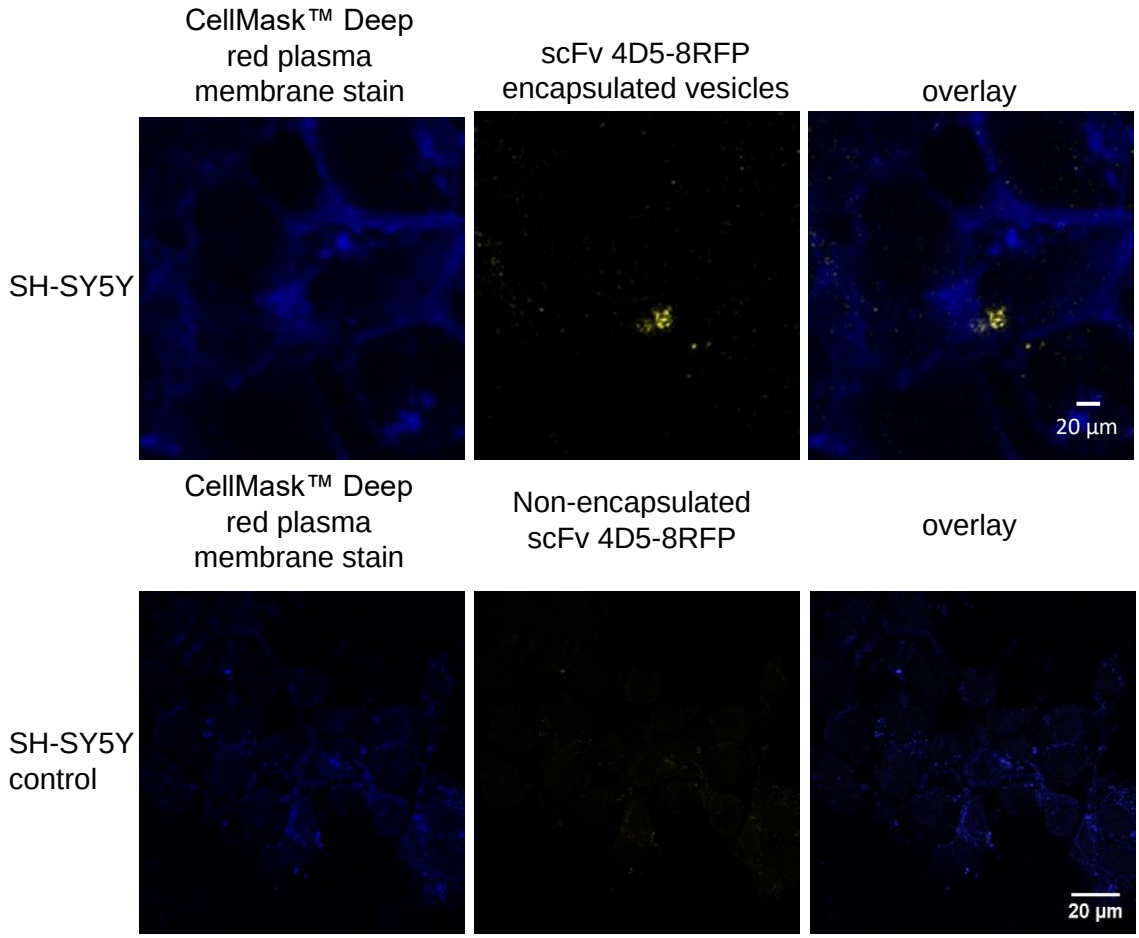

Figure 3.13. Uptake of antibody fragment encapsulated vesicles in SH-SY5Y neuroblastoma cell line. Confocal microscopic image of SH-SY5Y cells incubated for 2 hours at 37°C with BA vesicles encapsulating AF546 (yellow), counterstained with CellMask Deep plasma membrane marker (blue). Scale bar = 20 µm

3.4.7 In vivo work

To establish whether BA vesicles could cross biological barriers, and particularly the BBB, *in vivo* work was undertaken. Mice were injected intravenously with either non-encapsulated scFv 4D5-8RFP, encapsulated scFv 4D5-8RFP, empty vesicles, non-encapsulated AF546 or encapsulated AF546 (figure 3.14), with analysis of major organ vesicle content 30 minutes post-administration. Whilst brain tissue background fluorescence appeared to be increased upon treatment with either free AF546 or free antibody, punctate fluorescence was only observed in animals treated with encapsulated AF546, indicating entry of the vesicles into the brain tissue (figure 3.14). Similar results were seen in the kidney (figure 3.15), whereas the liver showed substantially enhanced tissue fluorescence upon delivery of vesicle encapsulated AF546 (figure 3.15). Encapsulated AF546 vesicles appear to have been opened, releasing the cargo, as AF546 is diffuse throughout the mouse lung tissue (figure 3.16).

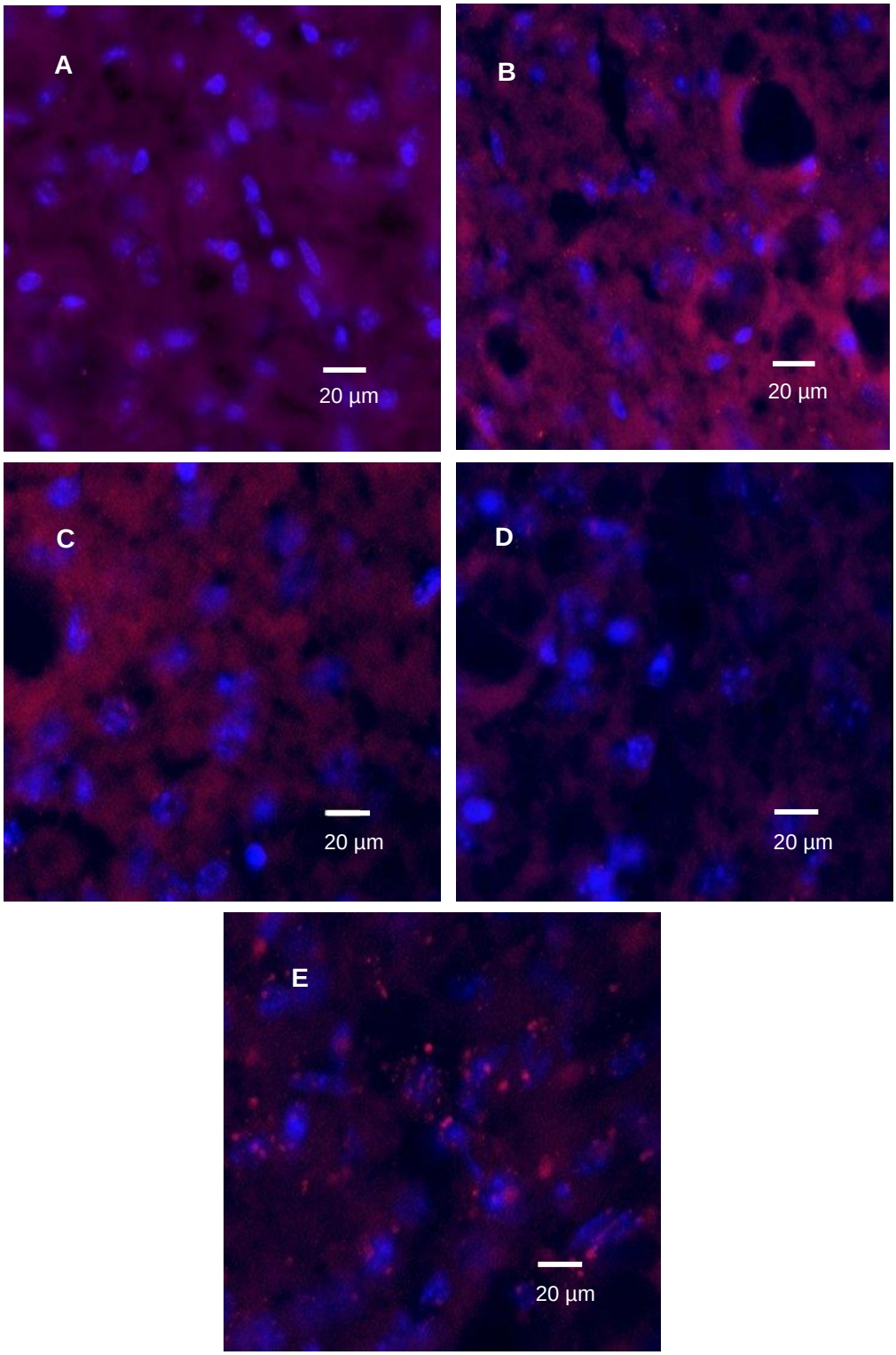

Figure 3.14. Fluorescent images of mouse brain tissue samples. **A)** Non-encapsulated scFv 4D5-8RFP, **B)** encapsulated scFv 4D5-8RFP, **C)** empty vesicles, **D)** non-encapsulated AF546 and **E)** encapsulated AF546. 30 minutes after intravenously injected in the tail vein, mice were sacrificed, and organs collected and frozen. Samples were sliced using the cryostat to 20 µm thick. Coronal sections were counterstained with nuclei stain, DAPI, and mounted onto slides using mowiol 488. Filters used were DAPI and RFP to visualise fluorescent dyes DAPI or AF546 and scFv 4D5-8RFP, respectively. Final concentration of AF546 was 18.72 µM, n=4, scale bar = 20 µm.

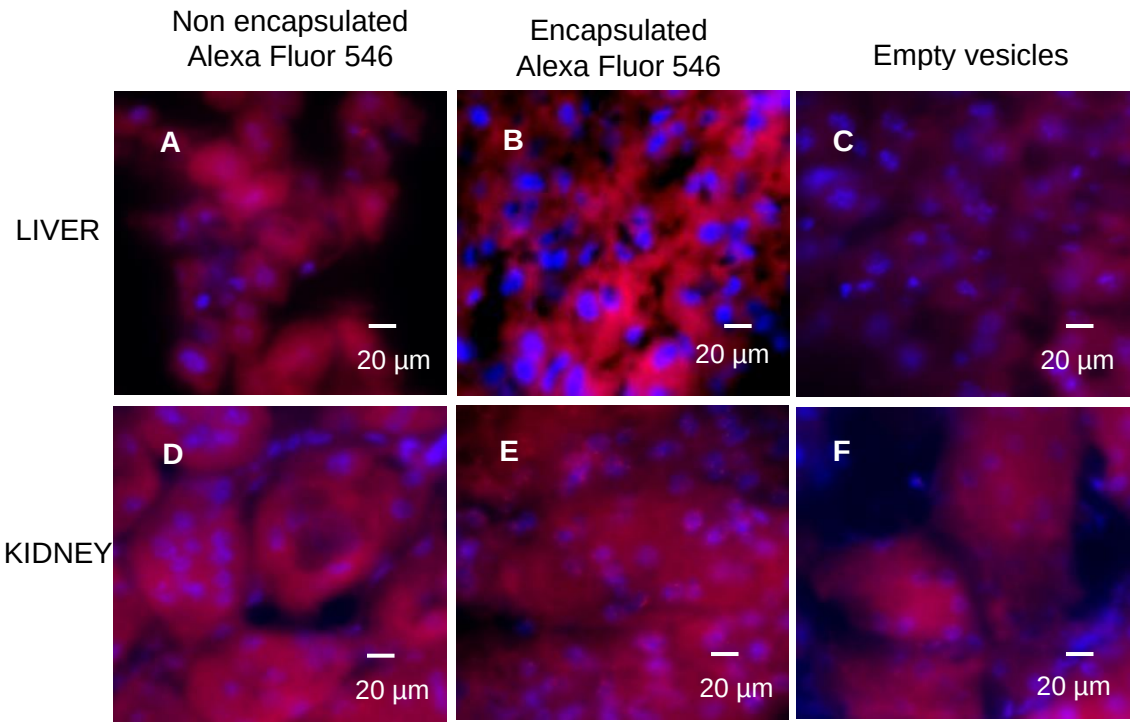

Figure 3.15. **Fluorescent image of mouse liver (A, B, C) and kidney (D, E, F) tissue samples. A), and D)** Non-encapsulated AF546, **B), and E)** encapsulated AF546 and **C), and F)** empty vesicles. 30 minutes after intravenously injected in the tail vain, mice were sacrificed, and organs collected and frozen. Samples were sliced using the cryostat to 20 µm thick. Coronal sections were counterstained with nuclei stain, DAPI, and mounted onto slides using mowiol 488. Filters used were DAPI and RFP to visualise fluorescent dyes DAPI or AF546, respectively. Final concentration of AF546 was 18.72 µM, n=4, scale bar = 20 µm.

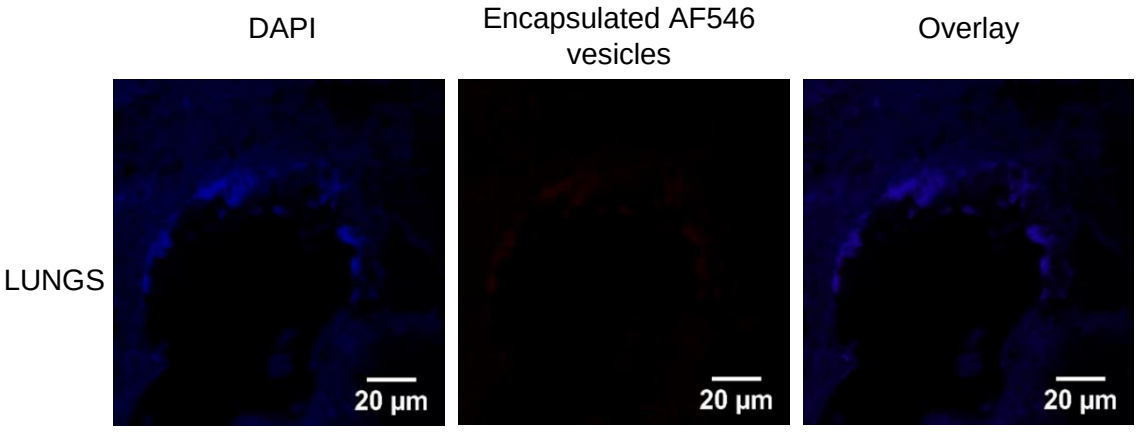

Figure 3.16. **Fluorescent image of mouse lung.** 30 minutes after intravenously injected in the tail vain, mice were sacrificed, and organs collected and frozen. Samples were sliced using the cryostat to 20 µm thick. Coronal sections were counterstained with nuclei stain, DAPI, and mounted onto slides using mowiol 488. Filters used were DAPI and RFP to visualise fluorescent dyes DAPI or AF546, respectively. Final concentration of AF546 was 18.72 µM, n=4, scale bar = 20 µm.

3.4.8 Homogenisation of tissue samples

To quantitatively assess the distribution of BA vesicles across major organs, AF546 content was measured in homogenised brain, lungs, kidney, subcutaneous adipose tissue- inguinal pad, liver and heart (figure 3.17). Heart and kidney levels of AF546 were not detectable, but all other tissues showed a positive signal. The highest value of encapsulated AF546 vesicles was located in the lungs (5.7 nmol/g) and the liver (3.2 nmol/g). The highest value of non-encapsulated AF546 was found in the lungs (15.7 nmol/g). For the distribution plot, only the non-encapsulated and encapsulated AF546 samples were included, as the RFP antibody fragment signal was not detectable.

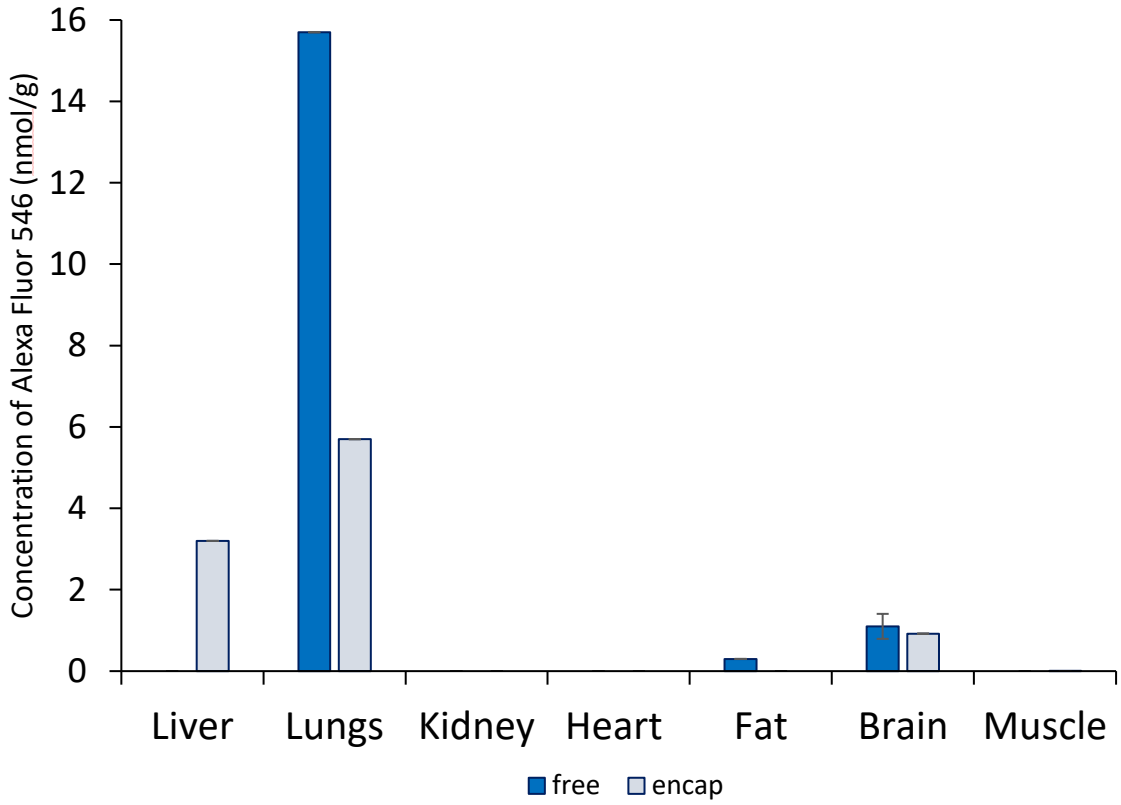

Figure 3.17. The distribution of encapsulated Alexa Fluor 546 vesicles and non-encapsulated Alexa Fluor 546 30 minutes after IV injection in model mouse. Organs from samples that were either treated with encapsulated AF546 vesicles or non-encapsulated AF546, were homogenised and fluorescence measured by CLARIOstar fluorescence plate reader (excitation filter 540-20 nm, emission filter 590-30 nm) (n=4).

3.5 Discussion

In this chapter, we have demonstrated that our novel anionic BA vesicles do not affect cell viability, are non-immunogenic and non-toxic in different brain-relevant cell lines, are taken up by cell lines whilst carrying different cargoes, and that these cargoes are released inside the cell. Moreover, vesicles could be detected in the brain within 30 minutes of intravenous administration in mice, demonstrating that BA vesicles possess the key features of a drug delivery system for the brain. Thus, demonstrating that our novel BA vesicles meet criteria recommended for developing a drug delivery system (Furtado *et al*, 2018). As discovered in the previous chapter (chapter 2) the vesicle material we had thought was GLH-20, was not, which was unexpected. As a result, analysis will be carried out in Chapter 4 to investigate further the material we have been using and how they can be synthesised. However, as these novel BA vesicles demonstrated the ability to cross biological barriers *in vitro*, further investigation was needed to see what these vesicles were but also their suitability as a drug delivery system.

3.5.1 Toxicity studies

The aim of undertaking in vitro studies is to evaluate, in a cost effective and time efficient manner, the potential of the vesicle to cause an adverse reaction *in vivo,* as well as to build upon knowledge (Dobrovolskaia and McNeil, 2013; Dusinska *et al*, 2017). Therefore, to determine the safety implications of the BA vesicles before further *in vitro* and *in vivo* studies could be undertaken, toxicity and inflammatory studies were carried out. The cytotoxicity and viability assays studied were the Annexin V apoptosis assay and PrestoBlue assay. Inflammatory studies were undertaken using the TNF-α ELISA assay. Thus, demonstrating that our novel anionic BA vesicles do not adversely influence cell viability and do not produce an immunogenic response. The apoptosis studies gave differing results indicating that they are not toxic to astrocytes in 24 hours but may produce a low cytotoxic response in hCMEC/D3 cells after 24 hours and after 7 days in HASTR/ci35. As there is some cytotoxicity observed PEGylation may overcome this.

Cell viability is a fundamental parameter of drug delivery (Puri *et al*, 2009). In order to ensure our BA vesicles are safe to use for future studies they need to demonstrate that they do not adversely influence cell health. Therefore, BA vesicles

were screened using the PrestoBlue assay to test cell viability. BA vesicles did not reduce cell viability of the hCMEC/D3 cells after 24 hours incubation using the PrestoBlue assay demonstrating their safety to be used in further *in vitro* and *in vivo* studies. Furthermore, due to the paucity of viability data for BA vesicles made from vernonia oil, this is the first time PrestoBlue viability assay has been performed to determine cell viability, and our results add to our knowledge of the properties of this material. We showed that our BA vesicles did not adversely affect cell viability, and as an important parameter of developing a drug delivery system, indicating that they are likely to be safe to use in future studies.

In order to measure the potential of an adverse immunogenic response to BA vesicles *in vitro*, TNF-α ELISA assay was performed. It is important to investigate all potential avenues of adverse responses that a drug delivery system may induce (Dobrovolskaia and McNeil, 2013) as there is a lack of information regarding the safety of BA vesicles (Fariya *et al*, 2014). Therefore, it is paramount to contribute to further evidence regarding BA vesicles for future studies. Proinflammatory cytokines, such as TNF-α, are expressed and secreted from activated microglia in response to injury and disease of the CNS (Nishioku *et al*, 2010; Chang et al, 2017). As a result, TNF-α is a measure of activated microglia function in the CNS (Nishioku *et al*, 2010; Varatharaj and Galea, 2017). Vesicles do not induce an inflammatory response to murine microglia cells, BV2, after 24-hour exposure. It was observed the vesicles induced a lower response than the negative control. Thus, indicating that the BA vesicles do not immunogenically compromise BV2s, and are unlikely to trigger an acute immune response *in vivo*, although more extensive immune profiling will be important to carry out before these vesicles can be taken to clinical use.

To further assess any potential risk, toxicity studies were undertaken to test the potential reactions BA vesicles may induce in different cell lines of the neurovascular unit, including astrocytes and endothelial cells. Apoptosis studies, using the Annexin V apoptosis assay, appear to demonstrate slightly differing results. Whilst the BA vesicles were shown to be non-toxic/pro-apoptotic after 24 hours exposure to astrocytes, this was not the case for hCMEC/D3 endothelia after 24-hour incubation and astrocytes after 7 days exposure. During the 7 day study the medium was changed only once, after 3 days of incubation, and replenished

with fresh medium containing the control or BA vesicles. The level of cytotoxicity is dose dependent and is observed at the highest concentrations in hCMEC/D3 cells. At the lower doses there are no cytotoxic response in the hCMEC/D3 cells. However, as the clinical dose is unknown, it would be dependent upon the drug encapsulated and the dose required to induce and effect (Kulkarni, Betageri and Singh, 1995; Ong *et al*, 2016). A further hypothesis for the cytotoxicity observed in the astrocytes may be that after 7 days the vesicles may become slightly cytotoxic.

It may be that as the material degrades it becomes toxic, impairing potential therapeutic effects of cargo delivery. The metabolism of the vesicle material may produce potential toxic by-products, inducing a cytotoxic response (Sukhanova *et al*, 2018), or it is possible that vesicles may damage mitochondria (Nyugen *et al,* 2015), or other cellular membranes (Farnoud and Nazemidashtarjandi, 2019). In order to investigate the mechanisms of cytotoxicity further studies would be undertaken including ATP assay to assess mitochondrial damage, TdT-mediated dUTP-biotin nick end labelling (TUNEL) assay to assess damage to DNA (Ansari *et al*, 1993; Kumar *et al*, 2017) or Amplex red assay can be used to measure ROS production (Kumar *et al*, 2017). If BA vesicles do have appreciable cytotoxicity following long-term exposure, modifying them through coating with, for example, polyethene glycol (PEG) is an option which may reduce toxicity, as has been shown for other vesicle lipids (Peng *et al*, 2013, Sukhanova *et al*, 2018).

The results from the PrestoBlue assay demonstrate that cell viability was not compromised. Whereas the results from the apoptosis assay indicate in the higher doses that the early apoptotic population of hCMEC/D3 cells were significantly reduced in comparison with the negative (medium only) control. Both assays are testing different parameters of cell health, the apoptosis assay is measuring the level of membrane integrity through phosphatidylserine binding with annexin V (Kumar *et al*, 2017), whilst PrestoBlue determines cell viability through the reducing capabilities of the mitochondria and cytoplasm (O'Brien *et al*, 2000; Hall *et al*, 2016). However, this may also be a variation of the different assays. Unfortunately, there is a paucity of toxicity studies of BAs, making it challenging to compare results (Fariya *et al*, 2014). More studies will need to be undertaken in order to observe and monitor these potentially low levels of cytotoxicity to see if they are reproduced in future studies.

It was also noted that the astrocytes from the 7-day, but not the 24-hour, study demonstrated low cytotoxic effect to actinomycin D, similar to that observed with the endothelial cells. Actinomycin D is a DNA intercalator which leads to the inhibition of transcription. However, it is apparent that there is lower apoptosis after 7 days exposure compared to 24 hours. One possible explanation may be that the astrocytes had recovered after the initial exposure to actinomycin D. Brodská *et al* (2016) observed the EC50 of actinomycin D decrease over a 48-hour period in leukaemia cell lines CML-T1, OCI-AML3 and HL-60. This may be a similar effect observed in this study.

3.5.2 Uptake kinetics

PI encapsulated vesicles have been taken up and released their payload in a range of different cell lines demonstrating that BA vesicles are a candidate for drug delivery. Thus, demonstrating that BA vesicles are released in different cell lines and across different species. PI encapsulated vesicles were observed to release their cargo in both human cell lines, SH-SY5Y and HEK-293T, as well as murine microglia cells, BV2, within 24 hours. Although only qualitative, PI release is appreciable in both HEK-293T and BV2 cell lines. Although present, there is considerably less uptake and less binding of PI to RNA and DNA in SHSY5Y cells than in HEK and BV2 cell lines. BV2 microglia are highly enzymatically active due to the presence of their lysosomes (Wu *et al*, 2013). Microglial lysosomes contain lipases, proteases and nucleases enabling them to perform their protective and degradative role, engulfing and destroying foreign substances and necrotic cells (Liu *et al*, 2007). HEK cells also express high enzymatic activity due to their role in excretion and removal of waste (Robinson and Goochee, 1991). This may account for the marked uptake in these two cell lines. The uptake kinetics may also be driven by the cell types used as was investigated and observed using pancreatic tumorigenic cell lines (Korang-Yeboah *et al*, 2015). This may be a further explanation for the diverse kinetics observed in the different cell types.

PI is unable to penetrate the cell membrane and bind to its target, RNA and DNA. PI should not be seen in any of the controls, as is the case with the HEK and SH-SY5Ycells. However, there is appreciable DNA binding observed with both controls for the BV2 and LN229. It has been observed that phospholipid membrane turnover

is a measurement of tumour proliferation which may explain the PI uptake observed in glioblastoma cells, LN229 (Podo *et al*, 1999). Macropinocytosis is the internalisation or invagination of plasma membrane and extracellular fluid through vesicle formation called macropinosomes (Lim and Gleeson, 2011; Ha *et al*, 2016; Palm, 2019). Macropinocytosis is an endocytic pathway which is over expressed in glioblastoma (Ha *et al*, 2016). Macropinocytosis was shown to invaginate a particle of 300 nm in size (Tan *et al*, 2013). However, this was observed in Chinese hamster ovarian cancer (CHO) cells and although not investigated, cell type may be a factor that influences parameters such as flexibility of macropinosomes as well as expression of macropinocytosis. Thus, indicating that we may see different expression in different cell lines which appears the case for cancer and macrophages (Ha *et al*, 2016; Solé-Domènech *et al*, 2016). While membrane turnover may be occurring for LN229 cells, it does not explain the penetration and binding for the murine microglial cell line, BV2. In order to survey the extracellular environment macrophages highly express the endocytic pathway macropinocytosis from harmful materials (Ha *et al*, 2016; Solé-Domènech *et al*, 2016). Perhaps microglia monitor their extracellular environment through macropinocytosis which may explain the uptake of PI, through non-selective macropinocytosis (Yin *et al*, 2017).

3.5.3 Distribution pattern and clearance

BA vesicles have also demonstrated the ability to cross the BBB in murine model, indicating the ability of the vesicles to be used as a drug delivery system to treat diseases of the brain. The mechanism by which the vesicles are able to traverse to the brain is not yet known. Despite the limited delivery mechanisms to transport molecules across the BECs into the brain, there are possible pathways. One hypothesis may be that the cells are taken up via pinocytosis, as mentioned above (section 3.5.2) (Tan *et al*, 2013). Interestingly, clathrin-mediated transport was observed as the main route of transcytosis for nanoparticles of a similar size and zeta potential as our vesicles (Neves *et al*, 2016). Thus, indicating receptor mediated transport as a potential route of transport.

As the vesicles have crossed the BBB it is important to investigate their potential as a drug delivery system *in vivo*. It is important to explore the biodistribution of the

vesicles within the brain tissue to elucidate where the vesicles are located and potential pathways to enhance delivery and targeting. As a result, the original study should be reprised, and the use of immunohistochemistry performed to determine the localisation and distribution of the BA vesicles *in vivo*. The antibodies used would include anti-glial fibrillary acidic protein (GFAP) for astrocytes, for endothelium anti-platelet endothelial cell adhesion molecule (PECAM-1 or CD31) and a primary antibody specific for microglia is anti-ionised calcium binding adaptor molecule 1 (Iba-1) (Singh-Bains *et al*, 2019). Nonetheless, in the absence of such results, it may be hypothesised that the vesicles are taken up by the microglial and macrophages, acting as the immune cells of the CNS (Gustafson *et al*, 2015). If this is found to be the case, then this could be a useful target for future treatment for neurological diseases. Activated microglial and macrophages are linked to the progression of a number of neurodegenerative diseases including AD, PD and glioblastomas (Zhang *et al*, 2016, Sørensen *et al*, 2018). There is increasing evidence that tumour-associated microglia and macrophages (TAMs) have an integral role in the microenvironment of the glioblastoma, reportedly constituting approximately 30% of the tumour (Li and Graeber, 2012; Sørensen *et al*, 2018). The tumours influence the TAMs to develop a distinct phenotype to support the progression of the tumour (Charles *et al*, 2011; Li and Graeber, 2012; Sørensen *et al*, 2018). Tumours with high TAMs appear to correlate with lower survival rates (Elechalawar *et al*, 2019), suggesting that targeting TAMs may be a viable treatment approach.

The distribution of the vesicles indicates high clearance via the lungs for both the encapsulated AF546 vesicles and non-encapsulated AF546. It has been reported that rapid clearance of cationic liposomes occurs by the lungs, liver and spleen (Thurston *et al*; 1998). As a result of the high vascularisation of the lungs, this distribution of the vesicles is expected. Our vesicles were also transported to the liver. Popov *et al* (2010) observed that 60 minutes after intravenous administration of cationic BA vesicles in mice, the liver displayed the highest value of radiolabelled vesicles. In a further study investigating the distribution of cationic BA vesicles, the kidneys were the organ expressing the highest clearance (Popov *et al*, 2012). However, this was not observed for either our encapsulated AF546 vesicles or free AF546.

3.5.4 Limitations

As one of the main aims was to encapsulate different cargoes it was important to investigate the potential of our vesicles to encapsulate not only tracer dyes but the antibody fragment scFv 4D5-8RFP. A limitation of this study is the concentration of the antibody fragment included in the original formulation (4.6 μM). Whilst this was a proof of concept study, increasing the concentration is a factor to investigate in future experiments. Therefore, it may appear that the signal of the antibody fragments was directly proportional to the concentration. Overall, the fluorescence of the RFP is thought to be several orders of magnitude lower than that of the Alexa Fluor (Siegel *et al*, 2013). Future studies will employ conjugation of AF546 to the antibody fragment to increase the fluorescent signal as well as increasing the concentration of the antibody fragments added to the material. It will also be paramount to reprise the viability and immunogenic assays with the antibody fragment encapsulated vesicles.

Whilst our study followed the recommendation by Monteiro-Riviera, Inman and Zhang (2009) as they suggest two or more independent studies to test for cytotoxicity, there were discrepancies in our *in vitro* findings. Further metabolic screening should be carried out in order to determine how the BA vesicles behave *in vitro*. Therefore, it is suggested to investigate the bioenergetic function of BA vesicles by measuring reactive oxygen species (ROS) production using, for example, the Amplex red assay (Kumar *et al*, 2017). Whilst *in vitro* testing was focused on the main cell types that we wanted to target for delivery to the brain, the cytotoxic response may differ in cells *in vivo*. Ideally *in vitro* studies would be performed on primary cell lines, which are more representative of *in vivo* conditions due to their sensitivity to environmental changes (Dusinska *et al*, 2017). However, due to the high throughput of immortalised cell lines this offers a more standardised platform, as well as cost effectiveness (Dusinska *et al*, 2017; Kumar *et al*, 2017). Such assays do not provide information regarding the mechanism/s of cell death (Adan *et al*, 2016).

The clinical dose of our BA vesicles is unknown and is very much dependent upon the dose of the drug that they encapsulate. Therefore, this is also very much dependent upon the encapsulation efficiency, which was very low (see section

2.4.9). At higher doses, based on the apoptosis assay results for hCMEC/D3 cells, the BA vesicle formulation may be toxic. However, the dose would be dependent upon the drug encapsulated within the vesicle as well as the encapsulation efficiency. It is also imperative to investigate and test the level of toxicity of BA vesicles encapsulated with therapeutic against the same dose of the drug alone.

In vivo toxicity was not explored. As *in vivo* testing will be systemic there are a number of other factors/parameters influencing the vesicles that may influence the effect of the BA vesicles that have not and need to be investigated (Dusinska *et al*, 2017). In particular, toxicity studies are recommended through the collection and examining of blood composition to investigate changes after exposure to vesicles (Marquis *et al*, 2009; Love *et al*, 2012; Winter *et al*, 2015). Changes can be compared to negative controls or pre-treatment samples (Marquis *et al*, 2009). Similarly, immunogenicity testing can be carried out, screening for increase in release of cytokines and chemokines (Marquis *et al*, 2009).

Our BA vesicles have not been formulated for a specific target. Whilst the initial studies were to investigate the uptake in biological barriers and then, *in vivo*, the potential as a drug delivery system to cross the BBB. They must be designed to be target specific, as this is a fundamental principle of development of a drug delivery system (Puri *et al*, 2009). One potential option is using a PEGylated folic acid compound (see section 3.5.5).

Whilst we know that the vesicles are opened, as observed in the release kinetics studies, we do not know the mechanism by which cargo is released. Other studies have demonstrated that their vesicles were designed with a release mechanism, the vesicles release their cargo in the presence of acetylcholinesterase due to the addition of acetylcholine head groups in the BA formulation (Popov *et al*, 2010; Dakwar *et al*, 2012; Popov *et al*, 2013). This is a fundamental parameter in the release kinetics, as it will determine not only release but target specificity of the vesicles. Puri *et al* (2009) suggest that creating a defect in the structure of the vesicles may trigger release of cargo either internally, enzymatic release or changes in pH, or externally, such as heat. Our vesicles may be pH sensitive and therefore, lysed within the lysosome of cells. However, this will need further investigation (section 3.5.5)

It is important to investigate how the BA vesicles are transported across cellular membranes, specifically the BBB. The mechanism by which the vesicles are endocytosed, for example clathrin-mediated endocytosis or caveolae- mediated transport, may influence their ability to transcytose (Salatin and Khosroushahi, 2017; Villaseñor *et al*, 2019). It is important to understand the mechanisms by which the drug delivery system traverses biological barriers to determine the pharmacokinetics and pharmacodynamics.

3.5.5 Future studies

As the efficacy of a chemotherapeutic is governed by its ability to penetrate the BBB rather than its efficacy to treat the tumour, there is a current focus on improving delivery, concentration and uptake of combinations of current chemotherapeutics (Pardridge, 2001; Ananda *et al*, 2011; Pinto *et al*, 2017).

One aspect which is imperative to investigate is the transport mechanism the vesicles use in order to penetrate the BBB. It is hypothesised that the mechanism by which the anionic vesicles are able to cross the cellular membrane is due to the caveolae mediated transport, by virtue of their lipid composition (Voigt, Christensen and Shastri, 2014). Voigt, Christensen and Shastri (2014) hypothesised that the interaction between the receptor and ligand was influenced by the hydrophobic and electrostatic interactions. They applied this to their highly anionic particles that they hypothesised were able to cross the cell membranes based on their high lipid content and, therefore, high affinity for lipid membranes, as well as the anionic surface charge of the nanoparticles which was believed to counteract the charge between the cell membrane and the particles. Therefore, this may explain how our anionic vesicles penetrated the mouse BBB.

As Voigt, Christensen and Shastri (2014) observed uptake of particles of a similar size and charge as our vesicles via caveolae mediated transport, this may be the mechanism by which our BA vesicles are able to cross the BBB. However, the size of caveolae, approximately 70 nm, indicates that this may not be likely (Bastini and Parton, 2010). A further confounding challenge may be the lower expression of caveolae-mediated transporters on BECs than other peripheral endothelial cells (Huang *et al*, 2018). However, in the BBTB increased expression of caveolae is observed (Zhan and Lu, 2012).

It has been observed that clathrin mediated transport was the mechanism utilised by lipid nanoparticles, produced with cetyl palmitate, to transcytose Caco-2 cells (Neves *et al*, 2016). As these nanoparticles are of a similar size and charge to our vesicles, it may be that our vesicles transcytose via the same pathway. As a result, all routes of entry should be explored by inhibiting each pathway with different concentrations of inhibitors to ensure that the dose is not lethal, but that it is able to exert its effect.

In order to carry out such studies this experiment may benefit from being tested using an *in vitro* BBB such as the static transwell plates or a dynamic flow system such as Kirkstall system. The inhibitor methyl-β-cyclodextrin has been recommended a suitable inhibitor for caveolae mediated transport (Ivanov, 2008) as it is involved in the extraction of cholesterol from the plasma membrane (Zidovetzki and Levitan, 2007). Amiloride or cytochalasin D are inhibitors of macropinocytosis (Ivanov, 2008). Amiloride acts as a Na^+/H^+ inhibitor reducing pH of the cytosol (Recouvreux and Commisso, 2017), whereas cytochalasin D inhibits polymerisation of actin (Dutta and Donaldson, 2012). Chloropromazine is a specific inhibitor of clathrin-mediate endocytosis (Ivanov, 2008) as it prevents the function of AP2 proteins, specific to formation of clathrin vesicles, as well as the sequestering of clathrin receptors and AP2 in endosomes preventing the recycling of clathrin to the membrane surface (Francia *et al*, 2019).

In order to investigate the intracellular behaviour of the BA vesicles further studies involving lysotracker should be employed (Wu *et al*, 2013). To further investigate the endocytic/transcytotic pathway of the BA vesicles, lysotracker will be encapsulated in the lumen of the BA vesicles, during the synthesising process. Lysotracker encapsulated vesicles will be incubated with confluent BV2s, the cell type representative of the microglia. The BA vesicles would be tracked and imaged continuously over a 24-hour time period, as from previous experimental work the vesicles appear to have been lysed well within this time frame.

It is important to investigate all routes of excretion in order to calculate the true clearance values. Future *in vivo* work would include the collection of urine and stools as well as blood to measure the fluorescence, alongside the homogenised tissue samples to investigate the overall fluorescence of all samples collected to

investigate more comprehensively the pathways and level of clearance. In this current study these samples were not collected. Therefore, this study should be reprised.

It would be pertinent to test the BA vesicles as a drug delivery system to treat diseases of the brain. It is suggested that the study would be reprised accompanying an animal model of CNS disease, such as 5xFAD as an AD mouse model (Jankowsky *et al*, 2017) or GL261 murine model (Oh *et al*, 2014). It is important to explore the distribution of the vesicles within the brain tissue to elucidate where the vesicles are located and potential pathways to enhance delivery and targeting (Sanavio *et al*, 2018).

Future work includes investigating the targeting of the vesicles in the brain. One potential route of exploration could be the inclusion of PEGylated folic acid during the synthesis of BA vesicles as suggested (Chapter 2, section 2.6). PEGylation is the addition of polyethylene glycol during the vesicle synthesis step in order to increase delivery to specific cells (Suk *et al*, 2016). PEGylation has been observed to reduce rapid clearance due to increased half-life resulting in increased circulation time (Zhang *et al*, 2016; Zhang, Mintzer and Uhrich, 2016). It has also been observed to reduce opsonisation but also reduce uptake in activated microglia (Papa *et al*, 2014). However, the lipid nanoparticles used in this study were PEGylated and the formulation was conjugated with folic acid. The high expression of the folate receptor (FR) in diseased brain suggests it may be used as a target in the delivery of therapeutics (Kamaly *et al*, 2009; Low, Henne and Doorneweerd, 2007; Pourgholi *et al*, 2016). Particularly as the folate receptor is not highly expressed in normal healthy cells (Low, Henne and Doorneweerd, 2007). As hypothesised, the vesicles may be taken up by the microglia. Therefore, in the diseased state these cells, referred to as TAMs, would be a potential target as they account for approximately 30% of the tumour mass (Søresen *et al*, 2018; Li and Graeber, 2012). The folate receptor is found in many isoforms including β which is expressed on TAMs of cancers such as liver, kidney, skin and glioblastoma (Elechalawar *et al*, 2019). This system has been used in a similar way, with a folate tagged PEGylated liposome in the imaging of ovarian tumours with a 4-fold increase in uptake within two hours (Kamaly *et al*, 2009). Therefore, the folate receptor may be used as a TAM-specific target, enabling delivery of BA vesicles

tagged with folate and encapsulating therapeutics to TAMs as part of the tumour microenvironment.

Kulkami and Feng (2013) investigated the effects of size and surface modification of nanoparticles and found nanoparticles smaller than 200 nm and coated with D-α-tocopheryl polyetheylene gycol 1,000 succinate (TPGS) appeared to avoid opsonisation. Therefore, surface modification may be a further factor to investigate to avoid first pass metabolism and improve targeting.

The route of administration in our *in vivo* study investigated intravenous administration. However, the route of delivery may influence the biodistribution of lipid nanoparticles (Chenthamara *et al*, 2019). Perhaps other non-invasive routes such as inhalation through intranasal administration, which also avoids first pass metabolism but is hypothesised to bypass the BBB and directly enter the brain via the trigeminal nerve, may influence the efficacy and delivery of the BA vesicles (Furtado *et al*, 2018; Chenthamara *et al*, 2019).

3.6 Conclusion

The BA vesicles used in our study have been shown to be non-toxic at low doses and do not influence cell viability. They do not induce an immunogenic response *in vitro*. Our BA vesicles have been observed to be lysed *in vitro* in different cell lines representative of the body as well as the diseased brain. They have also been shown to encapsulate cargoes of differing sizes from tracer dyes, such as AF546 and propidium iodide to larger fluorescently tagged antibody fragment scFv 4D5-8RFP. AF546 encapsulated vesicles have demonstrated the ability to cross the BBB. The BA vesicles used to cross the BBB were originally thought to be cationic GLH-20 vesicles. However, the zeta potential demonstrated that our BA vesicles are not only anionic but also novel. Therefore, demonstrating that our novel vesicles have the potential to be used as a drug delivery system to use to treat disease of the brain.

Chapter 4

4.1 Introduction

The initial studies of vesicles made with our preparation of GLH-20 from vernonia oil revealed that they possessed a negative zeta potential. Further investigation of these novel bolaamphiphilic (BA) vesicles in previous chapters, has shown them to be stable and to be taken up in a number of cell lines. They do not induce apoptosis or cause inflammation and are able to cross the BBB *in vivo* after 30 minutes. These vesicles are not the GLH-20 as they are anionic as demonstrated by the negative zeta potential. This highlights that the vesicles developed here are novel. Therefore, analysis will need to be undertaken to investigate what these vesicles are so that they can be reproducibly produced in the future as part of a potential brain delivery system.

Produced from the oil of the African sunflower, *Vernonia galamensis*, GLH-20 vesicles have shown the potential to cross the BBB. Vernonia oil has a high epoxide acid concentration (78%) making it attractive in comparison to other similar fatty acid oils, such as soybean and linseed, comprised of linoleic acid (Carlson *et al*, 1981; Grinberg *et al*, 1994). Vernolic acid, the single chain fatty acid of vernonia oil, is an attractive alternative to linoleic acid, due to its viscous properties (Grinberg *et al*, 1994). It is used in industry to provide stability, flexibility and durability in particular as a coating for steel plates (Carlson *et al*, 1981; Grinberg *et al*, 1994). BA compounds, synthesised from vernolic acid, can form a mono-layered membrane in the form of a raft, that when disrupted forms vesicles. BAs have been used in numerous applications and have been suggested as a drug delivery system (Dakwar *et al*, 2012; Kim *et al*, 2013; Gupta *et al*, 2015). Bors and Erdő (2019) suggest that cationic liposomes are more suitable drug delivery systems due to more effective interactions with biological barriers demonstrating enhanced uptake.

Anionic vesicles have been shown to cross the BBB in rats in low concentrations (Lockman *et al*, 2004). Highly anionic lipid nanoparticles are suggested to traverse the BBB despite the high charge of the nanoparticle, as the polarity of the BBB effectively cancels out the charge, thereby enabling the lipophilic interaction between the cell membrane and the nanoparticle (Voigt, Christensen and Shastri,

2014). These authors believe that the physiochemical modification facilitates the transcytosis of the particle through caveolae-mediated transport.

Grinberg *et al* (2008) synthesised cationic BA vesicles from vernonia oil. It appears that this study has, created a novel vesicle based on the synthesis of GLH-20 vesicles using vernonia oil (figure 4.1). The original synthesis of our BA vesicles followed a similar experimental procedure to Grinberg *at al* (2008). However, our vesicles were found to have a negative zeta potential. In order to understand this difference, high resolution mass spectrometry (HRMS) of the original material was performed. The analysis was then used to design a method to recreate and synthesise the vesicles used in the previous chapters. The newly synthesised vesicles were then characterised to ensure that they displayed the same physiochemical properties as the BA vesicles in the earlier part of this study.

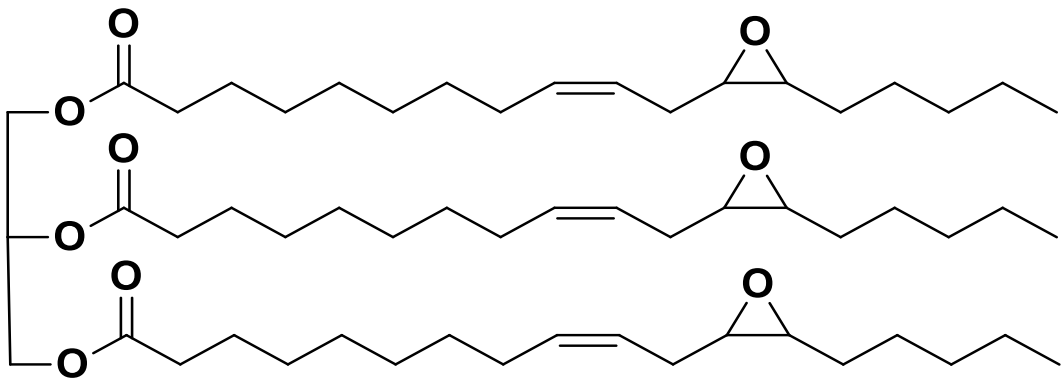

Figure 4.1. Schematic representation of vernonia oil. Starting material for the synthesis of GLH-20 vesicles shown to penetrate the BBB.

4.2 Aims:

1. To determine the material used for the synthesis of the original novel anionic BA vesicles from chapter 2 and 3

2. To develop a robust methodology for producing and purifying BA vesicles synthesised from vernonia oil to be used as a novel drug delivery system (DDS).

4.3 Experimental Procedures

4.3.1 Materials

Table 4.1 The list of materials and their suppliers used throughout chapter 4.

MATERIALS	SUPPLIER	ADDRESS
Candida Antarctica lipase B (CALB) (Novozym 435) (catalog # 06-3123)	Strem Chemicals	Newtown, Cambridge, UK
EtOH (catalog # 20821.330DP)	VWR Chemicals	Leicestershire, UK
Cholesterol (catalog # C8667), cholesteryl hemisuccinate (catalog # C6512)	Sigma Aldrich	Irvine, UK
acetic acid (catalog # 1038490), 1,10 decanediol (catalog # 10403515), chloroform (catalog # C2432), methanol (catalog # 10675112), propidium iodide (catalog # BMS500PI)	Thermo Fisher Scientific	Loughborough, Leicestershire, UK
Alexa Fluor 546 (catalog # A10237)	Invitrogen	Renfrewshire Scotland
PBS (catalog # BE17-516F)	Lonza	Slough, UK
Toluene (catalog # 108331), diethyl ether (catalog # 309966), chloroacetic acid (catalog # 800412), silica powder (catalog # S5130), thionyl chloride (catalog # 320536).	MERCK- Sigma Aldrich	Darmstadt, Germany
trimethyltin hydroxide (catalog # 71167.03), petroleum ether (catalog # 42085.K7), ethyl acetate (catalog # 22912.K2), dichloromethane (catalog # L13089 AP), tetrabutylammonium fluoride (catalog # L13303.09), anhydrous $MgSO_4$ (catalog # 33337.36)	Alfa Aesar- Fischer Scientific	Heysham, Lancashire, UK

4.3.2 General Procedures

Reactions employing air and/or moisture-sensitive reagents were performed under an atmosphere of nitrogen (unless otherwise specified) in flame-dried apparatus. Anhydrous reagents were handled under nitrogen using standard techniques.

Room temperature varied between 19-25°C. “Removed at reduced pressure” refers to the use of a rotary evaporator with the water bath temperature generally not exceeding 40°C.

4.3.2.1 Nuclear magnetic resonance

Nuclear magnetic resonance (NMR) was performed through Key Organics. The protocol used is outlines below.

Proton (^{1}H), carbon (^{13}C) and fluorine (^{19}F) nuclear magnetic resonance (NMR) spectra were recorded on a Bruker Avance 300 spectrometer operating at 300.1 MHz for ^{1}H, 75.5 MHz for ^{13}C and 282 MHz for ^{19}F, Bruker Avance II 400 operating at 400.1 MHz for ^{1}H and 100 MHz for ^{13}C. Chemical shifts were recorded at δ values in parts per million (ppm). Spectra were acquired in $CDCl_3$, DMSO-d_6, CD_3OD, acetone-d_6 or deuterium oxide at ambient temperature unless otherwise specified. For ^{1}H and ^{13}C NMR spectra recorded in $CDCl_3$, DMSO-d_6, CD_3OD and deuterium oxide, the peak due to residual $CDCl_3$ (7.27 ppm for ^{1}H, 77.00 ppm for ^{13}C), DMSO-d_6 (2.5 ppm for ^{1}H, 39.5 ppm for ^{13}C), CD3OD (3.31, 4.79 ppm for ^{1}H, 49 ppm for ^{13}C) or water (4.72 ppm for ^{1}H) was used as the internal reference. H NMR data are reported as follows: chemical shift (δ), relative integral, multiplicity (defined as: s = singlet, d = doublet, t = triplet, q = quartet, m = multiplet, bs = broad singlet), coupling constant(s) *J* (Hz), assignment.

4.3.2.2 High resolution mass spectrometry

High resolution mass spectrometry (HRMS) was performed by Dr Emmanuel Samuel at UCL. The protocol is outlined. HRMS was recorded on a Waters Micromass, LCT to Time of Flight mass spectrometer, coupled to a Waters 2975 HPLC. Chemical ionisation (CI) was recorded on a Waters Micromass GCT Time of Flight mass spectrometer. The parent ion (M, [M+H], [M+Na], [M+Acn+Na] or [M-H]) is quoted, followed by significant fragments with relative intensities.

4.3.2.3 Analytical thin layer chromatography

Analytical thin layer chromatography (TLC) was conducted on Merck pre-coated (25 μm) silical gel 60F_{254} plates or on aluminium-backed 0.2 mm thick silical gel 60 F_{254} plates (Merck) and the plates were visualised by treatment with either Seebach's 'magic' stain dip or alkaline potassium permanganate dip, followed by heating with a heat gun. The retention factor (Rf) quoted is rounded to the nearest 0.01. Flash chromatography was conducted using silica gel 60F_{254} as the stationary phase and the solvent indicated.

4.3.3 Synthesis of dichloroacetate diepoxystearate

This is a three-step procedure. The first step is the production of 6,7-epoxy stearic acid (i, figure 4.2), followed by the production of decane diepoxystearate (ii, figure 4.2) and finally the dichloroacetate diepoxy stearate (iii, figure 4.2).

A solution of vernonia oil in MeOH/H_2O was treated with NaOH at room temperature for 1 h. Due to non-specific opening of the epoxide this method was no longer used.

A mixture of vernonia oil and trimethyltin hydroxide in 1,2-dichloroethane was stirred at 80°C for 24 h (Nicolaou *et al*, 2005) to afford 6,7-epoxy stearic acid. 6,7-epoxy stearic acid was refluxed with 1,10 decanediol, *Candida antarctica* lipase B (CALB) (Novozym 435) in toluene for 24 h at 110°C to give decane diepoxystearate. Decane diepoxystearate and chloroacetic acid in toluene was heated at 85°C for 48 h to afford dichloroacetate diepoxystearate (Grinberg *et al*, 2008; Stern *et al*, 2014).

*4.3.3.1 **6,7-epoxy stearic acid*** (Nicolaou *et al*, 2005) (i, figure 4.2)

(Yield 88%). R_f 0.4 (pet ether: EtOAc, 60:40); *m/z* (ES^+) 296 [$(M+H)^+$], 100%. The data (figure 4.9) were in good agreement with the literature values (Grinberg ***et al***, 2005).

*4.3.3.2 **Decane diepoxystearate*** (Grinberg *et al,* 2008) (ii, figure 4.2)

(Yield 50%). R_f 0.4 (pet ether: Et_2O, 70:30); *m/z* (ES^+) 731.6190 [$(M+H)^+$]

4.3.3.3 Dichloroacetate diepoxystearate (Grinberg *et al*, 2008; Stern *et al*, 2014). (iii, figure 4.2)

(Yield 15%). R_f 0.4 (pet ether: Et_2O, 70:30); *m/z* (ES^-) 917.6098 [(M-H)-]

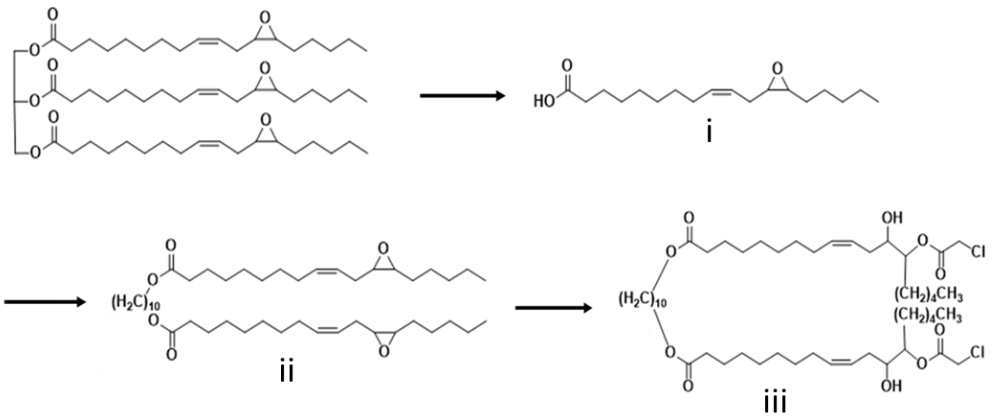

Figure 4.2. Schematic representation of the synthesis of dichloroacetate diepoxystearate. The starting material, vernonia oil, is used to produce step 1 6,7-epoxy stearic acid (i). The next step is the production of decane diepoxystearate (ii) and the final step produces dichloroacetate diepoxystearate (iii).

4.3.4 Diepoxystearate tetrol

The production of diepoxystearate was initially produced following the protocol for dichloroacetate diepoxystearate (section 4.3.3). This was later improved upon due to yield.

4.3.4.1 First attempt diepoxystearate tetrol

As following the protocol for dichloroacetate diepoxystearate the first two steps were produced (section 4.3.3.1 and 4.3.3.2). Decane diepoxystearate was suspended with distilled water was refluxed at 60°C for 9 days (Wang *et al*,2007). However, this reaction did not occur. Therefore, the protocol was improved.

4.3.4.2 Second attempt diepoxystearate tetrol

Hydrolysis of the esters has been followed and produced (section 4.3.3.1).

6,7-epoxy stearic acid was suspended with NaOH, dH_2O and MeOH and refluxed at 60°C for 24 h to afford 6,7-diol stearic acid (iv, figure 4.3). 6,7-diol steric acid was refluxed with 1,10 decanediol, *Candida antarctica* lipase B (CALB) (Novozym 435) in toluene for 24 h at 110°C to give diepoxystearate tetrol (v, figure 4.3). TET01 vesicles were synthesised from this final formulation.

4.3.4.2.1 6,7-diol stearic acid (iv, figure 4.3)

(Yield 31%). R_f 0.4 (pet ether: Et_2O, 80:20); *m/z* (ES^+) 313.45 [$(M+H)^+$].

4.3.4.2.2 Diepoxystearate tetrol (Grinberg *et al*, 2008) (v, figure 4.3)

(Yield 4.8%). R_f 0.4 (pet ether: Et_2O, 70:30); *m/z* (ES^+) 831.6177 [$(M+Acn+Na)^+$]

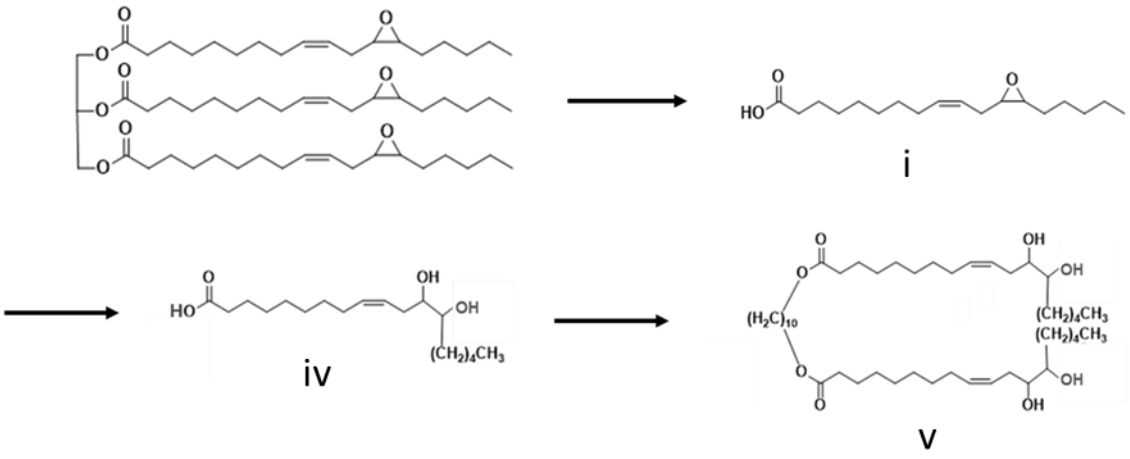

Figure 4.3. Schematic representation of the synthesis of diepoxystearate tetrol. The starting material, vernonia oil, is used to produce step 1 6,7-epoxy stearic acid (i). The next step is the production of 6,7-diol stearic acid (iv). The final step results in the production of the compound diepoxystearate tetrol with a low yield of 4.8% of the original material. Hence, this technique was optimised to improve and increase the overall yield.

4.3.4.3 Final attempt diepoxystearate tetrol

Hydrolysis of the esters has been followed and produced (section 4.3.3.1).

6,7-epoxy stearic acid was suspended with trifluoroacetic acid (TFA), tetrahydrofuran (THF) and dH_2O and stirred at room temperature for 48 h (Cory *et al*, 1990) to afford gave 6,7-diol stearic acid. 6.7-diol stearic acid was refluxed with *tert*-butyldimethylsilyl chloride (TBSCl), imidazole, 4-dimethylaminopyridine (DMAP) and dimethylformamide (DMF) for 24 hours at 80°C. to give 6,7-(tert-butyldimethylsilyl ether) stearic acid (Corey and Venkateswarlu, 1972). 6,7-(tert-butyldimethylsilyl ether) stearic acid in anhydrous dichloromethane (DCM) was added thionyl chloride at -5°C, and stirred for 1 hr at room temperature. 1,10-decanediol and stirred at room temperature for 1h to afford diester TBS intermediate. Diester TBS intermediate in THF at room temperature was added tetrabutylammonium fluoride (TBAF) afforded diepoxystearate tetrol

4.3.4.3.1 6,7-diol stearic acid (Cory *et al*, 1990)

(Yield 74%). R_f 0.4 (pet ether: Et_2O, 60:40); ***m/z*** (ES^+) 313.45 [$(M+H)^+$].

4.3.4.3.2 6,7-di(tert-butyldimethylsilyl ether) stearic acid (Corey and Venkateswarlu, 1972).

(Yield 81%). R_f 0.4 (pet ether: Et_2O, 60:40); ***m/z*** (ES^-) 541.4094 [$(M-H)^-$].

4.3.4.3.3 Diester TBS intermediate (D'Angelo and Smith, 2015)

(Yield 33%). R_f 0.4 (pet ether: Et_2O, 70:30); ***m/z*** (ES^-) 1224.9886 [$(M-H)^-$].

4.3.4.3.4 Diepoxystearate tetrol (Corey and Venkateswarlu, 1972).

(Yield 64%). R_f 0.4 (pet ether: Et_2O, 80:20); ***m/z*** (ES^+) 766.63227 [$(M+H)^+$].

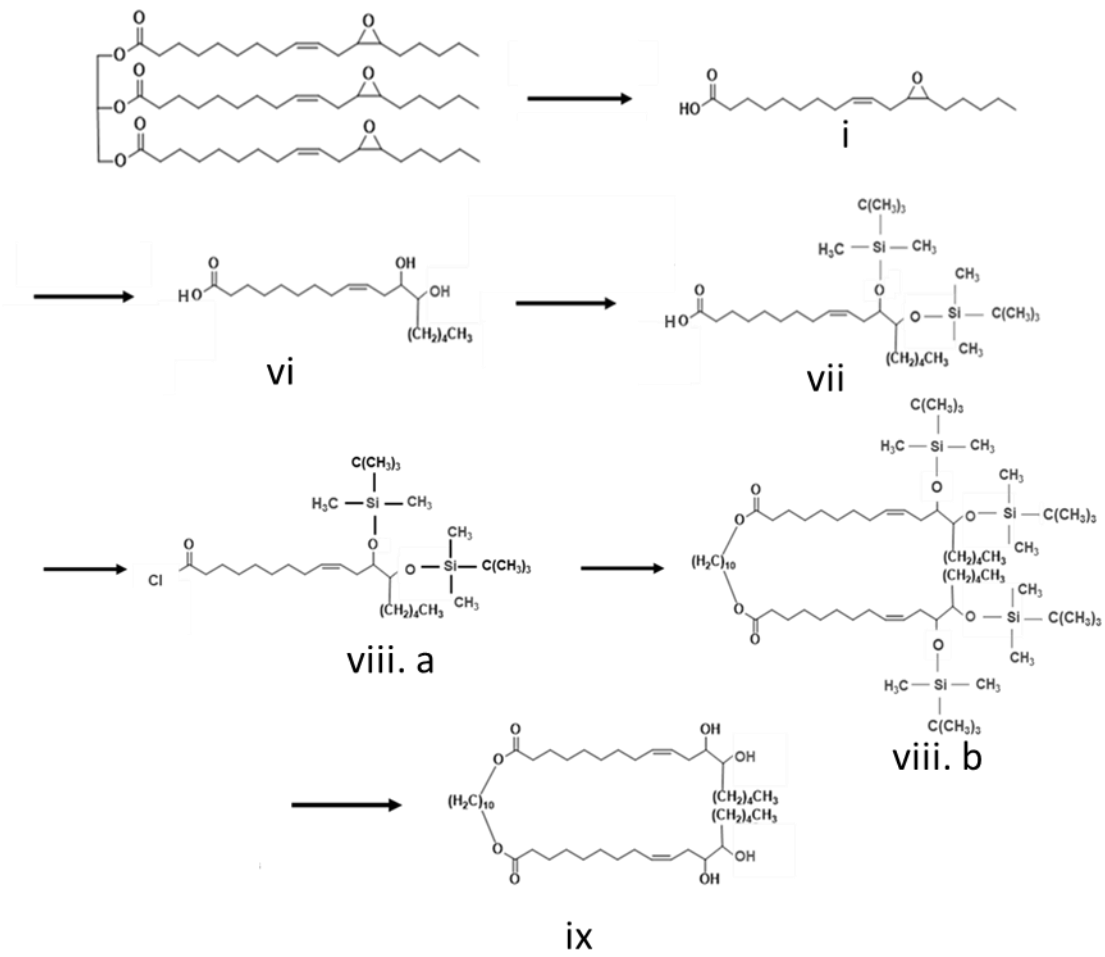

Figure 4.4. Schematic representation of the optimised synthesis of diepoxystearate tetrol. The starting material, vernonia oil, is used to produce step 1 6,7-epoxy stearic acid (i). The next step is the production of 6,7-diol stearic acid (vi). 6,7-di(tert-butyldimethylsilyl ether) stearic acid (vii) is the following product in the next synthesis step. The penultimate step is a two-step process which results in the product diester TBS intermediate (viii.a and viii.b). The final step results in the production of the compound diepoxystearate tetrol. The overall yield was improved to 64%.

4.3.5 Nanoparticle Tracking Analysis of vesicles

Nanoparticle Tracking Analysis (NTA) was performed using a NS300 NanoSight (Malvern Panalytical, Malvern, UK), configured with a sCMOS camera and a 405 nm diode laser. Samples were diluted in filter sterile, particle free PBS to ensure the number of particles were maintained with a flow rate of 20-40 particles in the field of view to maintain a concentration between 1 x 10^7-1 x 10^9 particles/ml. Camera settings were according to the manufacturer's instructions (Malvern Panalytical), recording 5 x 90 s videos per sample. Data were analysed using the NTA software (version 3.4). Triplicates of each experiment were performed.

4.4 Results

The original BA material, from chapters 2 and 3, unexpectedly produced novel anionic vesicles. They were also shown to cross the BBB. In order to determine what the novel BA vesicles were, so that we can develop a robust methodology for future synthesis, high resolution mass spectrometry (HRMS) was performed. Based on these results a new synthesis was undertaken to produce a version of the initial material from vernonia oil BA vesicles from this newly synthesised BA were characterised.

4.4.1 High resolution mass spectrometry of the original bolaamphiphilic material.

The original production of the vesicles was undertaken in 4 steps (see chapter 2, section 2.3.2). This should have resulted in vesicles with a positive zeta potential associated with the acetylcholine head group. As a result of the negative charge of these vesicles made with this material a sample of the original BA material was analysed by high resolution mass spectrometry (HRMS) to determine the molecular weight MW [M+H] (figure 4.5). Two predominant peaks were observed in the material with molecular weights of 924.7 and 767.7. Neither of these peaks are consistent with GLH-20 (chapter 2, figure 2.3), formula of $C_{58}H_{110}O_{14}N_2$, molecular weight, 1138.8572.

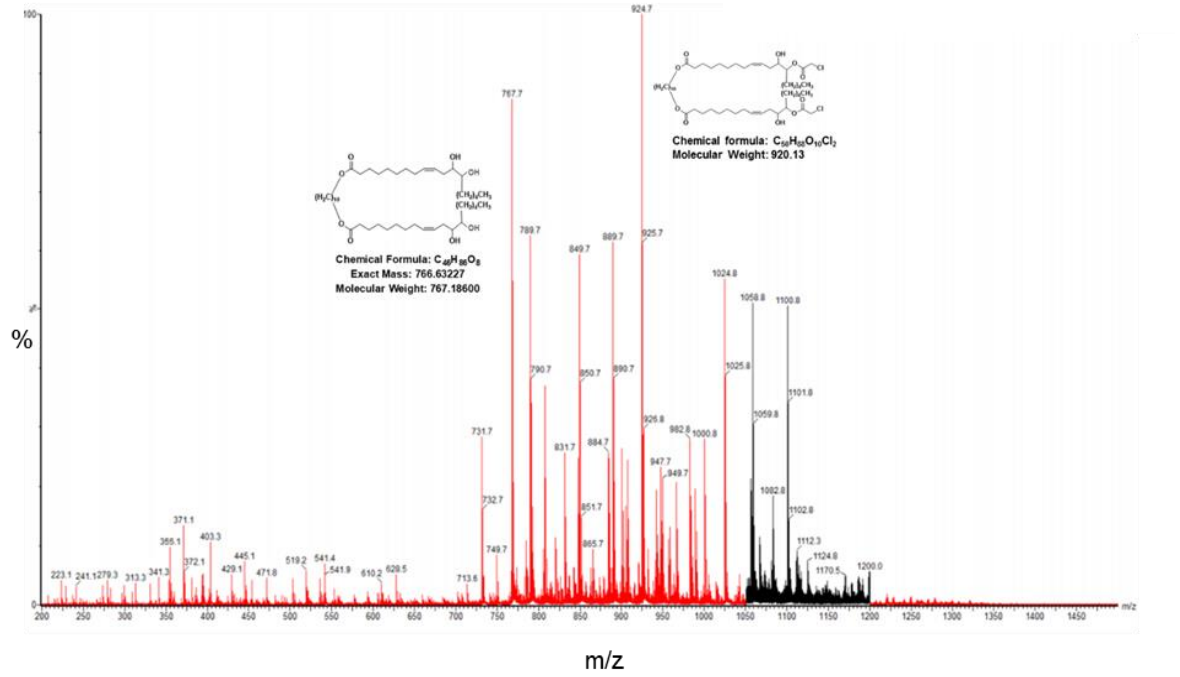

Figure 4.5 High Resolution Mass Spectrometry of the original material. The analysis revealed many compounds within the sample. However, the peaks demonstrate the relative abundance of the products and the two dominant peaks have masses of 924.7 and 767.7. From this analysis further investigations were undertaken to elucidate the nature of these species.

From analysis of the production scheme for GLH-20 the two peaks are intermediates of the GLH-20 production. The molecule with molecular weight of 924.7 is the penultimate product (dichloroacetate diepoxystearate). The other molecule (MW 767.7) is an intermediate of the product prior to dichloroacetate diepoxystearate (diepoxystearate tetrol). However, this material clearly formed vesicles that can penetrate cells. Therefore, we attempted to reprise production of this new material from vernonia oil to replicate the material found within the HRMS spectra.

4.4.2 Synthesis of novel material- FASCA01

The starting material is oil derived from *Vernonia galamensis*. The protocol used by Dr Sumi Lee and Professor Lawrence Williams (Rutgers) was followed for the initial steps. Hydrolysis of the esters is the first step followed by a coupling reaction with 1, 10-decanediol to link two of the derived fatty acids through esterification, to increase the hydrophobic chain. The stability of BA vesicles has been shown to be dependent upon the length of the hydrophobic chain (Popov *et al*, 2010). Figure 4.6 is the proposed procedure to be undertaken in order to synthesis the final product.

The analysis indicates the presence of two species (FASCA 01 and TET01). The final steps in the production included the opening of the epoxy group (figure 4.6). The purpose of this is to add polarity to the BA, consistent with the observed negative charge. Therefore, we set out to produce dichloroacetate diepoxystearate (FASCA 01) and analyse the properties.

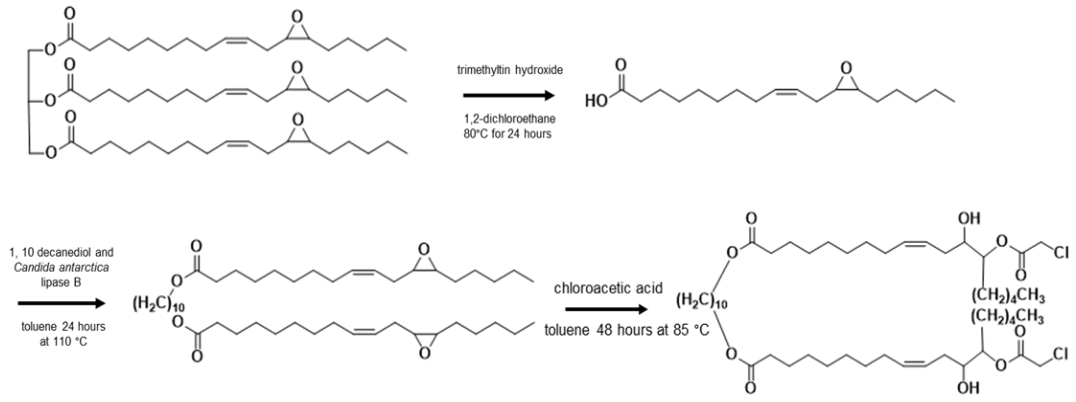

Figure 4.6. Schematic representation of the production of bolaamphiphile (FASCA 01). There are three steps involved in the production of BA; step 1; hydrolysis of the esters to produce 6,7-epoxy stearic acid, step 2; coupling of the 1,10 decanediol to link two molecules of stearic acid to produce decane diepoxystearate, step 3; opening of the epoxide through the addition of chloroacetic acid to produce dichloroacetate diepoxystearate.

4.4.2.1 Step 1-Hydrolysis of esters

1 g of vernonia oil (generously supplied by Professor Lawrence Williams), 1 g (5.5 mmol) of trimethyltin hydroxide and 50 ml of 1,2-dichloroethane was used to hydrolyse the esters of the starting material (figure 4.7). After 24 hours of reflux at 80°C, the material was cooled, and removal of solvent was performed by rotatory evaporation under vacuum. Hydrolysis was verified using thin layer chromatography (TLC), a chromatographic technique in which samples are separated on a stationary phase (a silica coated glass plate) in a mobile phase (the solvent to be used) by capillary action. The solvent employed here was petroleum ether (pet ether) (60°C – 80°C): ethyl acetate (EtOAc) in the ratio 3:2 and then analysed by staining with potassium permanganate (20 mM $KMnO_4$, 100 mM K_2CO_3, 5% w/v NaOH). Silica gel column chromatography was prepared with silica powder to purify the sample. Fractions containing the purified sample were collected and concentrated by rotatory evaporation under vacuum. The sample was

then analysed using high-resolution mass spectrometry (HRMS) and determined the molecular weight MW [M+H] 296.2351 (figure 4.8).

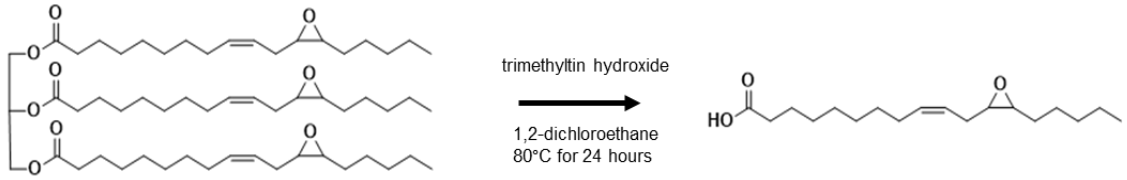

Figure 4.7. Schematic representation of the production of 6,7-epoxy stearic acid. Vernonia oil is the starting product which is hydrolysed with trimethyltin hydroxide and 1,2-dichloroethane at 80°C for 24 hours to produce 6,7-epoxy stearic acid. 6,7-epoxy stearic acid was confirmed by TLC and HRMS.

Silica gel column chromatography was used to separate and purify the products of the first hydrolysis reaction. The elution fractions were collected, and the solvent was removed for HRMS analysis (figure 4.8).

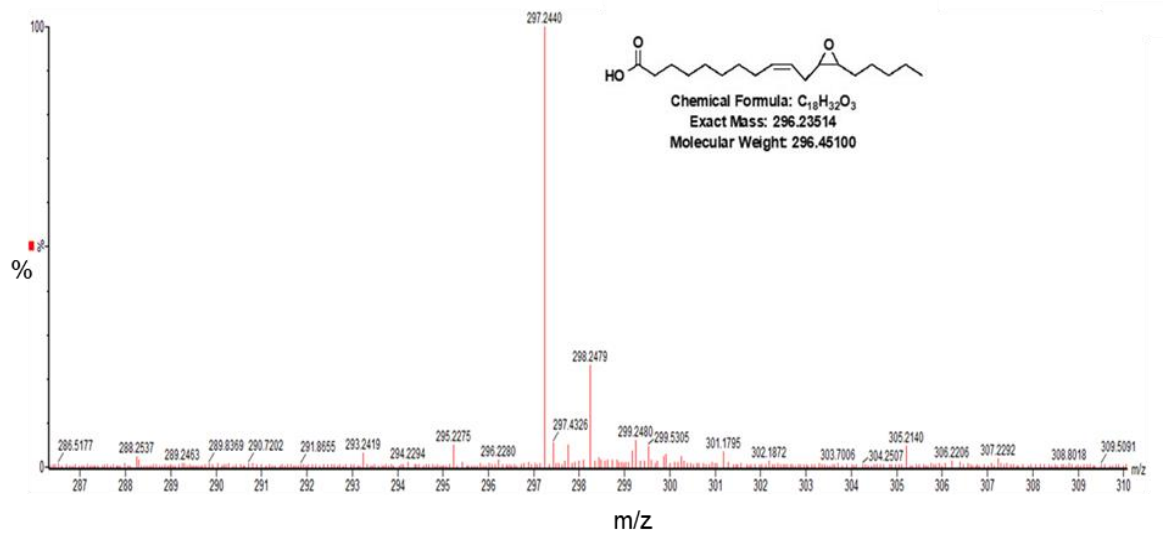

Figure 4.8. The resultant mass spectra from HRMS after the first step-hydrolysis of esters. The accurate mass measurement of product 1 was confirmed as 296.2351, chemical formula $C_{18}H_{32}O_3$.

The results from HRMS demonstrates that the hydrolysis of the starting material gave rise to the product 6,7-epoxy stearic acid. This was supported by the greatest peak demonstrating the relative abundance of this molecule in the sample.

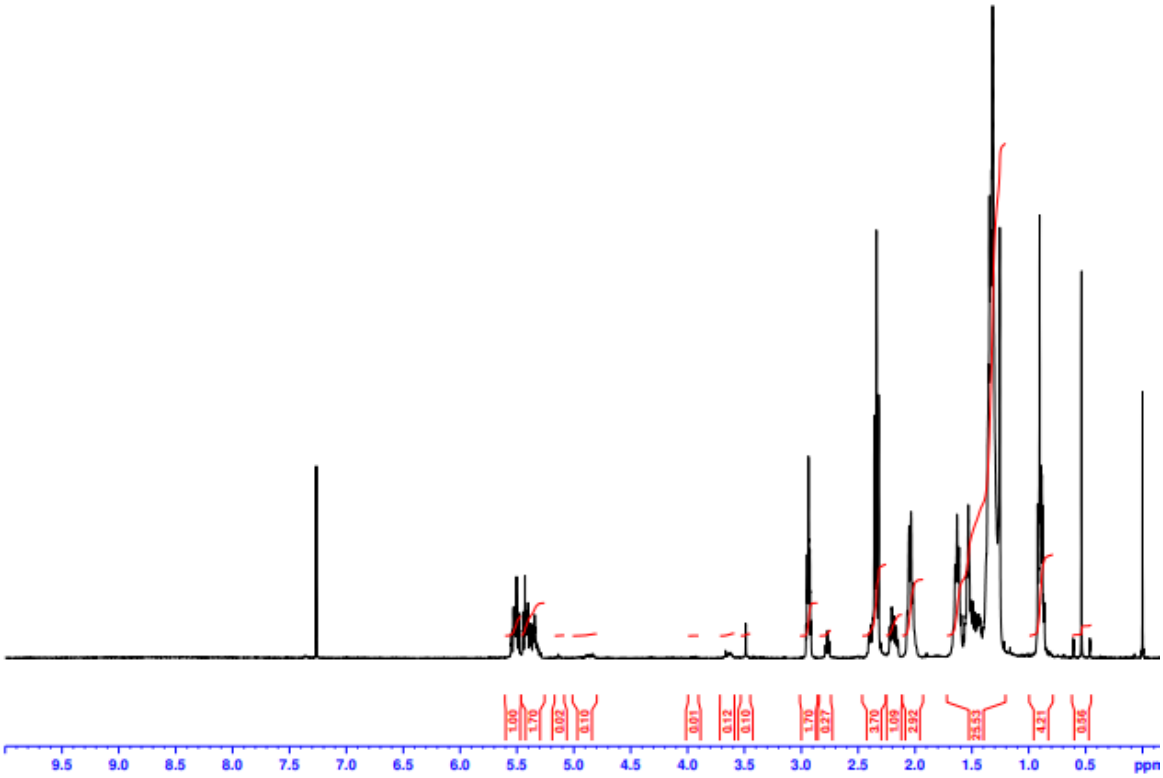

Figure 4.9. Proton NMR spectra of 6,7-epoxy stearic acid. Our analysis is in accordance with the literature.

NMR analysis of 6,7-epoxy stearic acid also supports the literature (Grinberg *et al*, 2005) (figure 4.9).

4.4.2.1.1 Step 2-Synthesis of decane diepoxystearate

0.55 g (1.85 mmol) of 6,7-epoxy stearic acid (product of step 1) was refluxed with 0.162 g (0.93 mmol) 1,10 decanediol, 0.0143 g of *Candida antarctica* lipase B (CALB) (Novozym 435) in 60 ml toluene with azeotropic distillation for 24 hours at 110°C (figure 4.10). Azeotropic distillation is a technique used to distil solutions that share a similar boiling point proving challenging to separate. Two distillation tubes are employed, one for dehydration and the other for separation of the solvent selected to purify the two samples, by altering the temperature, from the final product. Once the material had cooled to room temperature the lipase was filtered off. The solvent was removed by rotary evaporation under vacuum. In order to precipitate the product 70 ml of methanol was added to the cooled mixture and incubated overnight at 4°C. This was filtered and washed with cooled methanol. TLC was performed (using a mobile phase of 7:3 pet ether: Et_2O for a more accurate and less polar separation) and the TLC was stained with $KMnO_4$. The

sample was then analysed using high-resolution mass spectrometry (HRMS) and determined the molecular weight MW [M+H] 731.6190 (figure 4.11).

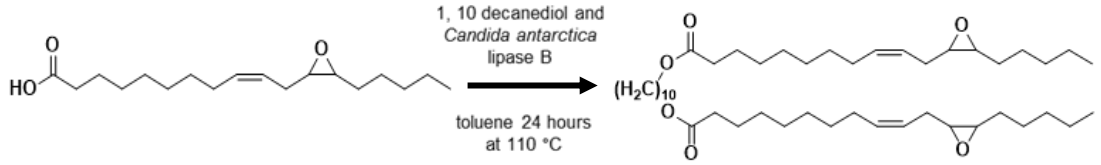

Figure 4.10. Schematic representation of the production of decane diepoxystearate. 6,7-epoxy stearic acid with 1, 10 decanediol, *Candida antarctica* lipase B and toluene was refluxed for 24 hours at 110°C. Decane diepoxystearate production was confirmed by HRMS.

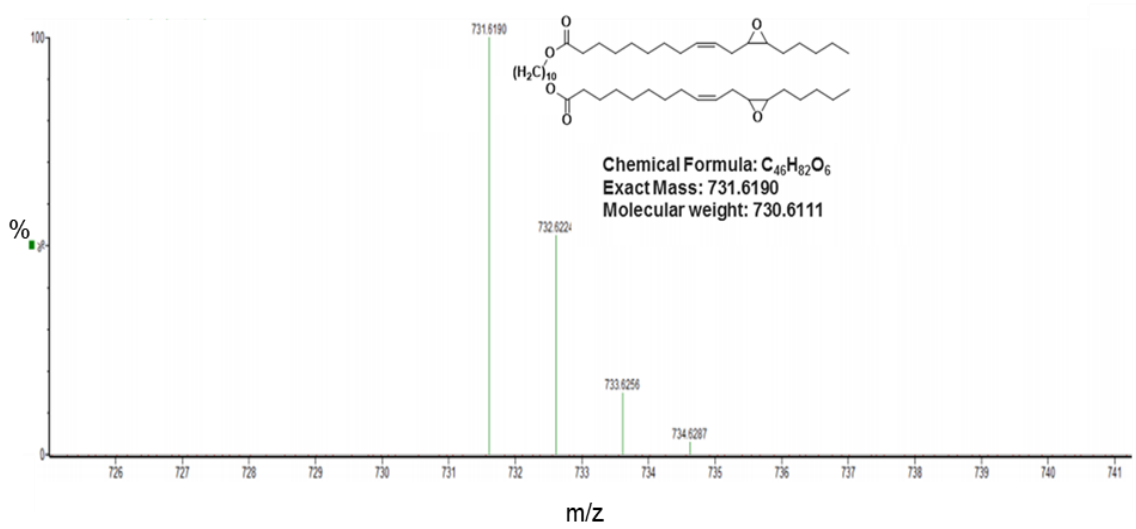

Figure 4.11. The resultant mass spectra from HRMS after the second step-coupling reaction. The accurate mass measurement of decane diepoxystearate was confirmed as 731.6190, chemical formula $C_{44}H_{78}O_6$.

Decane diepoxystearate is the intermediate that is required in order to produce the products of both predominant peaks from the HRMS analysis (figure 4.5).

4.4.2.1.2 Synthesis of dichloroacetate diepoxystearate

0.25 g of decane diepoxystearate (0.342 mmol) and 0.454 g of chloroacetic acid in 25 ml toluene was heated at 85°C for 48 hours (figure 4.12). The mixture was cooled, and a further 150 ml of toluene was added. The reaction mixture was washed with 6% (w/v) sodium bicarbonate solution ($NaHCO_3$) and then water. A separating flask was used to separate the aqueous from the organic phase. The organic phase was collected and dried out over anhydrous magnesium sulphate ($MgSO_4$) and filtered. The solvent was removed using a rotary evaporator under

vacuum. TLC was performed using a mobile phase of 7:3 pet ether: Et_2O and the staining with $KMnO_4$.

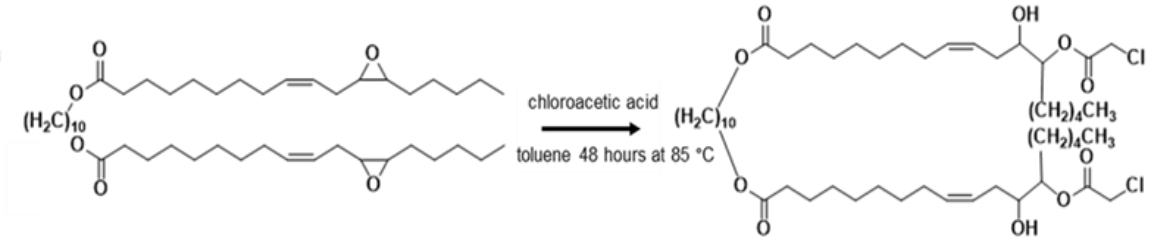

Figure 4.12. Schematic representation of the final product dichloroacetate diepoxystearate. FACSA 01 (dichloroacetate diepoxystearate) was produced from the heating of decane diepoxystearate, chloroacetic acid and toluene for 48 hours at 85°C. This was further separated, dried out and filtered before removing the solvent from the final product.

HRMS (figure 4.13) confirmed the addition of chloroacetic acid to decane diepoxystearate to produce dichloroacetate diepoxystearate (FACSA 01) as determined by the molecular weight MW [M-H]- as 917.6098.

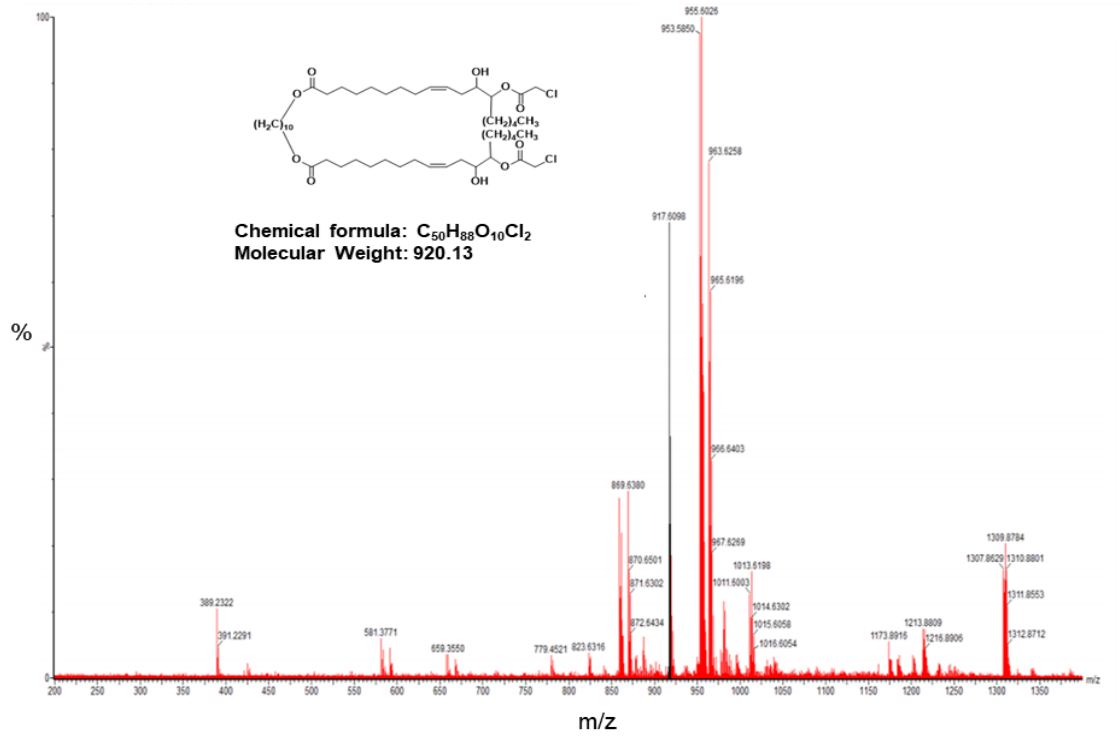

Figure 4.13. The resultant mass spectra from HRMS of the final product FACSA 01 (dichloroacetate diepoxystearate). The HRMS measurement of the final product was confirmed in negative mode [M-H]- as 917.6098, chemical formula $C_{50}H_{88}O_{10}Cl_2$.

4.4.3 Synthesis of novel material- TET01

The initial reaction, hydrolysis of the esters, has been maintained throughout the optimisation steps (section 4.4.2.1.). This method produced vesicles though the yield of bola material was low and the production time lengthy (figure 4.14).

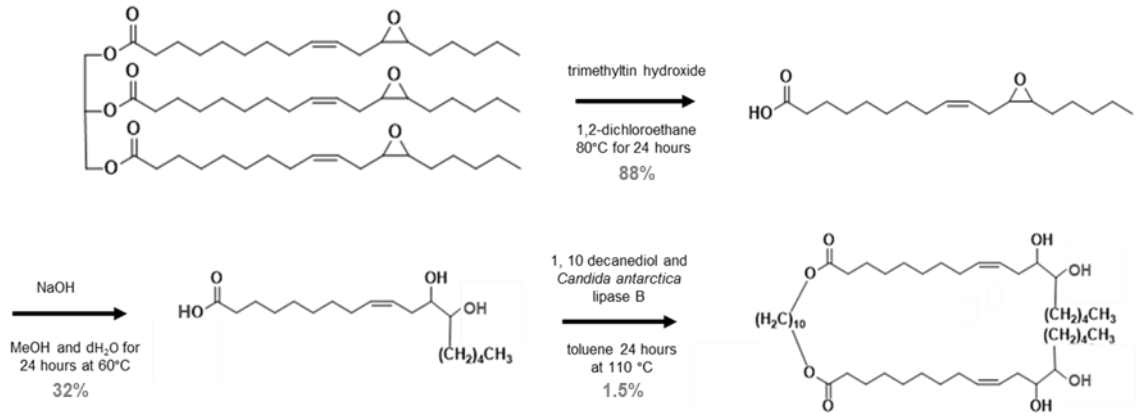

Figure 4.14. Schematic representation of the production of novel bolaamphiphile TET01. There are three steps involved in the production of BAs; step 1; hydrolysis of the esters, step 2; opening of the epoxide ring, step 3; coupling of 1,10 decanediol to link molecules of the ester diol.

4.4.3.1 Step 2- Formation of ester diol (6,7-diol stearic acid).

0.7435 g (2.5 mmol) 6,7-epoxy stearic acid was suspended with 0.3 g (7.5 mmol) NaOH, 10 ml dH_2O and 20 ml MeOH in a 50 mL flask, refluxed at 60°C (figure 4.15) and monitored by TLC for 24 hours using Seebach's 'magic' stain to identify the final product. After completion, the mixture was washed with 6% w/v $NaHCO_3$ solution and then water, dried over $MgSO_4$, and then filtered to give the crude product. Purification by silica gel column chromatography resolved the final product. TLC was performed using a mobile phase of 4:1 pet ether: Et_2O and the TLC was stained with Seebach's 'magic' stain.

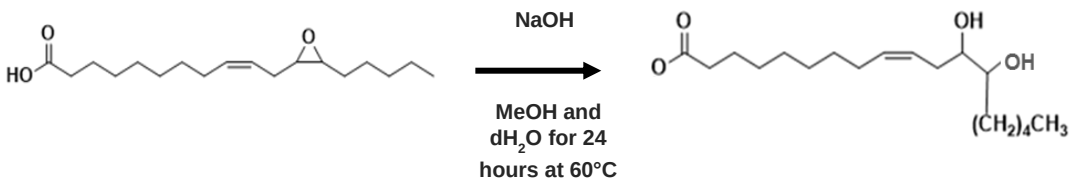

Figure 4.15. Schematic representation of the production of 6,7-epoxy stearic acid. Opening of the epoxide ring of 6,7-epoxy stearic acid was performed by the addition of potassium hydroxide and methanol for 72 hours at 60°C.

The sample was then analysed using high-resolution mass spectrometry (HRMS) and determined the molecular weight MW [M+H] 313.45, chemical formula $C_{18}H_{33}O_4$ (figure 4.16).

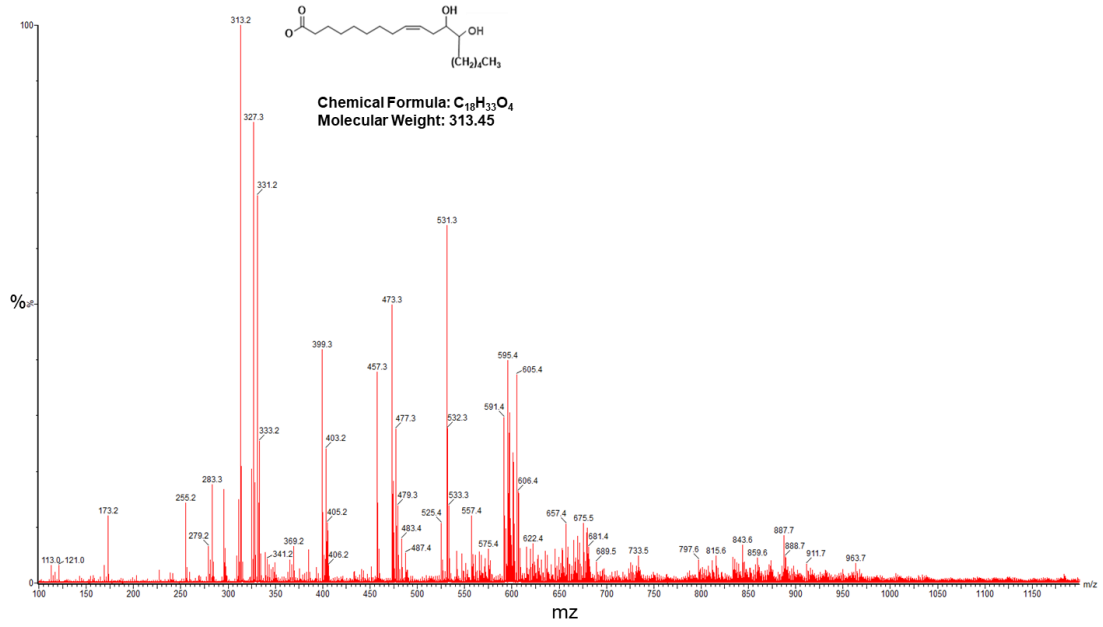

Figure 4.16. The resultant mass spectra from HRMS after the second step- opening of the epoxide ring. The accurate mass measurement of product 2, 6,7-diol stearic acid, was confirmed as 313.45, chemical formula $C_{18}H_{33}O_4$.

4.4.3.2 Final step- Coupling of 6,7-diol stearic acid molecules to 1,10 decanediol forming diepoxystearate tetrol.

0.3197 g (1.018 mmol) of 6,7-diol stearic acid (product of step 2) was refluxed with 0.09 g (0.517 mmol) 1,10 decanediol, 0.14 g of *Candida antarctica* lipase B (CALB) (Novozym 435) in 60 ml toluene with azeotropic distillation for 24 hours at 110°C (figure 4.17) as performed for the synthesis of decane diepoxystearate (section 4.4.2.1.1). The lipase was filtered off once the material had cooled to room temperature. The solvent was removed by rotary evaporation under vacuum. 70 ml of methanol was added to the cooled mixture to precipitate the product and incubated overnight at 4°C. This was filtered and washed with cooled methanol. Purification by silica gel column chromatography resolved the final product, diepoxystearate tetrol. TLC was performed using a mobile phase of 7:3 pet ether: Et_2O and the TLC was stained with Seebach's 'magic' stain.

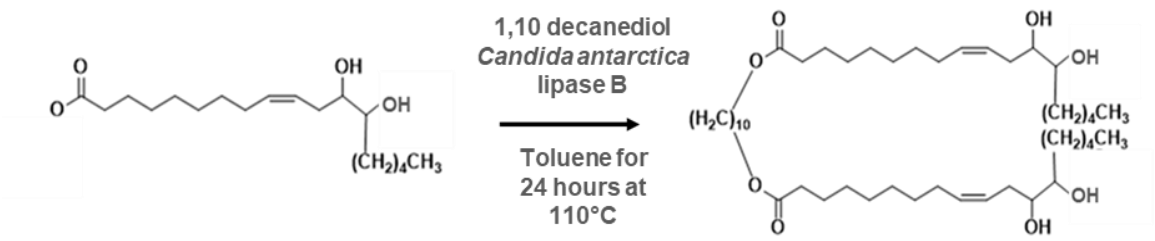

Figure 4.17. Schematic representation of the production of final product diepoxystearate tetrol. Diepoxystearate tetrol was produced from the coupling of 6,7-diol stearic acid, with 1,10 decanediol in the presence of catalyst *Candida antarctica* lipase B and toluene for 24 hours at 110°C. The product was confirmed by TLC and HRMS. This was purified through silica gel column chromatography.

The sample was then analysed using high-resolution mass spectrometry (HRMS) and determined by the molecular weight [M+Acn+Na]+ as 831.6177 (figure 4.18).

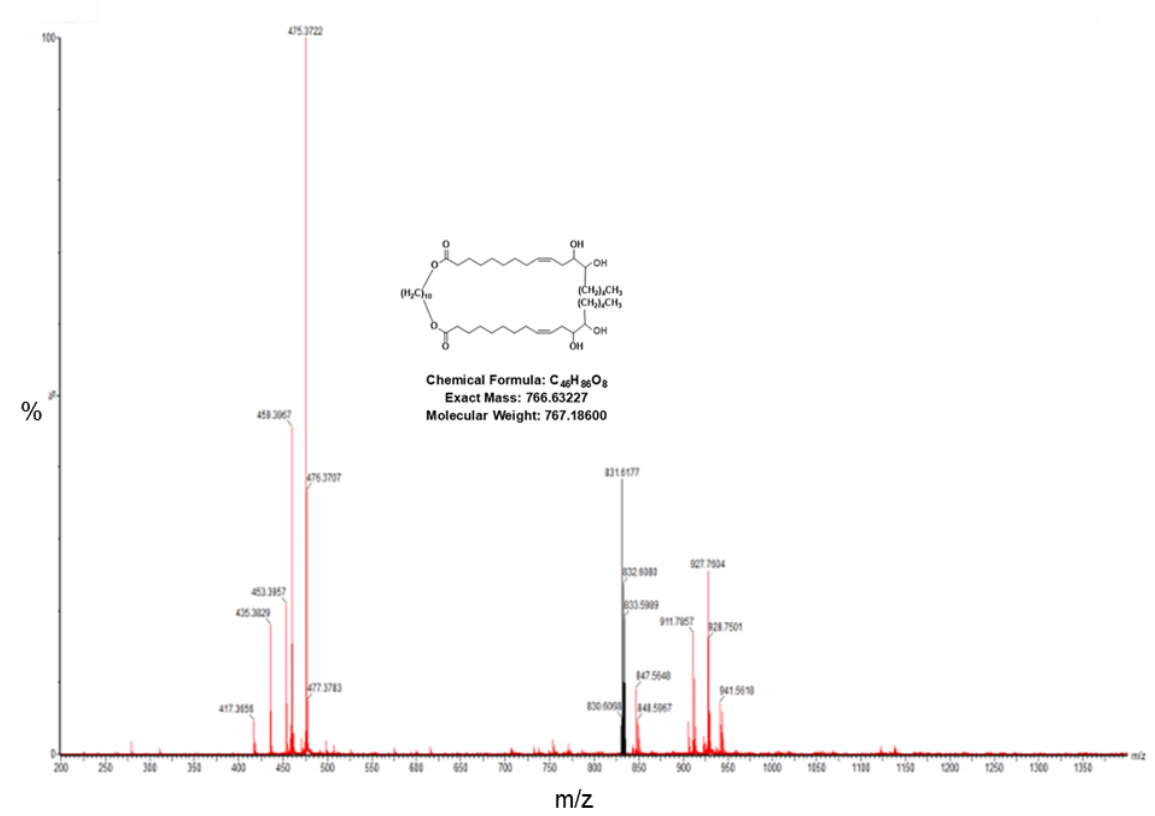

Figure 4.18. The resultant mass spectra from HRMS after the final step-synthesis of TET01 (diepoxystearate tetrol). The HRMS measurement of diepoxystearate was confirmed, peak in black, in positive mode [M+Acn+Na]+ as 831.6177, chemical formula $C_{46}H_{86}O_8$.

The yield was too low (4.8%). Therefore, a new technique was devised in order to increase yield. Vesicles were produced from this final synthesis and were characterised and analysed, as discussed further.

4.4.4 Optimisation of synthesis of novel material- TET01

Attempts were undertaken to improve yield and production time of the TET01 bola material. The protection of the hydroxyl groups initially with trimethylsilyl ethers and then *tert*-butyldimethylsilyl ethers was investigated (figure 4.19). The protection of the hydroxyl groups is designed to reduce potential non-specific interactions as well as increase the yield of the bola material.

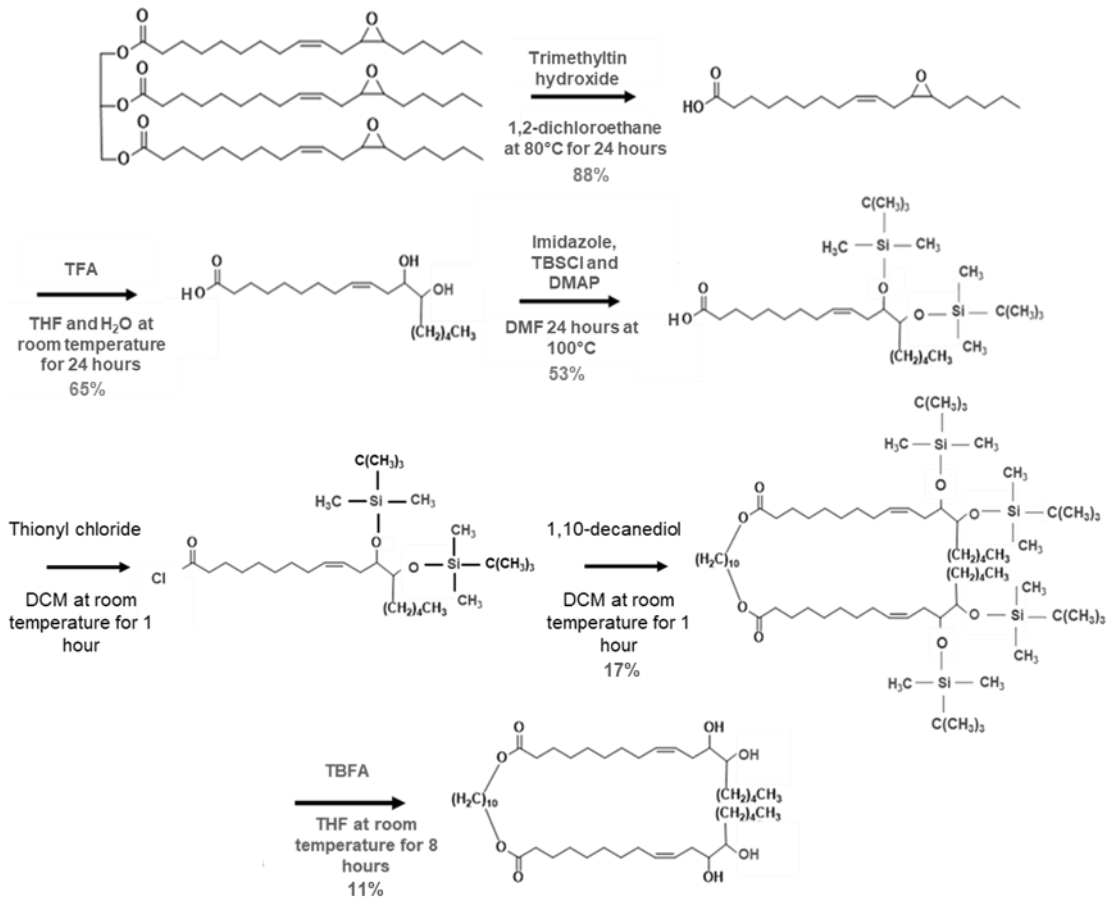

Figure 4.19. Schematic representation of the production of novel TET01 bolaamphiphile. There are three steps involved in the production of novel BA TET01, step 1; hydrolysis of the esters, step 2; opening of the epoxide ring, step 3; protecting the hydroxyl groups with tert-butyldimethylsilyl chloride (TBS-Cl), step 4a and 4b; 2 step reaction, first the formation of a chloride acid, followed by the coupling of 1,10 decanediol to extend the carbon chain, step 5; removal of TBS to produce diepoxystearate tetrol

4.4.4.1 Step 2- Formation of ester diol (6,7-diol stearic acid)

0.4465 g (1.508 mmol) 6,7-epoxy stearic acid was suspended in 100 µl trifluoroacetic acid (TFA), tetrahydrofuran (THF) (3 ml) and dH_2O (3 ml), mixed and

monitored by TLC for 48 hours at room temperature (figure 4.20). The eluent system used was pet ether: Et_2O (3:2), and Seebach's 'magic' stain. The mixture was washed with dH_2O and Et_2O and acidified with the addition of 1 M HCl (10 ml) to pH 3.8. The organic phase was dried over $MgSO_4$ and filtered to give the 6,7-diol stearic acid. The final yield was measured at 74%. This is an improvement over the 31% yield of the original synthesis.

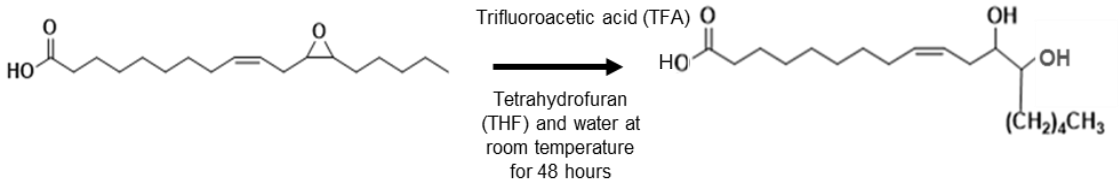

Figure 4.20. Schematic representation of the optimised production of 6,7-diol stearic acid. Opening of the epoxide ring of 6,7-epoxy stearic acid was performed by the addition of trifluoroacetic acid (TFA) as the reactant, tetrahydrofuran (THF) as the solvent and water at room temperature. 6,7-diol stearic acid was confirmed by TLC and HRMS. The chemical formula of the new product, 6,7-diol stearic acid, is $C_{18}H_{33}O_4$ with a molecular weight of 313.45.

The sample was then analysed using high-resolution mass spectrometry (HRMS) and determined the molecular weight MW [M+H] 313.3, chemical formula $C_{18}H_{33}O_4$ (figure 4.21).

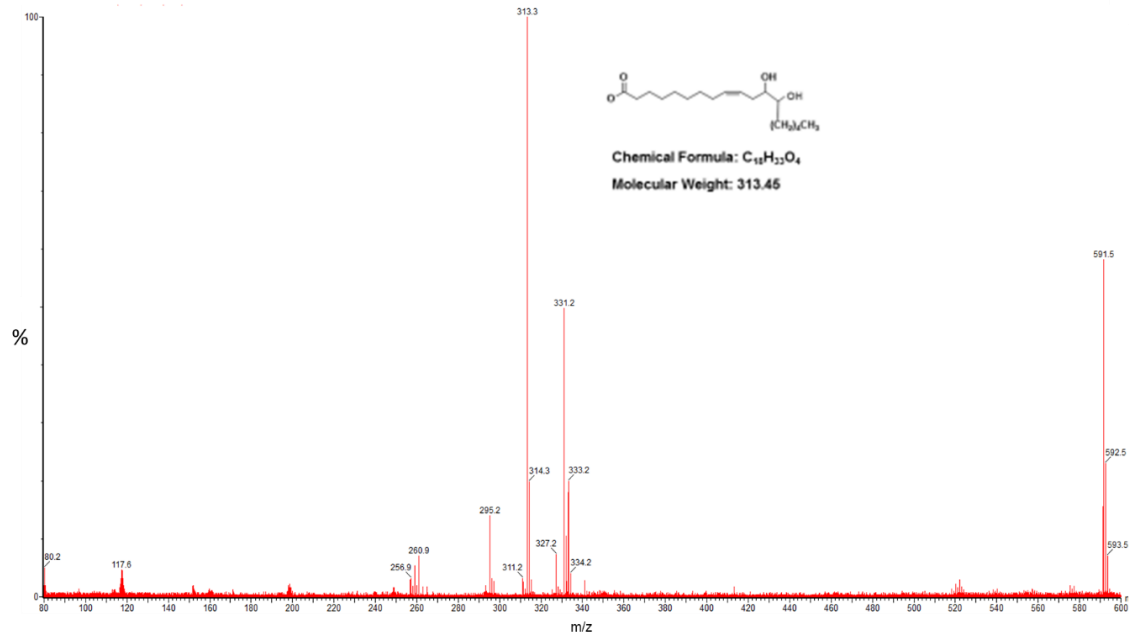

Figure 4.21. The resultant mass spectra from HRMS after the opening of the epoxide groups. The accurate mass measurement of product 6,7-diol stearic acid was confirmed, highest peak, as 313.3, chemical formula $C_{18}H_{33}O_4$

4.4.4.2 Step 3- Formation of 6,7-di(tert-butyldimethylsilyl ether) stearic acid

0.0354 g (0.1127 mmol) of 6,7-diol stearic acid was refluxed with 0.1 g (0.6635 mmol) *tert*-butyldimethylsilyl chloride (TBSCl) and 0.06 g (0.8814 mmol) imidazole in the presence of catalyst 0.025 g (0.2049 mmol) 4-dimethylaminopyridine (DMAP) and 50 ml dimethylformamide (DMF) for 24 hours at 80°C (figure 4.22). The reaction was monitored by TLC using eluent system pet ether: Et_2O (3:2), and Seebach's 'magic' stain to identify the final product. After completion, the mixture was washed with Et_2O and then water. Of the separated phases the organic phase was washed three times with Et_2O, dried over $MgSO_4$, and then filtered to give the crude product. Purification by silica gel column chromatography resolved the final product 6,7-*di(tert*-butyldimethylsilyl ether) stearic acid. Toluene was added prior to rotary evaporation to the purified mixture in order to aid removal of DMF.

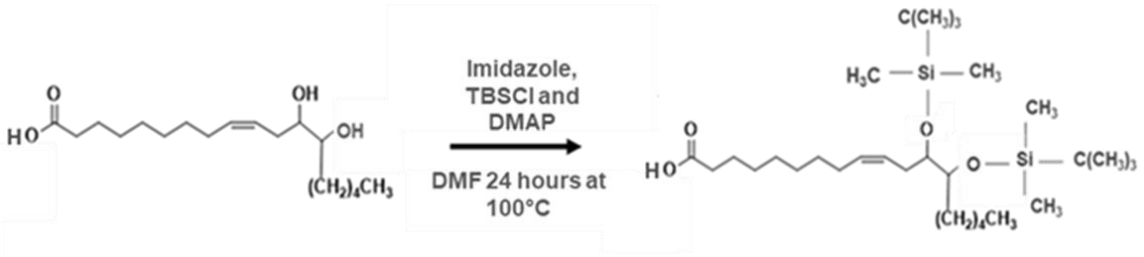

Figure 4.22. **Schematic representation of the production of 6,7-*di(tert*-butyldimethylsilyl ether) stearic acid.** 6,7-*di(tert*-butyldimethylsilyl ether) stearic acid was produced from the addition of *tert*-butyldimethylsilyl chloride and imidazole in the presence of catalyst 4-Dimethylaminopyridine (DMAP) and Dimethylformamide (DMF) 24 hours at 100°C. The product was confirmed by TLC and HRMS. This was further separated, dried out and filtered before removing the solvent from the final product.

The sample was then analysed using high-resolution mass spectrometry (HRMS) and determined the molecular weight MW [M-H]-541.4094, chemical formula $C_{18}H_{33}O_4$ (figure 4.23).

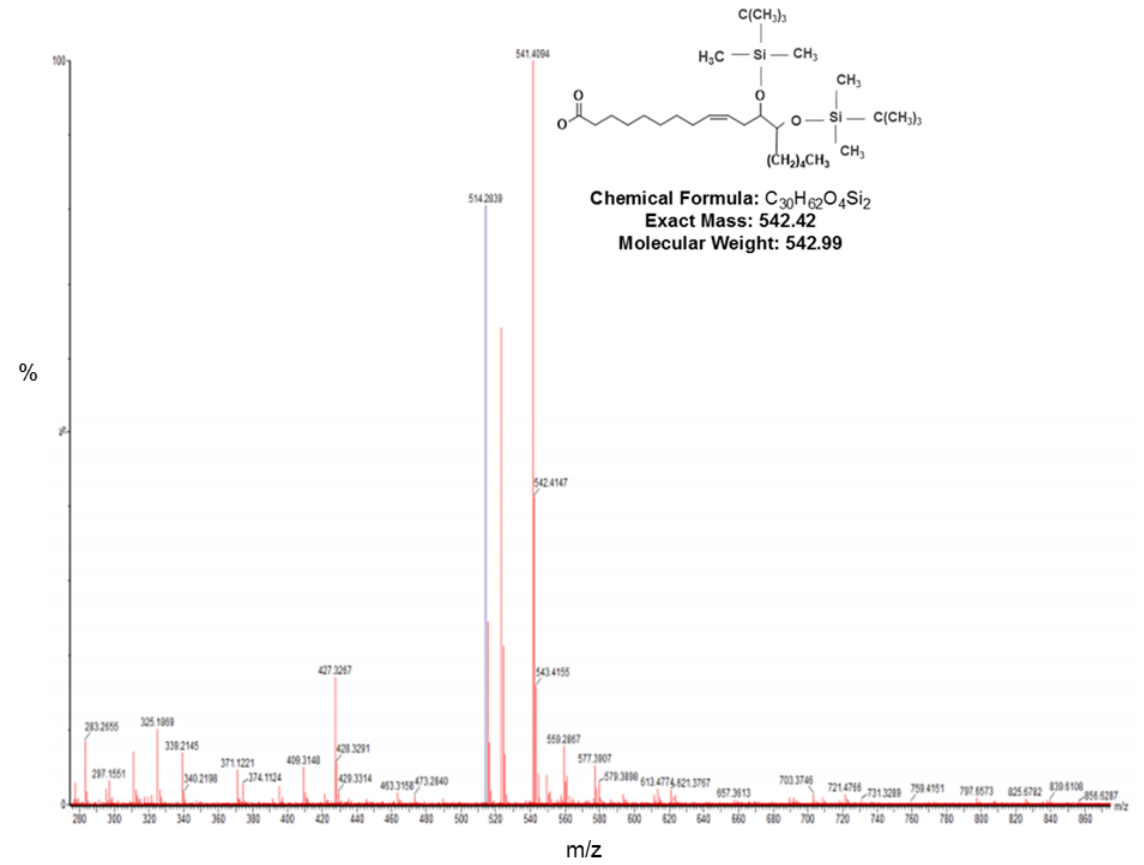

Figure 4.23. The resultant mass spectra from HRMS after the silyation of the epoxide groups. The accurate mass measurement of product 6,7-*di(tert*-butyldimethylsilyl ether) stearic acid was confirmed, highest peak, as 545.42, chemical formula $C_{24}H_{50}O_4Si_2$.

4.4.4.3 Step 4- Synthesis of diester TBS intermediate

0.2635 g of diester TBS intermediate (0.5749 mmol), was refluxed in anhydrous dichloromethane (DCM) was added thionyl chloride (0.10 ml) at -5°C. After stirring for 1 hour at room temperature, all starting material had dissolved. DCM and unreacted thionyl chloride were removed under reduced pressure. The product was redissolved in DCM (5 ml) under N_2 at 0°C. Next, 0.035 g 1,10-decanediol (0.20 mmol) was added. The reaction mixture was stirred at room temperature for 1h and was then quenched by the slow addition of ice cold $NaHCO_3$ solution and extracted with 50 ml EtOAc. The aqueous and organic phases were dried with $MgSO_4$ and the solvents removed under reduced pressure (figure 4.24). The resultant residue was purified by silica gel column chromatography, eluting with pet ether: Et_2O (7:3) to give diester TBS intermediate

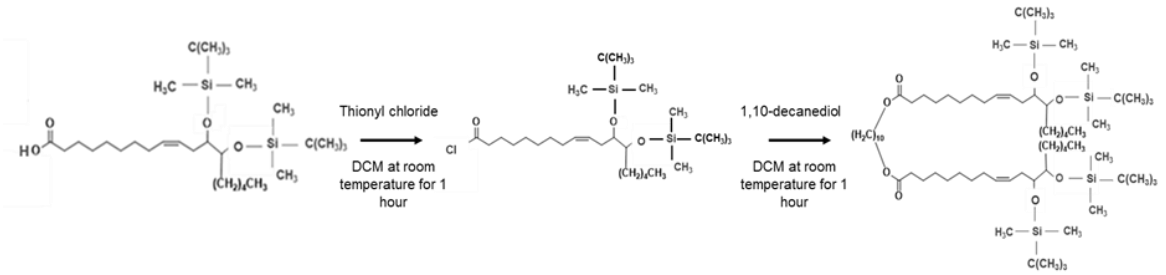

Figure 4.24. **Schematic representation of the two-step production of diester TBS intermediate.** Diester TBS intermediate was produced from the coupling of 6,7-*di(tert*-butyldimethylsilyl ether)stearic acid, in a two-step process initially with dichloromethane and thionyl chloride for 1 hour at room temperature. Then 1,10 decanediol is added for 1 hour at room temperature. The product was confirmed by TLC and HRMS. This was purified through column chromatography.

The sample was then analysed using high-resolution mass spectrometry (HRMS) and determined the molecular weight MW [M-H]- 1224.9886, chemical formula $C_{70}H_{142}O_8Si_4$ (figure 4.25).

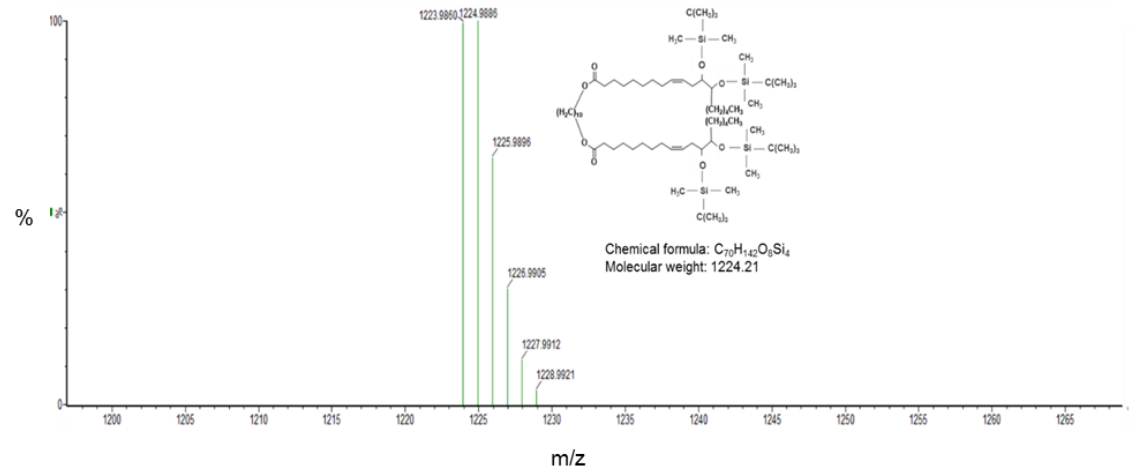

Figure 4.25. The resultant mass spectra from HRMS after the coupling of 6,7-*di(tert*-butyldimethylsilyl ether) stearic acid. The accurate mass measurement was confirmed, highest peak, as 1224.9886, chemical formula $C_{70}H_{142}O_8Si_4$.

4.4.4.4 Step 5- Synthesis of diepoxystearate tetrol-TET01

To a stirred solution of 0.10 g diester TBS intermediate (0.08 mmol) in 10 ml THF at room temperature 0.12 ml tetrabutylammonium fluoride (TBAF) was added. After 8 h at room temperature the mixture was then partitioned between aqueous phase (10 ml $NaHCO_3$) and organic phase (20 ml DCM). The aqueous and organic phases were dried with $MgSO_4$ and the solvents removed under reduced pressure. The resultant residue was purified by silica gel column chromatography, eluting with pet ether: Et2O (4:1) afforded the final product diepoxystearate tetrol (figure 4.26). The overall yield was improved from 4.8% to 64%.

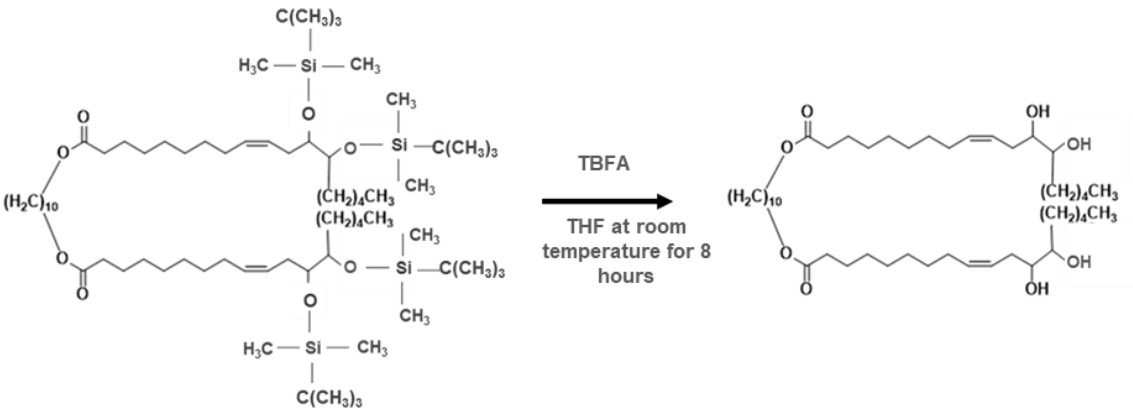

Figure 4.26. **Schematic representation of the production of the final product diepoxystearate tetrol.** Diepoxystearate tetrol was produced by the removal of TBS with TBAF for 8 hours at room temperature. The product was confirmed by TLC and HRMS.

The sample was then analysed using high-resolution mass spectrometry (HRMS) and determined the molecular weight MW [M+H] 766.63227, chemical formula $C_{18}H_{33}O_4$ (figure 4.27).

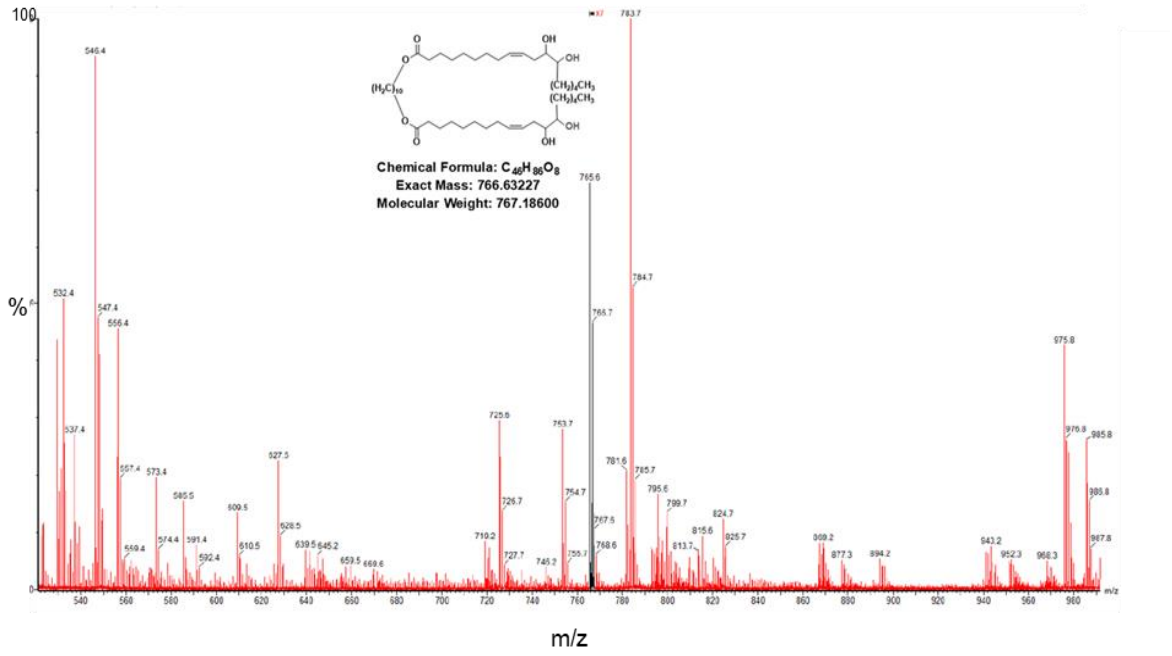

Figure 4.27. The resultant mass spectra from HRMS of the final product diepoxystearate tetrol. The accurate mass measurement of product diepoxystearate tetrol was confirmed, in black, as 766.63227, chemical formula $C_{46}H_{86}O_8$.

Each step of the synthesis for the production of diepoxystearate tetrol (TET01) and dichloroacetate diepoxystearate (FASCA 01) produced a yield, which was then used for the next step (section 4.3.3 and 4.3.4, figure 4.28). For the production of dichloroacetate diepoxystearate (FASCA 01) the yield of the first step, the production of 6,7-epoxy stearic acid, was 88% (figure 4.28). From this 88% of 6, 7-epoxy stearic acid, 50% of decane diepoxystearate was produced. This is an overall yield of 44% of the original starting material, vernonia oil (50% x 88%= 44%). The final synthesis step saw a yield of 15% dichloroacetate diepoxystearate produced, which was the equivalent of 6.6% of the starting material. Overall, this synthesis generated 66 mg of dichloroacetate diepoxystearate.

This was similar for the production of diepoxystearate tetrol (TET01). The final step of the second attempt synthesis produced 4.8% of diepoxystearate tetrol from the previous step 6,7-diol stearic acid. This is an overall yield of 15.2% of the original starting material, vernonia oil (figure 4.28). This is the equivalent of 15.2 mg of

diepoxystearate tetrol generated using this methodology. Due to the low yield production was optimised through the introduction of a novel methodology to improve the yield. The final yield of diepoxystearate tetrol was 64% of the previous product (diester TBS intermediate), generating 11% of the overall yield, equivalent to 111 mg of TET01 (figure 4.28).

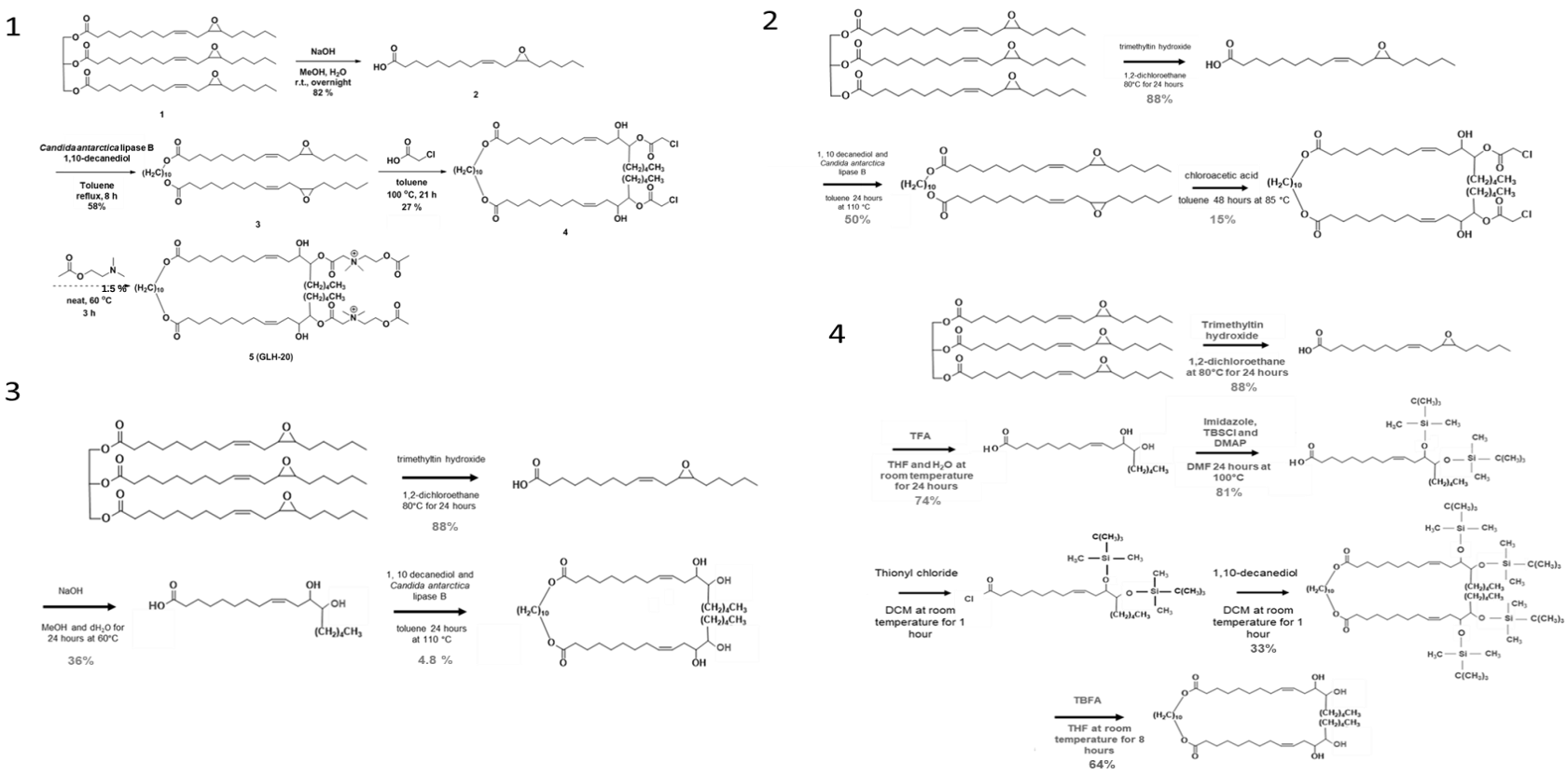

Figure 4.28 Summary schematic of (1) GLH-20, (2) FASCA 01, (3) TET01 (low yield) and (4) TET01 (optimised). The above schematic represents the synthesis of the final material used for the synthesis of the FASCA 01 and TET01 vesicles, with the initial yields and the improved yield for TET01. The original GLH-20 synthesis generated an overall yield of 1.5%, producing 15 mg of GLH-20 from 1 g of vernonia oil. The final yield for FASCA 01 is 15%, producing an overall yield of 66 mg from 1 g of vernonia oil. The final yield of TET01 produced generating only 15.2 mg (4.8% yield). As a result of the low yield the methodology was optimised to improve the yield to 64%, generating 111 mg of final material from 1g of starting material, vernonia oil. The initial synthesis of both FASCA 01 (2) and TET01 (3) were used for further characterisation. The limitation of starting material as well as their low yields limited the experiments performed.

4.4.5 Characterisation of FACSA 01 vesicles

Vesicles were synthesised (Chapter 2, section 2.3.5) with FACSA 01 (figure 4.6) material. The cargo to be synthesised with FACSA 01 material was either PBS (empty vesicles), AF546, or PI as described in Chapter 2 (section 2.3.5). Once synthesised the physical properties of the vesicles were characterised by DLS and zeta potential (Chapter 2, section 2.3.7 and 2.3.9, respectively) (table 4.2). The physiochemical properties of the resulting FACSA 01 vesicles were analysed by both DLS and zeta potential. DLS is a technique based on Brownian motion of particles in a suspension in order to provide a profile of the mean Z-average and PDI. The zeta potential is a measure of electrostatic repulsion/attraction between nanoparticles in solution and therefore, a measure of stability - the greater the electrostatic repulsion the less likely the vesicles will aggregate.

Newly produced vesicles, FASCA 01, were synthesised to encapsulate different tracer dyes, as was previously performed with our original BA material to investigate reproducibility.

Table 4.2. Dynamic light scattering, polydispersity index and zeta potential analysis of empty, Alexa Fluor 546 or propidium iodide encapsulated FACSA 01 vesicles (n=3).

Vesicles	Empty	AF546	Propidium iodide
Z-average (d.nm)(mean ± SEM)	163.4 ± 12.2	188.8 ± 16.8	493.9 ± 30.3
PDI (mean ± SEM)	0.4 ± 0.12	0.4 ± 0.12	0.6 ± 0.3
Zeta potential (mV) (mean ± SEM)	-45.7 ± 1.8	-37.5 ± 2.4	-6.0 ± 1.5

The z-average for PI vesicles (table 4.2) is the appreciably higher than the other z-average values. Whilst the zeta-potential is considerably lower than either empty or AF546 encapsulated FACSA 01 vesicles.

Stability rapidly decreases at both temperatures for FACSA 01 vesicles. Vesicles stored at 37°C are stable for longer than when FACSA 01 vesicles are stored at 4°C (table 4.3).

Table 4.3. **Stability of empty FACSA 01 vesicles stored at 4°C and 37°C over a five-day time frame (n=3).**

Zeta potential (mV) (mean ± SEM)	4°C	37°C
Day 1	-10.3 ± 2.3	-18.1 ± 1.5
Day 2	-8.6 ± 3.9	-11.6 ± 3.4
Day 3	-6.6 ± 0.7	-11.2 ± 0.7
Day 4	-6.5 ± 0.6	-8.4 ± 2.4
Day 5	-6.5 ± 0.9	-8 ± 0.1

4.4.6 Linear regression analysis to determine the encapsulation efficiency and concentration of Alexa Fluor 546 encapsulated in FACSA 01 vesicles.

To determine the concentration of AF546 encapsulated within purified FASCA 01 vesicles, fluorescence readings (excitation 540-20 nm, emission 590-30 nm) of the vesicles were measured and compared against the standard curve (Chapter 2, figure 2.4). Vesicles were purified by size exclusion chromatography. From the initial concentration of AF546 (125 mM) the highest concentration encapsulated in the FACSA 01 vesicles was 138.21 ± 41.3 µM (figure 4.29). A spectral analysis of the vesicles was previously performed (chapter 2, section 2.3.) which demonstrated that the material did not absorb light at any wavelength. It is not anticipated that the light emitted by the dye was being obscured/interfered with by the bola material.

The encapsulation efficiency was calculated, using equation 1 from chapter 2 (section 2.3.14):

$$encapsulation\ efficency\ (\%) = \frac{final\ concentration}{initial\ concentration} \times 100$$

The final concentration of F14 is 0.11%. The concentration of the fractions that were 0.14%.

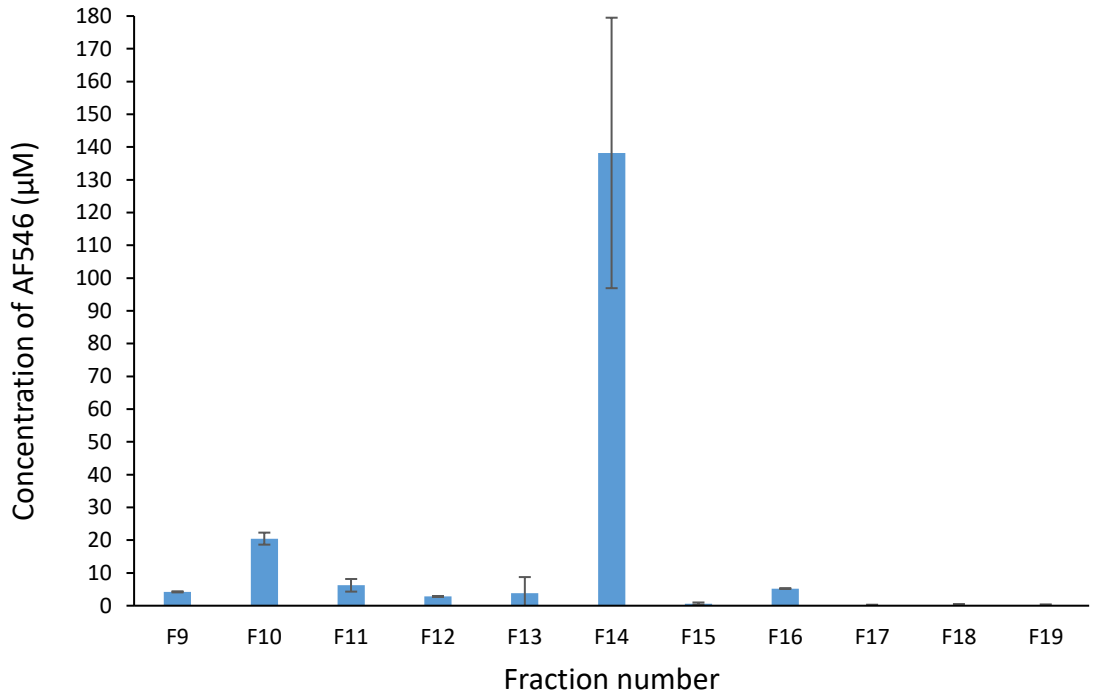

Figure 4.29. The encapsulation concentration of Alexa Fluor 546 encapsulated FACSA 01 vesicles as calculated from the linear regression (Figure 2.4). Preparations of vesicles that had been subjected to separation by sepharose CL-2B chromatography were examined using a CLARIOstar fluorescence plate reader (excitation filter 540-20 nm, emission filter 590-30 nm). From the measurements, fraction 14 of the purified vesicle population had the greatest concentration of AF546 (n=3).

4.4.7 Characterisation of TET01 vesicles

Vesicles were synthesised with the TET01 formulation (figure 4.14) and synthesised with either PBS (empty vesicles), AF546, or PI as described in Chapter 2 (section 2.3.5). Once synthesised the physical properties of the vesicles were characterised by DLS and zeta potential as described in chapter 2 (section 2.3.7) (table 4.4).

Table 4.4. Dynamic light scattering, polydispersity index and zeta potential analysis of empty, Alexa Fluor 546 or propidium iodide encapsulated TET01 vesicles (n=3).

Vesicles	Empty	Alexa Fluor 546	Propidium iodide
Z-average (d.nm) (Mean ± SEM)	223.7 ± 10.0	165.2 ± 130.0	157.5 ± 5.1
PDI (Mean ± SEM)	0.3 ± 0.063	0.7 ± 0.230	0.2 ± 0.01
Zeta potential (mV) (Mean ± SEM)	-46.6 ± 0.2	-23.0 ± 2.7	-2.8 ± 2.2

4.4.7.1 Preliminary Nanoparticle Tracking Analysis of TET01 vesicles

In order to determine the concentration of particles in the neat empty and PI encapsulated each neat formulation Nanoparticle Tracking Analysis (NTA) was performed (figure 4.30) and the vesicle size was also measured. From the NanoSight analysis the mean size of the vesicles was determined. 179.9 ± 6.1 nm was the mean size for the neat empty vesicles, and 161.6 ± 3.2 nm for the neat PI vesicles.

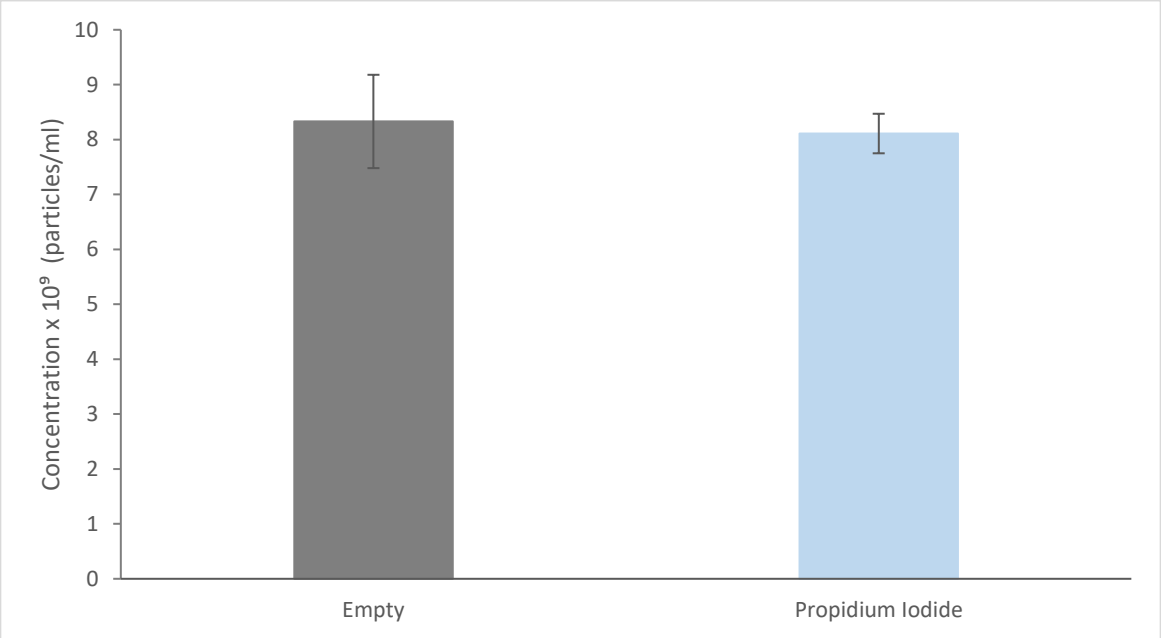

Figure 4.30. Concentration of empty TET01 vesicles or TET01 vesicles encapsulating propidium iodide determined from NanoSight Tracking Analysis.

4.5 Discussion

From the HRMS analysis of the original BA material, it was found that the material was not that of GLH-20, but rather a novel compound. The two predominant peaks indicate the presence of two species. Therefore, efforts were made to recreate the original BA material which was shown to produce stable vesicles that could cross the BBB *in vivo*. The production of FASCA 01 (dichloroacetate diepoxystearate), was characterised and profiled, using DLS and zeta potential. The production for TET01 (diepoxystearate tetrol) was lengthy and required modifications in an attempt to optimise the yield of the formulation. TET01 was however also characterised and profiled. Whilst the two formulations were not combined, this is strongly recommended for future studies given that both products form vesicles in isolation and that both products are apparent in the HRMS analysis.

4.5.1 Synthesis of FASCA 01 and TET01

The basis of the original formulation was taken from the experimental procedures used to synthesise the cationic vesicle- GLH-20. Grinberg *et al* (2008) reported the synthesis of BA compound GLH-20 to produce vesicles using the methylester of vernolic acid as a starting material.

The original formulation kindly gifted to us from Professor Lawrence Williams was interestingly not the cationic GLH-20 BA initially thought. The experimental procedure was followed from Grinberg *et al* (2008). However, the synthesis produced a novel material that had a negative zeta potential when made into vesicles inferring that a novel vesicle was being produced. After HRMS analysis, the original Rutgers derived material gave rise to two peaks which appeared to correspond to intermediate steps of the synthesis. The first was thought to be the penultimate step in the production of the GLH-20 vesicles containing the chloroacetic head groups (FACSA 01). The other peak was thought to correspond to the molecular weight of the coupled bola material with hydrolysed epoxide groups. As a result, further investigations were made to synthesise these materials and produce vesicles from them to assess their characteristics and their ability to act as a drug delivery system in order to treat diseases of the brain.

Initial attempts to hydrolyse the esters was undertaken with NaOH, MeOH and water. However, non-selective opening of the epoxide was also observed. Therefore, the method used was revised. As a result, a more selective methodology was employed, whilst avoiding non-specific side reactions. Trimethyltin hydroxide and 1,2-dichloroethane was employed for the first step (Nicolaou *et al*, 2005). This technique has been observed to reveal higher yield of carboxylic acids from esters (Nicolaou *et al*, 2005). The introduction of the technique increased the yield of vernolic acid (6,7-epoxy stearic acid) from 31% to 88%.

The second step, the formation of decane diepoxystearate, was then optimised. Initial attempts of refluxing 1,10 decanediol in toluene resulted in no formation of the product decane diepoxystearate. Therefore, the next attempts were performed in the presence of the catalyst 4-(dimethylamino)pyridine (DMAP) (Popov *et al*, 2010). DMAP is an effective catalyst for esterification reactions (Kamimura *et al*, 2008). However, this was unsuccessful as only a very low yield of decane diepoxystearate was observed. Therefore, Novozym 435, a lipase from *Candida antarctica* was employed (Grinberg *et al* 2008; Stern *et al*, 2014). This proved successful in that the reaction occurred and there was no trace of the coupling material, 1, 10 decanediol from TLC analysis, unlike the previous methods used. Grinberg *et al* (2008) reported an increase in yield from 30% to 85% with 10-fold increase of lipase. However, they also used a much higher concentration of 6,7-epoxy stearic acid than we did (92 g to our 0.55 g which is 160-fold greater), which may account for the higher yield. Although we did not increase the lipase 10-fold or increase the concentration of TET01 bola material the final yield was.50%. Nonetheless, this suggests that this step may require further optimisation.

The final synthesis step in the production of FACSA 01 (dichloroacetate diepoxystearate), afforded a final yield of 15%. This is less than the yield reported 28.5% for dichloroacetate diepoxystearate by Grinberg *et al* (2008). Vesicles were successfully produced from this material Their analysis will be discussed in parallel with vesicles made from the other intermediate found in the original synthesis, TET01.

For the initial synthesis of TET01, the same protocol was followed as FASCA 01, with the exception of the final step. The initial production of diepoxystearate tetrol

was adapted from Wang *et al* (2007). In this step the reaction is designed to selectively open the epoxide without hydrolysing the ester linkage. Due to the proton accepting and donating ability of water, acting as a nucleophilic solvent, it was expected to speed the reaction rate (Byers and Jamison, 2015). It may have been that the water was too weak a nucleophile to hydrate the epoxide in these conditions and may have not been selective enough (Vilotijere and Jamison, 2007). However, the reaction did not work. As a result, the synthesis was optimised attempted by another route. This was attempted as part of an overall revision of the pathway.

To further optimise both the yield and the time taken at each stage of the synthesis, with the exception of the first step (hydrolysis of the esters, formation of 6,7-epoxy stearic acid), improvements were implemented for the synthesis of diepoxystearate tetrol (TET01). As a result, the second step, synthesis of decane diepoxystearate (section 4.3.3.2), from the synthesis of FASCA 01, was substituted for the opening of the epoxy groups.

From the original investigations to hydrolyse the esters NaOH was observed to non-selectively open the epoxides. This was therefore employed as the initial technique used for the opening of the epoxide group. However, this was not effective as the reaction was slow with a low yield. Trifluoroacetic acid (TFA) has been used for opening of epoxy rings (Cory *et al*, 1990). The concentration of TFA used was designed to restrict the potential for non-selective reacting with alkenes as has been observed (Peterson *et al*, 1967). This initial reaction afforded a yield of 31% which was increased to 87% after optimisation.

Once the epoxide groups were opened the final step in the reaction was the coupling reaction. The initial attempts were performed with 1,10 decanediol and lipase Novozym 435 to afford diepoxystearate tetrol. Once this was completed, TET01 vesicles were produced and characterised as will be discussed further.

The final yield of diepoxystearate tetrol following this procedure was low (4.8%). One hypothesis for the low yield may be that the hydroxyl groups were not protected (Trader and Carlson, 2012). To prevent this from occurring it is recommended that alcohols are protected (Corey and Venkateswarlu, 1972). One such method is the derivatisation of the hydroxyl groups via silylation (Greene and Wuts, 1999; Patel

et al, 2007). Compounds such as trimethylsilane (TMS) or *tert*-butyldimethylsilane (TBS) may provide the protection required (Su *et al*, 2017). Initially, silylation was performed with TMS and afforded a yield of 80%. However, TMS is more susceptible to solvolysis, to attack by nucleophiles, as observed in the non-selective elimination of TMS during the final synthesis step (the coupling reaction), than TBS (Corey and Venkateswarlu, 1972). As observed in the non-selective elimination of TMS during the final synthesis step, the coupling reaction. As a result, the final product was not formed and so this method was replaced and further optimised with the use of TBS. TBS acts to protect the hydroxyl groups, transforming them to ethers, which is why it is more suitable that TMS (Corey and Venkateswarlu, 1972; Patschinski, Zhang, and Zipse, 2014). DMF used in the reaction acts as both the solvent and catalyst, aiding the mild conversion, optimising the yield (Patschinski, Zhang, and Zipse, 2014). This afforded a similar yield to TMS at 81% but there was no solvolysis as TBS is more suitable for enabling the final reaction to complete (Corey and Venkateswarlu, 1972).

The penultimate step, the coupling reaction, was a two-step reaction. The first step was the formation of the acid chloride (D'Angelo and Smith, 2015). Acid chloride is highly reactive and is therefore ideal as an intermediate for further reactions. The second reaction, the coupling with the 1,10 decanediol to produce diester TBS intermediate with a final yield was 33%.

Due to the high affinity of silicon for fluorine, the final step, the removal of the silylated protective groups (TBS), occurred with *tetrabutylammonium fluoride, with yield of 64% (*Corey and Venkateswarlu, 1972). This increase demonstrates that the optimisation was successful when compared to the yield of the TET01 characterised in this study (4.8%). It will be important to characterise this newly optimised TET01 material for future work.

Initially the protocol for the production of the bola material, both FASCA 01 and TET01, was comprised of three steps (figure 4.6 and 4.14). However, there were numerous limitations such as an exiguous yield and slow reaction time. Investigations were made to improve the overall yield of the initial studies. The synthesis of the desired BAs was optimised and produced through a final six step process. Previous BAs synthesised with vernonia oil also demonstrated the yield

decreasing with each production step (Grinberg *et al*, 2005 and 2008; Popov *et al*, 2010) such that the final step gave rise to a 42% yield (Popov *et al*, 2010). The overall yield was increased to 64%. This demonstrates that the optimisation steps have been successful at increasing the overall yield. The vesicles must be profiled for future studies, individually and in combination with the FASCA 01 formulation.

4.5.2 Characterisation of FASCA 01 and TET01

The importance of characterisation is to analyse the physiochemical properties of the drug delivery system (Singer *et al*, 2019). There are several parameters used to profile the drug delivery system including the particle size and size distribution, using DLS, and shape/morphology (Mourdikoudis, Pallares, and Thanh, 2018, Singer *et al*, 2019). In order to maintain reproducibility, we have used the techniques employed in our previous studies (chapter 2) as well reported in other studies investigating BA vesicles produced with vernonia oil (Grinberg *et a*l, 2008; Popov *et al*, 2012). The techniques used to characterise our vesicles include DLS, zeta potential, size exclusion column chromatography and NTA.

When comparing the overall size of our original BA vesicles to the newly synthesised FASCA 01 and TET01 vesicles the size of TET01 produces the largest and FASCA 01 the smallest (163.4 ± 12.2 nm and 223.7 ± 10.0 nm, respectively). Considering that essentially FASCA 01 is TET01 with the addition of chloroacetic acid it would be expected that they would be a similar size. There may be a number of reasons such as the formulation and stability of the vesicles or perhaps the synthesis technique. It will be of interest to investigate combining both materials together in a vesicle synthesis. This could be explored in future studies. However, this is not the case for the PI encapsulated vesicles which behave very differently. The size of PI encapsulated FASCA 01 vesicles appears to indicate that there is aggregation, especially as the size continued to increase despite attempts to sonicate to reduce the size, referred to as sonication induced aggregation (Taurozzi *et al*, 2010). The over sonication is adversely influencing the size and it might be of interest to investigate different techniques such as such as ethanol injection. It is a method designed to simplify the production of vesicles by dissolving the lipid material in ethanol and then injecting it into water, spontaneously forming vesicles (Huang *et al*, 2010; Shaker *et al*, 2017). Popov *et al* (2010) employed this method

for their GLH-20 vesicles, as did Kim *et al* (2020) for their GLH-20 and GLH-19 combination formulation. However, they also used the bath sonicator to form the vesicles. It may be more advantageous to investigate the formation of vesicles using a bath sonicator rather than a probe sonicator as it is an indirect method, providing lower energy levels than the probe and less likely to form aggregates (Taurozzi *et al*, 2010).

The NTA measurements of the vesicles appear to demonstrate a discrepancy between the two techniques, DLS and NTA, for the size distribution measurements for empty TET01 vesicles. NTA is a characterisation technique used for sizing particles and providing the concentration of particles within a sample (de Morais Ribeiro *et al*, 2018; Kim *et al*, 2019). NTA tracks the movement of individual particles undergoing Brownian motion and measures their size based on the light scattered during the tracking (Filipe *et al*, 2010; Kim *et al*, 2019). DLS measures the intensity of light scattered by particles under Brownian motion and the speed at which they move (Filipe *et al*, 2010; Bhattacharjee, 2016). Both techniques measure the particles based on the diffusion coefficient, measurement of the movement of a particle in medium and is dependent upon the frequency and size of each movement (Kriczek, 2015). However, DLS reports the size based on the intensity of light scattered, whereas NTA reports the size weighted by number (Kim *et al*, 2019). Both techniques have their merits and limitations. Light scattered from larger particles can skew the data in some instances when there is polydispersity within a sample (Filipe *et al*, 2010; Bhattacharjee, 2016; Stetefeld *et al*, 2016). NTA can be used to verify the size distribution of DLS as it may be more sensitive in measuring accurate size distribution for polydispersed particles (Kim *et al*, 2019). The discrepancy observed in our study has also been observed in others supporting the sensitivity of NTA for size distribution (de Morais Ribeiro *et al*, 2018). However, these studies have been reported using standard polystyrene beads rather than polydispersed heterogenous populations of particles to assess their strengths and limitations (de Morais Ribeiro *et al*, 2018). The concentration of the vesicles is the first time that this has been reported for BA vesicles synthesised from vernonia oil.

All the vesicles synthesised from TET01 and FACSA 01 formulations were less stable that the original BA vesicles. Stability reduces appreciably for FASCA 01 within 5 days regardless of the temperature at which they are stored. It appears

that the stability is modestly enhanced at 37°C than at 4°C however only by 2 days. From the HRMS analysis of the original BA material two predominant peaks were observed (figure 4.1). It may be suggested that the original BA material is stabilised as it is comprised of two species. As a result, the lack of stability observed for FASCA 01 and TET 01 may be due to the presence of only a single species within this formulation. Popov *et al* (2013), measured the zeta potential of individual formulations and in combination. GLH-20 was measured at +37.2 ± 2.0 mV, GLH-19 was + 44.1 ± 2.7 mV and in combination (GLH-20 and GLH-19) the zeta potential was +45.4 ± 0.6 mV. This appears to support our observations that combination of species provides more stability as opposed to the individual formulation. It is proposed that both FACSA 01 and TET01 should be included together to investigate the effect of two species on stability.

4.5.3 Encapsulation efficiency

The concentration of AF546 encapsulated by the original vesicles is low (0.04%). (chapter 2, section 2.4.10) in comparison to the FACSA 01 material (0.14%) and the initial concentration of AF546 added to the original synthesis (125 mM). A possible hypothesis may be that the FACSA 01 material and AF546 are interacting and binding more than the original material (Yeo and Park, 2004). Whilst it could be considered that the AF546 dye is interacting with the surface of the vesicle as well as being encapsulated lumen. However, this may be unlikely as AF546 is negatively charged molecule. It is unlikely to interact with the surface of a negatively charged compound such as FACSA 01.

The low encapsulation efficiency of the chromatographically separated peak fraction of AF546 original BA vesicles (section 2.4.9) and FASCA 01 vesicles demonstrates a need for future optimisation. The same future experiments are recommended as mentioned in Chapter 2 (section 2.6) - increasing concentration of the BA material (Harayqa and Domańska, 2014), increasing the concentration of the cargo (Derman, 2015) and incorporation of folate PEGylated lipid to the vesicle material (Cho *et al*, 2014).

The cargo encapsulated within may not be the only factor influencing the size of PI encapsulated FACSA 01 vesicles. These vesicles are considerably larger than the other vesicles with the same formulation. It is an appreciable increase in

comparison to the other vesicle sizes and appears to indicate flocculation, and poor stability. It appears that the repeated sonication increased the overall aggregation (Aoki *et al*, 1987; Taurozzi *et al*, 2010). Although, it may be the positive charge of the PI is adversely interacting with the FASCA 01 material. Perhaps indicating that the PI changes the behaviour of the material as this behaviour was not observed with the TET01 material or with other molecules. For future work it may be of interest to see if this is observed when both FASCA 01 and TET01 are mixed together.

4.6 Limitations and future work

In order to optimise further, future work should repeat the coupling reaction in the presence of *Candida antarctica* lipase B as a cataylst, as was performed in the initial synthesis (Grinberg *et al*, 2008). This is the only step from the original protocol that has not been optimised

A further limitation was the low yield of the FASCA 01 bola material. The protocol was not optimised during the production of FASCA 01, as we initially wanted to make the material, the yield was not the object at this point. However, it became apparent during the production of TET01 that optimisation was necessary as vernonia oil is a difficult commodity to source and so efficiency was needed to improve the yield at each step. Therefore, reprising the same optimisation steps as for the synthesis of TET01 is recommended for future production of FASCA 01 material.

A further limitation was the overall yield of both FASCA 01 and TET01, as well as the time and material constraints, as mentioned in the previous paragraph. This restricted more detailed experimentation. Therefore, NTA studies are preliminary and, in the future, will be expanded to include the concentration of all vesicles synthesised.

The vesicles do not appear as stable over time as the original BA vesicles. Perhaps a combination of both the tetrol (TET01) and chloroacetic (FACSA 01) BA material would provide the long-term stability. As the HRMS of the original material appears to demonstrate that there are two possible species this may explain the higher long-term stability observed. Popov *et al* (2010), investigated the stability as a measure of encapsulation. Combinations of at least two different vesicles within a sample

were tested over a period of 500 hours (21 days) for encapsulation stability. Although certain combinations, such as GLH-20 and GLH-19, were stable, GLH-20 were no longer stable after 13 days. GLH-19 was more stable when tested alone (approximately 50% stability after 21 days). GLH-19 appears to increase the stability of both formulations when together (GLH-19 increased GLH-20 vesicles stability by 10% for up to 21 days). Again, supporting the observations of combined formulations. As our original BA material demonstrated high stability for 4 months at 4°C. The stability was still considered high at the end of the third month. As two peaks were observed in the HRMS analysis it would be relevant to compare the influence of individual species to that of a mix of both formulations on stability. Therefore, it is recommended that both formulations are mixed together to investigate stability.

Cationic BA vesicle formulations GLH-19 and GLH-20 have recently been combined to improve drug delivery of encapsulated siRNAs to the brain and flank tumour (Kim *et al*, 2020). The individual profiles of each vesicle demonstrate that GLH-19 is more stable with higher binding affinity for the siRNAs that were used in the study, whereas GLH-20 was shown to have more efficient delivery and release kinetics. When both formulations were combined the vesicles indicated that the GLH-19/GLH-20 complex combined their individual traits and were shown to deliver siRNA *in vivo* to the brain. As our vesicles are anionic it will be of interest to investigate their potential as a drug delivery system using the individual formulations and in combination for future studies.

A further limitation was that there is no EM analysis of the vesicles performed, so we cannot confirm whether the vesicles are spherical, as the original material was shown to be. As is widely acknowledged, it is necessary to standardise such techniques to maintain reproducibility and alignment for testing and characterisation of drug delivery systems therefore such an analysis should be performed (Björnmalm, Faria, and Caruso, 2016; Mulverny *et al*, 2016; Gao and Lowry, 2018). This will need to be performed to confirm not only the shape but the size of the vesicles. EM, confocal microscopy with z-stacking may indicate where the vesicles are, for example if the cargo is interacting with the membrane of the vesicles or if they are encapsulated. In order to investigate this potential interaction, it is suggested that further studies are performed, in particular with vesicles

encapsulating the antibody fragment scFv 4D5-8RFP conjugated to AF546, as suggested in chapter 3 (section 3.5.4). Therefore, treating antibody fragment vesicles with proteinase K to measure the fluorescence using a fluorescent plate reader. If the antibody fragments are interacting with the surface rather than encapsulated in the lumen of the vesicles, the fluorescence would be expected to decrease.

The encapsulation efficiency must be improved. Initially both formulations should be combined to investigate the efficiency. It is also recommended that future studies increase either the concentration of the bola material, or the concentration of the molecule/drug to be encapsulated (Yeo and Parks, 2004; Harayqa and Domańska, 2014; Derman, 2015). A further suggestion is to synthesise the vesicles with polyethylene glycol (PEG) (Cho *et al*, 2014). This is not only to investigate the potential for the vesicles as candidates as potential drug delivery systems but also to compare the effects of these vesicles to that of the original BA material studied in chapters 2 and 3.

To ensure the safety of the FASCA 01 and TET01 formulations, as well as the combined formulation, toxicity studies will need to be performed. Further studies will include *in vitro* viability and immunogenicity assays. As we have yet to investigate the uptake of the FASCA 01 and TET01 vesicles, such studies will need to be undertaken in different cell lines. In order to investigate the opening of the vesicles future investigations are recommended to explore release kinetics using the encapsulated PI vesicles. It is recommended that the studies investigate the uptake and release of the individual as well as the combined formulations. These studies will be undertaken *in vitro,* prior to *in vivo* work-an *in vitro* BBB should be tested using either transwell plates of a flow dynamic system in which bi-tri cultures are grown (Helms *et al*, 2014). Transendothelial electrical resistance (TEER) measurements should be taken, using a voltohmmeter, of the *in vitro* BBB to ensure formation of the tight junctions of the brain endothelial cells (Helms *et al*, 2014). In order to evaluate the potential of the vesicles as a drug delivery system they should be tested *in vivo*.

Further studies would include the encapsulation of therapeutics such as etoposide which is able to cross the BBB but is effluxed rapidly by ATP transporters (Löscher

and Potschka, 2005). It would be of interest to investigate the encapsulation efficiency, after the modifications and optimisation suggested, and study the effects *in vitro* such as stability, uptake and efficacy.

4.7 Conclusions

The original BA material supplied by our collaborators which we thought to be GLH-20, was not. HRMS analysis, has revealed that the material comprised many components however, the main products are consistent with two intermediates that could be produced during GLH-20 synthesis. A simple synthetic procedure based on the GLH-20 synthesis was initially employed to see if they could be produced and then optimised to improve yield and reduce production time.

Vesicles have been characterised for each of the intermediates (FASCA 01 and TET01). The material was used to produce vesicles with less negative zeta potentials and z-averages to that of the initial BA material used for our *in vitro* and *in vivo* work (chapter 2 and chapter 3). However, it will be important to explore the potential of these vesicles *in vitro* and *in vivo*. A further synthesis needs to use both BA species mixed together to see if the resulting vesicle material is more stable. This should be explored in the future.

Chapter 5: General Discussion

5.1 Introduction

The incidence of diseases of the brain such as Alzheimer's disease, Parkinson's disease and glioblastoma are predicted to increase (Prince *et al*, 2016a; Feigin *et al*, 2017; Dorsey *et al*, 2018). This increase is due to the increasing population of elderly, the incidence of these diseases increasing with age, as well as better reporting of such cases globally (Prince *et al*, 2016b; Feigin *et al*, 2017). Despite all demonstrating different aetiologies, they do share one thing in common - there is no cure (Prince *et al*, 2016a). The treatment for diseases of CNS is only palliative and designed to reduce the symptoms rather than treat the underlying issue. One of the greatest barriers for treating diseases of the brain is the physical, pharmacological and functional barrier of the BBB, the interface between the vascular and central nervous systems. Whilst it has an important physiological function, protecting the brain from toxins, microbes and other foreign substances and maintaining the normal brain environment, it is also an excellent barrier against the entry of therapeutic agents to the CNS (Pardridge, 2012; Chaturvedi *et al*, 2019). The BBB is exquisitely effective at preventing drug entry, restricting approximately 98% of small molecules and the majority of large molecules from the brain parenchyma (Habgood *et al*, 2000; Pardridge, 2003), thus, limiting treatment opportunities.

There have been numerous invasive and non-invasive techniques developed to bypass the BBB and deliver drugs. Approaches span from the less invasive, such as liposomes, prodrugs, and the use of 'trojan horse' endogenous transporters, to more invasive techniques such as focused ultrasound and intracerebroventricular delivery. There are limitations for each of these methods including non-specific delivery, poor uptake in the brain, disruption of the BBB, and rapid clearance of the CSF. Clearly, novel drug delivery systems are needed. We hypothesised that BAs may offer a possible solution as a drug delivery system.

BAs are molecules composed of long carbon chains and polar head groups (Han *et al*, 2004), able to form monolayered spherical vesicles and encapsulate a higher payload than traditional liposomes (Puri *et al*, 2009; Fariya *et al*, 2014). Cationic BAs, including GLH-20, synthesised from vernonia oil from the African sunflower,

Vernonia galamensis, have been reported to cross the BBB and deliver protein sized molecules to the brain (Dakwar *et al*, 2012; Popov *et al,* 2012). Therefore, we have endeavoured to explore the potential of vesicles synthesised from vernonia oil as a potential drug delivery system to treat diseases of the brain.

5.2 Characterisation of novel, anionic bolaamphiphilic vesicles

Synthesis of GLH-20 material was performed in collaboration with Dr Sumi Lee and Professor Lawrence Williams (Rutgers, USA). As the GLH-20 BA is cationic, due to the presence of acetylcholine ester head groups, it was expected that our BA vesicles would demonstrate a positive zeta potential. However, this was not the case. Rather our BA vesicles were negatively charged demonstrating that they are anionic. Presumptively, that they are an unexpected, novel species. We investigated the potential of these novel vesicles as a drug delivery system, to determine the value of exploring their synthetic chemistry in house.

Tracer dyes, propidium iodide (PI) and Alexa Fluor 546 (AF546), were initially encapsulated in our BA vesicles. These were profiled, along with empty vesicles, using dynamic light scattering (DLS), transmission electron microscopy (TEM) (for empty vesicles only), zeta potential, and size exclusion chromatography. We also investigated the potential of BA vesicles to encapsulate a larger molecule such as the small variable antibody fragment scFv 4D5-8RFP. This was selected as it is smaller than an antibody, whilst still retaining the antigen binding site, and it has a built in marker in the guise of a red fluorescent protein within the architecture of the fragment. scFv 4D5-8RFP is specific to protein HER2 which is highly expressed in cancers such as breast and ovarian, as well as in some brain cancers. More importantly, this was a proof of concept study to investigate whether the vesicles could serve as a drug delivery system for therapeutic antibodies targeting brain specific antigens. Therapeutic use of antibodies can include as antibody drug conjugates. They are used to increase uptake to tumours through specific targeting as well as reducing non-target specific interactions of the cytotoxin by targetted delivery (Beck *et al*, 2017; Lu *et al*, 2020). Many of these are still in clinical trials (Corraliza-Gorjón *et al*, 2017) but if any show promise in targeting brain tumours they will require delivery across the BBB. The size of antibody drug conjugates can range in size from 300-1000 Da which may influence delivery (Beck *et al*, 2017). The maximum size of molecule that our BA vesicles has not yet been determined.

The size of the antibody encapsulated vesicle was larger than the empty vesicles or the vesicles encapsulating the tracer dyes. However, this stands to reason as the molecule is considerably larger at 52 kDa than the tracer dyes which are smaller than 1 kDa.

Further characteristics of the vesicles were monitored to investigate their drug delivery potential. AF546 encapsulated vesicles were profiled for their long-term stability as well as their encapsulation efficiency. AF546 encapsulated vesicles demonstrated that over a four-month period the stability did reduce by 25%, but the zeta potential was still > -30 mV at this time point, indicating that our BA vesicles had a high degree of stability when stored at 4°C Popov *et al* (2010) observed stability of their cationic GLH-20 vesicles decreasing after 13 days. This demonstrates that our BA vesicles with their high electrostatic repulsion are more stable, remaining discrete and therapeutically usable for a minimum of 4 months.

The encapsulation efficiency for AF546 was measured using a fluorescent plate reader analysing all the fractions that had been purified by size exclusion chromatography and in which a signal was detectable. Whilst the efficiency is low, appreciable amounts of the test AF546 tracer could be detected. These data will serve as a baseline for future studies investigating techniques to enhance and optimise encapsulation. It is known that efficiency is in part dependent upon the dose of the therapeutic to be encapsulated (Bozzuto and Molinari, 2015).

Our vesicles have demonstrated a similar size and charge to studies investigating the potential of anionic nanoparticles as drug delivery systems. These studies have demonstrated that anionic particles cross biological barriers *in vitro* as well as the BBB *in vivo* (Lockman *et al*, 2004; Chattopadhyay *et al*, 2008; Voigt, Christensen, and Shastri, 2014). This supports our contention that our novel anionic vesicles may have potential as a drug delivery system. In order to investigate this further *in vitro* uptake studies were performed.

5.3 Uptake and kinetic studies

AF546 encapsulated anionic vesicles prepared in this study were used in the preliminary *in vitro* uptake studies to investigate their capabilities. They were shown to be taken up by the neuronal cell line SH-SY5Y within two hours of exposure.

Further experiments were undertaken to investigate their ability to be taken up by different cell lines.

Uptake and kinetic studies were performed in the kidney cell line - HEK-293T, microglial BV2s, neuroblastoma - SH-SY5Y and glioblastoma - LN229, with our novel BA vesicles encapsulating antibody fragment, scFv 4D5-8RFP, or PI. Vesicles encapsulating this antibody fragment were shown to be taken up *in vitro* in SH-SY5Y cells. PI binds to nucleic acids and is also unable to cross intact membranes, thus making this a useful tool to measure the uptake and release of our vesicles, as PI should be excluded from healthy cells. Initial studies with PI encapsulated vesicles showed them to be opened after 24 hours incubation in HEK-293, BV2s, and SH-SY5Y cells to differing degrees, with the lowest nuclear staining observed in the SH-SY5Y cells. Whilst this shows uptake it does not provide an accurate time frame as to when the vesicles are taken up and lysed. To further investigate the uptake kinetics, the study was reprised in glioblastoma, LN229 cells. As PI is excluded from healthy cells the premise is that only encapsulated PI will be able to enter the cell, and only once the vesicle has been lysed will we see fluorescence as PI binds to nucleic acids. We were able to measure not only uptake but lysis of the PI encapsulated vesicles through the increase of fluorescence signal as the PI bound. Cells were incubated at different time intervals and uptake was measured using flow cytometry. Uptake was observed within 30 minutes and increased over the four-hour time frame measured. This demonstrated that not only were the vesicles being taken up, but they were lysed, releasing their payload. Although we know the vesicles are releasing their cargo, we do not know the mechanism by which this occurs. This may be cell type specific, as has been suggested previously (Korang-Yeboah *et al*, 2015), but will be an important topic for future studies to address. One avenue to explore will be with vesicles containing a tracer dye such as lysotracker. These will allow tracking of the vesicles microscopically to investigate in which cellular compartment they are taken up and when they are lysed.

5.4 Safety of the vesicles

To test the safety and utility of our BA vesicles as a drug delivery system, we undertook a range of viability and immunogenicity studies *in vitro,* including the annexin A5 apoptosis assay, PrestoBlue cell viability assay, and measurement of

secreted TNF-α by ELISA. This study used cell lines representative of the BBB and of those that the vesicles may encounter within the brain, namely immortalised human endothelial cells hCMEC/D3, murine microglia BV2s and immortalised human astrocytes HASTR/ci35. The vesicles were found to induce a small degree of cytotoxicity in hCMEC/D3 after 24 hours and HASTR/ci35 after 7 days exposure when given at a high dose (50 µg/ml). Importantly however, this dose is significantly greater than might be expected to be used *in vivo*, where administration of 3.5 µg per mouse was shown to be sufficient to enable tracer delivery to the brain. This suggests that toxic effects of the vesicles are unlikely to prove a major limiting factor. There is a lack of toxicity studies regarding vesicles produced from vernonia oil and of BA nanoparticles in general, further demonstrating the need for such studies to be carried out and reported (Fariya *et al*, 2014). Nonetheless, strategies to improve vesicle targeting and reduce exposure, such as PEGylation, may prove valuable for future study (Peng *et al*, 2013, Sukhanova *et al*, 2018).

5.5 In vivo studies

BA vesicles encapsulating antibody fragment, scFv 4D5-8RFP, or tracer molecules were shown to be taken up *in vitro*, but the critical test for any potential drug delivery system is whether uptake also occurs *in vivo*. Accordingly, we administered BA vesicles intravenously to 7-week old male C57BL/6 mice, treating groups with either encapsulated AF546 vesicles, non-encapsulated AF546, encapsulated antibody fragment, non-encapsulated antibody fragment or empty vesicles. Importantly, encapsulated AF546 vesicles were taken up and could be detected within the brain after 30 minutes circulation time. This demonstrated that our novel anionic vesicles are able to cross the BBB. Lockman *et al* (2004) have previously observed that anionic nanoparticles can cross the BBB more effectively than cationic nanoparticles. Cationic vesicles, GLH-20 produced from vernonia oil, were shown to cross the BBB in 30 mins, however this study observed high clearance of these vesicles in the kidneys (Popov *et al*, 2012). Our vesicles were effectively cleared in the lungs and liver, as has been shown in studies of similar particle clearance mechanisms (Thurston *et al*; 1998; Popov *et al*, 2010; Zhang *et al*, 2015). Together, these data demonstrate that our novel vesicles have the potential to be used as a drug delivery system.

5.6 Synthesis of novel bolaamphiphilic material.

Having shown the potential of BAs as a drug delivery system, we wanted to more fully characterise the chemical properties of these vesicles, and to establish an effective chemical synthetic pathway. High resolution mass spectrometry (HMRS) analysis indicated the presence of two species, both intermediates of the original GLH-20 formulation, the penultimate product (FASCA 01) and a further intermediate (TET01). Therefore, attempts to reconstruct this material were undertaken. This was a time-consuming process as the protocol needed optimisation at almost every step to increase the yield. The initial protocol was a three-step procedure with the first step being hydrolysis of the esters, followed by a coupling reaction to extend the carbon chain and finally the opening of the epoxide group with the addition of chloroacetic acid (FASCA 01) or without (TET 01). The first step was the hydrolysis of the esters, using the original starting material, vernonia oil. Initially the procedure followed the methodology reported by Grinberg *et al* (2005 and 2008) and Stern *et al* (2014) in order to produce the intermediates (FASCA 01 and TET01) seen in the HRMS analysis. Both intermediates were produced and the overall yield for TET01 was increased from 4.8% to 64%. Although the process requires future yield optimisation for FASCA 01, both formulations were synthesised into vesicles encapsulating tracer dyes. Profiling of these vesicles with DLS, zeta potential, size exclusion chromatography and nanoparticle tracking analysis confirmed that whilst they produced vesicles the characteristics differed to that of the original material in that they had poorer stability. It is recommended that the two formulations be combined as both compounds were present in the original HRMS analysis. Whilst we have demonstrated that these vesicles can been recreated, further optimisation and testing is required.

5.7 Future work

Whilst future studies will include calculating. the encapsulation efficiency of scFv 4D5-8RFP vesicles it is important to point out that the encapsulation efficiency is relative to the drug and dose encapsulated within the vesicle. The most important factor is ensuring that they have an effective, deliverable payload, that the encapsulation does not compromise biological activity and that the molecule can reach its target site (Bozzuto and Molinari, 2015). Nonetheless, due to the

encapsulation efficiency being low for vesicles in our studies, it remains important to investigate improving this efficiency. A number of variables can be trialled, increasing the concentration of bola material, increasing the concentration of drug/molecules to be encapsulated and PEGylation. Future work will include encapsulating different tracer dyes to further investigate how the external environment influences the internal environment of the vesicle, as well as lysotracker to investigate how the vesicles are lysed, and investigate the uptake mechanism in the presence of various inhibitors. Production of the vesicles will be further optimised, particularly by investigating mixing both formulations together (FASCA 01 and TET01) to increase stability. The recent study on combined GLH-19 and GLH-20 vesicles being successfully used to deliver siRNA to mouse brains attests to the potential of this approach (Kim *et al*, 2020). Uptake studies, viability and immunogenic assays will be performed *in vitro* in different cell lines. Ideally, *in vivo* studies will be performed using the newly synthesised vesicles that consist of these anionic molecules (FASCA 01 and TET01).

5.8 Conclusion

Novel anionic vesicles have been synthesised encapsulating a range of different cargoes. They have been shown to be taken up and released *in vitro*. They have also crossed the BBB *in vivo*, 30 minutes after intravenous injection. We have developed a novel methodology for the synthesis of these novel vesicles. These vesicles have shown the potential to be useful as a drug delivery system.

6 REFERENCES

Abbott, A. (2011). Novartis to shut brain research facility. Drug giant redirects psychiatric efforts to genetics. *Nature* 480(7376):161–162.

Abbott, N, J. (2013). Blood-brain barrier structure and function and the challenges for CNS drug delivery. *Journal of Inherited Metabolic Disease* 36:437-449

Abbott, N, J., Patabendige, A, K., Dolman, D, E, M., Yusof, S, R., and Begley, D, J. (2010). Structure and function of the blood-brain barrier. *Neurobiology of Disease* 37(1):13-25

Abbott, N, J., Pizzo, M, E., Preston, J, E., Janigro, D., and Thorne, R, G. (2018). The role of brain barriers in fluid movement in the CNS: is there a 'glymphatic' system? *Acta Neuropathologica*. 135:387-407

Abbott, N, J., Ronnback, L., and Hanson, E. (2006). Astrocyte-endothelial interactions at the blood-brain barrier. *Nature Reviews Neuroscience* 7:41-53

Abyadeh, M., Zarchi, A, A, K., Faramarzi, M, A., and Amani, A. (2017). Evaluation of factors affecting size and size distribution of chitosan-electrosprayed nanoparticles. *Avicenna Journal of Medical Biotechnology* 9(3):126-132

Adan, A., Kiraz, Y., and Baran, Y. (2016). Cell proliferation and cytotoxicity Assays. *Current Pharmaceutical Biotechnology* 17(14): 1213-1221

Ai, Y., Markesbery, W., Zhang, Z., Grondin, R., Elseberry, D., Gerhardt, G, A., and Gash, D, M. (2003). Intraputamenal Infusion of GDNF in Aged Rhesus Monkeys: Distribution and Dopaminergic Effects. *The Journal of Comparative Neurology* 461:250-261

Ajay., Bemis, G, W., and Murcko, M, A. (1999). Designing Libraries with CNS Activity. *Journal of Medicinal Chemistry* 42(24):4942-4951

Alavijeh, M, S., and Palmer, A, M. (2010). Measurement of the pharmacokinetics and pharmacodynamics of neuroactive compounds. *Neurobiology of Disease* 37:38-47

Almutairi, M, M, A., Gong, H., Yu, Y, G., Chang, Y., and Shi, H. (2016). Factors controlling permeability of the blood-brain barrier. *Cellular and Molecular Life Sciences* 73:57-77

Alvarez-Erviti, L., Seow, Y., Yin, H., Betts, C., Lakhal, S. and Wood, M, J. (2011). Delivery of siRNA to the mouse brain by systemic injection of targeted exosomes. *Nature Biotechnology*, 29(4):341-345.

Alvarez, J, I., Katayama, T., and Prat, A. (2013). Glial Influence on the Blood Brain Barrier. *Glia* 61:1939-1958

Alzheimer's Association. (2018). Alzheimer's disease facts and figures. *Alzheimer's & Dementia*. 14(3):367-429

Ananda, S., Nowak, A.K., Cher, L., Dowling, A., Brown, C., Simes, J., Rosenthal, M.A. and Cooperative Trials Group for Neuro-Oncology (COGNO). (2011). Phase 2 trial of temozolomide and pegylated liposomal doxorubicin in the treatment of patients with glioblastoma multiforme following concurrent radiotherapy and chemotherapy. *Journal of Clinical Neuroscience* 18(11):1444-1448.

Andreone, B, J., Chow, B, W., Tata, A., Lacoste, B., Ben-Zvi, A., Bullock, K., Deik, A, A., Ginty, D, D., Clish, C, B., and Gu, C. (2017). Blood-Brain Barrier Permeability Is Regulated by Lipid Transport-Dependent Suppression of Caveolae-Mediated Transcytosis. *Neuron* 94:581-594

Aoki, M., Ring, T, A., and Haggerty, J, S. (1987). Analysis and modelling of the ultrasonic dispersion technique. *Advanced Ceramic Materials (USA) 2*(3A).

Arvanitis, C, D., Ferraro, G, B., and Jain, R, K. (2019). The blood brain barrier and blood-tumour barrier in brain tumours and metastases. *Nature Reviews Cancer* 20:26-41

Aryal, M., Fischer, K., Gentile, C., Gitto, S., Zhang, Y, Z., and McDannold, N. (2017). Effects on P-Glycoprotein Expression after Blood0Brain Barrier Disruption Using Focused Ultrasound and Microbubbles. *PLoS ONE* 12(1):e0166061

Ashraf, T., Kao, A., and Bendaya, R. (2014). Functional Expression of Drug Transporters in Glial Cells: Potential Role on Drug Delivery to the CNS. *Advances in Pharmacology* 71:45-111

Ashraf, T., Kis, O., Banerjee, N., and Bendayan, R. (2012). Drug transporters at brain barriers: expression and regulation by neurological disorders. *Advances in Experimental Medicine and Biology* 763:20-69

Baeten, K, M., and Akassoglou, K. (2011). Extracellular Matrix and Matrix Receptors in Blood- Brain Barrier Formation and Stroke. *Developmental Neurobiology* 71(11):1018-1039

Baker, S, L., Munasinghe, A., Kaupbayeva, B., Kang, N, R., Certiat, M., Murata, H., Matyjaszewski, K., Lin, P., Colina, C, M., and Russell, A, J. (2019). Transforming protein-polymer conjugate purification by tuning protein solubility. *Nature Communications* 10(1):1-12.

Ballabh, P., Braun, A., and Nedergaard, M. (2004). The blood-brain barrier: an overview: structure, regulation, and clinical implications. *Neurobiology of Disease* 16(1): 1-13

Banks, W, A. (2019). The blood–brain barrier as an endocrine tissue. *Nature Reviews Endocrinology* 15(8):444-455.

Banks, W, A., and Greig, N, H. (2019). Small molecules as central nervous system therapeutics: old challenges, new directions, and a philosophic divide. *Future Medicinal Chemistry* 11(6):489-493

Barabutis, N., Uddin, M, A. and Catravas, J, D. (2019). Hsp90 inhibitors suppress p53 phosphorylation in LPS-induced endothelial inflammation. *Cytokine*, 113:427-432.

Bart, J., Groen, H, J, M., Hendrikse, N, H., van der Graaf, W, T, A, Vaalburg, W., and de Vries, E, G, E. (2000). The blood-brain barrier and oncology: new insights into function and modulation. *Cancer Treatment Reviews* 26:449-462

Bastini, M., and Parton, R, G. (2010). Caveolae at a glance. *Journal of Cell Science*.123:3831-3836

Bell, R, D., Winkler, E, A., Sagare, A, P., Singh, I., LaRue, B., Deane, R., and Zlokovic, B, V. (2010). Pericytes control key neurovascular functions and neuronal phenotype in the adult brain and during brain aging. *Neuron* 68(3):409-427.

Benarroch, E, E. (2014). Brain glucose transporters: Implications for neurological disease. *Clinical Implications of Neuroscience Research* 82(15):1374-1379

Benlimame, N., Le, P, U., and Nabi, I, R. (1998). Localisation of autocrine motility factor receptor to caveolae and clathrin-independent internalisation of its ligand to smooth endoplasmic reticulum. *Molecular Biology of the Cell*. 9:1773-86

Beck, A., Goetsch, L., Dumontet, C., and Corvaïa, N. (2017). Strategies and challenges for the next generation of antibody-drug conjugates. *Nature Reviews Drug Discovery* 16(5):315-337

Bergström, M., and Långström, B. (2005). Pharmacokinetic studies with PET. In *Imaging in Drug Discovery and Early Clinical Trials* (pp. 279-317). Birkhäuser Basel.

Berlier, J, E., Rothe, A., Buller, G., Bradford, J., Gray, D, R., Filanoski, B, J., Telford, W, G., Yue, S., Liu, J., Cheung, C, Y., and Chang, W. (2003). Quantitative comparison of long-wavelength Alexa Fluor dyes to Cy dyes: fluorescence of the dyes and their bioconjugates. *Journal of Histochemistry & Cytochemistry* 51(12):1699-1712.

Bernard-Arnoux, F., Lamure, M., Ducray, F., Aulagner, G., Honnorat, J., and Armoiry, X. (2016). The cost-effectiveness of tumour-treating fields therapy in patients with newly diagnosed glioblastoma. *Neuro-Oncology* 18(8):1129-1136

Bhattacharjee, S. (2016). DLS and zeta potential–what they are and what they are not? *Journal of Controlled Release* 235:337-351.

Bicker, J., Alves, G., Fortuna, A., and Falcão, A. (2014). Blood-brain barrier models and their relevance for a successful development of CNS drug delivery systems: A review. *European Journal of Pharmaceutics and* Biopharmaceutics 87:409-432

Björnmalm, M., Faria, M., and Caruso, F. (2016). Increasing the impact of materials in and beyond bio-nano science. *Journal of the American Chemical Society* 138(41)13449-13456.

Blanchette, M., and Daneman, R. (2015). Formation and maintenance of the BBB. *Mechanisms of Development* 138:8-16

Bobo, H, R., Laske, D, W., Akbasak, A., Morrison, P, F., Dedrick, R, L., and Oldfield, E, H. (1994). Convection-enhanced delivery of macromolecules in the brain. *Proceeding of the National Academy of Sciences* 91:2076-2080

Bodor, N., and Buchwald, P. (2002). Barriers to remember: brain-targeting chemical delivery systems and Alzheimer's disease. *Drug Discovery Today*. 7(14):766-774

Bors, L, A., and Erdő, F. (2019). Overcoming the Blood–Brain Barrier. Challenges and Tricks for CNS Drug Delivery. *Scientia Pharmaceutica* 87(1):1-28.

Bozzuto, G., and Molinari, A. (2015). Liposomes as nanomedical devices. *International Journal of Nanomedicine* 10:975-999

Brasnjevic, I., Steinbusch, H, W, M., Schmitz, C., and Martinez-Martinez, P. (2009). Delivery of peptide and protein drugs over the blood-brain barrier. *Progress in Neurobiology* 87:212-251

Brem, H., Mahaley, M, S., Vick, N, A., Black, K, L., Schold, S, C., Burger, P, C., Friedman, A, H., Ciric, I, S., Eller, T, W., Cozzens, J, W., and Kenealy, J, N. (1991). Interstitial chemotherapy with drug polymer implants for the treatment of recurrent gliomas. *Journal of Neurosurgery* 74(3):441-446

Brightman, M, W., and Reese, T, S. (1969). Junctions between intimately apposed cell membranes in the vertebrate brain. *Journal of Cell Biology* 40(3):648-77

Brodská, B., Holoubek, A., Otevřelová, P., and Kuželová, K. (2016). Low-Dose Actinomycin-D Induces Redistribution of Wild-Type and Mutated Nucleophosmin Followed by Cell Death in Leukemic Cells. *Journal of Cellular Biochemistry* 117(6):1319-1329.

Brown, V, I., and Greene, M, I. (1991). Molecular and cellular mechanisms of receptor-mediated endocytosis. *DNA and Cell Biology* 10(6):399-409

Byers, J, A., and Jamison, T, F. (2013). Entropic factors provide unusual reactivity and selectivity in epoxide-opening reactions promoted by water. *Proceedings of the National Academy of Sciences* 110(42):16724-16729.

Çalış, S., Atar, K, Ö., Arslan, F, B., Eroğlu, H., and Çapan, Y. (2019). Nanopharmaceuticals as Drug-Delivery Systems: For, Against, and Current Applications. In *Nanocarriers for Drug Delivery* pp. 133-154.

Candela, P., Gosselet, F., Miller, F., Buee-Scherrer, V., Torpier, G., Cecchelli, R., and Fenart, L. (2008). Physiological Pathway for Low-Density Lipoproteins across the Blood-Brain Barrier: Transcytosis through Brain Capillary Endothelial Cells In Vitro. *Endothelium* 15:1-11

Castro, D, M., Dillon, C., Machnicki, G., and Allegri, R, F. (2010). The economic cost of Alzheimer's disease: Family or public-health burden? *Dementia and Neuropsychologia* 4(4):262-267

Chalikwar, S, S., Mene, B, S., Pardeshi, C, V., Belgamwar, V, S., and Surana, S, J. (2013). Self-assembled, chitosan grafted PLGA nanoparticles for intranasal delivery: design, development and ex vivo characterization. *Polymer-Plastics Technology and Engineering* 52(4):368-380.

Chan, G, N., Hoque, M, T., and Bendayan, R. (2013). Role of nuclear receptors in the regulation of drug transporters in the brain. *Trends in Pharmacological Sciences* 34(7):361-372

Chang, R., Yee, K, L. and Sumbria, R, K. (2017). Tumor necrosis factor α Inhibition for Alzheimer's Disease. *Journal of Central Nervous System Disease* 9:1179573517709278.

Charles, N, A., Holland, E, C., Gilberston, R., Glass, R., and Kettenmann, H. (2011). The brain tumour microenvironment. *Glia* 59:1169-1180

Chattopadhyay, N., Zastre, J., Wong, H, L., Wu, X, Y., and Bendayan, R. (2008). Solid lipid nanoparticles enhance the delivery of the HIV protease inhibitor, Atazanavir, by a human brain endothelial cell line. *Pharmaceutical Research* 5(10):2262-2271

Chaturvedi, S., Rashid, M., Malik, M, Y., Agarwal, A., Singh, S, K., Gayen, J, R., and Wahajuddin, M. (2019). Neuropharmacokinetics: a bridging tool between CNS drug development and therapeutic outcome. *Drug Discovery Today* 24(5):116-1175

Chenthamara, D., Subramamiam, S., Ramakrishnan, S, G., Krishnaswamy, S., Essa, M, M., Lin, F, H., and Qoronfleh, M, W. (2019). Therapeutic efficacy of nanoparticles and routes of administration. *Biomaterials Research* 23(20):1-29

Clarke, L, E., Liddelow, S, A., Chakraborty, C., Münch, A, E., Heiman, M., and Barres, B, A. (2018). Normal aging induces A1-like astrocyte reactivity. *Proceedings of the National Academy of Sciences* 115(8):E1896-E1905

Clogston, J, D., and Patri, A, K. (2011). Zeta potential measurement. In: McNeil, S, E. (ed). Characterisation of Nanoparticles Intended for Drug Delivery. Humana Press, Totowa, NJ, pp 63–70.

Cohen-Pfeffer, J, L., Gururangan, S., Lester, T., Lim, D, A., Shaywitz, A, J., Westphal, M., and Slavc, I. (2017). Intracerebroventricular Delivery as a Safe, Long-Term Route of Drug Administration. *Paediatric Neurology* 67:23-35

Coomber, B, L., and Stewart, P, A. (1986). Three-dimensional reconstruction of vesicles in endothelium of blood-brain barrier versus highly permeable microvessels. *The Anatomical record* 215(3):256-61

Cording, J., Günther, R., Vigolo, E., Tscheik, C., Winkler, L., Schlattner, I., Lorenz, D., Haseloff, R, F., Schmidt-Ott, K, M., Wolburg, H., and Blasig, I, E. (2015). Redox

regulation of cell contacts by tricellulin and occluding: Redox-sensitive cysteine sites in tricellulin regulate both tri- and bicellular junctions in tissue barriers as shown in hypoxia and ischemia. *Antioxidants and Redox Signalling* 23(13):1035-1049

Corey, E, J., and Venkateswarlu, A. (1972). Protection of Hydroxyl Groups as tert-Butyldimethylsilyl Derivatives. *Journal of the American Chemical Society* 94(17):6190-6191

Corraliza-Gorjón, I., Somovilla-Crespo. B., Santamaria, S., Garcia-Sanz, J, A., and Kremer, L. (2017) New strategies using antibody combinations to increase cancer treatment effectiveness. *Frontiers in Immunology*. 8(1804):1-31

Cory, R, M., Ritchie, B, M., and Shrier, A, M. (1990). A versatile synthesis of butenolides total synthesis of (+/-)-mintlactone. *Tetrahedron Letter* 31(47):6789-6792

Crone, C., and Christensen, O. (1981). Electrical resistance of a capillary endothelium. *The Journal of General Physiology* 77(4):349-371

Cummins, P, M. (2012). Occludin: One Protein, Many Forms. *American Society for Microbiology* 32(2):242-250

D'Angelo, J. and Smith, M. B. (2015). Common Fundamental Reactions in Organic Chemistry. *Hybrid Retrosynthesis* 77–149*.*

Dakwar, G, R., Hammad, I, A., Popov, M., Linder, C., Grinberg, S., Heldman, E; and Stepensky, D. (2012). Delivery of proteins to the brain by bolaamphiphilic nano-sized vesicles. *Journal of Controlled Release*. 160(2): 315-321

Danaei, M., Dehghankhold, M., Ataei, S., Davarani, F, H., Javanmard, R., Dokhani, A., Khorasani, S., and Mozafari, M, R. (2018). Impact of particle size and polydispersity index on the clinical applications of lipidic nanocarrier systems. *Pharmaceutics* 10(2):57-74

Daneman, R. (2012). The Blood-Brain Barrier in Health and Disease. *Annuals of Neurology* 72(5):648-672

Daneman, R., and Prat, A. (2015). The Blood-Brain Barrier. *Cold Spring Harbour Perspectives in Biology*. 7(1):a020412

Daneman, R., Zhou, L., Agalliu, D., Cahoy, J, D., Kaushal, A., and Barres, B, A. (2010). The mouse blood-brain barrier transcriptome: a new resource for understanding the development and function of brain endothelial cells. *PLoS ONE* 5(10):e13741

Davalos, D., Grutzendler, J., Yang, G., Kim, J, V., Zuo, Y., Jung, S., Littman, D, R., Dustin, M, L. and Gan, W, B. (2005). ATP mediates rapid microglial response to local brain injury in vivo. *Nature Neuroscience* 8(6):752-758

De Jong, W, H., and Borm, P, J, A. (2008). Drug delivery and nanoparticles: Applications and hazards. *International Journal of Nanomedicine* 3(2):133-149

de Lange, E, C. (2004). Potential role of ABC transporters as a detoxification system at the blood–CSF barrier. *Advanced Drug Delivery Reviews* 56(12), pp.1793-1809.

de Morais Ribeiro, L, N., Couto, V, M., Fraceto, L, F., and de Paul, E. (2018). Use of nanoparticle concentration as a tool to understand the structural properties of colloids. *Scientific Reports* 8:982

De Witt Hamer, P, C. (2010). Small molecule kinase inhibitors in glioblastoma: a systematic review of clinical studies. *Neuro-oncology*. 12(3), pp.304-316.

Derecki, N, C., Cronk, J, C., and Kipnis, J. (2013). The role of microglia in brain maintenance: implication for Rett syndrome. *Trends in Immunology* 34(3):144-150

DiMasi, J, A., Feldman, L., Seckler, A., and Wilson, A. (2010). Trends in risks associated with new drug development: success rates for investigational drugs. *Clinical Pharmacology & Therapeutics* 87(3):272-277.

Djupesland, P, G. (2013a). Nasal drug delivery devices: characteristics and performance in a clinical perspective- a review. *Drug Delivery and Translational Research* 3:42-62

Djupesland, P, G., Mahmoud, R, A., and Messina, J, C. (2013b). Accessing the brain: the nose may know the way. *Journal of Cerebral Blood Flow and Metabolism* 33:793-794

Dobrovolskaia, M, A., and McNeil, S, E. (2013). Understanding the correlation between in vitro and in vivo immunotoxicity tests for nanomedicines. *Journal of Controlled Release* 172(2):456-466.

Doherty, G, J., and McMahon, H, T. (2009). Mechanisms of Endocytosis. *Annual Review of Biochemistry*. 78:857-902

Dorsey, E. R., Elbaz, A., Nichols, E., Abd-Allah, F., Abdelalim, A., Adsuar, J, C., Ansha, M, G., Brayne, C., Choi, J, Y. J., Collado-Mateo, D., Dahodwala, N., Do, H, P., Edessa, D.,Endres, M., Fereshtehnejad, S, M., Foreman, K, J., Gankpe, F, G., Gupta, R., Hankey, G, J., Hay, S, I., Hegazy, M, I., Hibstu, D, T., Kasaeian, A., Khader, Y., Khalil, I., Khang, Y, H., Kim, Y, J., Kokubo, Y., Logroscino, G., Massano, J., Ibrahim, N, M., Mohammed, M, A., Mohammadi, A., Moradi-Lakeh, M., Naghavi, M., Nguyen, B, T., Nirayo, Y, L., Ogbo, F, A., Owolabi, M, O., Pereira, D, M., Postma, M, J., Qorbani, M., Rahman, M, A., Roba, K, T., Safari, H., Safiri, S., Satpathy, M., Sawhney, M., Shafieesabet, A., Shiferaw, M, S., Smith, M., Szoeke, C, E., Tabarés-Seisdedos, R., Truong, N, T., Ukwaja, K, N., Venketasubramanian, N., Villafaina, S., Weldegwergs, K., Westerman, R.,Wijeratne, T., Winkler, A, S., Xuan, B, T., Yonemoto, N., Feigin, V, L., Vos, T., and Murray, C, J, L. (2018). Global, regional, and national burden of Parkinson's disease, 1990 – 2016: a systematic analysis for the Global Burden of Disease Study 2016. *Lancet Neuorology* 17:939-953

Dréan, A., Rosenberg, S., Lejeune, F, X., Goli, L., Nadaradjane, A, A., Guehennec, J., Schmitt, C., Verreault, M., Bielle, F., Mokhtari, K., Sanson, M., Carpentier, A.,

Delattre, J, Y., and Idbaih, A. (2018). ATP binding cassette (ABC) transporters: expression and clinical value in glioblastomas. *Journal of Neuro-Oncology* 138:479-486

Dusinska, M., Rundén-Pran, E., Schnekenburger, J., and Kanno, J. (2017). Toxicity tests: in vitro and in vivo. In *Adverse effects of engineered nanomaterials* (pp. 51-82). Academic Press.

Dutta, D., and Donaldson, J, G. (2012). Search for inhibitors of endocytosis. *Cellular Logistics* 2(4):203-208

Eggen, B, J, L., Raj, D., Hanisch, U, K., and Boddeke, H, W, G, M. (2013). Microglial Phenotype and Adaptation. *Journal of Neuroimmune Pharmacology* 8:807-823

Elechalawar, C, K., Bhattacharya, D., Ahmed, M, T., Gora, H., Sridharan, K., Chaturbedy, P., Sinha, S, H., Jaggarapu, M, M, C, S., Narayan, K, P., Chakravarty, S. and Eswaramoorthy, M. (2019). Dual targeting of folate receptor-expressing glioma tumour-associated macrophages and epithelial cells in the brain using a carbon nanosphere–cationic folate nanoconjugate. *Nanoscale Advances* 1(9):3555-3567.

Engin, A, B., and Hayes, A, W. (2018). The Impact of Immunotoxicity in Evaluation of the Nanomaterials Safety. *Toxicology Research and Application* 2:1-9

Erdő, F., Bors, L, A., Farkas, D., Bajza, A., and Gizurarson, S. (2018). Evaluation of intranasal delivery route of drug administration for brain targeting. *Brain Research Bulletin* 143:155-170

Escamilla, G, H., and Newkome, G, R. (1994). Bolaamphiphiles from golf balls to fibres. *Angewandte Chemie International Edition in English* 33(19):1937-1940

Faraco, G., Park, L., Anrather, J. and Iadecola, C. (2017). Brain perivascular macrophages: characterization and functional roles in health and disease. *Journal of Molecular Medicine* 95(11):1143-1152.

Fariya, M., Jain, A., Dhawan, V., Shah, S., and Nagarsenker, M, S. (2014). Bolaamphiphiles: a pharmaceutical review. *Advanced pharmaceutical bulletin* 4(Suppl 2):483

Feigin, V, L., Abajobir, A, A., Abate, K, Hassen., Abd-Allah, F., Abdulle, A, M., Abera, S, F., Abyu, G, Y., Ahmed, M, B., Aichour, A, N., Aichour, I., Aichour, M, T, E., Akinyemi, R, O., Alabed, S., Al-Raddadi, R., Alvis-Guzman, N., Amare, A, T., Ansari, H., Anwari, P., Ärnlöv, J., Asayesh, H., Asgedom, S, W., Atey, T, M., Avila-Burgos, L., Avokpaho, E, F, G, A., Azarpazhooh, M, R., Barac, A., Barboza, M., Barker-Collo, S, L., Bärnighausen, T., Bedi, N., Beghi, E., Bennett, D, A., Bensenor, I, M., Berhane, A., Betsu, B, D., Bhaumik, S., Birlik, S, M., Biryukov, S., Boneya, D, J., Bulto, L, G., Carabin, H., Casey, D., Castañeda-Orjuela, C, A., Catalá-López, F., Chen, H., Chitheer, A, A., Chowdhury, R., Christensen, H., Dandona, L., Dandona, R., de Veber, G, A., Dharmaratne, S, D., Do, H, P., Dokova, K., Dorsey, E, R., Ellenbogen, R, G., Eskandarieh, S., Farvid, M, S., Fereshtehnejad, S, M.,

Fischer, F., Foreman, K, J., Geleijnse, J, M., Gillum, R, F., Giussani, G., Goldberg, E, M., Gona, P, N., Goulart, A, C., Gugnani, H, C., Gupta, R., Gupta, R., Hachinski, V., Hamadeh, R, R., Hambisa, M., Hankey, G, J., Hareri, H, A., Havmoeller, R., Hay, S, I., Heydarpour, P., Hotez, P, J., Jakovljevic, M, M, J., Javanbakht, M., Jeemon, P., Jonas, J, B., Kalkonde, Y., Kandel, A., Karch, A., Kasaeian, A., Kastor, A., Keiyoro, P, N., Khader, Y, S., Khalil, I, A., Khan, E, A., Khang, Y, H., Khoja, A, T, A., Khubchandani, J., Kulkarni, C., Kim, D., Kim, Y, J., Kivimaki, M., Kokubo, Y., Kosen, S., Kravchenko, M., Krishnamurthi, R, V, Kuate, B., Kumar, D, G, A., Kumar, R., Kyu, H, H., Larsson, A., Lavados, P, M., Li, Y., Liang, X., Liben, M, L., Lo, W, D., Logroscino, G., Lotufo, P, A., Loy, C, T., Mackay, M, T., Magdy , H., Magdy, A, E, H, M., Majeed, E, R, A., Malekzadeh, R., Manhertz, T., Mantovani, L, G., Massano, J., Mazidi, M., McAlinden, C., Mehata, S., Mehndiratta, M, M., Memish,Z, A., Mendoza, W., Mengistie, M, A., Mensah, G, A., Meretoja, A., Mezgebe, H, B., Miller, T, R., Mishra, S, R., Mohamed, N., Mohammadi, I, A., Mohammed, K, E., Mohammed, S., Mokdad,A, H., Moradi-Lakeh, M., Moreno-Velasquez, Musa, K, M., Naghavi, M., Ngunjiri, J, W., Nguyen, C, T., Nguyen, G., Nguyen, Q, L., Nguyen, T, H., Nichols, E., Ningrum, D, N, A., Nong, V, M., Norrving, B., Noubiap, , J, N., Ogbo, F, A., Owolabi, M, O., Pandian, J, D., Parmar, P, G., Pereira, D, M., Petzold, M., Phillips, M, R., Piradov, M, A.,. Poulton, R, G., Pourmalek, F., Qorbani, M., Rafay, A., Rahman, M., Rahman, M, H., Rai, R, J., Rajsic, S., Ranta, A., Rawaf, S., Renzaho, A, M, N., Rezai, M, S., Roth, G, A., Roshandel, G., Rubagotti, E., Sachdev, P., Safiri, S., Sahathevan, R., Sahraian, M, A., Samy, A, M., Santalucia, P., Santos, I, S., Sartorius, B., Satpathy, M., Sawhney, M., Saylan, M, I., Sepanlou, S, G., Shaikh, M, A., Shakir, R., Shamsizadeh, M., Sheth, K, N., Shigematsu, M., Shoman, H., Silva, D, A, S., Smith, M., Sobngwi, E., Sposato, L, A., Stanaway, J, D., Stein, D, J., Steiner, T, J., Stovner, L, J., Suliankatchi-Abdulkader, R., Szoeke, C, L., Tabarés-Seisdedos, R., Tanne, D., Theadom, A, M., Thrift, A, G., Tirschwell, D, L., Topor-Madry, R., Tran, B, X., Truelsen, T., Tuem, K, B., Ukwaja, K, N., Uthman, O, A., Varakin, Y, Y., Vasankari, T., Venketasubramanian, N., Vlassov, V, V., Wadilo, F., Wakayo, T., Wallin, M, T., Weiderpass, E., Westerman, R., Wijeratne, T., Wiysonge, C, S., Woldu, M, A., Wolfe, C, D, A., Xavier, D., Xu, G., Yano, Y., Yimam, H, H., Yonemoto, N., Yu, C., Zaidi, Z., Zaki, M, E, S., Zunt, J, R., Murray, C, J, L., and Vos,T. (2017). Global, regional, and national burden of neurological disorders during 1990 – 2015: a systematic analysis for the Global Burden of Disease Study 2015. *Lancet Neurology* 16:877-897

Fenhart, L., Casanova, A., Dehouck, B., Duhem, C., Slupek, S., Cecchelli, R., and Betbeder, D. (1999). Evaluation of effect of charge and lipid coating on the ability of 60 nm nanoparticles to cross an in vitro model of the blood-brain barrier. *Journal of Pharmacology and Experimental Therapeutics* 291(3):1071-1022

Filipe, V., Hawe, A., and Jiskoot, W. (2010). Critical evaluation of nanoparticle tracking analysis (NTA) by NanoSight for the measurement of nanoparticles and protein aggregates. *Pharmaceutical Research* 27(5):796-810

Filipe, V., Hawe, A., and Jiskoot, W. (2010). Critical evaluation of NTA by NanoSight measurement of nanoparticles and protein aggregates. *Pharmaceutical Research* 27(5):796-811

Flynn, M., Zammarchi, F., Tyrer, P. C., Akarca, A. U., Janghra, N., Britten, C. E., Havenith, C, E., Levy, J, N., Tiberghien, A., Masterson, A., Barry, C., D'Hooge, F., Marafioti, T., Parren, P, W., Williams, D, G., Howard, P, W., van Berkel, P, H., and Hartley, J. A. (2016). ADCT-301, a Pyrrolobenzodiazepine (PBD) Dimer-Containing Antibody Drug Conjugate (ADC) Targeting CD25-Expressing Hematological Malignancies. *Molecular Cancer Therapeutics*. doi:10.1158/1535-7163.MCT-16-0233

Franceschi, S., de Viguerie, N., Riviere, M., and Lattes, A. (2000). Synthesis and aggregation of two-headed surfactants bearing amino acid moieties. *New Journal of Chemistry* 23(4):447-452

Francia, V., Rejer-Smit, C., Boel, G., and Salvati, A. (2019). Limits and challenges in using transport inhibitors to characterise how nano-sized drug carriers enter cells. *Nanomedicine* 14(12):1533-1549

Freskgård, P, O., and Urich, E. (2017). Antibody therapies in CNS diseases. *Neuropharmacology*. 120:38-55

Fu, Y., and Kao, W, J. (2010). Drug release kinetics and transport mechanisms of non-degradable and degradable polymeric delivery systems. *Expert Opinion on Drug Delivery* 7(4):429-444

Fuhrhop, J, H., and Fritsch, D. (1986). Bolaamphiphiles form ultrathin, porous, and unsymmetric monolayer lipid membrane. *Accounts of Chemical Research* 19(5);130-137

Fuhrhop, J, H., and Wang, T. (2004). Bolaamphiphiles. *Chemical Reviews* 104(6):2901-2937

Fuhrhop, J, H., Spiroski, D., and Boettcher, C. (1993). Molecular Monolayer Rods and Tubules Made of α-(L-Lysine),ω -(Amino) Bolaamphiphiles. *Journal of the American Chemical Society* 115:1600-1601

Fujimoto, K. (1995). Freeze-fracture replica electron microscopy combined with SDS digestion for cytochemical labeling of integral membrane proteins. Application to the immunogold labeling of intercellular junctional complexes. *Journal of Cell Science*. 108(11):3443-3449.

Fung, L, K., Shin, M., Tyler, B., Brem, H., and Saltzman, W, M. (1996). Chemotherapeutic Drugs Released from Polymers: Distribution of 1,3-bis(2-chloroethyl)-1-nitrosourea in the Rat Brain. *Pharmaceutical Research* 13(5):671-682

Fuoss, R, M., and Edelson, D. (1951). Bolaform Electroytes. I. Di-(β-trimethylammonium Ethyl) Succinate Dibromide and Related Compounds 1. *Journal of American Chemical Society* 73(1):267-273

Furi, I., Momen-Heravi, F. and Szabo, G. (2017). Extracellular vesicle isolation: present and future. *Annals of Translational Medicine*, 5(12).

Furtado, D., Björnmalm, M., Ayton, S., Bush, A, I., Kempe, K., and Caruso, F. (2020). *Overcoming the blood-brain barrier: The role of nanomaterials in treating neurological diseases.* Advanced Materials 30(1801362):1-66

Gabathuler, R. (2010). Approaches to transport therapeutic drugs across the blood-brain barrier to treat brain diseases*. Neurobiology of Disease* 37:48-57

Gabizon, A., Shmeeda, H., and Barenholz, Y. (2003). Pharmacokinetics of Pegylated Liposomal Doxorubicin. *Clinical Pharmacokinetics* 42(5):419-436

Ganipineni, L, P., Danhier, F., and Préat, V. (2018). Drug Delivery challenges and future of chemotherapeutic nanomedicine for glioblastoma treatment. *Journal of Controlled Release* 281:42-57

Gao, H. (2016). Progress and perspectives on targeting nanoparticles for brain drug delivery. *Acta Pharmaceutica Sinica B* 6(4):268-286

Gao, X., and Lowry, G, V. (2018). Progress towards standardised and validated characterisations for measuring physiochemical properties of manufactured nanomaterials relevant to nano health and safety risks. *NanoImpact* 9:14-30

Garcia-Garcia, E., Andrieux, K., Gil, S., and Couvreur, P. (2005). Colloidial carriers and blood-brain barrier (BBB) translocation: A way to deliver drugs to the brain? *International Journal of Pharmaceutics*. 298: 274-292

Garinot, M., Fiévez, V., Pourcelle, V., Stoffelbach, F., des Rieux, A., Plapied, L., Theate, I., Freichels, H., Jérôme, C., Marchand-Brynaert, J., and Schneider, Y, J. (2007). PEGylated PLGA-based nanoparticles targeting M cells for oral vaccination. *Journal of Controlled Release* 120(3):195-204.

Gastfriend, B, D., Palecek, S, P., and Shusta, E, V. (2018). Modeling the blood-brain barrier: Beyond the endothelial cells. *Current Opinion in Biomedical Engineering*. 5:6-12

Gautam, A., and Pan, X. (2016). The changing model of big pharma: impact of key trends. *Drug Discovery Today* 21(3):379-384

Gdowski, A., Ranjan, A., Mukerjee, A., and Vishwanatha, J. (2015). Development of biodegradable nanocarriers loaded with a monoclonal antibody. *International Journal of Molecular Sciences* 16(2):3990-3995.

Gjerløff, T., Jakobsen, S., Nahimi, A., Munk, O, L., Bender, D., Alstrup, A, K, O., Vase, K, H., Hansen, S, B., Brooks, D, J., and Borghammer, P. (2014). In Vivo Imaging of Human Acetylcholinesterase Density in Peripheral Organs Using 11C-Donepezil: Dosimetry, Biodistribution, and Kinetic Analyses. *The Journal of Nuclear Medicine* 55(11):1818-1824

Goldwirt, L., Beccaria, K., Carpentier, A., Farinotti, R., and Fernandez, C. (2014). Irinotecan and temozolomide brain distribution: A focus on ABCB1. *Cancer Chemotherapy and Pharmacology* 74:185-193

Gomez-Nicola, D., and Perry, V, H. (2015). Microglial dynamics and role in the healthy and diseased brain: a paradigm of functional plasticity. *The Neuroscientist* 21(2):169-184.

Gonclaves, D, M., de Liz, R., and Grad, D. (2011). The Inflammatory Process in Response to Nanoparticles. *The Scientific World Journal* 11:2441-2442

Goulatis, L, I., and Shusta, E, V. (2017). Protein engineering approaches for regulating blood-brain barrier transcytosis. *Current Opinion in Structural Biology* 45:109-115

Goutal, S., Gerstenmayer, M., Auvity, S., Caillé, F., Mériaux, S., Buvat, I., Larrat, B., and Tournier, N. (2018). Physical blood-brain barrier disruption induced by focused ultrasound does not overcome the transporter-mediated efflux of erlotinib. *Journal of Controlled Release* 292:210-220.

Graff, C, L., and Pollack, G, M. (2004). Nasal drug administration: Potential for targeted central nervous system delivery. *Journal of Pharmaceutical Sciences* 94(6):1187-1195

Greene, T, W., and Wuts, P, G. (1999). *Protective groups in organic synthesis*. New York: John Wiley and Sons. pp 114.

Grinberg, S., Kolot, V., Linder, C., Shaubi, E., Kas'yanov, V., Deckelbaum, R, J., and Heldman, E. (2008). Synthesis of novel cationic bolaamphiphiles from vernonia oil and their aggregated structures. *Chemistry and Physics of Lipids* 153(2):85-97

Grinberg, S., Kolot, V., and Mills, D. (1994). New chemical derivatives based on *Vernonia galamensis* oil. *Industrial Crops and Products* 3:113-119

Grinberg, S., Linder, C., Kolot, V., Waner, T., Wiesman, Z., Shaubi, E., and Heldman, E. (2005). Novel cationic amphiphilic derivatives from vernonia oil: synthesis and self-aggregation into bilayer vesicles, nanoparticles, and DNA complexants. *Langmuir* 21(17):7638-7645.

Grinberg,S., Kipnis, N., Linder, C., Kolot, V., and Heldman, E. (2010). Asymmetric bolaamphiphiles from vernonia oil designed for drug delivery. *European Journal of Lipid Science and Technology.* 112(1): 137-151

Guillemin, G, J., and Brew, B, J. (2004). Microglia, macrophages, perivascular macrophages, and pericytes: a review of function and identification. *Journal of Leukocyte Biology* 75(3):388-397.

Gumbleton, M., Abulrob, A, G., and Campbell, L. (2000). Caveolae: an alternative membrane transport compartment. *Pharmaceutical Research* 17:1035-48

Guo, L., Ren, J., and Jiang, X. (2012). Perspectives on Brain-Targeting Drug Delivery Systems. *Current Pharmaceutical Biotechnology* 13:2310-2318

Gupta, K., Afonin, K, A., Viard, M., Herrero, V., Kasprzak, W., Kagiampakis, I., Kim, T., Koyfman, A, Y., Puri, A., Stepler, M., Sappe., KewalRamani, V, N., Grinberg, S., Linder, C., Heldman, E., Blumenthal, R., and Shaprio, B, A. (2015). Bolaamphiphiles as carriers for siRNA delivery: from chemical syntheses to practical applications. *Journal of Controlled Release* 213:142-151

Gustafson, H, H., Holt-Casper, D., Grainger, D, W., and Ghandehari, H. (2015). Nanoparticle uptake: The phagocyte problem. *Nano Today*. 10(4):487-510

Ha, K, D., Bidlingmaier, S, M., and Lui, B. (2016). Macropinocytosis exploitation by cancers and cancer therapeutics. *Frontiers in Physiology* 7(381):1-10

Haar, C, P., Hebbar, P., Wallace IV, G, C., Das, A., Vandergrift III, W, A., Smith, J, A., Giglio, P., Patel, S, J., Ray, S, K., and Banik, N, L. (2012). Drug Resistance in Glioblastoma: A Mini Review. *Neurochemical Research* 37(6):1192-1200

Habgood, M, D., Begley, D, J., and Abbott, N, J. (2000). Determinants of passive drug entry into the central nervous system. *Cellular and Molecular Neurobiology* 20(2):231-53

Hadian, Z., Sahari, M, A., Moghimi, H, R., and Barzegar, M. (2014). Formulation, characterization and optimization of liposomes containing eicosapentaenoic and docosahexaenoic acids; a methodology approach. *Iranian Journal of Pharmaceutical Research* 13(2):393-404

Haeren, R, H, L., van de Ven, S, E, M., van Zandvoort, M, A, M, J., Vink, H., van Overbeeke, J, J., Hoogland, G., and Rijkers, K. (2016). Assessment and imaging of the cerebrovascular glycocalyx. *Current Neurovascular Research* 13:1-12

Hall, M D., Simeonov, A., and Davis, M, I. (2016). Avoiding fluorescence assay interference- The case for diaphorase. *Assay and Drug Development Technologies* 14(3):175-179.

Hambardzumyan, D., Gutmann, D, H., and Kettermann, H. (2016). The role of microglia and macrophages in glioma maintenance and progression. *Nature Neuroscience* 19(1):20-27

Han, F., Huang, J., Zheng, B., and Li, Z. (2004). Surface properties of bolaamphiphiles in ethanol/water mixed solutions. *Colloids and Surfaces A: Physiochemical and Engineering Aspects* 242:115-122

Hanif, F., Muzaffar, K., Perveen, K., Malhi, S, M., and Simjee, S, U. (2017). Glioblastoma Multiforme: A Review of its Epidemiology and Pathogenesis through Clinical Presentation and Treatment. *Asian Pacific Journal of Cancer Prevention* 18(1):3-9

Harder, B, G., Blomquist, M, R., Wang, J., Kim, A, J., Woodworth, G, F., Winkles, J, A., Loftus, J, C., and Tran, N, L. (2018). Developments in the Blood-Brain Barrier Penetrance and Drug Repurposing for Improves Treatment of Glioblastoma. *Frontiers in Oncology* 8:462 doi: 10.3389/fonc.2018.00462

Harris, E, S., and Nelson, W, J. (2010). V-E Cadherin: At the Front, Centre, and Sides of Endothelial Cell Organisation and Function. *Current Opinion in Cell Biology* 22(5):651-658

Hartz, A. M., and Bauer, B. (2011). ABC transporters in the CNS—An inventory. *Current Pharmaceutical Biotechnology.* 12: 656–673.

He, Q., Liu, J., Liang, J., Liu, X., Li, W., Liu, Z., Ding, Z., and Tuo, D. (2018). Towards improvements for penetrating the blood-brain barrier-recent progress from a material and pharmaceutical perspective. *Cells* 7(4):24-45

Hegi, M, E., and Stupp, R. (2015). Withholding temozolomide in glioblastoma patienets with unmethylated *MGMT* promoter-still a dilemma? *Neuro-Oncology* 17(11):1425-1427

Heldman, E., Linder, C., Grinberg, S., Popov, M., and Hollander, I. (2014). Delivery of Tenofovir to the Brain by Novel Nano-Vesicles for the Treatment of Neuro-HIV (S10.003). *Neurology* 82(10 Supplement): S10-003

Henry, A, G., Hislop, J, N., Grove, J., Thorn, K., Marsh, M., and von Zastrow, M. (2012). Regulation of Endocytic Clathrin Dynamics by Cargo Ubiquitination. *Developmental Cell* 23(3):519-532

Hervé, F., Ghinea, N., and Scherrmenn, J, M. (2008). CNS Delivery Via Adsorptive Transcytosis. *The American Association of Pharmaceutical Sciences Journal* 10(3):455-472

Hommelgaard, A, M., Roepstorff, K., Vilhardt, F., Torgensen, M, L., Sandvig, K., and van Deyrs, B. (2005). Caveolae: stable membrane domains with a potential for internalisation. *Traffic*. 720-4

Huang, Q., Zhong, W., Hu, Z., and Tang, X. (2018). A review of the role of cav-1 in neuropathology and neural recovery after ischemic stroke. *Journal of Neuroinflammation* 15:348

Huang, X., Caddell, R., Yu, B., Xu, S., Theobald, B., Lee, L, J., and Lee, R.J. (2010). Ultrasound-enhanced microfluidic synthesis of liposomes. *Anticancer Research* 30(2):463-466.

Hunter, A, J., Lee, W, H., and Bountra, C. (2018). Open innovation in neuroscience research and drug discovery. *Brain and Neuroscience Advances* 2:1-6

Huotari, J., and Helenius, A. (2011). Endosome maturation. *The European Molecular Biology Organisation Journal* 30:3481-3500

Hynynen, K., McDannold, N., Sheikov, N, A., Jolesz, F, A., and Vykhodtseva, N. (2003). Local and reversible blood-brain barrier disruption by noninvasive focused ultrasound at frequencies suitable for trans-skull sonications. *NeuroImage* 24:12-20

Ishida, T., Harashima, H., Kiwada, H. (2002). Liposome clearance*. Bioscience Research* 22:197-224

Ivanov, A, I. (2008). Pharmacological inhibition of endocytic pathways: is it specific enough to be useful? *Methods in Molecular Biology* 440:15-33

Jackson, S., ElAli, A., Virgintino, D., and Gilbert, M, R. (2017). Blood-brain barrier pericyte importance in malignant gliomas: what we can learn from stroke and Alzheimer's disease. *Neuro-Oncology* 19(9):1173-1182

Jain, A, K., and Thareja, S. (2019). In vitro and in vivo characterisation of pharmaceutical nanocarriers used for delivery. *Artificial Cells, Nanomedicine, and Biotechnology*. 47(1):534-539

Jang, S, C., Kim, O, Y., Yoon, C, M., Choi, D, S., Roh, T, Y., Park, J., Nilsson, J., Lotvall, J., Kim, Y, K. and Gho, Y, S. (2013). Bioinspired exosome-mimetic nanovesicles for targeted delivery of chemotherapeutics to malignant tumours. *ACS Nano*, 7(9):7698-7710.

Jankowsky, J, L., and Zheng, H. (2017). Practical considerations for choosing a mouse model of Alzheimer's disease. *Molecular neurodegeneration* 12(1):89.

Janowicz, P, W., Leinenga, G., Götz, J., and Nisbet, R.M. (2019). Ultrasound-mediated blood-brain barrier opening enhances delivery of therapeutically relevant formats of a tau-specific antibody. *Scientific Reports* 9(1):1-9.

Jesus, S., Soares, E., Costa, J., Borchard, G., and Borges, O. (2016). Immune response elicited by an intranasally delivered HBsAg low-dose adsorbed to poly-ε-caprolactone based nanoparticles. *International Journal of Pharmaceutics* 504(1-2):59-69.

Jin, H., Zhang, H., Ma, T., Lan, H., Feng, S., Zhu, H. and Ji, Y. (2018). Resveratrol protects murine chondrogenic ATDC5 cells against LPS-induced inflammatory injury through up-regulating MiR-146b. *Cellular Physiology and Biochemistry*, 47(3):972-980.

Jones, A, R., and Shusta, E, V. (2007). Blood–brain barrier transport of therapeutics via receptor-mediation. *Pharmaceutical Research* 24(9):1759-1771

Joseph, E., and Singhvi, G. (2019). Multifunctional nanocrystals for cancer therapy: A potential nanocarrier. In *Nanomaterials for Drug Delivery and Therapy* (pp. 91-116). William Andrew Publishing.

Kabanov, A, V., and Batrakov, E, V. (2017). Polymer Nanomaterials for Drug Delivery Across the Blood Brain Barrier. In: Ikezu, Y., and Gendleman, H. (eds) *Neuroimmune Pharmacology*. Springer, Cham 847-868

Kalluri, R. and LeBleu, V, S. (2020). The biology, function, and biomedical applications of exosomes. *Science*, *367*(6478).

Kamaly, N., Kalber, T., Thanou, M., Bell, J, D., and Miller, A, D. (2009). Folate receptor targeted bimodal liposomes for tumour magnetic resonance imaging. *Bioconjugate Chemistry* 20(4):648-655.

Kessler, A, F., Frömbling, G, E., Gross, F., Hahn, M., Dzokou, W., Ernestus, R, I., Löhr, M., and Hagermann, C. (2018). Effects of tumour treating fields (TTFields) on glioblastoma cells are augmented by mitotic checkpoint inhibition. *Cell Death Discovery* 4:77 doi 10.1038/s41420-018-0079-9

Khamisipour, G., Jadidi-Niaragh, F., Jahromi, A, S., Zandi, K., and Hojjat-Farsangi. (2016). Mechanisms of tumour cell resistance to the current targeted-therapy agents. *Tumour Biology* 37:10021-10039

Khan, A, R., Liu, M., Khan, M, W., and Zhai, G. (2017). Progress in brain targeting drug delivery system by nasal route. *Journal of Controlled Release* 268:364-389
Kim, A., Ng, W, B., Bernt, W., and Cho, N, J. (2019). Validation of size estimation of nanoparticle tracking analysis on polydisperse macromolecule assembly. *Scientific Reports* 9:2639

Kim, T., Afonin, K, A., Viard, M., Koyfman, A, Y., Sparks, S., Heldman, E., Grinberg, S., Linder, C., Blumenthal, R.P., and Shapiro, B.A. (2013). In silico, in vitro, and in vivo studies indicate the potential use of bolaamphiphiles for therapeutic siRNAs delivery. *Molecular Therapy-Nucleic Acids* 2:e80.

Kim, T., Viard, M., Afonin, K, A., Gupta, K., Popov, M., Salotti, J., Johnson, P, F., Linder, C., Heldman, E., and Sharpiro, B, A. (2020). Characterisation of cationic bolaamphiphile vesicles for siRNA delivery into tumours and brain. *Molecular Therapy Nucleic Acids* 20:359-372

Kita, K., and Dittrich, C. (2011). Drug delivery vehicles with improved encapsulation efficiency: taking advantage of specific drug-carrier interaction. *Expert Opinion on Drug Delivery* 8(3):329-342

Kobus, T., Vykhodyseva, N., Pilatou, M., Zhang, Y., and McDannold, N. (2016*). Safety Validation of Repeated Blood-brain Barrier Disruption Using Focused Ultrasound. Ultrasound in Medicine and* Biology 42(2):481-92

Korang-Yeboah, M., Gorantla, Y., Paulos, S, A., Sharma, P., Chaudhary, J., and Palaniappan, R. (2015). Polycaprolactone/maltodextrin nanocarrier for intracellular drug delivery: formulation, uptake mechanism, internalisation kinetics, and subcellular localisation. *International Journal of Nanomedicine* 10:4763-4781

Kovtun, O., Tillu, V, A., Ariotti, N., Parton, R, G., and Collins, B, M. (2015). Cavin family proteins and the assembly of caveolae. *Journal of Cell Science*. 128(7):1269-1278

Krause, G., Winkler, L., Mueller, S, L., Haselhoff, R, F., Pointek, J., and Blasig, I, E. (2008). Structure and function of claudins. *Biochimica et Biosphysica Acta (BBA)-Biomembranes* 1778(3):631-645

Kristensson, K., and Olsson, Y. (1971). Uptake of exogenous proteins in mouse olfactory cells. *Acta Neuropathologica* 19(2):145-154

Kruczek, B. (2015). Diffusion Coefficient. In: Drioli, E., and Giorno, L. (eds). *Encyclopedia of Membranes*. Springer: Berlin (pp. 1-4)

Kulkarni, S, A., and Feng, S, S. (2013). Effects of particle size and surface modification on cellular uptake and biodistribution of polymeric nanoparticles for drug delivery. *Pharmaceutical research* 30(10):2512-2522.

Kulkarni, S, B., Betageri, G, V., and Singh, M. (1995). Factors affecting microencapsulation of drugs in liposomes. *Journal of Microencapsulation* 12(3):229-246

Kumar, V., Sharma, N., and Maitra, S, S. (2017). In vitro and in vivo toxicity assessment of nanoparticles. *International Nano Letters* 7(4):243-256.

Kunitake, T., and Okahata, Y. (1978). Synthetic bilayer membranes with anionic head groups. *Bulletin of the Chemical Society of Japan* 51(6):1877-1879

Kunwar, S., Chang, S., Westphal, M., Vogelbaum, M., Sampson, J., Barnett, G., Shaffrey, M., Ram, Z., Peipmeier, J., Prados, M., Croteau, D., Pedain, C., Leland, P., Husain, S, R., Joshi, B, H., and Puri, R, K. (2010). Phase III randomised trial of CED of IL13-PE38QQR vs Gliadel wafers for recurrent glioblastoma. *Neuro-Oncology* 12(8):871-881

Kuo, Y, C., and Chen, Y, C. (2015). Targeting delivery of etoposide to inhibit the growth of human glioblastoma multiforme using lactoferrin- and folic acid-grafted ploy(lactide-*co*-glycolide) nanoparticles. *International Journal of Pharmaceutics* 479:138-149

Kutuzov, N., Flyvbjerg, H., and Lauritzen, M. (2018). Contributions of the glycocalyx, endothelium, and extravascular compartment to the blood-brain barrier. *Proceedings of the National Academy of the United States of America* 115(40):E9429-E9438

Lajoie, J, M., and Shusta, E, V. (2015). Targeting Receptor-Mediated Transport for Delivery of Biologics Across the Blood-Brain Barrier. *The Annual Review of Pharmacology and Toxicology* 55:31.1-31.19

Langen, U, H., Ayloo, S., and Gu, C. (2019). Development and Cell Biology of the Blood-Brain Barrier. *Annual Review of Cell and Developmental Biology* 35:12.1-12.23

Lauschke, K., Frederiksen, L., and Hall, V, J. (2017). Paving the way toward complex blood-brain barrier models using pluripotent stem cells. *Stem Cells and Development* 26(12):857-874

Leandro, K., Bicker, J., Alves, G., Falcão, A., and Fortuna, A. (2019). ABC transporters in drug-resistant epilepsy: mechanisms of upregulation and therapeutic approaches. *Pharmacological Research*. 144:357-376

Leonard, R, C, F., Williams, S., Tulpule, A., Levine, A, M., and Oliveros, S. (2009). Improving the therapeutic index of anthracycline chemotherapy: focus on liposomal doxorubicin (Myocet™). *The Breast* 18(4):218-22

Li, S, P., Lin, Z, X., Jiang, X, Y. and Yu, X, Y. (2018). Exosomal cargo-loading and synthetic exosome-mimics as potential therapeutic tools. *Acta Pharmacologica Sinica*, 39(4):542-551.

Li, W., and Graeber, M, B. (2012). The molecular profile of microglia under the influence of glioma. *Neuro-Oncology* 14(8):958-978

Li, X., Corbett, A, L., Taatizadeh, E., Tasnim, N., Little, J.P., Garnis, C., Daugaard, M., Guns, E., Hoorfar, M. and Li, I, T. (2019). Challenges and opportunities in exosome research—Perspectives from biology, engineering, and cancer therapy. *APL Bioengineering*, 3(1):011503.

Lian, T., and Ho, R, J, Y. (2001). Trends and Developments in Liposome Drug Delivery Systems. *Journal of Pharmaceutical Sciences* 90(6):667-680

Liddelow, S, A., and Barres, B. (2017). Reactive Astrocytes: Production, Function and Therapeutic Potential. *Immunity* 46:957-968

Lim, J, P., and Gleeson, P, A. (2011). Macropinocytosis: an endocytic pathway for internalising large gulps. *Immunology and Cell Biology* 89:836-843

Lim, J., Yeap, S, P., Che, H, X., and Low, S, C. (2013). Characterization of magnetic nanoparticle by dynamic light scattering. *Nanoscale Research Letters* 8(1):381

Liu, M., Eguchi, N., Yamasaki, Y., Urade, Y., Hattori, N., and Urabe, T. (2007). Focal cerebral ischemia/reperfusion injury in mice induces hematopoietic prostaglandin D synthase in microglia and macrophages. *Neuroscience* 145(2):520-529.

Liu, Q., Shen, Y., Chen, J., Gao, X., Feng, C., Wang, L., Zhang, Q., and Jiang, X. (2011). Nose-to-Brain Transport Pathways of Wheat Germ Agglutinin Conjugated PEG-PLA Nanoparticles. *Pharmaceutical Research* 29(2):546-558

Lochhead, J, J., and Thorne, R, G. (2012). Intranasal delivery of biologics to the central nervous system. *Advanced Drug Delivery Reviews* 64:614-628

Lockman, P, R., Koziara, J, M., Mumper, R, J., and Allen, D, D. (2004). Nanoparticle surface charges alter blood0brain barrier integrity and permeability. *Journal of Drug Targeting*. 12(9-10): 635-41

Lorusso, D., Di Stefano, A., Carone, V., Fagotti, A., Pisconti, S., and Scambia, G. (2007). Pegylated liposomal doxorubicin-related palmar-plantar erythrodysesthesia (‘hand-foot’syndrome). *Annals of Oncology* 18(7), pp.1159-1164.

Löscher, W., and Potschka, H. (2005). Blood-brain barrier active efflux transporters: ATP-binding cassette gene family. *NeuroRx* 2(1):86-98

Louis, D, N., Ohgaki, H., Wiestler, O, D., Cavenee, W, K., Burger, P, C., Jouvet, A., Scheithauer, B, W., and Kleihues, P. (2007). The 2007 WHO Classification of Tumours of the Central Nervous System. *Acta Neuropathologica* 114:97-10

Love, S, A., Maurer-Jones, M, A., Thompson, J, W., Lin, Y, S., and Haynes, C, L. (2012). Assessing nanoparticle toxicity. *The Annual Review of Analytical Chemistry* 5:181-205

Low, P, S., Henne, W, A. and Doorneweerd, D, D. (2008). Discovery and development of folic-acid-based receptor targeting for imaging and therapy of cancer and inflammatory diseases. *Accounts of Chemical Research* 41(1):120-129.

Lu, C, T., Zhao, Y, Z., Wong, H, L., Cai, J., Peng, L., and Tian, X, Q. (2014). Current approaches to enhance CNS delivery of drugs across the brain barrier. *International Journal of Nanomedicine* 9:2241-2257

Lu, R., Martin, T, A., and Jiang, W, G. (2013). The role of claudin-5 in the blood-brain barrier and brain metastases. *Molecular Medicine Reports* 9(3):779-785

Lu, R, M., Hwang, Y, C., Liu, I, J., Lee, C, C., Tsai, H, Z., and Wu, H, C. (2020). Development of thereapeutic antibodies for the treatment of diseases. *Journal of Biomedical Science* 27(1):1-30

Lu, W. (2012). Adsorptive-Mediated Brain Delivery Systems. *Current Pharmaceutical Biotechnology* 13(12):2340-2348

Luissint, A, C., Artus, C., Glacial, F., Ganeshamoorthy, K., and Couraud, P, O. (2012). Tight junctions at the blood brain barrier: physiological architecture and disease-associated dysregulation. *Fluids and Barriers of the CNS* 9:23

Mäger, I., Meyer, A, H., Li, J., Lenter, M., Hilderbrandt, T., Leparc, G., and Wood, M, J, A. (2016). Targeting blood-brain-barrier transcytosis- perspectives for drug delivery. *Neuropharmacology* 120:4-7

Maggi, L., and Mantegazza, R. (2011). Treatment of myasthenia gravis. *Clinical Drug Investigation* 31(10):691-701.

Magnus, P, D., Sarkar, T., and Djuric, S. (1982). Organosilicon Compounds in Organic Synthesis. *Comprehensive Organometallic Chemistry* 7:515-659

Maguire, C, M., Rösslein, M., Wick, P., and Prina-Mello, A. (2018). Characterisation of particles in solution–a perspective on light scattering and comparative technologies. *Science and Technology of Advanced Materials* 19(1):732-745.

Mahringer, A., and Fricker, G. (2016). ABC transporters at the blood-brain barrier. *Expert Opinion on Drug Metabolism and Toxicology* 12(5):499-508

Mahringer, A., Ott, M., Reimold, I., Reichel, V., and Fricker, G. (2011). The ABC of the blood-brain barrier- regulation of drug efflux pumps. *Current Pharmaceutical Design* 17 (26):2762-2770

Maiti, P., Manna, J. and Dunbar, G, L. (2017). Current understanding of the molecular mechanisms in Parkinson's disease: targets for potential treatments. *Translational Neurodegeneration*. 6(1):28.

Manallack, D, T. (2007). The pKa Distribution of Drugs: Application to Drug Discovery. *Perspectives in Medicinal Chemistry* 1:25-38

Mannhold, R. (2005). The impact of lipophilicity in drug research: a case report on β-blockers. *Mini-Reviews in Medical Chemistry* 5: 197–205

Mariano, C., Palmela, I., Pereira, P., Fernandes, A., Falcão, A, S., Cardoso, F, L., Vaz, A, R., Campos, A, R., Gonçalves-Ferreira, A., Kim, K, S., and Brites, D. (2013). Tricellulin expression in brain endothelial and neural cells. *Cell and Tissue Research* 351(3):397-407.

Markiv, A., Beatson, R., Burchell, J., Durvasula, R, V., and Kang, A, S. (2011). Expression of recombinant multi-coloured fluorescent antibodies in gor -/trxB- E. coli cytoplasm. *BMC Biotechnology* 11(117):1-10

Marquis, B, J., Love, S, A., Braun, K, L., and Haynes, C, L. (2009). Analytical methods to assess nanoparticle toxicity. *Analyst* 134:425-439

Mayor, S., and Pagano, R, E. (2007). Pathways of clathrin-independent endocytosis. *Molecular Cell Biology* 8:603-612

McArthur, S., Loiola, R, A., Maggioli, E., Errede, M., Virgintino, D., and Solito, E. (2016). The restorative role of annexin A1 at the blood-brain barrier. *Fluids and Barriers of the CNS* 13:17-31

Mehn, D., Caputo, F., Rösslein, M., Calzolai, L., Saint-Antonin, F., Courant, T., Wick, P., and Gilliland, D. (2017). Larger or more? Nanoparticle characterisation methods for recognition of dimers. *RSC Advances* 7(44):27747-27754.

Mentkowski, K, I., Snitzer, J, D., Rusnak, S. and Lang, J, K. (2018). Therapeutic potential of engineered extracellular vesicles. *The AAPS journal*, 20(3):50.

Meresse S., Dehouck M, P., Delorme P., Fruchart J, C., and Cecchelli R. (1991) Lipoproteins and reconstituted blood-brain barrier. In *Pharmaceutical Applications of Cell and Tissue Culture to Drug Transport,* pp. 217– 229.

Michell-Robinson, M, A., Touil, H., Healy, L, M., Owen, D, R., Durafourt, B, A., Bar-Or, A., Antel, J, P., and Moore, C, S. (2015). Roles of microglia in brain development, tissue maintenance and repair. *Brain* 138(5):1138-1159.

Miller, D, S. (2015). Regulation of ABC transporters blood-brain barrier: the good, the bad, and the ugly. *Advances in Cancer Research* 125:43-70

Miller, D, S., and Cannon, R, E. (2014). Signalling pathways that regulate basal ABC transporter activity at the blood-brain barrier. *Current Pharmaceutical Design* 20(10):1463-71

Mishra, V., Bansal, K, K., Verma, A., Yadav, N., Thakur, S., Sudhakar, K., and Rosenholm, J, M. (2018). Solid lipid nanoparticles: Emerging colloidal nano drug delivery systems. *Pharmaceutics* 10(4):191.

Mohs, R, C., and Greig, N, H. (2017). Drug discovery and development: Role of basic biological research. *Alzheimer's and Dementia: Translational Research and Clinical Interventions* 3:651-657

Moller, W., Saba, G, K., Haussinger, K., Becker, S., Keller, M., and Schuschnig, U. (2011). Nasally inhaled pulsating aerosols: lung, sinus and nose deposition. *Rhinology* 49(3):286-91

Molofsky, A, V., Krenick, R., Ullian, E., Tsai, H, H., Deneen, B., Richardson, W, D., Barres, B, A., and Rowitch, D., H. (2012). Astrocytes and disease: a neurodevelopmental perspective. *Genes and Development* 26:891-907

Morgan, P., Van Der Graaf, P., Arrowsmith, J., Feltner, D, E., Drummond, K, S., Wegner, C, D., and Street, S, D, A. (2012). Can the flow of medicines be improved? Fundamental pharmacokinetic and pharmacological principles toward improving Phase II survival. *Drug Discovery Today* 17(9/10):419-424

Mourdikoudis, S., Pallares, R, M., and Thanh, N, T, K. (2018). Characterisation techniques for nanoparticles: comparison and complementarity upon studying nanoparticle properties. *Nanoscale* 10:12871-12934

Mulvaney, P., Parak, W, J., Caruso, F., and Weiss, P, S. (2016). Standardising nanomaterials. *ACS Nano* 10(11):9763-9764

Muralidharan, P., Mallory, E., Malapit, M., Hayes, D., and Mansour, H, M. (2014). Inhalable PEGylated phospholipid nanocarriers and PEGylated therapeutics for respiratory delivery as aerosolized colloidal dispersions and dry powder inhalers. *Pharmaceutics* 6(2):333-353.

Nagpal, K., Singh, S, K., Mishra, D, N. (2013). Drug targeting to brain: a systematic approach to study the factors, parameters and approaches for prediction of permeability of drugs across BBB. *Expert Opinion on Drug Delivery* 10(7):1-30

Nakai, E., Park, K., Yawata, T., Chichara, T., Kumazawa, A., Nakabayashi, H., and Shimizu, K. (2009). Enhanced MDRI expression and chemoresistance of cancer stem cells derived from glioblastoma. *Cancer Investigation* 27:901-908

Neuwelt, E, A., Bauer, B., faulke, C., Fricker, G., Iadecola, C., Janigro, D., Leybaert, L., Molnar, Z., O'Donnell, M., Povlishock, J., Saunders, N., Sharp, F., Stanimirovic, D., Watts, R., and Drewes, L. (2011). Engaging Neuroscience to Advance Translational Research in Brain Barrier Biology. *Nature Reviews Neuroscience* 12(3):169-182

Neves, A, R., Queiroz, J, F., Lima, S, A, C., Figueiredo, F., Fernandes, R., and Reis, S. (2016). Cellular uptake and transcytosis of lipid-based nanoparticles across the intestinal barrier: relevance for oral drug delivery. *Journal of Colloid and Interface Science* 463:258-265.

Nimmerjahn, A., Kirchhoff, F., and Helmchen, F. (2005). Resting Microglial Cells Are Highly Dynamic Surveillants of Brain Parenchyma in Vivo. *Science* 308(5726):1314-1318

Nishioku, T., Matsumoto, J., Dohgu, S., Sumi, N., Miyao, K., Takata, F., Shuto, H., Yamauchi, A., and Kataoka, Y. (2010). Tumour necrosis factor-α mediates the blood–brain barrier dysfunction induced by activated microglia in mouse brain microvascular endothelial cells. *Journal of Pharmacological Sciences* 112(2):251-254.

Nitta, T., hata, M., Gotoh, S., Seo, Y., Sasaki, H., Hashimoto, N., Furuse, M., and Tsukita, S. (2003). Size-selective loosening of the blood-brain barrier in claudin-5-deficient mice. *Journal of Cell Biology* 161(3):653-660

Nuraje, N., Bai, H., and Su, K. (2013). Bolaamphiphilic molecules: Assembly and applications. *Progress in Polymer Science* 38(2):302-343.

Obermeier, B., Daneman, R., and Ransohoff, R, M. (2013). Development, maintenance and disruption of the blood-brain barrier. *Nature Medicine* 19:1584-1596

O'Brien, J., Wilson, I., Orton, T., and Pognan, F. (2000). Investigation of the Alamar Blue (resazurin) fluorescent dye for the assessment of mammalian cell cytotoxicity. *European Journal of Biochemistry* 267(17):5421-5426.

Ogawa, M., Kosaka, N., Regino, C.A., Mitsunaga, M., Choyke, P, L., and Kobayashi, H. (2010). High sensitivity detection of cancer in vivo using a dual-controlled activation fluorescent imaging probe based on H-dimer formation and pH activation. *Molecular bioSystems* 6(5):888-893.

Oh, K., Kim, S, R., Kim, D, K., Seo, M, W., Lee, C., Lee, H, M., Oh, J, E., Choi, E, Y., Lee, D, S., Gho, Y, S. and Park, K, S. (2015). In vivo differentiation of therapeutic insulin-producing cells from bone marrow cells via extracellular vesicle-mimetic nanovesicles. *ACS Nano*, 9(12):11718-11727.

Oh, T., Fakurnejad, S., Sayegh, E, T., Clark, A, J., Ivan, M, E., Sun, M, Z., Safaee, M., Bloch, O., James, C, D., and Parsa, A, T. (2014). Immunocompetent murine models for the study of glioblastoma immunotherapy. *Journal of Translational Medicine*. 12(107):1-10

Ohgaki, H., and Kleihues, P. (2012). The Definition of Primary and Secondary Glioblastoma. *Clinical Cancer Research* 19(4):764-772

Ohtsuki, S., and Terasaki, T. (2007). Contribution of Carrier-Mediated Transport Systems to the Blood-Brain Barrier as a Supporting and Protecting Interface for the Brain: Importance for CNS Drug Discovery and Development. *Pharmaceutical Research* 24(9):1745-1758

Okamoto, C, T. (1998). Endocytosis and Transcytosis. *Advanced Drug Delivery Reviews* 29:215-228

Olanow, C, W., Gauger, L, L., and Cedarbaum, J, M. (1991). Temporal Relationships between Plasma and Cerebrospinal Fluid Pharmacokinetics of Levodopa and Clinical Effect in Parkinson's disease. *Annals of Neurology* 29:556-559

Oldendorf, W, H., Cornford, M, E., and Brown, W, J. (1977). The large apparent work capillary endothelial cells in brain and other tissues of the rat. *Annals of Neurology* 1(5):409-417

Ong, C, B., Mohammad, A, W., Rohani, R., Ba-Abbad, M, M., and Hairom, N, H, H. (2016). Solar photocatalytic degradation of hazardous Congo red using low-temperature synthesis of zinc oxide nanoparticles. *Process Safety and Environmental Protection* 104:549-557.

Ong, S, G, M., Ming, L, C., Lee, K, S., and Yuen, K, H. (2016). Influence of the encapsulation efficiency and size of liposome on the oral bioavailability of griseofulvin-loaded liposomes. *Pharmaceutics* 8(25):1-17

Osada, T., Gu, Y, H., Kanazawa, M., Tsubota, Y., Hawkins, B. T., Spatz, M., Milner, R., and del Zoppo, G, J. (2011). Interendothelial claudin-5 expression depends on cerebral endothelial cell-matrix adhesion by β_1-integrins. *Journal of Cerebral Blood Flow and Metabolism* 31:1972-1985

Palm, W. (2019). Metabolic functions of macropinocytosis. *Philosophical Transactions of the Royal Society B* 374(1765):20180285.

Panchuk-Voloshina, N., Haugland, R, P., Bishop-Stewart, J., Bhalgat, M, K., Millard, P, J., Mao, F., Leung, W, Y., and Haugland, R.P. (1999). Alexa dyes, a series of new fluorescent dyes that yield exceptionally bright, photostable conjugates. *Journal of Histochemistry & Cytochemistry* 47(9):1179-1188.

Papa, S., Ferrari, R., De Paola, M., Rossi, F., Mariani, A., Caron, I., Sammali, E., Peviani, M., Dell'Oro, V., Colombo, C., and Morbidelli, M. (2014). Polymeric nanoparticle system to target activated microglia/macrophages in spinal cord injury. *Journal of Controlled Release* 174:15-26.

Papasani, M, R., Wang, G, K., and Hill, R, A. (2012). Gold Nanoparticles: The Importance of Physiological Principles to Devise Strategies for Targeted Drug Delivery. *Nanomedicine*. 8:804−814.

Pardridge, W, M. (1995). CNS drug design based on principles of blood-brain barrier transport. *Journal of Neurochemistry* 70(5):1781-1792

Pardridge, W, M. (2001). *Brain Drug Targeting: The Future of Brain Drug Development* Cambridge, UK: Cambridge University Press

Pardridge, W, M. (2002). Drug and gene delivery to the brain: the vascular route. *Neuron* 36(4):555-558

Pardridge, W, M. (2003). Blood-Brain Barrier Drug Targeting: The Future of Brain Drug Development. *Molecular Interventions* 3(2): 90-105

Pardridge, W, M. (2005). The Blood-Brain Barrier: Bottleneck in Brain Drug Development. *The Journal of the American Society for Experimental NeuroTherapies* 2(1):3-14

Pardridge, W, M. (2009). Alzheimer's disease drug development and the problem of the blood brain barrier. *Alzheimer's and Dementia* 5:427-432

Pardridge, W, M. (2012*).* Drug transport across the blood-brain barrier. *Journal of Cerebral Blood Flow and Metabolism* 32:1959-1972

Pardridge, W, M. (2016). CSF, blood-brain barrier, and brain drug delivery. *Expert opinion on Drug Delivery* 13(7): 963-975

Pardridge, W, M. (2017). Delivery of Biologics Across the Blood-Brain Barrier with Molecular Trojan Horse Technology. *BioDrugs* 31:503-519

Parton, R, G., and del Pozo, M, A. (2013). Caveolae as plasma membrane sensors, protectors and organisers. *Molecular Cell Biology* 14(2):98-112

Parton, R, G., Joggerst, B., and Simons, K. (1994). Regulated internalisation of caveolae. *Journal of Cell Biology* 127:1199-215

Patching, S, G. (2017). Glucose Transporters at the Blood-Brain Barrier: Function, Regulation and Gateways for Drug Delivery. *Molecular Neurobiology* 54:1046-1077

Patel, G, B., and Sprott, D, G. (1999). Archaeobacterial ether lipid liposomes (acrchaeosomes) as novel vaccine and drug delivery systems. *Critical Reviews in Biotechnology* 19(4):317-357

Patel, P., Chang, C, T., Kang, N., Lee, G, J., Powell, W, S., and Rokach, J. (2007). Reductive deprotection of silyl groups with Wilkinson's catalyst/catechol borane. *Tetrahedron letters* 48(30):5289-5292.

Patel, V, R., and Agrawal, Y, K. (2011). Nanosuspension: An approach to enhance solubility of drugs. *Journal of Advanced Pharmaceutical Technology & Research*2(2):81.

Pathan, S, A., Iqbalm, Z., Zaidi, S, M, A., Talegaonkar, S., Vohra, D., Jain, G, K., Azeem, A., Jain, N., Lalani, J, R., Khar, R, K., and Ahmad, F, J. (2009). CNS Drug Delivery Systems: Novel Approaches. *Recent Patents on Drug Delivery and Formulation* 3:71-89

Patschinski, P., Zhang, C., and Zipse, H. (2014). The Lewis Base-Catalysed Silylation of Alcohols- A Mechanistic Analysis. *The Journal of Organic Chemistry* 79:8348-8357

Perez, A, P., Mundiña-Weilenmann, C., Romero, E, L., and Morilla, M, J. (2012). Increased brain radioactivity by intranasal ^{32}P-labeled siRNA dendriplexes within in situ-forming mucoadhesive gels. *International Journal of Nanomedicine* 7:1373-1385

Peterson, P, E., Bopp, R, J., Chevli, D, M., Curran, E, L., Dillard, D, E., and Kamat, R, J. (1967). Solvents of low nucleophilicity. IX. Inductive and participation effects in carbonium ion reactions in acetic, formic, and trifluoroacetic acid. *Journal of the American Chemical Society* 89(23):5902-5911.

Pfeiffer, C., Rehbock, C., Hühn, D., Carrillo-Carrion, C., de Aberasturi, D, J., Merk, V., Barcikowski, S., and Parak, W, J. (2014). Interaction of colloidal nanoparticles with their local environment: the (ionic) nanoenvironment around nanoparticles is different from bulk and determines the physico-chemical properties of the nanoparticles. *Journal of the Royal Society Interface* 11(96):20130931

Pinto, M, P., Arce, M., Yameen, B., and Vilos, C. (2017). Targeted brain delivery nanoparticles for malignant gliomas. *Nanomedicine* 12(1):59-72

Po, H, N. and Senozan, N, M. (2001). The Henderson-Hasselbalch equation: its history and limitations. *Journal of Chemical Education* 78(11):1499-1503

Podo, F. (1999). Tumour phospholipid metabolism. *NMR in Biomedicine: An International Journal Devoted to the Development and Application of Magnetic Resonance In Vivo* 12(7):413-439.

Pointek, J., Winkler, L., Wolburg, H., Müller, S, L., Zuteger, N., Piehl, C., Wiesner, B., Krause, G., and Blasig, I, E. (2008). Formation of tight junctions: determinants of homophilic interaction between classic claudins. *Federation of American Societies for Experimental Biology* 22 (1):146-58

Popov, M., Grinberg, S., Linder, C., Warner, T., Levi-Hevroni, B., Deckelbaum, R, J., and Heldman, E. (2012). Site-directed decapsulation of bolaamphiphilic vesicles with enzymatic cleavable surface groups. *Journal of Controlled Release* 160: 306-314

Popov, M., Hammand, I, A., Bachar, T., Grinberg, S., Linder, C., Stepensky, D., and Heldman, E. (2013). Delivery of analgesic peptides to the brain by nano-sized bolaamphiphilic vesicles made of monolayer membranes. *European Journal of Pharmaceutics and Biopharmaceutics* 85:381-389

Popov, M., Linder, C., Deckelbaum, R, J., Grinberg, S., Hansen, I, H., Shaubi, E., Warner, T., and Heldman, E. (2010). Cationic vesicles from novel bolaamphiphilic compounds. *Journal of Liposome Research* 20(2): 147-159

Pourgholi, F., Farhad, J, N., Kafil, H, S., and Yousefi, M. (2016). Nanoparticles: novel vehicles in treatment of glioblastoma. *Biomedicine & Pharmacotherapy* 77:98-107.

Press, A, T., Ramoji, A., vd Lühe, M., Rinkenauer, A, C., Hoff, J., Butans, M., Rössel, C., Pietsch, C., Neugebauer, U., Schacher, F, H., and Bauer, M. (2017). Cargo–carrier interactions significantly contribute to micellar conformation and biodistribution. *NPG Asia Materials* 9(10):e444-e444.

Preston, J, E., Abbott, J, N., and Begley, D, J. (2014). Transcytosis of macromolecules at the blood-brain barrier*. Advances in Pharmacology* 71:147-163

Prince, M., Ali, G, C., Guerchet, M., Prina, M, A., Albanese, E., and Wu, Y, T. (2016a). Recent global trends in the prevalence and incidence of dementia, and survival with dementia. *Alzheimer's Research and Therapy*. 8(23):1-13

Prince, M., Comas-Herrera, A., Knapp, M., Guerchet, M., and Karagiannidou, M. (2016b). World Alzheimer report 2016: improving healthcare for people living with dementia: coverage quality and costs now and in the future, 2016. *Alzheimer's Disease International*

Pulgar, V, M. (2019). Transcytosis to cross the blood brain barrier, new advancements and challenges. *Frontiers in Neuroscience* 12:1019.

Puri, A., Loomis, K., Smith, B., Lee, J, H., Yavlovich, A., Heldman, E., and Blumenthal, R. (2009). Lipid-based nanoparticles as pharmaceutical drug carriers: from concepts to clinic. *Critical Reviews in Therapeutic Drug Carrier Systems* 26(6).

Qosa, H., Miller, D, S., Pasinelli, P., and Trotti, D. (2015). Regulation of ABC Efflux Transporters at Blood-Brain Barrier in Health and Neurological*. Disorders. Brain Research* 1628:298-316

Recouvreux, M, V., and Commisso, C. (2017). Macropinocytosis: a metabolic adaptation to nutrient stress in cancer. *Frontiers in Endocrinology* 8(261):1-7

Redzic, Z. (2011). Molecular biology of the blood-brain barrier and cerebrospinal fluid barrier: similarities and differences. *Fluids and Barriers of the CNS*. 8:3

Reichel, A. (2015). Pharmacokinetics of CNS Penetration. Edited by Li Di and Edward H. Kerns., *Blood–Brain Barrier in Drug Discovery: Optimizing Brain Exposure of CNS Drugs and Minimizing Brain Side Effects for Peripheral Drugs*. First Edition. John Wiley and Sons.

Rizk, M, L., Zou, L., Savic, R, M., and Dooley, K, E. (2017). Importance of Drug Pharmacokinetics at the Site of Action. *Clinical Translation in Science* 10:133-142

Robey, R, W., Pluchino, K, M., Hall, M, D., Fojo, A, T., Bates, S, E., and Gottesman, M, M. (2018). Revisiting the role of ABC transporters in multidrug-resistant cancer. *Nature Reviews Cancer* 18(7):452-464

Robinson, P, S., and Goochee, C, F. (1991). Kidney-specific enzyme expression by human kidney cell lines generated through oncogene transfection. *Journal of Cellular Physiology* 148(1):54-59.

Rothberg, K, G., Heuser, J, E., Donzell, W, C., Ying, Y, S. Glenner, J, R., and Anderson, R, G. (1992). Caveolin, a protein component of caveolae membrane coats. *Cell* 68:673-82

Sabbagh, M, N., Hendrix, S., and Harrison, J, E. (2019). FDA position statement "Early Alzheimer's disease: Developing drugs for treatment, Guidance for Industry". *Alzheimer's and Dementia: Translational Research and Clinical Interventions* 5:13-19

Saito, Y., and Wright, E, M. (1984). Regulation of bicarbonate transport across the brush border membrane of the bull-frog choroid plexus. *Journal of Physiology* 350:327-342

Salatin, S., and Khosroushahi, A, Y. (2017). Overviews on the cellular uptake mechanism of polysaccharide colloidal nanoparticles. *Journal of Cellular Molecular Medicine* 21(9):1668-1686

Sanavio, B., Librizzi, L., Pennacchio, P., Beznoussenko, G, V., Sousa, F., Silva, P, J., Mironov, A, A., Frassoni, C., Stellacci, F., De Curtis, M. and Krol, S. (2018). Distribution of superparamagnetic Au/Fe nanoparticles in an isolated guinea pig brain with an intact blood brain barrier. *Nanoscale*, 10(47):22420-22428.

Sanchez- Covarrubias, L., Slosky, L. M., Thompson, B. J., Davis, T. P., and Ronaldson, P. T. (2014). Transporters at CNS barrier sites: obstacles or opportunities for drug delivery? *Current Pharmaceutical Design* 20(10):1422–1449

Saraiva, C., Praça, C., Ferreira, R., Santos, T., Ferreira, L., and Bernardino, L. (2016). Nanoparticle-mediated brain drug delivery: overcoming blood–brain barrier to treat neurodegenerative diseases. *Journal of Controlled Release* 235:34-47.

Sarin, H. (2010). Physiologic upper limits of pore size of different blood capillary types and another perspective on the dual pore theory of microvascular permeability. *Journal of Angiogenesis Research* 2(14):1-19

Savage, D, T., Hilt, J, Z., and Dziubla, T, D. (2019). In vitro methods for assessing nanoparticle toxicity. *Methods in Molecular Biology* 1894:1-29

Scarff, C, A., fuller, M, J, G., Thompson, R, F., and Iadaza, M, G. (2018). Variations on negative stain electron microscopy: tools for tackling challenging systems. *Journal of Visualised Experiments* 132:57199

Schmid, S, L. (1997). Clathrin-Coated Vesicle Formation and Protein Sorting: An Integrated Process. *Annual Review of Biochemistry* 66:511-48

Scott, C, C., Vacca, F., and Gruenberg, J. (2014). Endosome maturation, transport and functions. *Seminars in Cell and Developmental Biology* 31:2-10

Sezonov, G., Joseleau-Petit, D., and D'Ari, R. (2007). *Escherichia coli* physiology in Luria-Bertani broth. *Journal of Bacteriology*. 189(23):8746-8749

Shaker, S., Gardouh, A, R., and Ghorab, M, M. (2017). Factors affecting liposomes particle size prepared by ethanol injection method. *Research in Pharmaceutical Sciences* 12(5):346.

Sharif, Y., Jumah, F., Coplan, L., Krosser, A., Sharif, K., and Tubbs, R, S. (2018). The blood brain barrier: A review of its anatomy and physiology in health and disease. *Clinical Anatomy* 31(6):812-823

Sharma, A., and Sharma, U, S. (1997). Liposomes in drug delivery: progress and limitations. *International Journal of Pharmaceutics* 154:123-140

Shimizu, T., and Masuda, M. (1997). Stereochemical Effect of Even-Odd Connecting Links on Supramolecular Assemblies Made of 1-Glucosamide Bolaamphiphiles. *Journal of the American Chemical Society* 119(12):2812-2818

Shimizu, T., Masuda, M., and Minamikawa, H. (2005). Supramolecular nanotube architectures based on amphiphilic molecules. *Chemical Reviews* 105(4):1401-1444

Shinozaki, Y., Shibata, K., Yoshida, K., Shigetomi, E., Gachet, C., Ikanaka, K., Tanaka, K, F., and Koizumi, S. (2017). Transformation of Astrocytes to a Neuroprotective Phenotype by Microglia via $P2Y_1$ Receptor Downregulation. *Cell Reports* 19(6):1151-1164

Siegel, A, P., Baird, M, A., Davidson, M, W., and Day, R, N. (2013). Strengths and weaknesses of recently engineered red fluorescent proteins evaluated in live cells using fluorescence correlation spectroscopy. *International Journal of Molecular Sciences* 14:20340-20358

Siepmann, J. and Göpferich, A. (2001). Mathematical modeling of bioerodible, polymeric drug delivery systems. *Advanced Drug Delivery Reviews* 48(2-3):229-247.

Singer, A., Barakat, Z., Mohapatra, S. and Mohapatra, S, S. (2019). Nanoscale Drug-Delivery Systems: In Vitro and In Vivo Characterization. In *Nanocarriers for Drug Delivery* (pp. 395-419).

Singh, A, K., Achazi, K., Schade, B., Böttcher, C., Haag, R., and Sharma, A, K. (2018). Synthesis of non-ionic bolaamphiphiles and study of their self-assembly and transport behaviour for drug delivery applications. *Royal Society of Chemistry Advances* 8:31777-31782

Singh-Bains, M, K., Linke, V., Austria, M, D., Tan, A, Y., Scotter, E, L., Mehrabi, N, F., Faull, R, L., and Dragunow, M. (2019). Altered microglia and neurovasculature in the Alzheimer's disease cerebellum. *Neurobiology of Disease* 132:104589.

Sisa, C., Kholia, S, R., Naylor, J., Herrera Sanchez, M, B., Bruno, S., Deregibus, M, C., Camussi, G., Inal, J, M., Lange, S., and Hristova, M. (2019). Mesenchymal stromal cell derived extracellular vesicles reduce hypoxia-ischaemia induced perinatal brain injury. *Frontiers in physiology* 10:282.

Skarlatos, S., Yoshikawa, T., and Pardridge, W, M. (1995). Transport of [^{125}I] transferrin through the rat blood-brain barrier*. Brain Research* 683:164-171

Sohet, F., Lin, C., Munji, R.N., Lee, S.Y., Ruderisch, N., Soung, A., Arnold, T.D., Derugin, N., Vexler, Z.S., Yen, F.T. and Daneman, R. (2015). LSR/angulin-1 is a tricellular tight junction protein involved in blood–brain barrier formation. *Journal of Cell Biology 208*(6): 703-711.

Solé-Domènech, S., Cruz, D, L., Capetillo-Zarate, E., and Maxfield, F, R. (2016). The endocytic pathway in microglia during health, aging and Alzheimer's disease. *Ageing Research Reviews* 32:89-103

Sonvico, F., Clementino, A., Buttini, F. Colombo, G., Pescina, S., Guterres, S, S., Pohlmann, A, R., and Nicoli, S. (2018). Surface-modified nanocarriers for nose-to-brain delivery: from bioadhesion to targeting. *Pharmaceutics* 10(34):1-34

Sørensen, M, D., Dahlrot, R, H., Boldt, H, B., Hansen, S., and Kristensen, B, W. (2018). Tumour-associated microglia/macrophages predict poor prognosis in high-grade and correlate with aggressive tumour subtype. *Neuropathology and Applied Neurobiology* 44:185-206

Sørensen, M. D., Fosmark, S., Hellwege, S., Beier, D., Kristensen, B, W., and Beier, C. P. (2015). Chemoresistance and chemotherapy targeting stem-like cells in malignant glioma. In: *Cell Biology in Neoplasms of the Central Nervous System* (111-138). Springer International Publishing

Srinivasan, B., and Kolli, A, R. (2019). Transepithelial/Transendothelial Electrical Resistance (TEER) to Measure the Integrity of Blood-Brain Barrier. *Neuromethods*. 142:99-114

Stamatovic, S, M., Johnson, A, M., Keep, R, F., and Andjelkovic, A, V. (2016). Junctional proteins of the blood-brain barrier: New insights into function and dysfunction. *Tissue Barriers* 4:1

Stathopulos, P, B., Scholz, G, A., Hwang, Y, M., Rumfeldt, J, A., Lepock, J, R., and Meiering, E, M. (2004). Sonication of proteins causes formation of aggregates that resemble amyloid. *Protein Science* 13(11):3017-3027.

Stern, A., Guidotti, M., Shaubi, E., Popov, M., Linder, C., Heldman, E., and Grinberg, S. (2014). Steric environment around acetylcholine head groups of bolaamphiphilic nanovesicles influences the release rate of encapsulated compounds. *International Journal of Nanomedicine* 9:561-574

Stetefeld, J., McKenna, S, A., and Patel, T, R. (2016). Dynamic light scattering: a practical guide and applications in biomedical sciences. *Biophysical Reviews* 8(4):409-427.

Stewart, P, A. (2000). Endothelial Vesicles in the Blood-Brain Barrier: Are They Related to Permeability? *Cellular and Molecular Neurobiology* 20(2):149-163

Strazielle, N., and Ghersi-Egea, J, F. (2015). Efflux transporters in the blood-brain interfaces of the developing brain. *Frontiers in Neuroscience* 9(21):1-11

Su, Y., Xia, S., Zhong, R., and Wang, L. (2017). Phytohormonal quantification based on biological principles. *Hormone Metabolism and Signalling in Plants* 13:431-470.

Suk, J, S., Xu, Q., Kim, N., Hanes, J., and Ensign, L, M. (2016). PEGylation as a strategy for improving nanoparticle-based drug and gene delivery. *Advanced drug delivery reviews* 99:28-51.

Suman, J, D., Laube, B, L., and Dalby, R. (1999). Comparison of nasal deposition and clearance of an aerosol generated by nebulizer and an aqueous spray pump. *Pharmaceutical Research* 16(10):1648-52

Sun, B., and Chiu, D, T. (2005). Determination of the Encapsulation Efficiency if Individual vesicles using single-vesicle photolysis and confocal single molecule detection. *Analytical Chemistry* 77:2770-2776

Surmeier, D, J. (2018). Determinants of dopaminergic neuron loss in Parkinson's disease. *The FEBS Journal*. 285(19), pp.3657-3668.

Sweeney, M., Sagare, Am P., and Zlokovic, B, V. (2018). Blood-brain barrier breakdown in Alzheimer's disease and other neurodegenerative disorders. *Nature Reviews Neurology* 14(3):133-150

Takano, T., Tian, G-F., Peng, W., Lou, N., Libionka, W., Han, X., and Nedergaard, M. (2006). Astrocyte-mediated control of cerebral blood flow. *Nature Neuroscience* 9:260–267

Tamai, I., and Tsuji, A. (2000). Transport-Mediated Permeation of Drugs Across the Blood-Brain Barrier*. Journal of Pharmaceutical Sciences* 89(11):1371-1388

Tan, Y., Fleck, R, A., Asokanathan, C., Yuen, C, T., Xing, D., Zhang, S., and Wang, J. (2013). Confocal microscopy study of pertussis toxin and toxoids on CHO-cells. *Human vaccines & immunotherapeutics* 9(2):332-338.

Taurozzi, J, S., Hackley, V, A., and Wiesner, M, R. (2011). Ultrasonic dispersion of nanoparticles for environmental, health and safety assessment–issues and recommendations. *Nanotoxicology* 5(4):711-729.

Temsamani, J., Scherrmann, J, M., Rees, A, R., and Kaczorek, M. (2000). Brain drug delivery technologies: novel approaches for transporting therapeutics. *Pharmaceutical Science and Technology Today* 3(5):155-162

Thomas, C, M., and Smart, E, J. (2008). Caveolae structure and function*. Journal of Cellular and Molecular Medicine* 12(3):796-809

Thomas, W, E. (1999). Brain macrophages: on the role of pericytes and perivascular cells. *Brain Research Reviews* 31(1):42-57.

Thomsen, M. S., Routhe, L. J., and Moos, T. (2017). The vascular basement membrane in the healthy and pathological brain. *Journal of Cerebral Blood Flow and Metabolism*. 37(10):3300–3317

Thurston, G., McLean, J. W., Rizen, M., Baluk, P., Haskell, A., Murphy, T. J., Hanahan, D., and McDonald, D, M. (1998). Cationic liposomes target angiogenic endothelial cells in tumors and chronic inflammation in mice. *Journal of Clinical Investigation* 101:1401–1413.

Tietz, S., and Englehardt B. (2015). Brain Barriers: Crosstalk between complex tight junctions and adherens junctions. *Journal of Cell Biology* 209(4):493-506

Trader, D, J., and Carlson, E, E. (2012). Chemoselective hydroxyl group transformation: an elusive target. *Molecular BioSystems* 8(10):2484-2493.

Tremblay, M, E., Stevens, B., Sierra, A., Wake, H., Bessis, A., and Nimmerjahn, A. (2011). The Role of Microglial in the Healthy Brain. *The Journal of Neuroscience* 31(45):16064-16069

Tsuji, A. (2005). Small Molecular Drug Transfer across the Blood-Brain Barrier via Carrier-Mediated Transport Systems. *The Journal of the American Society for Experimental NeuroTherapeutics* 2(1):54-62

Ungewickell, E, J., and Hinrichsen, L. (2007). Endocytosis: clathrin-mediated membrane budding. *Current Opinion in Cell Biology* 19(4):417-425.

Van Norman, G.A. (2016). Drugs, devices, and the FDA: Part 1: an overview of approval processes for drugs. *JACC: Basic to Translational Science 1*(3):170-179.

van Tellingen, O., Yetkin-Arik, B., de Gooijer, M, C., Wesseling, P., Wurdinger, T., and de Vries, H, E. (2015). Overcoming the blood-brain barrier for effective glioblastoma treatment. *Drug Resistance Updates* 19:1-12

Vandenberghe, R., Rinne, J, O., Boada, M., Katayama, S., Scheltens, P., Vellas, B., Tuchman, M., Gass, A., Fiebach, J, B., Hill, D., Lobello, K., Li, D., McRae, T., Lucas, P., Evans. I., Booth, K., Luscan., G., Wyman, B, T., Hua, L., Yang, L., Brashear, H, R., Black, R, S., and for the Bapineuzumab 3000 and 3001 Clinical Study Investigators. (2016). Bapineuzumab for mild to moderate Alzheimer's disease in two global randomised, phase 3 trials. *Alzheimer's Research and Therapy* 8:18

Varatharaj, A. and Galea, I. (2017). The blood-brain barrier in systemic inflammation. *Brain, Behaviour, and Immunity* 60:1-12.

Verhaak, R.G., Hoadley, K.A., Purdom, E., Wang, V., Qi, Y., Wilkerson, M.D., Miller, C.R., Ding, L., Golub, T., Mesirov, J.P., Alexe, G., Lawrence, M., O'Kelly, M., Tamayo, P., Weir, B, A., Gabriel, S., Winckler, W., Gupta, S., Jakkula, L., Feiler, H, S., Hodgson, J, G., James, C, D., Sarkaria, J, N., Brennan, C., Kahn, A., Spellman, P, T., Wilso, R, K., Speed, T, P., Gray, J, W., Meyerson, M., Getz, G., Perou, C, M., Hayes, D, N., and The Cancer Atlas Research Network. (2010). Integrated genomic analysis identifies clinically relevant subtypes of glioblastoma characterized by abnormalities in PDGFRA, IDH1, EGFR, and NF1. *Cancer Cell* 17: 98–110.

Villaseñor, R., Lampe, J., Schwaniger, M., and Collin, L. (2019). Intracellular transport and regulation of transcytosis across the blood-brain barrier. *Cellular and molecular Life Sciences* 76:1081-1092

Vogelbaum, M, A., and Aghi, M, K. (2015). Convection-enhanced delivery for the treatment of glioblastoma. *Neuro-Oncology* 17(2):ii3-ii8

Voges, J., Reszka, R., Gossmann, A., Dittmar, C., Richter, R., Garlip, G., Kracht, L., Coenen, H, H., Sturm, V., Wienhard, K., and Heiss, W.D., 2003. Imaging-guided convection-enhanced delivery and gene therapy of glioblastoma. *Annals of*

Neurology: Official Journal of the American Neurological Association and the Child Neurology Society 54(4):479-487.

Voigt, J., Christensen, J. and Shastri, V.P., 2014. Differential uptake of nanoparticles by endothelial cells through polyelectrolytes with affinity for caveolae. *Proceedings of the National Academy of Sciences 111*(8), pp.2942-2947.

Von Hoff, D, D., Layard, M, W., Basa, P., Davis, H, L., Von Hoff, A, L., Rozencweig, M., and Muggia, F, M. (1979). Risk factors for doxorubicin-induced congestive heart failure. *Annals of Internal Medicine* 91(5):710-717.

Vykhodtseva, N., McDannold, N., and Hynynen, K. (2008). Progress and Problems in the Application of Focused Ultrasound for Blood-Brain Barrier Disruption. *Ultrasonics* 48(4):279-296

Wang, D., Wang, C., Wang, L., and Chen, Y. (2019). A comprehensive review in improving delivery of small-molecule chemotherapeutic agents overcoming the blood-brain/brain tumour barriers for glioblastoma treatment. *Drug Delivery* 26(1):551-565

Wang, S., Voisin, M, B., Larbi, K, Y., Dangerfield, J., Scheiermann, C., Tran, M., Maxwell, P, H., Sorokin, L., and Nourshargh, S. (2006). Venular basement membranes certain specific matrix protein low expression regions that act as exit points for emerging neutrophils. *Journal of Experimental Medicine* 203:1519-1532

Warren, K, E. (2018). Beyond the blood: brain barrier: the importance of central nervous system (CNS) pharmacokinetics for the treatment of CNS tumours, including diffuse intrinsic potine glioma. *Frontiers in Oncology* 8(239):1-11

Watabe, T., Naka, S., Ikeda, H., Horitsugi, G., Kanai, Y., Isohashi, K., Ishibashi, M., Kato, H., Shimosegawa, E., Watabe, H., and Hatazawa, J. (2014). Distribution of Intravenously Administered Acetylcholinesterase Inhibitor and Acetylcholinesterase Activity in the Adrenal Gland: 11C-Donepezil PET Study in the Normal Rat. *PLoS One* 9(9):e107427

Westin, U., Piras, E., Jansson, B., Bergström, U., Dahlin, M., Brittebo, E., and Björk, E. (2005). Transfer of morphine along the olfactory pathway to the central nervous system after nasal administration to rodents. *European Journal of Pharmaceutical Sciences*. 24(5):565-573

Wijaya, J., Fukuda, Y., and Schuetz, J, D. (2017). Obstacles to brain tumour therapy: Key ABC transporters. *International Journal of Molecular Sciences* 18(2544):1-35

Wimo, A., Guerchet, M., Ali, G, C., Wu, Y, T., Prina, A, M., Winblad, B., Jönsson, L., Liu, Z., and Prince, M. (2017). The worldwide costs of dementia 2015 and comparisons with 2010. *Alzheimer's & Dementia* 13(1):1-7.

Winkler, E, A., Bell, R, D., and Zlokovic, B, V. (2014). Central nervous system pericytes in health and disease. *Nature Neuroscience* 14(11):1398-1405

Winter, E., Dal Pizzol, C., Locatelli, C., and Crezkynski-Pasa, T, B. (2015). Development and Evaluation of lipid nanoparticles for drug delivery: study of toxicity in vitro and in vivo. *Journal of Nanoscience and Nanotechnology* 15:1-10

Wolburg-Buchholz, K., Mack, A, F., Steiner, E., Pfeiffer, F., Englehardt, B., and Wolburg, H. (2009). Loss of astrocyte polarity marks blood-brain barrier impairment during experimental autoimmune encephalomyelitis*. Acta Neuropathologica* 118(2):219-233

Wolf, S, A., Boddeke, H, W, G, M., and Kettermann, H. (2017). Microglia in Physiology and Disease. *Annual Review of Physiology* 79:619-43

Wong, A, D., Ye, M., Levy, A, F., Rothstein, J, D., Bergles, D, E., and Searson, P, C. (2013). The blood-brain barrier: an engineering perspective. Frontiers in Neuroengineering 6:7 doi: 10.3389/fneng.2013.00007.

Wu, H, Y., Chung, M, C., Wang, C, C., Huang, C, H., Liang, H, J., and Jan, R, T. (2013). Iron oxide nanoparticles suppress the pathway of IL-1bate via the secretory lysosomal pathway in murine microglial cells. *Particle and Fibre Toxicology* 10(1):46

Wu, H., Hu, K., and Jiang, X. (2008). From nose to brain: understanding transport capacity and transport rate of drugs. *Expert Opinion on Drug Delivery* 5:1159-1168

Xiong, J., Mao, D, A., and Liu, L, Q. (2015). Research progress on the role of ABC transporters in the drug resistance mechanism of intractable epilepsy. *BioMed Research International* 2015(4):1-10

Xu, L., Guo, R., Xie, Y., Ma, M., Ye, R., and Liu, X. (2015). Caveolar: molecular insights and therapeutic targets for stroke. *Expert Opinion* 19(5):1-18

Yan, M., Schwaederle, M., Arguello, D., Millis, S, Z., Gatalica, Z., and Kurzrock, R. (2015). HER2 expression status in diverse cancers: review of results from 37,992 patients. *Cancer and Metastasis Reviews* 34(1):157-164.

Yeo, Y., and Park, K. (2004). Control of encapsulation efficiency and initial burst in polymeric microparticle systems. *Archives of Pharmacal Research* 27(1):1.

Yin, J., Valin, K, L., Dixon, M, L., and Leavenworth, J, W. (2017). The Role of Microglia and Macrophages in CNS Homeostasis, Autoimmunity, and Cancer. *Journal of Immunology Research* 5150678:1-12

Zamanian, J, L., Xu, L., Foo, L, C., Nouri, N., Zhou, L., Giffard, R, G., and Barres, B, A. (2012). Genomic analysis of reactive astrogliosis. *Journal of Neuroscience* 32:6391-6410

Zammarchi, F., Chivers, S., Williams, D. G., Adams, L., Mellinas-Gomez, M., Tyrer, P., Crobett, S., D'Hooge, F., Dissanayake, S., Sims, S., Havenith, K., Howard, P, W., Hartley, J, A., and van Berkel, P, H. (2016). ADCT-502, a novel pyrrolobenzodiazepine (PBD)-based antibody-drug conjugate (ADC) targeting low

HER2-expressing solid cancers. Presented at: *28th EORTC-NCI-AACR Symposium on Molecular Targets and Cancer Therapeutics*

Zeng, L., An, L., and Wu, X. (2011). Modelling drug-carrier interaction in the drug release from nanocarriers. *Journal of drug delivery*. 2011(370308):1-15

Zhan, C., and Lu, W. (2012). The Blood-Brain/Tumour Barriers: Challenges and Chances for Malignant Gliomas Targeted Drug Delivery. *Current Pharmaceutical Biotechnology* 13:2380-2387

Zhang, F., Lin, y, A., Kannan, S., and Kannan, R, M. (2016). Targeting specific cells in the brain with nanomedicines for CNS therapies. *Journal of Controlled Release* 240:212-226

Zhang, F., Xu, C, L., and Liu, C, M. (2015). Drug delivery strategies to enhance the permeability of the blood-brain barrier for treatment of glioma. *Drug Design, Development and Therapy* 9:2089-2100

Zhang, J., Stevens, M, F, G., and Bradshaw, D, T. (2012). Temozolomide: mechanisms of action, repair and resistance. *Current Molecular Pharmacology* 5(1):102-114.

Zhang, Y., Mintzer, E., and Uhrich, K, E. (2016). Synthesis and characterisation of PEGylated bolaamphiphiles with enhanced retention in liposomes. *Journal of Colloid and Interface Science* 482:19-26

Zidovetzki, R., and Levitan, I. (2007). Use of cyclodextrins to manipulate plasma membrane cholesterol content: Evidence, misconceptions and control strategies. *Biochimica et Biophysica Acta* 1768:1311-1324

Zlokovic, B, V. (2011). Neurovascular pathways to neurodegeneration in Alzheimer's disease and other disorders. *Nature Reviews Neuroscience* 12(12):723-738.